CHARACTERIZATION OF RefZ, A DEVELOPMENTALLY CONTROLLED REGULATOR OF *Bacillus subtilis* FtsZ

A Dissertation

by

EMILY E. BROWN

Submitted to the office of graduate and professional studies of
Texas A&M University
in partial fulfillment of the requirements for the degree of

DOCTOR OF PHILOSOPHY

Chair of Committee,	Jennifer K. Herman
Committee Members,	James C. Hu
	Dorothy E. Shippen
	Frank M. Raushel
Head of Department,	Gregory D. Reinhardt

August 2018

Major Subject: Biochemistry

Copyright 2018 Emily E. Brown

ABSTRACT

Bacillus subtilis is a soil bacterium capable of differentiating into a spore form resistant to both desiccation and heat. Sporulation begins with a single cell possessing two copies of a single, circular genome arranged with an *oriC* at each cell pole and the termini near midcell. Cell division occurs at the cell quarter over one chromosome, producing two disproportionately sized compartments and capturing approximately one quarter of one chromosome in the newly formed forespore compartment. While it is known that a specific region of the chromosome is reproducibly captured in the forespore, the mechanism underlying the precision of capture is unknown. Here we describe a role for a DNA-binding protein called RefZ and its cognate binding motifs (*RBMs*) in the precise capture of DNA in the forespore through regulation of FtsZ. RefZ is conserved across the *Bacillus* genus and remains an inhibitor of cell division in a species-swapping experiment. The *RBMs* are also conserved in their positioning relative to the *oriC* across the *Bacillus*, suggesting that the function of the *RBMs* is both important and position-dependent in the genus. In *B. subtilis*, the *RBMs* flank the region of the chromosome captured at the time of cell division, and we find that RefZ binds the five *oriC*-proximal *RBMs* with similar apparent affinity in units of two and four. In the absence of RefZ or when the *RBMs* are mutated, chromosomal regions normally excluded from the forespore are captured, suggesting that RefZ-*RBM* complexes play a role in regulating the position of cell division relative to the chromosome during sporulation. Misexpression of RefZ during vegetative growth disrupts FtsZ rings in a manner that requires DNA binding. We investigate the hypothesis that RefZ-*RBM* complexes mediate precise chromosome capture by regulating

FtsZ dynamics. We identified and characterized 10 RefZ loss-of-function variants (rLOFs) capable of binding *RBM*s, yet unable to inhibit cell division. Using single-cell analysis, we show that the rLOFs do not capture a wildtype complement of DNA in the forespore, instead phenocopying a Δ*refZ* mutant. These results suggest that RefZ acts through FtsZ to accomplish chromosome capture. To better understand the molecular basis of RefZ's activity, the structure of RefZ was solved and RefZ and the rLOFs were further characterized. Our data suggest RefZ can exist as a monomer or dimer, and that RefZ's oligomerization state both on and off DNA, likely control its capacity to influence FtsZ dynamics *in vivo*.

DEDICATION

My parents played a major role in my decision to begin graduate school and have been my chief support during graduate school. When I was growing up, my Dad was always reading about science, planting in the garden, or building something. He shared his curiosity for nature and desire to understand the world with me. I was schooled by my Mom, who also assisted me with scholarship applications for college and graduate school. I dedicate this dissertation to them, Clark and Mary Brown.

ACKNOWLEDGEMENTS

I would like to thank the many people who helped me during my graduate studies at Texas A&M University. Special thanks to Thomas and Nancy Baber for allowing me to live with their family for my first three months in College Station. Thank you to Kent and Judy Marshall, Larry and Helen Joiner, and Rachael Mews for prayers and encouragement. Thank you to my roommates Hannah Hattaway, Tingting Zhao, and Coral Bunch for warm hearts and lots of laughter. Thank you to Ezgi Krimili for being the best friend anyone could ever ask for.

I will now acknowledge several key people that played an important role in my development as a scientist. Danish Khan helped me catch up on a lot of biochemistry and molecular microbiology during my first year of graduate school. Thank you for your patience to teach me, I would never have succeeded without you. Inna Krieger taught me to screen for crystals, use a fluorimeter, operate Chimera, and motivated me when I needed it. Special thanks also to Su Tang who does science with excellence. Thanks for teaching me gel filtration, discussing my project, and mounting and shooting my crystals in summer 2017.

It has been a privilege to be a part of the Herman Lab research group. Qutaiba thank you for being like a father to me and always making lab a fun happy place. Yi Duan thanks for proofreading this dissertation and for all the other things you helped me with. Anthony, you are more than a friend definitely a brother. Thanks for your friendship, humor, and help in the lab. Allyssa, thank you for being a real trooper on this project; your enthusiasm for science always brightens up the room. Sarah it has been a pleasure

knowing you and sharing wine and coffee on the weekends. Thanks for the many times you helped out in lab, managing our laziness, and covering for us when we didn't do our jobs! Tingfeng, so grateful to know you. Thank you for always offering helpful advice on my project and being a fun soul in lab. Matt Theodore, your dedication to hard work is contagious. Thanks for bringing an atmosphere of diligence, kindness, and encouragement to lab.

The most important person in my PhD journey is my boss, Jennifer Herman. You were God's gift to me. You are the most hard-working person I know and you always put others before yourself. Your life is a gift to humanity. The Herman lab environment is something you create by nurturing people with a deep spirit of love. Thank you for all the times you encouraged me, helped me, gave me new ideas, and reassured me. You are also an excellent scientist, one of the best, and certainly my favorite.

Finally I thank God. Thank you for this privilege to study and use the mind You gave me to learn about this fascinating bacteria called *Bacillus subtilis*. Thank you for Your promises, Your salvation, and Your love. "How precious to me are your thoughts, O God! How vast is the sum of them! If I would count them, they are more than the sand." Psalm 139.

CONTRIBUTORS AND FUNDING SOURCES

Contributors

This work was supervised by a dissertation committee consisting of Dr. Jennifer Herman [Graduate Advisor and Chair of Committee] and Dr. Dorothy Shippen [Committee Member] of the Department of Biochemistry and Biophysics and Dr. Jim Hu [Committee Member] of the Department of Biochemistry and Biophyscis and Dr. Frank Raushel [Committee Member] of the Department of Chemistry.

Experiments in Chapter II were done in collaboration with Allyssa K. Miller and Ben T. Mercado. Ben T. Mercado performed the bioinformatics analysis (Fig. 2.1C, 2.1D, and 2.2) showing conservation of the *RBM*s across the genera of *Bacillus*. Allyssa K. Miller performed the experiements presented in Figures 2.3, 2.9, 2.10, 2.11, and 2.12. I I performed the experiments presented in Figures 2.4, 2.5, 2.6, and 2.7 for the paper. I also performed the analysis and experiments for the remainin Figures in Chapter II.

Experiments in Chapter III were performed in collaboration with Allyssa K. Miller, Dr. Inna V. Krieger and Dr. Jim C. Sacchettini. Experiments in Figs 3.1, 3.2, 3.3, 3.9 were performed by Allyssa K. Miller. The solution and structure refinement was carried out by Dr. Inna V. Krieger and Dr. Jim C. Sacchettini in the Department of Biochemistry and Biophysics at Texas A&M University. Purification of the rLOFs in the results was aided greatly by an undergraduate researcher, Ryan Otto. All other work including crystallography screening was completed by myself independently.

Funding sources

The work in this dissertation was funded in part by the Start-up funding of Dr. Jennifer Herman from the Department of Biochemistry and Biophysics, with the funding number 02-248312. Additionally the work in this dissertation was funded by Award 1514629 from the National Science Foundation. The authors are responsible for the contents in this dissertation. Information in this dissertation does not necessarily represent the official views of the Department of Biochemistry and Biophysics.

TABLE OF CONTENTS

LIST OF FIGURES

LIST OF TABLES

CHAPTER I: INTRODUCTION

Every living organism alive on planet earth today is the result of a well-played symphony of cellular physiology that culminates in the replication of genetic material and its passage to progeny. In order to maintain viability during growth, organisms must couple chromosome replication and segregation with cell division to ensure that each daughter cell inherits at least one copy of the chromosome. Consequently, survival depends on the precise coordination of macromolecule within three-dimensional space. Therefore an outstanding fundamental question is: how do cells coordinate chromosome organization with the complex process of cell division? Prokaryotes have reduced complexity when compared to eukaryotes and therefore offer many advantages for studying fundamental questions. Within bacteria, *Bacillus subtilis* sporulation in particular affords a unique platform for studying the coordination between cell division and chromosome organization. This is because sporulation involves only two copies of the chromosome and a distinct chromosome organization pattern (1, 2). Additionally cell division during sporulation is asymmetric and requires that the cell overcome the regulation that normally inhibits polar division during vegetative growth. In this dissertation, I will describe my contribution to understading how cell division is coordinated with chromosome positioning during *Bacillus subtilis* sporulation.

The genus of *Bacillus*

A historical look at Bacillus

The genus *Bacillus* is comprised of Gram-positive endospore forming bacteria from the phylum Firmicutes (3). *Bacillus* had a prominent historical role in the development of modern microbiology, molecular genetics and biochemistry (3). Louis Pasteur used a heat-inactivated strain of *Bacillus anthracis* in 1870 to create the first antibacterial vaccine (3). *B. anthracis* was also used to test the application of Koch's postulates (1890) to determine the causative agents of disease (3).

Spore formation affords protection and pathogenicity to Bacillus

Spore formation is a particularly fascinating biological phenomenon because a spore can preserve genetic information for extended periods of time. There are reports of viable *Bacillus* spores isolated from samples thousands of years old, and even one report, albeit controversial, of viable spores from a bee gut in 25-40 million year old amber (4). The ability of spores to withstand harsh environments in the gut, soil, and even canned goods contributes to the pathogenicity of several endospore formers that cause disease. The spores of *Clostridium difficile* allow it to survive the acidic environment of the stomach and germinate in the colon to cause pseudomembranous colitis when the gut has been cleared of competitor bacteria by antibiotic therapy (5). The spores of *C. botulinum* (the responsible agent for botulism a very dangerous type of food poisoning) allow it to survive some methods of food preservation (6). There are also several notable pathogenic *Bacillus* species, including *B. anthracis*, the causative agent of anthrax, and *B. thuringiensis* an agriculturally important insect pathogen (4, 7). *Bacillus* spores can

survive extreme temperatures, desiccation, and UV irradiation, making them difficult to eradicate. Formation of a protective endospore allows *Bacillus* to wait out unfavorable conditions (heat, desiccation, and chemicals) that kill competing bacteria (8). When conditions improve the spores germinate and vegetative cells can rapidly multiply in an environment cleared of competitors (8, 9). Endospore formation also enhances virulence by allowing *Bacillus* to tightly adhere to surfaces and withstand normal cleaning procedures (10). The mechanisms underlying spore adhesion are not fully understood, but electrostatic properties, hydrophobicity, saccharic matrix, and appendages play a role (9, 11).

The study of sporulation in *Bacillus* pathogens was curtailed by the dangers of working with these microorganisms. Therefore, much of the foundational work related to sporulation was conducted in a "domesticated" laboratory strain, *B. subtilis* 168. This strain 168 was isolated in 1947 by P. R. Bulkholder and N. H. Giles as a tryptophan auxotroph for the study of aromatic amino acid biosynthesis (12). *B. subtilis* 168 has a number of genetic differences from the environmental strains of *B. subtilis*, most notably it is defective in biofilm formation and has a frameshift mutation in the surfactin biosynthesis gene (*sfp*) important for swarming motility (13). *B. subtilis* grew in popularity as a model organism due to its genetic tractability (it is naturally transformable) and the ease with which it could be induced to sporulate (3). By the 1970s, *B. subtilis* was the paradigm model organism for the Gram-positive world and groundbreaking work in *Bacillus* led to the discovery of alternative sigma factors and insight into transcriptional regulation (3). In 1997 the first *Bacillus subtilis* genome was published (3). Today we

know *B. subtilis* has at least 4,107 genes, although only ~1,500 have experimentally determined functions (3).

Reservoirs for Bacillus

Soil is a common natural reservoir for *Bacillus* (7). However, through interaction with plants and the organisms that consume plants, *Bacillus* also takes up residence in the gastrointestinal tracts of animals (7). The effect of *Bacilli* (beneficial, symbiotic, parasitic or pathogenic) depends upon factors intrinsic to both the *Bacillus* species and the animal host. *B. thuringiensis* is used to control Japanese beetles and caterpillar larvae respectively because it produces an insecticidal toxin called Bt. Bt is widely used as as a biological control agent, and is present in more than 90% of bioinsecticides sold. During *B. thuringiensis* sporulation, Bt toxin is produced as a proteinaceous crystal. Upon ingestion by an insect, the crystals are solubilized and the protoxins are proteolytically cleaved to the active form which bind to receptors in the insect gut(14). This results in pore formation and ion leakage in the cells along the intestinal wall, ultimately causing death of caterpillar larvae (14). *Bacillus* may also form a beneficial relationship with its host by making nutrients more available and competitively preventing growth of antagonistic bacteria (4). The recent explosion in gut microbiome research has led to a heightened interest in spore-based probiotics since spores have an excellent shelf life and can survive the journey to the lower GI (4).

The mechanisms of B. subtilis sporulation

In response to nutrient stress, *B. subtilis* can initiate the developmental program of sporulation which culminates in preservation of one copy of the chromosome in a highly resistant cell type called a spore (2). The natural soil environment of *Bacillus* commonly presents harsh environmental conditions and starvation (2). *Bacillus* can respond with a variety of survival strategies including chemotaxis, induction of competence, antibiotic production, several types of motility and finally sporulation (2). Sporulation is considered the last resort of all survival strategies (2). Given this information, it should not come as a surprise that the cellular decision to enter sporulation is extremely complex and highly regulated (2).

Decision making cascade preceding sporulation

The master transcriptional regulator for sporulation is Spo0A (1). Detection of nutrient limitation leads to activation of a phosphorylation cascade in which several kinases (KinA, KinB, KinC, KinD and KinE) contribute to the gradual accumulation of Spo0A-P, and ultimately initiation of sporulation (1, 2). KinA is most important and has three PAS domains which have been characterized in other kinases as sensors for oxygen availability and redox potential (1). Spo0A-P may bind to 10% of all *B. subtilis* genes, and can act as both an activator and a repressor (2). Spo0A-P activates transcription of the key genes *spoIIA*, *spoIIE* and *spoIIG* (2). σ_H also plays a critical role in the initiation of sporulation, activating more than eighty genes (2).

Establishment of the axial filament

A key response to the cellular decision to sporulate is the establishment of a chromosomal arrangement that is optimal for packaging of a single chromosome into the spore (15, 16). The axial filament is a condensed (*oriC-ter ter-oriC*) chromosomal arrangement where two copies of the chromosome are anchored to opposite cell poles. One copy of the chromosome will nurture the forespore in the mother cell and the other will be packaged into the spore. A correct chromosome arrangement is a prerequisite for precise chromosome capture at the time of polar division, which is the focus of this dissertation.

Genetic asymmetry between mother cell and prespore

After establishment of the axial filament, the cell division machinery is repositioned from midcell to one or both cell poles (2). Importantly, rearrangement of the chromosome is not required for repositioning of the Z-ring, though it is important for precise capture of the forespore-destined chromosome (17). At the selected pole a divisome will assemble which is similar but not identical to the midcell divisome of vegetative growth (2). Importantly, the divisome will assemble and septation occurs around the spore-destined chromosome, initially trapping only ~30% of the chromosome inside the prespore compartment (2). Thus, polar division creates a genetic asymmetry that promotes specific, compartmentalized gene expression patterns within the mother cell and forespore (2). The known players in precise chromosome capture will be discussed in the first chapter of this dissertation, while chapters two and three are the investigation of the role of the DNA-binding protein RefZ in chromosome capture.

Activation of forespore specific gene expression

The compartmentalized gene expression program in the forespore is initiated by sigmaF (2). SigmaF is held inactive by the presence of anti-sigma factor SpoIIAB (2). SpoIIAA (an anti-anti-sigma factor) associates with the prespore side of the asymmetric division site (2) and when dephosphorylated by SpoIIE (18) interacts with SpoIIAB-sigmaF with the consequence that sigmaF is freed (2). SigmaF then associates with RNA polymerase in the forespore and promotes transcription of forespore-specific genes. The levels of SpoIIE and SpoIIAB are important for this activation cascade. After septation, SpoIIE in the mother cell is degraded by FtsH, but the concentration of SpoIIE increases in the forespore. The phosphatase activity of SpoIIE is activated after the asymmetric septum is formed. At the same time the concentration of SpoIIAB falls because of its intrinsic instability and the fact that it's position on the chromosome makes it one of the last genes to be pumped into the forespore (2)*; spoIIAB* is located nearly opposite the *oriC* outside of the forespore-captured region of the chromosome. This allows SpoIIE in the forespore to travel to the pole where it dephosporylates SpoII-AA.

The asymmetric capture of the chromosome is important for the criss-cross signal cascade for the two parallel gene expression programs in the mother and forespore (19, 20). When sigmaF is activated in the forespore it causes sigmaE activation in the mother cell which turns on about 46 genes that reprogram the mother cell to nurture forespore development, one of which is sigmaG (19). SigmaG then turns on sigmaK in the mother cell (19). SigmaE in the mother cell in turn activates sigmaG in the forespore (19). Immediately following septation, compartmentalized sigmaF can only activate the part of

its regulon initially captured in the forespore (21). Therefore, gene expression in the forespore is controlled both through comparmentalization of genes and transcriptionally by sigmaF. The sigmaF regulon has a left chromosomal arm biased distribution and there are a cluster of genes around the Rac binding sites (*ram* sites), which are immediately expressed following septation (19). SigmaF regulon genes excluded from the *ori*-proximal region are not initially expressed.

Pumping of the forespore chromosome by SpoIIIE

After the initial prespore chromosome capture, around 10-15 min pass and then the remainder of the chromosome is pumped into the forespore by FtsK-like DNA translocase SpoIIIE (2, 22). FtsK is a well-studied *E.coli* protein involved in chromosome partitioning during vegetative growth (22). More specifically, FtsK directionally pumps chromosomal material in the midcell division plane (the *ter* region) toward the appropriate daughter cell to prevent a block in the cell cycle (23). FtsK also helps in the resolution of chromosome dimers, which result from chromosome entanglement during recombination (22). SpoIIIE is expressed constitutively also functioning to remove trapped chromosomes from under the septum (22). *B. subtilis* has another DNA translocase, SftA, that is not membrane associated but is recruited by the divisome component FtsA to remove chromosomes from underneath the divisome (23). Only SpoIIIE is essential to sporulation.

The directionality of pumping in FtsK is biased by directional KOPS sequences present on the chromosome in the *ter* region (22). For SpoIIIE the sequences implicated in directionally pumping are called SRSs, and binding and recognition of these sequences

is required for directional pumping *in vitro (22, 23)*. The directionality of the SpoIIIE and FtsK pump is toward the chromosome dimer resolution site or *dif* site (22, 23). These sites are scattered across the chromosome but have highest density near the *ter* region (22, 23). In *E. coli* resolution of chromosome dimers (cantenes) is mediated by formation of Holliday junctions by the recombinases XerD and XerC (22, 23). In *B. subtilis* RipX and CodV are the corresponding recombinases (22, 23).

In vitro and *in vivo* studies suggest there are at least two SpoIIIE channels formed in the septum, one around each arm of the chromosome (22, 24). Data suggest SpoIIIE assembles two sets of end-to-end hexamers in the cytoplasmic membrane of both the forespore and the mother cell. SpoIIIE strips the chromosome of proteins as it pumps (22, 25). It is not yet understood how the end of the chromosome is resolved into the forespore since the chromosome is a closed loop (22, 24). RefZ has a positive self-interaction with SpoIIIE (discussed in Chapter II), the functional significance of which is unclear.

Final stages of sporulation

After septation and during/after chromosome transport, the forespore is engulfed by the mother cell, resulting in a double membrane-bound compartment with a layer of peptidoglycan in between. Spore development proceeds with the thickening and modification of peptidoglycan (cortex) between the inner and outer membrane, coating of the spore with an inner and outer layer of proteins, and replacement of cytoplasmic water molecules with dipocolinic acid. Eventually the mother cell undergoes a programmed cell lysis to release the mature spore, which remain dormant until germinant signals are received (26).

Chromosome organization

For prokaryotic and eukaryotic cells, chromosome organization is essential for survival and preservation of life. Faithful replication and equal segregation protect genetic transfer to daughter cells. Chromosome organization is not random and must be compatible with replication, repair, and gene expression mechanisms. Moreover, as the cell cycle progresses chromosomes often need to be reorganized for segregation. Our knowledge of chromosome organization has advanced in recent years due to developments in genomics techniques, which allow study of global chromosome architecture and light microscopy techniques which allow visualization of specific chromosomal loci in live cells. However, chromosome organization remains an active area of research as many mysteries, including the tight coordination of chromosome replication and segregation with cell division, remain unclear.

B. subtilis sporulation affords an excellent system to study the coordination of chromosome replication and segregation. My dissertation studies uncover the mechanisms of a specialized nucleoid occlusion system that functions during *Bacillus* sporulation where two copies of the chromosome are anchored to opposite cell poles and condensed in an (*oriC-ter ter-oriC*) arrangement. As a preface to my work, I will review what is currently known about both eukaryotic and prokaryotic chromosome compaction and organization mechanisms.

Chromosome compaction in eukaryotes

If stretched end to end, the human genome would be >2 m in length, yet when properly compacted it fits within 3 um (less than the diameter of the nucleus) (27). Similarly, a typical bacterial chromosome is 1,000 times longer than the cell (28).

For eukaryotes, the basic unit of chromosome compaction is the nucleosome, which is 146 base pairs of DNA wrapped around a histone octamer (Fig. 1.1A) (29). Each histone octamer is comprised of four dimers (29). Each dimer will be one of the core histones H2A, H2B, H3 and H4 (29). A plethora of epigenetic signals are "written" on histones as post-translational modifications which restrict or promote access to the DNA, often by controlling compaction (29). Association of histones with DNA is unstable, therefore histones can rapidly disassemble and reassemble on the DNA during replication, transcription, and repair (29). The nucleosomes linearly compact DNA 7-fold and associate to form chromatin fibers (Fig. 1.1A) which fold into the higher-order structures that allow DNA to fit inside the nucleus (29).

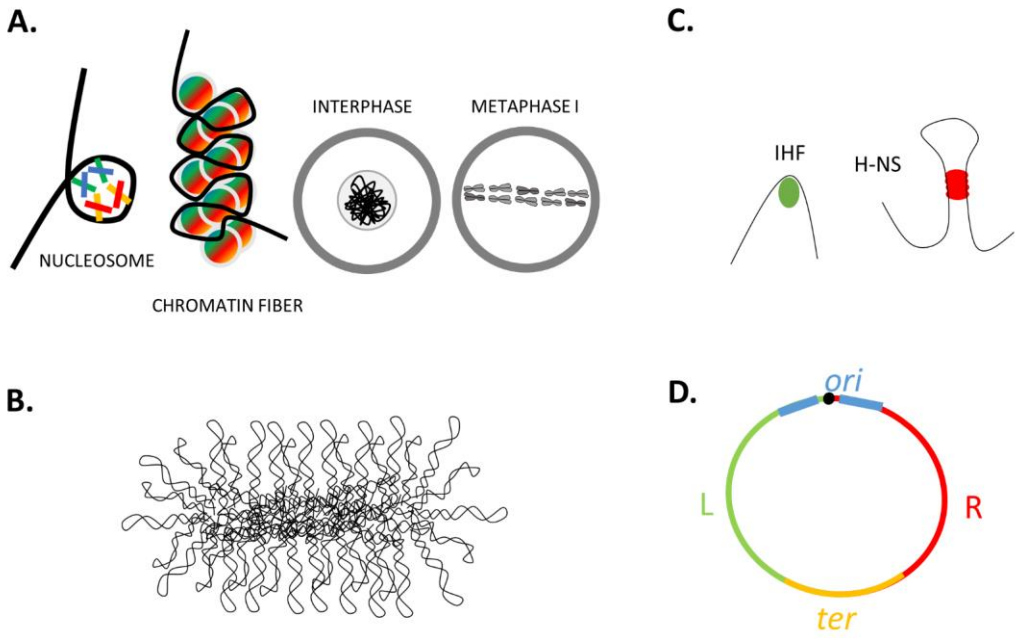

Figure 1.1. Chromosome organization in eukaryotes and bacteria. (A) The basic structure of chromatin is the nucleosome. 146 bp of DNA are wrapped around each histone. The nucleosomes look like beads on a string and are folded into a chromatin fiber. The chromatin fiber is looped and compacted into a 250 nm fiber. These fibers are coiled to produce compacted chromatids, which align at the metaphase plate. **(B)** The bacterial chromosome has a condensed core with more frequently accessed regions of the chromosome protruding from the condensed core as loops giving it a "bottlebrush" appearance. **(C)** IHF and HU are DNA-bending proteins that fold the nucleoid. H-NS and MatP are DNA-bridging proteins that have long-range interactions which result in further ordered compaction of the chromosome. **(D)** The *E.coli* chromosome has been separated into several major macrodomains: *ori*, *ter*, and right and left arm macrodomains.

Gene expression differences are reflected in the extent of DNA packaging (30). In general genes that are highly expressed are positioned on loops emanating from more tightly packed chromatin, whereas genes that are not frequently expressed will be buried deeper in the compacted chromosomal core (30).

At interphase each linear chromosome resides at a given space within the nucleus called a chromosome territory (CT) (31). The larger chromosomes with more heterochromatin regions seem to be positioned near the nucleus periphery while smaller gene dense chromosomes are more likely to be found at the nucleus center (31, 32). Individual CT's are further organized into multi-megabase regions that are active

(euchromatin) or inactive (heterochromatin) (31, 33). Sub-megabase or topologically associating domains (TADs) are the next level deep in chromosome organization and are defined as regions that interact more frequently within the domain than externally to a different domain (31, 33). TADs are comprised of chromatin loops but the folding and organizational units have not been well characterized (31, 33). As the cells prepare to divide, 3D chromosome organization undergoes a major reorganization and compaction from interphase to metaphase (31, 33). Chromosomes adopt a more general compact pattern of organization involving linear and axial compaction (31). The structural maintenance of chromosome (SMC) complexes have an important role in compacting the chromosomes into the sister chromatids that align at the metaphase plate (Fig. 1.1A) (33, 34).

Chromosome compaction in prokaryotes

In most bacteria, the chromosome is circular but some are linear (28). The structure of the compacted bacterial chromosome has been described as a bottlebrush (Fig. 1.1B) (35). The core is dense with loops consisting of twisted DNA emanating from the core (35). Compaction is a collaborative effort between protein-assisted condensation and supercoiling of the chromosome (35, 36).

The hierarchical organization of the bacterial chromosome begins with macrodomains which are megabases in size (28). The definition for a macrodomain is a collection of loci within the chromosome that interact more frequently than with other regions of the chromosome same as TADs for eukaryotes (28). The *E.coli* chromosome has four macrodomains: *ori*, *ter*, and left and right arms (Fig. 1.1D) (28). Within a

macrodomain, or in some organisms where macrodomains have not been observed, chromosome organizational units of 100-200 kb have been identified and given the term CID (chromosomal interaction domain) (28, 37). Within CIDs there are plectomeres (also called supercoil domains) which are loops of supercoiled DNA with a size around 10 kb (28). Plectomeres are tethered at their base by proteins. The result of frequent unwinding of DNA for transcription creates regions free of plectonemes which may act as boundaries constraining movement of supercoils and other chromosome-like structure (28). Three separate experiments (EM imaging, rate of recombination as a function of genomic distance, and rates of transcription after dsDNA breaks) have suggested that for each *E.coli* chromosome there are ~400 plectomeres (28). Protein-assisted chromosome compaction is mediated by nucleoid associated proteins (NAPs). Some NAPs are involved in DNA wrapping/bending (HU), DNA bridging (HNS, MatP), and still others function in tethering and clipping (SMC).

In *E. coli* the histone-like, positively-charged protein HU has two subunits, α and β which can form homo or heterodimers. These may further associate to form an octamer (38). DNA bends around the octamer through insertion of proline residues into the minor groove (39). A HU variant with higher affinity to DNA causes overcompaction of the chromosome; conversely the absence of HU leads to a diffuse chromosome structure and anucleate daughter cells (40, 41). Integration host factor (IHF) is another *E.coli* DNA-bending protein contributing to chromosomal compaction which can bend DNA to 160° (28). Both IHF and HU mediate short-range chromosomal folding (Fig. 1.1C) (42). In *B. subtilis*, HBsu and HPB9 are the only characterized histone-like proteins (43, 44) and are

similar to HU in *E.coli* (44). HBsu is essential and associates nonspecifically to DNA as a homodimer (44).

E.coli protein Histone-like Nucleoid Structuring protein (H-NS) is a global organizing protein that facilitates larger scale compaction (42). It binds and bridges DNA through self-interaction of both its C-terminal DNA-binding domain and N-terminal oligomerization domain (28). H-NS binds hundreds of sites scattered across the chromosome with a preference for curved or AT-rich DNA (28). H-NS can also spread along DNA, modulating gene expression and preventing transcription of horizontally acquired DNA elements (28).

To properly compact the *ter* macrodomain, *E.coli* relies on a DNA-binding protein called MatP and 23 binding sites (*matS)* enriched over a 800 kb region (45). MatP is a 17 kDa protein that dimerizes and forms a tetramer by interaction of its coiled-coil domain (46). Tetramer formation results in DNA bridging and chromosome compaction (46). MatP displaces *E.coli's* SMC (MukBEF) from the *ter* encouraging association of MukBEF with the origin instead (47). If MatP is deleted, the chromosome is less compacted and the *ter* is segregated prematurely (45).

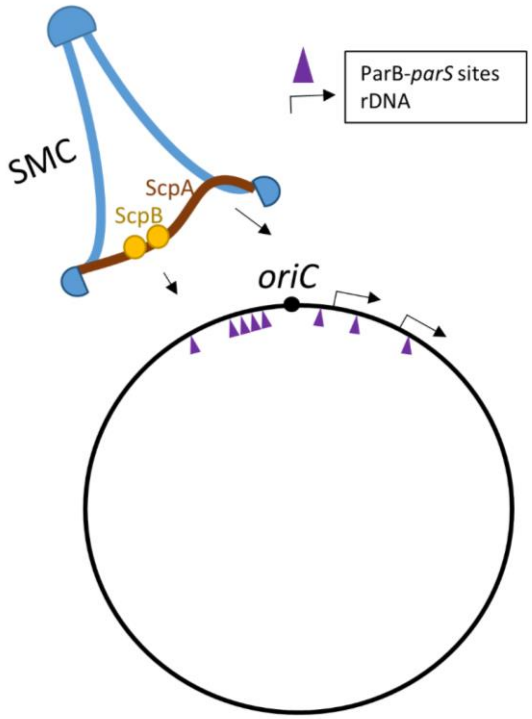

Figure 1.2. The condensin complex in *Bacillus subtilis* is composed of the SMC, ScpA, and ScpB. SMC is a dimeric clip protein, which can take on a variety of conformations to control and condense DNA. The hinge domain is at the bottom of the V while the ATPase domain of the SMC is at the open end of the V. ScpA and ScpB are important partner proteins required for proper function of the SMC complex. The SMC complex loads onto both ParB-*parS* sites (purple carets) and rDNA (promoter arrow).

The SMC complexes, also called condensins, comprise an important class of proteins for chromosome compaction (28). A more detailed look into this system is required because in *B. subtilis* the SMC cooperates with the ParABS system to properly segregate the chromosomes at the onset of sporulation which is a prerequisite for correct chromosome capture (34). Additionally ParA is from the same family as MinD which is a key player in bacterial cell division and both of these proteins act as positional agents in the cell (48).

The SMC is a clip-like protein that exists from humans to bacteria but are not conserved necessarily in sequence (49). MukB, the first member described in this protein family, was identified as a mutant that generated a high frequency of anucleate daughter cells (50). Most archaea, as well as both Gram-positive and Gram-negative bacteria have one SMC-like protein, whereas eukaryotes contain multiple SMC proteins (51). SMC proteins in eukaryotes are part of a five subunit complex that mediates sister chromatid cohesion during S-phase and mitosis, when chromosomes are separated (49, 52). In *E. coli*, the SMC-like complex consists of MukBEF. MukBEF is responsible for establishing megabase scale DNA contacts which, in conjunction with HU, condense and properly fold the macrodomains of the chromosome (53). In *B. subtilis* the condensin complex is composed of SMC, Segregation and Condensation Protein A (ScpA), and ScpB (Fig. 1.2). The SMC protein is composed of a coiled-coil domain with an ATPase domain at the head domain (54). Dimerization of SMC forms a V-shape with an ATPase domain on each end of the open end of the V (54). ScpA and ScpB form a core complex with a stoichiometry of 1:2 and associate with the SMC via the C-terminal domain of ScpA (55). They are both required for proper function of the SMC and are thought to regulate the ATPase activity

(55, 56). Although the exact mechanism remains unclear, most data suggest SMC can entrap/encircle DNA within the V in a variety of topologies, and that opening and closing of both ends of the ring allow the SMC to function like a handcuff to control and compact DNA (54). In *Bacillus subtilis* the SMC loads onto the chromosome at eight centromeric DNA sequences called *parS* sites and at rDNA near the origin of replication (*oriC*) (Fig. 1.2) (34, 57, 58). SMC-ScpAB loading onto rDNA may function primarily to condense the *oriC*-proximal region of the chromosome while SMC-ScpAB loading at the *parS* centromere would compact regions beyond the *oriC* (57). The current model is that the SMC-ScpAB loads onto newly replicated bacterial centromere-like *parS* sites like a handcuff individualizing them from the template chromosome and juxtapositioning the right and left arms to each other (34, 56).

Chromosome segregation in prokaryotes

Bacillus sporulation requires two copies of the chromosome. One copy of the chromosome will nurture the forespore in the mother cell and the other will be packaged into the spore. Through segregation and anchoring the origins of replication to opposite cell poles the cell separates the chromosomes and maximizes the chance of an origin being captured in the prespore compartment. Our current knowledge of the mechanisms by which chromosomes are segregated are discussed below.

Eukaryotes have a dedicated phase of the cell cycle for replication S-phase (synthesis) followed by a dedicated phase for segregation M-phase (mitosis) (59). After compaction the chromosomes align at the metaphase plate where they become attached to

microtubules via kinetochores (59). Anaphase begins when the mitotic spindle contracts or when the microtubules pull sister chromatids to opposite poles (59).

In contrast, bacteria overlap chromosome replication and segregation with cell division. During rapid growth, bacteria immediately segregate their *oriC*s towards the cell pole or the future cell pole before replication is complete. Malfunction of chromosome segregation at any point could result in either breakage of the chromosome by the division machinery or anucleate daughter cells, both of which ultimately result in cell death.

The ParABS system

Much of the current knowledge for bacterial chromosome segregation is a result of studying the ParABS plasmid partitioning systems, which ensure some plasmids are properly inherited by daughter cells (28, 60). In nearly 65% of bacteria, a chromosomally encoded system homologous to the ParABS plasmid system helps to ensure proper chromosome segregation (28). Many important discoveries in bacterial chromosome segregation with the ParABS system have been in the Gram-negative bacterium *Caulobacter crescentus*. *C. crescentus* is an alpha-proteobacterium with a single, circular chromosome (Fig. 1.3A) (61). The *oriC* is at the cell pole closest to an extension of the cell body called the stalk while the *ter* region is near the opposite cell pole.

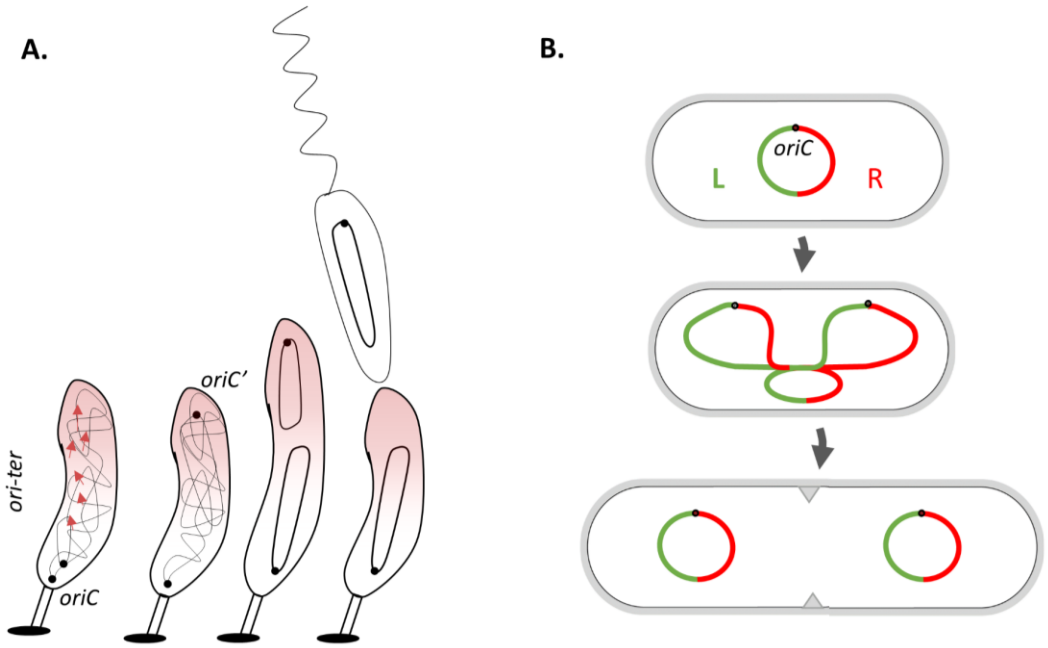

Figure 1.3. Chromosome organization-segregation cycle for *C. crescentus* and *E. coli.* (A) *C. crescentus* exhibits the *c*hromosome organization-segregation cycle of *ori-ter* where chromosomes are replicated and segregated in parallel with the longitudinal axis of the cell. After chromosome replication *parS* motifs near the *oriC* are condensed by binding and bridging of ParB to a nucleoprotein patch. This centromere like element has affinity for nucleoid associated ParA which has an increasing gradient density (maroon) towards the opposite cell pole. The ParB-*parS* complex travels up the gradient releasing ParA as it moves. Released ParA must bind ATP before nonspecifically reassociating with the nucleoid. **(B)** *E. coli exhibits* the chromosome organization-segregation cycle of *left-ori-right*. In this pattern the left and right arms are not parallel but lie east and west of the cell's absolute middle. They are replicated and segregated in a manner that maintains this orientation.

The ori-ter pattern in C. crescentus

There are two described patterns for the chromosome organization-segregation cycle in bacteria. *Caulobacter crescentus* exhibits the first pattern known as *ori-ter* in which the right and left arms of the chromosome run parallel to the long axis of the cell (Fig. 1.3A) (28). *parS* is a DNA sequence near or at *oriC* (62) and following chromosomal replication there are two copies of the *parS* site. ParB (DNA-binding protein) spreads on these *parS* sites, bridging adjacent *parS* sites creating a nucleoprotein patch for each chromosome (62). ParA is a deviant Walker A-type ATPase from the same family as MinD that dimerizes upon binding ATP, which stimulates nonspecific DNA-binding (48, 62). ParA has a gradient distribution biased toward the new cell pole that is dependent on interaction with the nucleoid (63). Bound ParA will interact with the nearest ParB-*parS* nuceloprotein patch, resulting in segregation of one origin towards the new (flagellated) cell pole. Elasticity of the chromosome is thought to help drive translocation of ParB-*parS* up the ParA gradient; this is called the DNA-relay model. In the early days of studying the parABS system the predominant model was a ParA filament model that acted like a mitotic spindle to draw the origin to the new cell pole (28, 64). In this model, ParB-*parS* interaction caused depolymerization of the ParA filament (64). Today, the favored model for function of the ParABS system is the DNA-relay model mentioned above (28). Thus in *Caulobacter* after replication the new chromosome is segregated to the opposite pole by the ParABS system. Following segregation and cell division, the original stalk cell remains and a flagellated swarmer is released (65). The new pole eventually becomes a stalked pole, thus the *ori-ter* configuration of the chromosome is maintained (28).

The left-ori-right pattern in E. coli

E.coli exhibits the second organization-segregation pattern known as *left-ori-right* (Fig. 1.3B) (35). For this chromosome pattern the chromosomal arms do not lie parallel to one another along the long axis of the cell (35). Instead the origins are near midcell (future cell pole) with the left and right arms lying "east" and "west" respectively of the cell's absolute middle (Fig. 1.3B) (35). *E. coli* lacks the ParABS system but possesses MukBEF which is important for cell viability and proper chromosome organization (66). In a MukB null the chromosomes do not properly segregate following replication to restore the *left-ori-right* pattern of chromosome organization, instead the *oriC* remains at the old cell pole (66).

During *E. coli* replication, the DNA ahead of the replication fork becomes overwound causing positive supercoils (67). In order to relieve the stress, the replication fork rotates, which results in interlinks (twisting of two strands of DNA) behind the replication fork (67). Before chromosome segregation can occur these ~450,000 interlinks must be resolved (47). It is known that topoisomerases, specifically TopoIV and DNA gyrase, have essential roles in resolution of the twisted strands, and that resolution is required for chromosome segregation (47). DNA gyrase works ahead of the replication fork to relax positive supercoiling while TopoIV works behind and in front of the replication fork (47).

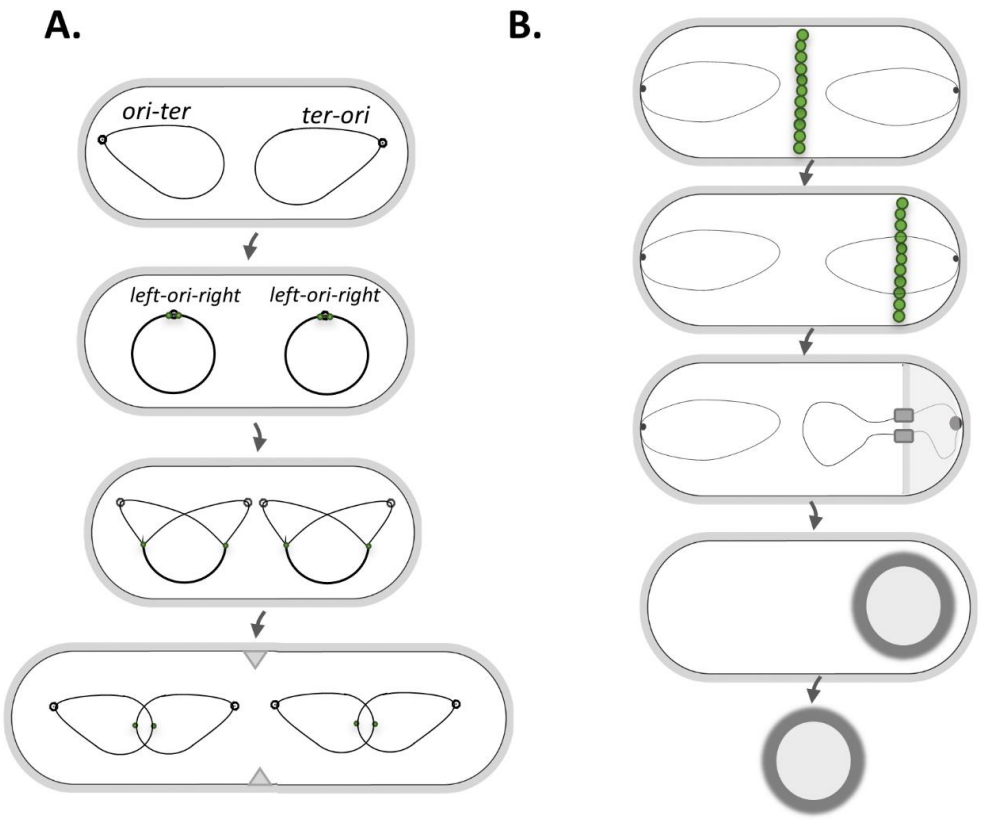

Figure 1.4. Organization-segregation cycle for *B. subtilis* (A) The *B. subtilis* chromosome organization-segregation cycle oscillates between *ori-ter* and *left-ori-right* during rapid growth. Immediately after replication the chromosomes are oriented in the *ori-ter* pattern. After replication they resolve to the *left-ori-right* pattern. As replication proceeds the origins are pulled toward the opposite and new cell poles reestablishing the *ori-ter* pattern. **(B)** During sporulation SirA, Sda, and Spo0A stop DNA replication initiation lowering the *Bacillus* chromosome copy number to just two per cell and generates the axial filament. The cell division machinery is redistributed to both poles, but only one pole is selected for division. Genetic asymmetry promotes spore and mother cell specific gene expression programs. The remainder of the chromosome is pumped into the forespore by SpoIIIE. Development proceeds and eventually the mother cell lyses releasing the mature spore.

The combination of patterns in B. subtilis

Bacillus exhibits both *ori-ter* and *left-ori-right* chromosome segregation patterns (Fig. 1.4A) (68). DNA replication begins when DnaA binds regions at the *oriC*, resulting in the assembly of large nucleoprotein complex, which unwinds the AT rich DNA duplex in the region. Replisome components then load onto the replication forks and proceed bidirectionally towards the *ter*. During vegetative growth there can be more than eight partial copies of the chromosome per cell. Newly replicated chromosomes in *Bacillus* adopt the *ori-ter* pattern (Fig. 1.4A) (68). However, after initiation of replication near the cell pole, the template DNA of *Bacillus* resolves back to the *left-ori-right* pattern and the *oriC*s move toward midcell (Fig. 1.4A) (68).

The ParABS and SMC complexes are both required for the organization-segregation pattern observed in *B. subtilis*. In *B. subtilis*, the ParABS system is comprised of Soj (ParA), Spo0J (ParB) and *parS*, respectively. This system functions differently in *B. subtilis* than in *C. crescentus*. Ten *parS* sites have been identified, eight of which are within the *oriC*-proximal region of the chromosome; the remaining two *parS* sites lie outside of this region (69). Following chromosomal replication there will be two copies of the *parS* sites. Spo0J binds the *oriC*-proximal *parS* sites bridging to adjacent sites which create nucleoprotein complexes similar to *C. crescentus'* ParB-*parS (69)*. Thus a mere 20 dimers of Spo0J can condense kilobases of DNA (70). Spo0J-*parS* recruits the SMC complex which individualizes the chromosomes from each other. Soj forms an ATP dependent dimer that can bind to DNA similar to *C. crescentus'* ParA. However, Soj does not form a cloud-like gradient, as in *C. crescentus*. In cells lacking both Spo0J the *oriC*-proximal region of the chromosome is disorganized and origins are not correctly separated

(69, 71). Soj was shown to contribute to the relocalization of newly replicated origins towards the nucleoid periphery (68). After replication, Spo0J-*parS* pulls the newly replicated origins towards the nucleoid periphery through interaction with Soj, resulting in an *ori-ter* configuration (68). When another replication cycle is triggered, Soj releases ParB-*parS* and the chromosomes relax into the *left-ori-right* pattern (68).

Chromosome segregation in B. subtilis during sporulation

Chromosome orientation at sporulation onset

In preparation for sporulation *Bacillus* must reduce the chromosome copy number to just two per cell. Replication initiation fires more than once in fast growth conditions for *B. subtilis*, leading to the possibility for up to eight partial chromosomal copies in a given cell (72). Chromosome copy number is controlled in part by a Spo0A-P regulated gene encoding an inhibitor of DnaA called *sirA* (72). SirA prevents additional rounds of DNA replication in cells committed to sporulation by interacting directly with DnaA (72, 73). Another protein, Sda, prevents sporulation in cells that have not yet finished division or are undergoing DNA repair (1). Sda expression occurs in bursts as DnaA initiates replication (1). Proteolysis of Sda by ClpXP after the burst provides an opportunity for some diploid cells to enter sporulation (1). Sda's mechanism of action is to inhibit KinA by blocking autophosphorylation and preventing phospho-transfer to SpoOF (1).

To form a spore the cell needs to establish a specific chromosome configuration: the axial filament. The axial filament is an elongated configuration of two chromosome copies each with their *oriC*-proximal regions anchored to the cell pole and with the chromosomal arms lying parallel to the long axis of the cell (42). The chromosomes are

tethered by interaction between RacA (Remodeling and Anchoring of the Chromosome) bound to its cognate sites enriched around *oriC* and the polarly-localized membrane-associated protein DivIVA (42, 74). DivIVA is a negative curvature-sensing protein composed of coiled-coil domains (75). DivIVA is conserved across Gram-positive bacteria and its coiled coil structure is reminiscent of that of eukaryotic tropomyosins (75). In addition to serving as the membrane anchor for RacA, DivIVA plays a critical role in the regulation of cell division. RacA binds to 25 RacA binding motifs (*ram*s) enriched around the *oriC*-proximal region of the chromosome (76). RacA-*ram* interactions to adjacent RacA-*ram* sites form an adhesive patch which anchors the chromosome to the pole through direct interaction between RacA and DivIVA (76). Nonspecific binding of RacA across the genome via its N-terminal winged HTH mediates chromosomal compaction by a mechanism similar to MatP (42). Consistent with a similar mechanism MatP and RacA have structural similarity both containing a HTH domain and a C-terminal coiled coil domain (42). RacA transcription is controlled by Spo0A and sigmaH and peak levels reach about 3,000 copies per cell or 3 uM (42). RacA is essential for formation of the axial filament and proper capture of DNA in the forespore. Soj also functions in *oriC* segregation during sporulation and is important for high fidelity of *oriC* capture in the forespore (69).

Important players for correct chromosome capture

To characterize the precise region of the chromosome initially captured in the forespore at the time of division, both population and single-cell based assays for chromosome "trapping" have been developed (69, 77, 78). The single cell version of this

assay is the most sensitive and provides the most detailed picture of chromosomal regions that are either excluded or present in the forespore (69). The assay is performed in a strain containing a SpoIIIE DNA pumping mutant SpoIIIE36, which freezes the chromosome at the initial capture position. Although SpoIIIE36 prevents pumping, sigmaF still becomes activated in the forespore. Therefore a fluorescent reporter gene fused to a sigmaF controlled promoter (such as P_{spoIIQ}) will be transcribed only if the locus is captured in the forespore. The reporters can be placed at various places around the chromosome and the use of multiple fluorescent markers allows for simultaneous assay of more than one chromosomal region at a time. Thus, this highly sensitive assay allows for quantitation of precise chromosome capture during *B.subtilis* sporulation at the single cell level.

Many proteins are required for correct chromosome capture. The capture of the *oriC* and the left and right *oriC*-proximal chromosomal arms region are the best characterized (Fig. 1.5). Three major defects have been studied: 1) mislocalization of the *oriC* in the mother cell, but retention of the left and right *oriC*-proximal arms in the forespore 2) capture of *oriC*, but miscapture of the *oriC*-proximal arm regions and 3) miscapture of both regions. Failure to capture the *oriC* results in the forespore-destined chromosome being pumped completely out of the forespore; if this occurs, cells divide at the opposite pole in a second attempt to capture *oriC* (79). Null mutants of *divIVA*, *comN*, *minD*, *minJ*, *soj*, *racA*, and *sirA* show a reduced frequency of *oriC* capture in the forespore, but retain the arm regions in the forespore, suggesting these proteins function primarily in correct *oriC* organization/capture, but not in proper capture of the arms(80, 81). Spo0J, which has been implicated in chromosome condensation and recruitment/loading of the SMC complex around *oriC* (69) is important for proper capture of both oriC and the

chromosomal arms(17). RefZ, which is important for the timely redistribution of FtsZ from midcell to the pole (82) shows an altered pattern of chromosomal arm capture during sporulation (83). More specifically, a Δ*refZ* mutant more frequently captures regions of both the left and right arms that are generally excluded from the forespore (83). RefZ's highly conserved binding sites are also required for proper arm capture and RefZ interacts with the DNA pump SpoIIIE by bacterial two-hybrid (83). These results hint that RefZ may influence chromosome capture by influencing the position of the *RBM*s relative to the DNA pump that assembles around the chromosomal arms during septation.

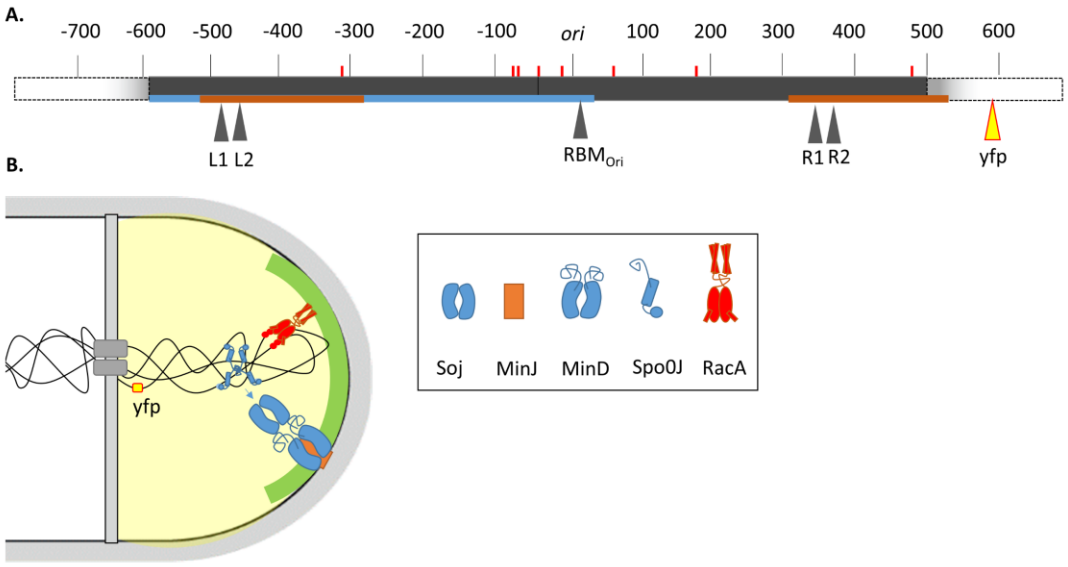

Figure 1.5 The *oriC*-proximal region of the *Bacillus* chromosome captured in the prespore. (A) The dark gray line is the region of the chromosome captured in WT cells. Red vertical lines are RacA binding sites. The blue horizontal line represents the region Spo0J organizes. Brown horizontal lines correspond to the regions found to be retained in the forespore even when *ori* was captured out (17). The grey carets denote positions of the RefZ Binding motifs (*RBM*s). The yellow caret is yfp under sigmaF control at position +51. **(B)** Tethering of the axial filament by RacA-*ram* and Spo0J-*parS*-Soj. RacA binds to *ram* sites and condenses the chromosome. The coiled coil domain of RacA interacts with DivIVA (green). Only one RacA-*ram* complex is shown for simplicity. Spo0J binds the *parS* sites and through oligomerization organizes the chromosome. Spo0J-*parS* interacts with Soj which jumps back and forth between the nucleoid and pole. MinD interacts with MinJ, which is targeted to the pole through DivIVA. The *yfp* reporter is shown captured in the forespore resulting in forespore luminescence.

Bacterial cell division

There is a close relationship between chromosome organization and cell division. FtsZ is a key, highly conserved protein required for bacterial cell division. FtsZ has a similar protein fold to eukaryotic tubulin, but only possesses ~10% amino acid sequence homology (84). In 1991 FtsZ was discovered to coalesce at the midcell of *E.coli* to form the so-called "Z-ring." FtsZ remained at the leading edge of the invaginating cell envelope at midcell and decreased in size as the cell was separated into two daughter cells (85). This discovery led to the hypothesis that, similar to eukaryotes, some bacterial proteins might function as structural scaffolds to facilitate cell morphogenesis (86). Decades of work have revealed that the cell division machinery is exceedingly complex consisting of over 10 essential proteins in *E. coli* (FtsA, B, I, K, L, N, Q, W, Z and ZipA) (87). Loss of any of these proteins results in cell filamentation and eventual death(87).

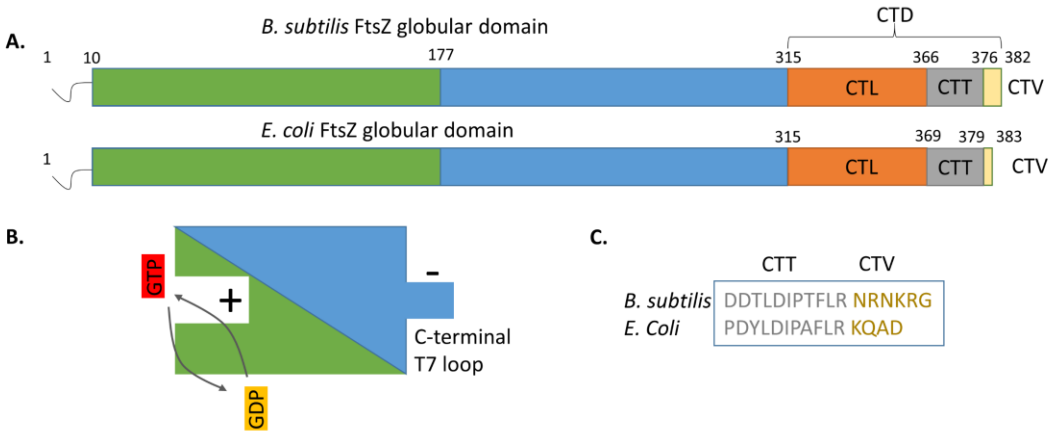

Figure 1.6. Domain structure of *B. subtilis* and *E. coli* FtsZ. (A) *B. subtilis* and *E. coli* FtsZ's have five domains: an unstructured N-terminal region (residues 1-10); N-terminal globular domain which contains the Rossman fold for GTP binding (residues 11-177); C-terminal globular domain which includes the T7 loop that inserts into the + end of another FtsZ monomer to create a functional GTPase active site (residues 178-315); CTL (unstructured) (residues 316-366); CTT (13 highly conserved residues); CTV (not conserved, with four residues for *E. coli* and six residues for *B. subtilis*). **(B)** GTP and GDP are exchanged at the + end of the subunit while the T7 loop is at the – end. **(C)** Amino acid sequence for the CTT and CTV of *B. subtilis* and *E. coli* FtsZ.

The current model for FtsZ function

FtsZ, like tubulin, is a polymerizing GTPase. Fluorescent microscopy experiments suggest the FtsZ polymerization initiates from one or two locations at midcell, after which bidirectional spreading leads to a circumferential Z-ring (84). The Z-ring is a helix, but because the helix pitch is short it appears as a ring (88, 89). The current model for Z-ring assembly (based primarily on research performed with *E. coli*) is that monomeric FtsZ assembles head-to-tail, short (120-200 nm), single-stranded polymers that then associate through lateral interactions (86). FtsZ assembly and subunit exchange are activated by GTP.

In 1998 the first FtsZ structure was solved, a GDP- bound form from *Methanococcus jannaschii*, revealing FtsZ was composed of at least two domains connected by a central helix (90). Today, based on extensive structural, biochemical, and genetic analysis, FtsZ is considered to possess five domains: 1) an unstructured N-terminus (not conserved) 2) a globular core (conserved), a C-terminal linker (not conserved), a C-terminal tail (conserved), and a C-terminal variable region (not conserved) (Fig. 1.6A) (91). FtsZ binds GTP uniquely compared to canonical P-loop nucleotide binding proteins and G-proteins (84, 88). The N-terminal globular region of FtsZ is a Rossman fold, which contains tubulin's signature nucleotide binding motif GGGTGTG (88). There are four loops T1, T2, T3, T4 (tubulin loops), which make contact with the phosphate backbone of the GTP (90). T1 is similar to a P-loop,consisting of a strand-helix-loop (90). T4 contains the nucleotide binding motif (90). The nucleotide binding pocket of FtsZ is denoted as the + end of the FtsZ subunit (Fig. 1.6B) (88). The insertion of the synergy (T7) loop (NxDFxD) from the opposite (-) end of another FtsZ

subunit into the + end of the FtsZ subunit creates a functional GTPase active site by providing the key catalytic residues for hydrolysis (Fig. 1.6B) (88, 92). GTP hydrolysis, but not GTP binding is dependent on magnesium (90).

For *B. subtilis* and *E. coli*, the intracellular concentrations of FtsZ do not vary through the cell cycle but are around 2-6 uM and 10 uM, respectively (93, 94). Seventy percent of total FtsZ is cytoplasmic, and only 30% is involved in FtsZ ring formation (84). For *B. subtilis* there is enough FtsZ in the mature ring to encircle the cell approximately 2.5 times as a polymer (88). How the remaining cytoplasmic FtsZ remains diffuse is unclear, since the concentration is above the *in vitro* critical threshold for assembly (88). One possibility is that the membrane tethers are limiting and sequestered to the Z-ring, thus maintaining only polymerized FtsZ at the Z-ring (88). Another possibility is negative regulatory proteins prevent polymerization interaction with membrane tethers (88).

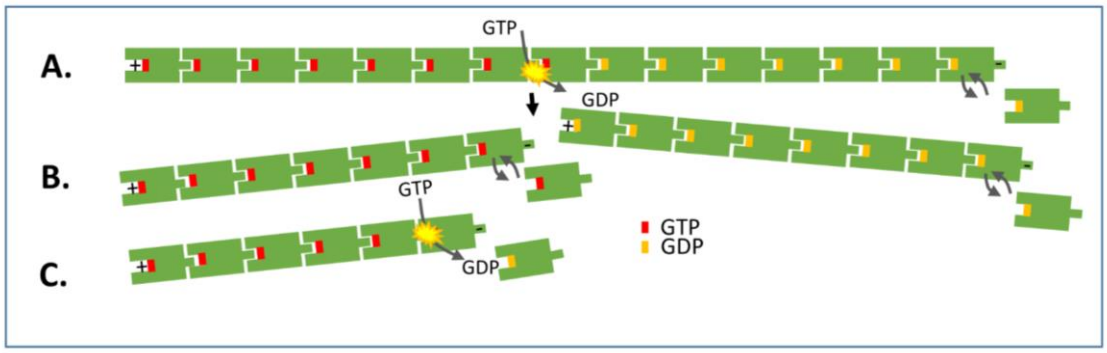

Figure 1.7. Mechanisms for FtsZ subunit exchange from the negative end of the FtsZ polymer. **(A)** An FtsZ polymer with a GTP biased distribution towards the positive end of the polymer. Shown also is the release of a GDP-bound monomer from the negative end of a polymer. At the middle of the filament GTP-hydrolysis mediated filament breakage is shown. GTP hydrolysis leading to filament breakage is a model, not a description of how the assembly/disassembly functions **(B)** Release of a GTP-bound monomer from the negative end of a polymer without hydrolysis **(C)** Release of a GTP-bound monomer from the negative end of a polymer with hydrolysis.

E. coli FtsZ assembly dynamics

FtsZ dynamics turns out to be complex and probably slightly different for each bacterial species. *E. coli* FtsZ dynamics are the most studied and therefore are focused on here. The standard short polymers of *E. coli* FtsZ observed *in vitro* are 120-200 nm (30-50 subunits) long and one subunit in width (88). Since this length is not sufficient to encircle the cell, the Z-ring must be comprised of staggered and laterally interacting polymers, a model that has been demonstrated experimentally (95, 96). It was recently shown that *in vivo* FtsZ polymers move dynamically by the addition of FtsZ monomers at the head of the filament and the dissociation of monomers from the tail of the polymer, which is proposed to drive the cell wall synthesis machinery (86, 97). This is called treadmilling and the rate of movement is 30 nm/sec (86, 98).

FtsZ subunit exchange can proceed by different mechanisms. I will adapt the previously described model for FtsZ subunit exchange (99) to be congruent with the recent discovery of FtsZ treadmilling (97, 98). Treadmilling of FtsZ implies growth of the polymer occurs from the positive end of the FtsZ polymer and disassembly occurs from the negative end of the polymer (97, 98).

In the absence of regulatory proteins, which could modulate GTPase activity, one anticipates a gradient of GTP in the FtsZ polymer since GTP-bound subunits are added to the positive end (Fig. 1.7A). FtsZ subunit exchange may proceed from the negative end of the polymer in the following ways: 1) The release of a GDP-bound monomer from the negative end of a polymer (Fig. 1.7A) 2) Release of a GTP-bound monomer from the negative end of a polymer without hydrolysis (Fig. 1.7B) 3) Release of a GTP-bound monomer from the negative end of a polymer with hydrolysis (Fig. 1.7C) (99).

The effects of GTP hydrolysis on FtsZ subunit exchange remain controversial and there are currently two models for how it occurs (99). In the first model (Fig. 1.7A), GTP hydrolysis within an assembled FtsZ polymer results in a weakening of the longitudinal bond to the next subunit that ultimately causes the polymer to break, although not necessarily immediately (99). Breakage of the filament creates a new negative end from which GTP-bound FtsZ monomers can dissociate. This new negative end would double the rate of subunit exchange without altering the rate of exchange for a given polymer. In the second model, GTP-hydrolysis affects subunit exchange only by increasing the rate at the ends of the polymer (99). In the latter model, the cooperative assembly of FtsZ maintains the assembled filament at the FtsZ-GDP interface of the polymer and therefore GTP-hydrolysis doesn't lead to a broken polymer (99). Subunit exchange at the end of FtsZ may also occur without GTP hydrolysis (Fig. 1.7B) (99).

Although not commonly emphasized, terminal subunit exchange without GTP hydrolysis is estimated to account for half of the total subunit exchange (99). This accounts for the observation that the nucleotide exchange rate for FtsZ is faster than the rate of GTP hydrolysis. Initially it was postulated that nucleotides within the FtsZ polymer could be exchanged; however, excess GDP in solution does not accelerate FtsZ disassembly (99). Instead the faster nucleotide exchange rate can be explained by the exchange of subunits from the negative end of FtsZ polymer in the absence of GTP hydrolysis (99).

E. coli FtsZ cooperativity

Assembly of *B. subtilis* and *E. coli* FtsZ is cooperative, but the mechanisms are likely distinct due to differences in bundling properties of the proteins (91). FtsZ has structural homology to tubulin, and therefore was anticipated to exhibit microtubule-like cooperativity (100). Microtubules (polymers associated into a tube via lateral interactions) have two phases of assembly. In the "nucleation" phase, association of α and β tubulin is slow because the subunit contacts are weak. The subsequent "growth" phase is fast because subunits can make lateral contacts as well as subunit to subunit contacts (100).

E. coli FtsZ has weaker lateral contacts than microtubules, and the rate of GTP turnover, ionic strength, macromolecular crowding, and *in vivo* bundling proteins all affect FtsZ lateral contacts. Under standard polymerization conditions *in vitro, E. coli* FtsZ forms stable, single-stranded polymers without lateral interactions (100). Only in the presence of crowding agents such as methyl cellulose or diethylaminoethyl (DEAE) dextran, or divalent cations Ca2+ or Mg2+ does *E.coli* FtsZ make lateral contacts to form sheets, bundles, helices, and pipes. The GTPase rate of *E.coli* FtsZ also affects the length of the polymer, which in turn affects FtsZ's propensity to bundle (short polymers have weaker lateral interactions than longer polymers).

In vivo, regulatory proteins like ZapA and ZipA promote lateral contacts between the FtsZ polymers. These results indicate that while tubulin can form lateral interactions spontaneously, *E. coli* FtsZ needs some assistance (100). Consistent with this conclusion, the lateral contacts, which confer cooperativity to tubulin, involve surfaces that are not conserved in *E. coli* FtsZ (100).

Some reports in the literature state that *E.coli* FtsZ assembly is not cooperative (100). Subsequent studies demonstrated that GTP-mediated FtsZ assembly in *E. coli* is cooperative but by longitudinal interactions rather than lateral (100, 101). Initially cooperativity was reported by the observation that a critical concentration of FtsZ was required for assembly and GTPase activity (94). Later, using an FtsZ mutant L68W with tryptophan fluorescence reporting on FtsZ assembly kinetics, a lag phase, a nucleation step (monomer to dimer), an elongation phase (dimer to trimer and beyond), and equilibrium were observed (102, 103). Therefore *E. coli* FtsZ assembly is cooperative; a trimer presents a slightly more favorable conformation for addition of a subunit than a dimer and a dimer more than a monomer (101). FtsZ cooperativity in *E. coli* requires that subunits have long distance communication with one another and the mechanism for how this occurs in a linear polymer is not straightforward (101).

Lateral interactions of B. subtilis FtsZ

Unlike *E. coli* FtsZ, *B. subtilis* FtsZ may assemble cooperatively in a manner more analogous to tubulin. *B. subtilis* FtsZ formed bundles of filament rings and sheets under conditions where *E. coli* FtsZ forms only polymers (91). Light scattering with *B. subtilis* FtsZ also produces a stronger signal in comparison to *E. coli* because the filaments are bundled and bulkier (91). Increased lateral interactions also slow GTP hydrolysis, therefore the difference in propensity to bundle is also observed in the GTPase rate for *E. coli* (5.4 GTP/FtsZ/min) and *B. subtilis* (2.25 GTP/FtsZ/min) (91). Note, the rate of GTP turnover for *B. subtilis* is half that observed for *E. coli (91)*. The region of FtsZ conferring its bundling properties is the extreme C-terminal variable region (CTV) (Fig. 1.4) (91).

This is based on the observation that swapping the positively charged CTV of *B. subtilis* FtsZ (NRNKRG) with the neutral *E. coli* (KQAD), is sufficient to swap their bundling behaviors (91). Therefore the *B. subtilis* CTV is both necessary and sufficient to confer strong lateral interactions which result in bundling and higher order structures reminiscent of microtubules (91). Electrostatic interactions are likely the primary determinant driving bundling (91), as substitutions in the CTV that swap charges perturb bundling, while those that conserve charge support bundling (91). Moreover, when the concentration of a salt that could disrupt ionic interactions (KCl) was increased, the light scattering signal dropped 40 fold, consistent with reduced bundling (91).

FtsZ ring constriction in *E.coli* persists for approximately 10 min, or half the cell cycle under the growth conditions examined (88). Constriction could happen as a result of subunit release from the constricting ring or because the fibers slide across each other and compact (84). In support of the subunit release model, the intensity of a fluorescently labeled Z-ring fades with constriction (88). FtsZ treadmilling continues as constriction occurs, suggesting that released FtsZ is somehow prevented from being reincorporated into the Z-ring.

FtsZ regulation

Intracellular FtsZ concentration does not regulate ring formation

Although a minimum concentration of FtsZ is required for polymerization in the cell, the concentration of FtsZ does not regulate Z-ring assembly in the cell (84). Hence increasing the amount of FtsZ in the cell does not result in more frequent midcell ring formation (84). However, increasing FtsZ levels does overcome inhibition at the cell

poles in both *B. subtilis* and *E. coli,* as there is an increased frequency of Z-rings at the poles when FtsZ is overexpressed intracellularly (84). Consistent with this, FtsZ concentration is upregulated during sporulation in *B. subtilis* as part of the mechanism to redistribute FtsZ toward the cell poles to allow for polar division (84).

The intrinsically disordered tail of FtsZ

As the key scaffolding protein for the cell division machinery, FtsZ acts like a Hub protein. Hub proteins often use intrinsically disordered peptides which can adopt a variety of ordered conformations to make contacts with many proteins to ensure effective control of a physiological process (104, 105). FtsZ's C-terminal domain (CTD) functions as an intrinsically disordered peptide (106). The CTD is comprised of the CTL, CTT, and CTV (Fig. 1.6A). For *M. jannaschii* FtsZ, the CTD is quite short, whereas in some bacteria it can be as long as 300 residues. For *E.coli* and *B. subtilis* the CTD is ~50 residues in length (Fig. 1.4) (84). Due to flexibility, the CTD is not resolved in most FtsZ structures (88). In different organisms the CTD possesses both structural and sequence disparity that likely reflect specialized functions and interaction partners. The disordered unconserved linker, which ranges widely in length across bacterial species (88), is after the globular domain of FtsZ. The sequence of FtsZ's CTL seems to be unimportant for the interactions studied so far. After the linker is a conserved CTT (C-terminal tail), an 11 amino acid sequence which mediates many important interactions to regulatory proteins (88). The interactions of several key FtsZ regulators with this region are explored in the next section. At the extreme C-terminus is the CTV (C-terminal variable region), which as discussed already, has been implicated in the lateral interactions of FtsZ.

Membrane tethers

The first steps in Z-ring assembly are recruitment and attachment of FtsZ to the membrane. In *E. coli*, the known protein players in membrane anchoring are FtsA and ZipA (107). FtsA, the best characterized anchor protein, is an actin homolog capable of dimerization and oligomerization. It contains a membrane targeting sequence (MTS) that is inserted into the inner membrane in a membrane-potential dependent manner (87, 108). FtsA oligomerizes allowing direct tethering of FtsZ to the cytoplasmic membrane, an important step in the early stages of divisome assembly in *E. coli* (107). As cytokinesis progresses, FtsA is released from its oligomerized state and has a secondary function in recruitment of late-stage divisome proteins (107). The point of contact between FtsZ and FtsA is the CTT (109). A single amino acid change, D373G, disrupts interaction between FtsZ and FtsA (109). The crystal structure of *Thermotoga maritima* FtsA in complex with the C-terminal tail of FtsZ (4A2A) reveals FtsA has an actin-like fold composed of four subdomains (1A, 1B, 2A, 2B) (110). The tail of FtsZ interacts with subdomain 2B, consistent with previous genetic work (110).

ZipA is another essential membrane protein from *E. coli* that stabilizes Z-rings in vivo and promotes FtsZ bundling i*n vitro* (87). It has an N-terminal transmembrane helix and essentiality can be bypassed by a gain-of-function mutation in FtsA (108). A co-crystal structure of *E. coli* ZipA with the tail of FtsZ shows the tail binding as a beta strand followed by a helix (111). Consistent with the structure, biochemical characterization showed the critical amino acids contacts on the FtsZ tail to be several hydrophobic residues in the CTT (I374, F377, and L378) (111). ZipA and FtsA have different patterns

of FtsZ recruitment to the membrane; FtsA can only recruit polymerized FtsZ while ZipA can recruit monomeric and polymerized FtsZ (112). If FtsZ is recruited to the membrane by ZipA, static bundles of FtsZ form, but if FtsZ is recruited by FtsA the filament is dynamic and rapid disassembly ensues after which monomeric FtsA can no longer be attached to the membrane (112).

For *B. subtilis* the membrane anchors are FtsA, EzrA, and SepF. In *B. subtilis*, FtsA is not essential, although a null mutant is filamentous (108, 113). FtsA has also not been extensively characterized in *B. subtilis*, though it has been shown to dimerize in an ATP-dependent fashion (113). EzrA has been likened to *E. coli* ZipA since both have an N-terminal transmembrane helix and make direct contact with FtsZ (108). EzrA is a membrane protein that interacts directly with FtsZ to prevent or promote Z-ring assembly at midcell and the cell poles (114, 115). EzrA has a secondary function of recruiting PBP1 (a transglycosylase) to the septum to insert new peptidoglycan during septation (114, 115). EzrA has a spectrin fold; in eukaryotes spectrins help to tether actin to other membrane bound proteins (114, 115). In a similar manner, EzrA may tether FtsZ (tubulin homolog) and FtsA (actin homolog) to the membrane-associated proteins involved in cell envelope synthesis (114, 115). The model for EzrA is analogous to a C-shape inserted into the cytoplasmic side of the membrane (Fig. 1.8) (114, 115). This arc could entrap FtsZ polymers preventing lateral interactions (Fig. 1.8A). Alternatively the EzrA arcs may wrap the leading edge of the invaginating septum and FtsZ may interact with the outside of the EzrA arc (Fig. 1.8A) (114, 115).

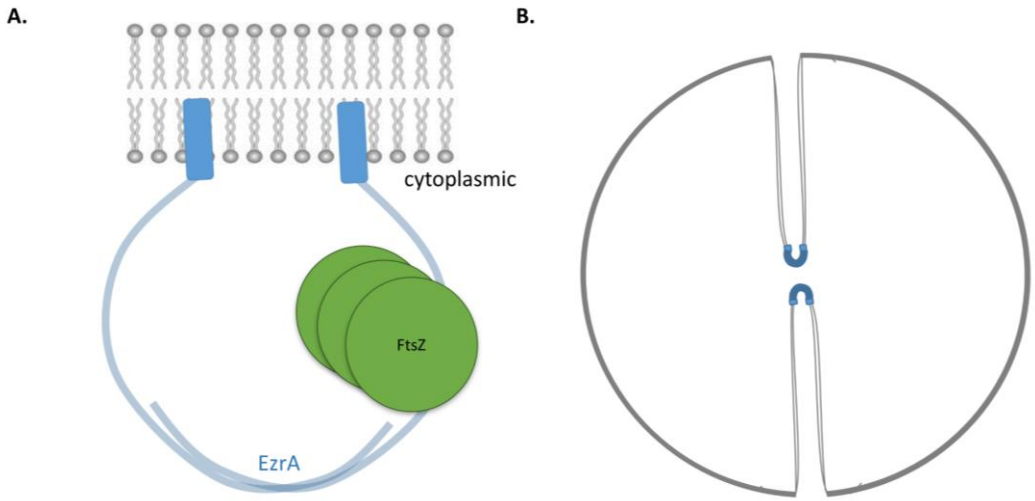

Figure 1.8. Models for EzrA and SepF activity (A) In one model for EzrA the transmembrane helix inserts into the cytoplasmic side of the membrane while the EzrA arcs dimerize to form a circle. FtsZ may interact with the inside or outside of the arc. If FtsZ is entrapped within the EzrA arc, then lateral association of FtsZ will be prevented. **(B)** Illustration of how SepF and possibly EzrA (depicted as blue caps) may associate with the leading edge of the invaginating membrane to position FtsZ filaments.

SepF has an N-terminal amphipathic helix and assembles into 50 nm rings *in vitro* (116). When mixed with FtsZ polymers, SepF bundles the FtsZ polymers into microtubule-like tubes (116). Conserved across Gram-positive bacteria, the current model for SepF function is that arcs wrap around the leading edge of the invaginating septum (Fig. 1.8B), promoting association and alignment of FtsZ polymers in parallel (108).

Positional Regulation of Z-rings

Across bacterial species the physical position of FtsZ may differ but the division site selection remains very precise. In *E.coli* and *B. subtilis* the divisome is placed within 2% of the absolute middle at the population level (86). Both positive and negative regulation for FtsZ positioning is likely required to achieve this precision (86). Even after decades of work, the precise positioning mechanisms remain vague. Selection of the division site is partially dependent on DNA replication initiation. Replication initiation is required for proper placement but not assembly of the FtsZ ring in both *B. subtilis* and *E. coli* (84). The most well characterized systems for positioning the Z-ring are Min and NO. In *E.coli* Min- cells have an equal distribution of FtsZ rings between midcell and the poles (86). The NO system is dispensable in *E. coli*, except in the absence of Min and thus seems to be primarily a failsafe; however, NO may have a more subtle role in chromosome organization which we do not currently appreciate (86). In *B. subtilis,* Z-rings can still form at absolute midcell when the Min system is completely inactivated (117). Moreover, under certain growth conditions, both *E. coli* and *B. subtilis* can continue to divide with a midcell bias even without Min and NO (117, 118), indicating

other uncharacterized systems for Z-ring positioning exist (119). Recently, an example of a positive regulation system was identified in *E. coli (118, 119)*.

The MinCDE system of E. coli

In *E. coli*, the Min system is composed of three proteins MinC, MinD, and a topological determinant MinE (Fig. 1.9) (120). MinC and MinD associate to form a polar zone of inhibition at the membrane which is chased by the oscillator ring composed of MinE (Fig. 1.9) (120). MinC directly antagonizes the FtsZ filament and is positioned through interaction with membrane bound MinD (Fig. 1.9). MinD binds ATP, which stimulates dimerization creating the interaction interface for MinC and MinE. Dimerization also increases MinD's affinity for the membrane (48). As the MinE ring moves toward the pole MinC and MinD are displaced from the membrane (Fig. 1.9). MinE undergoes a complete conformational change to interact with MinD, which causes an increase in MinD's ATPase activity resulting both MinD and MinC being released from the membrane. MinE can then be released from the membrane or it can hop to another subunit of MinD (48). The hopping of MinE when a high concentration of an MinD is present on the membrane is thought to cause the oscillation of MinD which results in the time-averaged gradient of MinC inhibitor. This excludes FtsZ polymerization except at midcell (Fig. 1.9) (120).

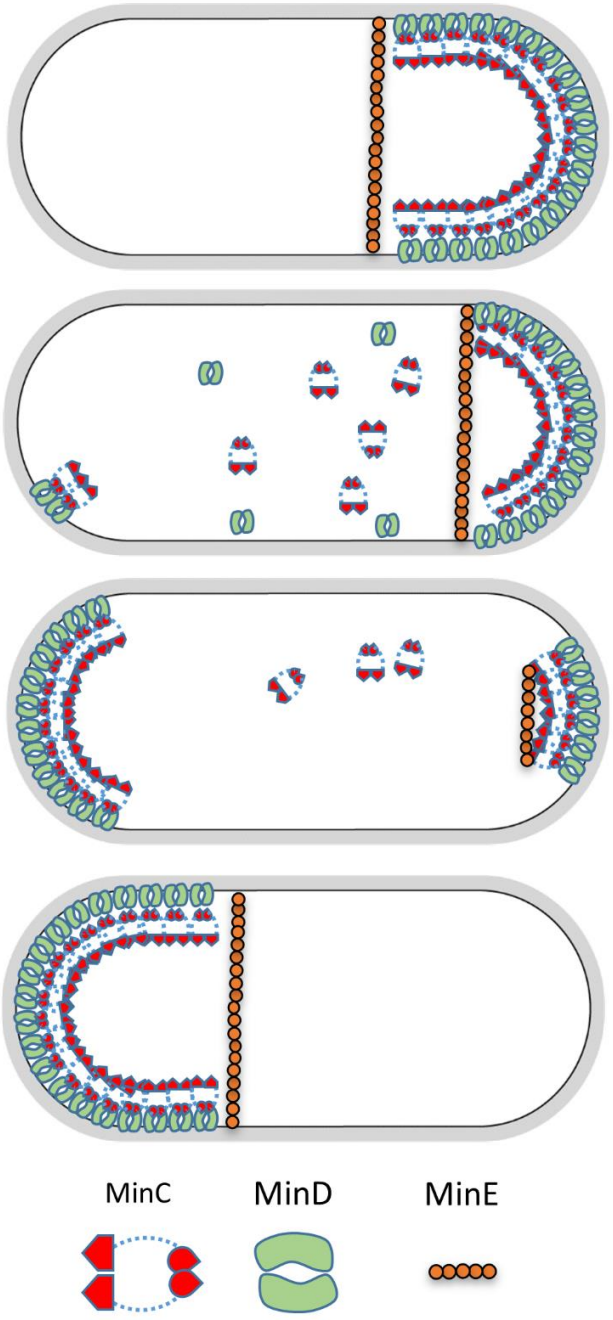

Figure 1.9 MinCDE system in *E.coli.* The Min system is composed of two proteins MinCD and a topological determinant. In *E.coli* the topological determinant is MinE. The MinE ring (orange) oscillates across the cell depolymerizing MinCD which then moves to the other side of the cell. The result is a gradient of MinCD in the cell which has the highest concentration at the cell poles and lowest concentration at midcell. This arrangement makes FtsZ polymerization at midcell more likely.

MinCDJ and DivIVA in B. subtilis

B. subtilis lacks MinE and instead the topological determinant is MinJ. MinJ is localized by interaction with DivIVA, a protein that senses and localizes to regions of specific negative membrane curvature such as the curved cell pole (121). During vegetative growth (recall DivIVA is important for chromosome tethering to the pole at sporulation) DivIVA localizes to midcell and forms a ring on both sides of the cell division plane at the onset of cytokinesis (121). There DivIVA recruits MinJ, which recruits MinD, and in turn, MinC (121). MinC is thought to prevent FtsZ released from the constricting Z-ring from reassembling to form another ring adjacent to the already established site of cell division (121). This ensures division happens only once preventing FtsZ assembly on either side of the midcell divisome, an event that could result in the production of annucleate minicells. DivIVA rings collapse into a patch at the poles after cells have completely separated (121). Membrane association of *B. subtilis* MinD is independent of ATP binding. Instead ATP-binding of MinD causes interaction with partner proteins MinJ and MinC (48).

Mechanism for MinC's antagonism of FtsZ

There are two structures of MinC: *Salmonella typhimurium* (3GHF) (122) and *Thermotoga maritima* (1HF2) (123) which reveal a two domain protein connected by a flexible linker (124). Extensive mutational analysis of MinC and FtsZ in *E. coli* has identified that MinC targets FtsZ with a two-pronged approach. First the CTD of FtsZ makes contact with the MinC C-terminal domain, and then the globular domain of FtsZ (Helix 10) makes contact with the N-terminal domain of MinC (125, 126). The

mechanism is the same for *Bacillus* (124). MinC's C-terminal domain is conserved across Gram-positive and Gram-negative bacteria, but the N-terminal domain is not (127). When FtsZ polymerizes, the CTD is converted into a multivalent ligand (128). MinC has a higher affinity for the multivalent CTD and is therefore targeted to FtsZ polymers not FtsZ monomers (128). This is a mechanism for targeting a spatial regulator only to Z-rings as opposed to cytoplasmic FtsZ (128). Such targeting is presumably how low copy regulators, like MinC, avoid being saturated by FtsZ monomers (128). MinC's globular contact to FtsZ is proposed to weaken or break the FtsZ filament. This contact is likely to be driven by electrostatic interactions since the patch of residues identified on FtsZ's globular surface is highly negatively charged and the interaction is pH sensitive and inhibited by salt (129).

Nucleoid Occlusion (NO) in E. coli

The nucleoid has an important role in FtsZ positioning. Intrinsic properties of the nucleoid such as negative charge and bulkiness may inhibit FtsZ polymerization (104, 130). Specific protein systems that interact with the nucleoid to prevent FtsZ assembly and are synthetically lethal with inactivation of the Min system are collectively called nucleoid occlusion systems (Fig. 1.10) (NO).

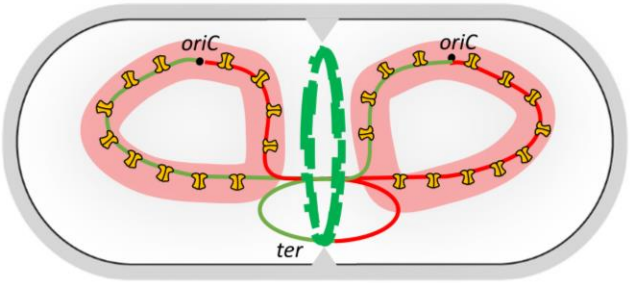

Figure 1.10. Nucleoid Occlusion in *E. coli.* SlmA (yellow homodimer) binds to SBS sites scattered across the chromosome except near the *ter* macrodomain. Absence of SlmA in the *ter* macrodomain relieves NO mediated inhibition of FtsZ allowing for midcell division since the *ter* is the last region to segregate.

In *E.coli* the NO system consists of a DNA-binding protein SlmA that binds to specific DNA motifs (SBSs), scattered across the chromosome except near the *ter* region (Fig. 1.10). SlmA prevents division from occurring over the nucleoid via a direct interaction with FtsZ (104, 131). SlmA was identified in a genetic screen for proteins that are Synthetic Lethal with Min (slm) (131). Like RefZ, SlmA is a member of the TetR protein family and has two domains (132). The N-terminal domain of SlmA contains helices, of which α1, α2, and α3 form the HTH DNA-binding motif (132). ChIP-seq identified 52 *in vivo* sites of enrichment for SlmA and SlmA's 12 bp concensus DNA motif, GTGAGTACTCAC, was identified (132). The positions of the SBS sites are genome-wide except for a noticeable absence of sites from the *ter* and right macrodomain (Fig. 1.10) (132). Interestingly the SBS sites were also found to be enriched in regions thought to be close to the cell membrane (133). The *ter* is the last region of the chromosome to be replicated during cell division and is present at midcell at that time

(132). Absence of SlmA-SBS complexes in the *ter* region makes division permissive, and any nucleoid trapped under the division machinery can be removed by FtsK (Fig. 1.10).

The C-terminal domain of SlmA is composed of helices α4-α9 and contains the dimerization interface and a hydrophobic cleft where SlmA binds its ligand: the C-terminal tail of FtsZ (132). The SlmA-SBS structure revealed SlmA binds the SBS as a pair of dimers (133). Consistent with this finding, isothermal titration calorimetry (ITC) showed a 4:1 (SlmA-SBS) ratio for a 12 bp SBS, and an electrophoretic gel mobility shift analysis with a fragment containing one SBS displayed two mobility shifts (133). SlmA binds to DNA differently than other TetR proteins, in that it significantly distorts the DNA (133). The dimer is probably anchored by this distortion and the distortion is hypothesized to be responsible for cooperative binding of the second dimer (133). ITC revealed additional spreading of SlmA on adjacent DNA after binding of the dimer pair (133). Importantly this interaction does not occur without an SBS, suggesting it is not non-specific association with the DNA *(133).* Therefore it has been hypothesized that SlmA binds as a dimer of dimers and changes in the DNA conformation allow binding of two additional SlmA dimers (133). No more than eight monomers of SlmA have been observed at a single SBS site (133).

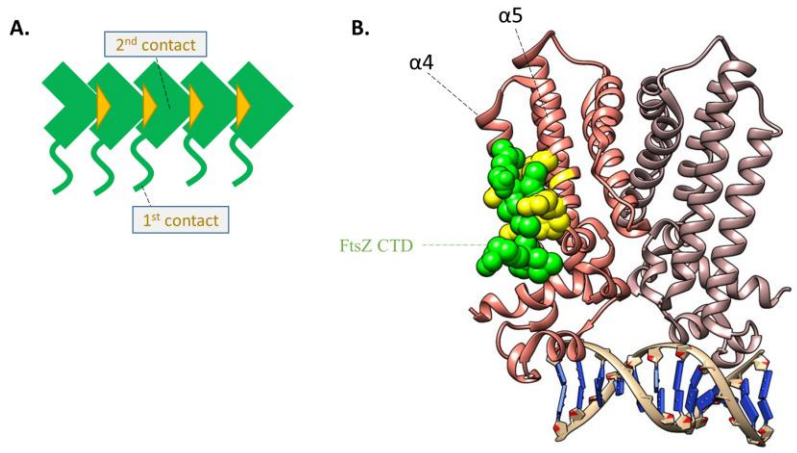

Figure 1.11 SlmA's mechanism of FtsZ antagonism is 2-pronged (A) SlmA makes two contacts to the FtsZ filaments similar to MinC. The first contact is to the CTD of FtsZ shown as a green line. The second contact is to the globular domain of FtsZ. **(B)** The FtsZ CTD (green spherical model) binds to a narrow hydrophobic grove between α4 and α5. Residues identified as important for this interaction on SlmA are shown as yellow spheres.

Similar to MinC, SlmA's mechanism of FtsZ antagonism also requires two contacts: the first is to FtsZ's CTD, and the second is to FtsZ's C-terminal globular domain (Fig. 1.11A) (134). The first contact between SlmA and FtsZ's CTD targets SlmA to membrane bound FtsZ polymers (134). Recall when FtsZ polymerizes the CTD is converted into a multivalent ligand. Membrane anchors FtsA and ZipA associate with this multivalent CTD tethering FtsZ to the membrane (104). It has been proposed that SlmA competitively displaces the FtsZ CTD from interaction with these membrane anchors(134). Because SlmA must first contact the multivalent CTD of FtsZ this provides a mechanism for SlmA to target FtsZ polymers not monomers(104). This is important because the copy number of FtsZ, FtsA, and ZipA in the cell far exceed the copy number of SlmA meaning its mechanism of antagonism must be substoichiometric (104). SlmA

makes contact with the CTD of FtsZ near the region where other TetR protein family members bind to ligands. In the C-terminal regulatory domain, SlmA does not have a large cavity or an accessible entrance to the small potential pocket (132), instead SlmA has a narrow hydrophobic groove between α4 and α5 that becomes more exposed upon DNA binding to which the FtsZ CTD inserts into (104). The FtsZ CTD does not adopt a helix conformation when contacting SlmA like it does when contacting FtsA or ZipA. Instead it binds in an extended conformation along nearly the entire length of the subunit. When SlmA is not bound to the SBS it is thought to adopt multiple structural conformations only some of which expose the hydrophobic cleft (104). The DNA bound state of SlmA locks the protein in a conformation which optimally exposes the hydrophobic cleft where the CTD of FtsZ binds (104).

The second contact SlmA makes to the FtsZ globular domain is a shared interaction interface with the regulator MinC and likely results in breakage of the displaced FtsZ filament (132, 135),(134). The exact mechanism by which SlmA promotes FtsZ disassembly is unclear (104). SlmA has a slight effect on FtsZ's GTPase activity. One group reported the SlmA-SBS complex increased FtsZ's GTPase activity by 36% (119, 135) while another group reported only a 10% increase (133). The exact role of binding to DNA in SlmA's antagonism of FtsZ is also not known. SlmA's interaction with the SBS likely localizes it in the cell and concentrates its antagonism, but binding to the SBS also increases SlmA's affinity for FtsZ, and SlmA inhibits FtsZ polymerization approximately 100 times more in the presence of an SBS. However, overexpression of SlmA lacking the helix-turn-helix motif required for DNA binding can also inhibit cell division, suggesting that DNA binding is not formally required (119, 135).

Nucleoid Occlusion (NO) in B. subtilis

The main player for the NO system in *B. subtilis* is Noc, a ParB (Spo0J) homolog that associates with the membrane in a DNA-dependent manner (130, 136). There are around 4500-7500 molecules of Noc per cell and 74 binding motifs (NBS) have been identified, scattered across the chromosome except near the *ter* (130, 136). The NBS site is a 14 bp inverted repeat with the consensus ATTTCCCGGGAAAT (130, 136). The mobility shift for Noc used a 24 bp probe and thus the propensity for spreading could not be observed in this assay (130, 136). Inactivation of Noc is also synthetic lethal with inactivation of the Min system, similar to what was observed for *E.coli'*s SlmA (130, 136). Noc overexpression prevents asymmetric division during sporulation, an event which requires assembly of FtsZ over the nucleoid (130, 136).

To date no cell division proteins have been found to interact directly with Noc, suggesting that NO in *B. subtilis* operates by a distinct mechanism from SlmA (130, 136). Consistent with this idea, Noc belongs to the parB/MinD class of proteins, structurally different from the TetR-like family (130, 136). Since Noc is associated with the membrane, one plausible mechanism for its action against FtsZ is that it disrupts the association of FtsZ with membrane anchors, SepF and FtsA (130, 136). However, this mechanism would have to involve non-specific interactions, as the N-terminal membrane targeting signal can be replaced with other membrane targeting signals without perturbing Noc function (130, 136). Another possibility is that the Noc-SBS nucleoprotein complexes at the membrane physically crowd and prevent assembly of membrane

anchored FtsZ (130, 136) as the nucleoid itself tethered to the membrane has been proposed to act as a physical barrier to assembly of FtsZ (130, 136).

Asymmetric cell division during *B. subtilis* sporulation

The asymmetric division during *B. subtilis* sporulation requires a switch in the positioning of FtsZ from midcell to the pole. The integral membrane protein SpoIIE is important for facilitating this switch and is observed first at midcell before the FtsZ and SpoIIE redistribute via an extending spiral towards both poles (18). After FtsZ is redistributed to the cell quarters, which are the two potential sites for the septation of sporulation, one of the Z-rings will develop into a septum and the other will dissolve (18). In the absence of SpoIIE, there is a delay in shifting of the FtsZ ring to the pole (18). SpoIIE's other role in sporulation is that of initiating the forespore specific transcription program which was previously discussed.

Regulator of FtsZ (RefZ)

RefZ, the topic of this dissertation, is also important for repositioning FtsZ to the cell poles. RefZ is a TetR-like DNA-binding protein, conserved by gene synteny in the *Bacillus* genus of polar spore formers with the gene encoding the FtsZ regulator *ezrA (82).* In a Δ*refZ* mutant, the formation of a polar Z-ring is slightly delayed. This is similar to the phenotype observed for *spoIIE,* though less severe (82). However, RefZ appears to act through a different pathway than SpoIIE, as a Δ*refZ* Δ*spoIIE* mutant, is more severely delayed in polar Z-ring formation than either single mutant (82). RefZ localizes initially to the site of asymmetric septation before or during redeployment of FtsZ from midcell. This localization depends upon the ability of RefZ to bind to DNA via its helix-turn-helix

(82). There are five RefZ binding motifs (*RBM*) on each *Bacillus* chromosome. Two *RBMs* (RBM_{L1} and RBM_{L2}) are at -484 kb and -446 kb near the left boundary for chromosome capture (Fig. 1.5A). One *RBM* (RBM_{ori}) is at 3 kb. The other two *RBMs* (RBM_{R1} and RBM_{R2}) are at +342 kb and +367 kb near the right boundary for chromosome capture (82). The orientation of the axial filament would likely position RBM_{L1} RBM_{L2} RBM_{R1} and RBM_{R2} near the asymmetric septum suggesting *RefZ-RBM* interactions might be responsible for the observed localization to the asymmetric septum.

An attractive model would be that RefZ binds the *RBMs* to accomplish timely repositioning of FtsZ and precise chromosome capture. RefZ may self associate bridging the left chromosome arm to the right chromosome arm to organize the chromosome for pumping into the forespore. RefZ may bind to the *RBMs* as a dimer of dimers similar to the NO occlusion regulator of FtsZ SlmA. The interaction between RefZ and FtsZ may be direct such as is the case for SlmA. In support of this model, when overexpressed during vegetative growth RefZ prevents stable Z-ring assembly at midcell (82). RefZ missexpression is lethal in the absence of MinD and can be used to isolate suppressors to identify potential protein interaction partners (82). All suppressing mutations were in FtsZ and mapped primarily to the MinC-FtsZ interaction surface near α10. Overexpressing FtsZ overcame RefZ missexpression (82). Therefore RefZ may promote stable Z-ring assembly by initiating Z-ring formation at the poles or by inhibiting midcell FtsZ assembly (82). In Chapters II and III of this dissertation the testing of these hypotheses is described and the outcome reported.

Tetracycline repressor protein family

History of the TetR protein family

As RefZ is a member of the TetR protein family, a brief review will be given of the TetR family's structure, ligands, and function. As transcription factors that regulate gene expression, the TetR family of regulatory proteins are key players in the modulation of bacterial physiology (137, 138). Bacteria colonize nearly every environmental niche on planet earth. Growth in such a vast array of environments requires a quick adaptive response to unstable pH, temperature, osmotic pressure, and nutrient availability. The first member of the TetR family to be characterized and the protein for which the family gets its name is TetR (137, 138). TetR is the transcriptional repressor of an operon in Gram-negative bacteria encoding an antibiotic exporter that confers resistance to tetracyclines. TetR's ability to bind DNA is regulated allosterically by tetracycline. Upon binding tetracycline, TetR undergoes a conformational change that releases it from its operator site, leading to increased transcription of tetA the gene encoding the efflux pump for tetracycline (139).

2,353 TetR family members have been identified, and of those ~240 have been characterized to some extent (137, 138). Most TetR family proteins with experimentally determined functions act as transcriptional regulators; however, others (SlmA and RefZ) appear to have specialized roles in positionally regulating FtsZ through interactions with motifs located at sites around the nucleoid (83, 140).

Structure of the TetR protein family

More than 100 X-ray crystal structures exist for distinct members of the TetR family (141). The structure of TetR like proteins is a homodimer with a conserved Helix-Turn-Helix (HTH) DNA-binding motif. The homodimer is composed of two nearly identical monomers each of which has ten alpha helices (α1-α10) connected by loops and turns. The HTH domain is created by α1, α2, and α3, which mediate contact with DNA. Structures for TetR proteins in complex with the DNA have been solved for at least seven proteins (138). Comparison of the structures demonstrates that TetRs do not have a conserved mode for DNA recognition and binding (138). While all utilize the HTH, DNA contact can be mediated by contact with either the DNA phosphate backbone or interactions with DNA bases (138). Moreover, the number of dimer units that associate with a single operator is variable. For example, TetR binds to a 15 bp operator as a single dimer (142) whereas other members of the family (eg. QacR and SlmA) bind to a longer operator (20+ bp) as two dimers (Fig. 1.12). The regulatory region of the TetR protein family helices (α5-α10) is connected to the HTH domain by α4. In addition to linking the regulatory and HTH domain, α4 is responsible for transmitting structural changes induced by ligand binding from the regulatory region to the HTH. The dimer contacts are mostly found on α6, α8 and α9 (137, 138). There is no conservation of primary amino acid sequence across this protein family aside from the HTH domain.

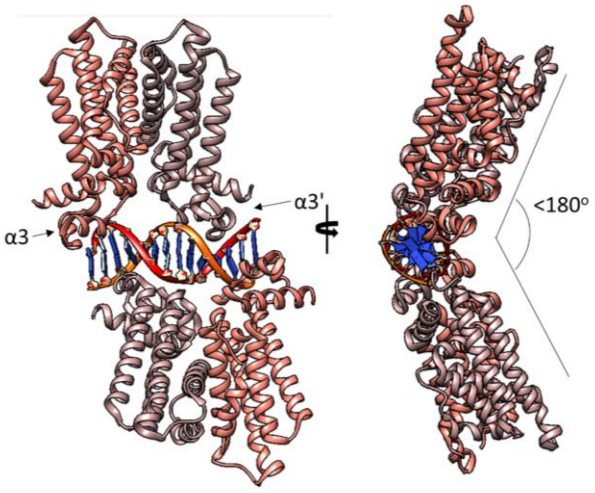

Figure 1.12 Structure of SlmA-SBS (4GCL). SlmA binds as a dimer of dimers to the SBS. Each homodimer straddles a minor groove placing a3 and a3' into successive major grooves. (Right panel) The proteins orient as a wide V when viewed looking down the DNA axis.

Helix-Turn-Helix motif

The HTH motif is used through all domains of life (eukaryotes, prokaryotes, and archaea) for specific recognition of DNA sequences (143). The HTH is a tri-helical motif with three major classifications: tetra-helical bundle, the winged-helix and the ribbon-helix–helix type (143). For the simple HTH, the first two alpha helices cross at 120°. The third helix is called the recognition helix and fits into the major groove. Functionally, the HTH fold has roles in transcriptional repression and activation, DNA repair, chromosome organization, and protein-protein interactions (143). There is no simple code for relating DNA sequence recognition to a protein's HTH motif as DNA structure encodes further complexity (144). Three-dimensional recognition motifs such as the HTH recognize properties of the DNA bases (ATGC) as well as the 3D shape of DNA (144).

How do DNA-binding proteins find their specific target site in the vast genomic sea, and how do they accomplish it so quickly? Protein-DNA interactions are highly

specific and occur 100X faster than the diffusion limit and 1000X faster than the rate of protein-protein interactions (145). The thermodynamic challenge is recognition of a specific DNA sequence and binding to it (145). The kinetic challenge is the time required to find the specific site (145). One model is facilitated diffusion which is the constraint of the 3D search space to 1D by nonspecific interactions with DNA that permit diffusional sliding along the DNA until the target is found (145).

C-terminal regulatory domains of TetR family proteins

The C-terminal regulatory region of the TetR family is important for dimerization and ligand binding, both of which may modulate the specificity and affinity of DNA-binding. All TetR proteins characterized thus far bind to DNA as dimers; binding as a monomer or an odd multiple to DNA has not been observed. However, the state of many TetR proteins in solution is disputed, and may vary by protein. TetR family proteins have been observed as both monomeric and dimeric species by by gel filtration, native gels, analytical centrifugation, and chemical crosslinking.

In order for dimer formation to be favorable in solution, the free energy for dimer formation must overcome the loss of translational and rotational degrees of freedom of the monomer in solution (146). Unless the amount of surface area buried upon dimer formation results in a free energy change that exceeds the losses of two monomers in solution, the protein will remain monomeric. This explains why a number of TetR protein family members are monomeric in solution. The intriguing question then becomes, why are these TetR proteins only observed as dimer multiples on DNA? This paradox can be resolved if the free energy required for binding a highly cooperative DNA site is much

less than the free energy of dimer formation (146). In this case, the protein would exist only as a monomer in solution, binding of an independent monomer to the binding motif would never be observed, and the protein would always bind as a dimer (or multiple dimers) on the DNA (146).

TetR DNA interaction is allosterically regulated by binding of a wide variety of ligands in the C-terminal regulatory region: fatty acids, metal cofactors, bile acids, antibiotics, toxic compounds, sugars, and nucleotides. The diversity of ligands is reflective of the broad range of TetR function (138). Several of the proteins can even bind different ligands in the same pocket (138). Helices α5, α6, and α7 form a triangular pocket for ligand binding while α4 acts like a lid for this pocket. The ligands enter the pocket via the side, top or front of the domain (138). Symmetric (ligand binding in both monomers) or asymmetric (ligand binding in one monomer) binding may cause a conformational change resulting in the distance between α3 and α3' of the HTH distance being incompatible with straddling the major groove (141). For TetR and QacR, a structural change in α6 causes a pendulum motion from α4 which widens the DNA-binding domain gap to be incompatible with the width of the major groove (138). Alternatively ligand binding may not trigger a conformational change but instead rigidify the protein, preventing the flexibility required for accessing the DNA binding conformation (141). Interestingly, the TetR family exhibits extensive variability in the apo structures for the distance between helix 3-3' (33.3 to 63.4 A) (141). This is likely just a crystallization artifact, which reflects flexibility of helix 3-3' while searching for the DNA-binding conformation (141).

CHAPTER II: A DNA-BINDING PROTEIN DEFINES THE PRECISE REGION OF CHROMOSOME CAPTURE DURING *Bacillus* SPORULATION [1]

Introduction

A major goal of bacterial cell biology is to identify and characterize the primary determinants underlying the cell's 3D organization and to understand how spatial organization is exploited to regulate physiology. Although not generally thought of as a primary platform from which bacteria organize cellular activities, the nucleoid is well positioned to serve a significant role as a topological marker because it is highly organized and occupies an expansive central space in the cytoplasm (147).

The importance of the nucleoid in cellular organization is best understood in the context of division site selection. The signals for divisome assembly are tightly coupled with nucleoid positioning, thus ensuring that each daughter cell inherits at least one copy of the chromosome. In fast-growing *Bacillus subtilis* and *Escherichia coli*, the bulk nucleoid is localized in the middle two-quarters of the cell, with the least amount of DNA present at the cell poles; at the end of replication, there is also less DNA present between replicated chromosomes at midcell. The nucleoid occlusion proteins of *E. coli* (SlmA) and *B. subtilis* (Noc) are DNA-binding proteins that inhibit FtsZ polymerization (131, 148) when bound to DNA motifs enriched around the nucleoid except near the midcell-localized chromosomal terminus regions (132, 135, 136).

[*] Adapted with permission from "A DNA-binding protein defines the precise region of chromosome capture during *Bacillus* sporulation" by Miller A.K., Brown E.E., Mercado B.T., and Herman J.K., et al, 2016. Molecular Microbiology, 99(1):111-22. Copyright 2016 by John Wiley & Sons, Inc.

In addition to growing by binary fission, *B. subtilis* is also capable of developing into a resting cell type called a spore. During early stages of sporulation, *B. subtilis* harbors two chromosome copies, stretched across the cell in an *oriC-ter-ter-oriC* arrangement called the axial filament (1, 149). The *oriC*-proximal regions are anchored to the cell poles through interactions between the conserved morphogenic protein DivIVA and the DNA-binding protein RacA (150). Shortly thereafter, an asymmetric septation creates two disproportionately sized cell compartments. The smaller compartment, or forespore, eventually becomes the mature spore while the larger "mother" cell nurtures the forespore during development.

To create the two compartments, FtsZ redistributes from midcell toward one or both poles through a spiral-like intermediate (74). Polar coalescence of FtsZ during sporulation is driven in part by increasing levels of FtsZ, expressed from a developmental promoter called P2 (151, 152), as well as synthesis of SpoIIE, a bifunctional protein shown to interact with FtsZ (153). RefZ (Regulator of FtsZ), a DNA-binding protein upregulated early in sporulation, was also shown to promote the timely redistribution of FtsZ toward the cell pole (82). Artificial expression of RefZ during exponential growth inhibits cell division by disrupting Z-rings, a phenotype that can be suppressed by mutant variants of FtsZ or by FtsZ overexpression (82). The mechanism by which RefZ influences FtsZ dynamics is not currently understood.

In contrast to vegetative growth, during which nucleoid occlusion inhibits FtsZ assembly over the nucleoid, the polar division of sporulation occurs directly over one chromosome, initially capturing approximately 25% of the *oriC*-proximal region in the forespore compartment (16, 69). This transient genetic asymmetry promotes differential

transcriptional programs in the forespore and mother cell that are required for spore development (154). Assembly of the FtsK-like DNA pump, SpoIIIE, prevents the chromosome from being guillotined by the polar division septum (24). Following assembly, SpoIIIE translocates the remainder of the chromosome into the forespore compartment (155).

Several proteins have been implicated in *oriC* capture in the forespore (17, 69, 72, 150). However, it is less clear how the cell manages to reproducibly define the boundary where cell division takes place around the forespore-destined chromosome (16, 69). In this work we show that spatially conserved DNA motifs (*RBM*s) help define the precise location of cell division with respect to the chromosome during sporulation. More specifically, our data support a model in which the FtsZ-regulating protein, RefZ, associates with *RBM*s localized near the site of polar division to regulate the position of cell division relative to the chromosome during sporulation.

Results

RefZ and its DNA binding sites are conserved across the Bacillus genus

During sporulation, RefZ is enriched at several regions on the chromosome harboring a mostly palindromic, 20 bp motif referred to as an *RBM* (RefZ Binding Motif) (Fig. 2.1B) (82). The *RBM* is sufficient for interaction with RefZ, as its placement at ectopic sites leads to specific enrichment of the ectopic regions following RefZ immunoprecipitation (82). Five out of six of the *RBM*s map to the *oriC*-proximal quadrant of the *B. subtilis* circular chromosome, while RBM_T, which is degenerate and lacks the conserved central palindrome, is located near the terminus (Fig. 2.1A and 2.1B).

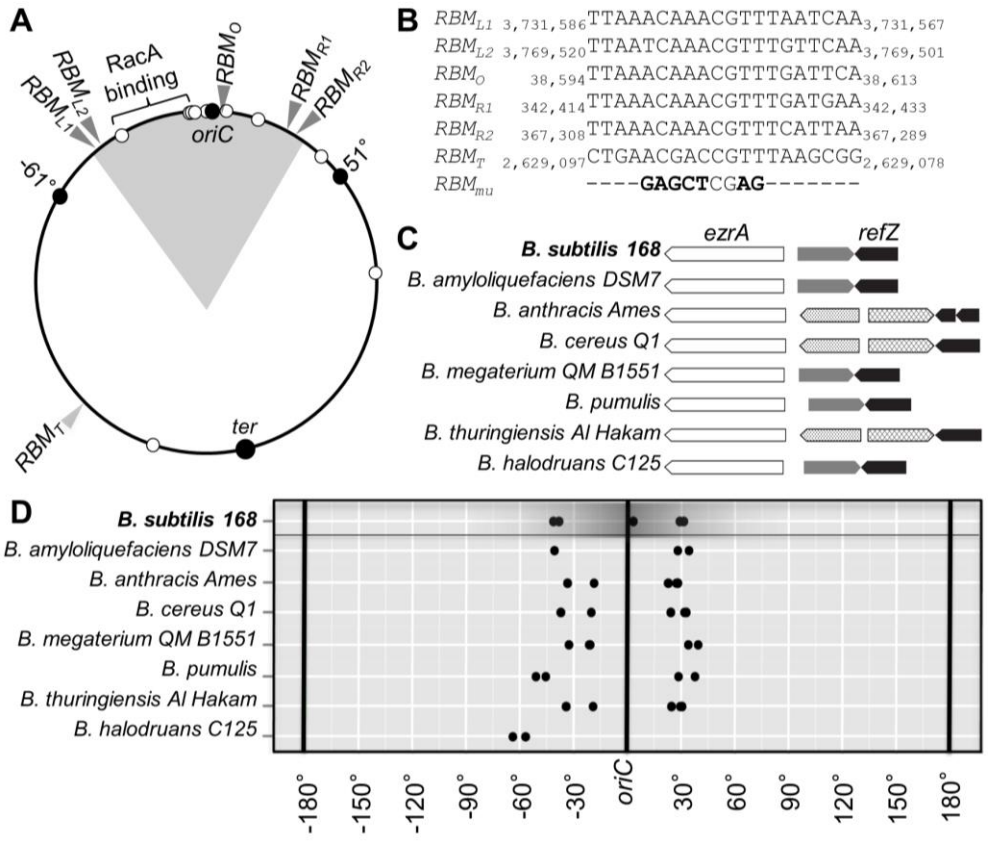

Figure 2.1. RefZ and *RBM*s are conserved across the *Bacillus* genus. (*A*) Location of *RBM*s on the *B. subtilis* chromosome. The shaded region indicates the approximate region of chromosome initially captured in the forespore at the time of polar division. Eighty percent of RacA binding sites are located on the left arm between chromosome coordinates 3,805,000 and 4,211,500 in the labeled region. Spo0J binding sites are shown as white circles. (*B*) Chromosomal coordinates (*B. subtilis* 168) and alignment of the five *oriC*-proximal *RBM*s. *RBMmu* denotes the point mutations introduced into each *RBM* to create the null strain, *RBM5mu*. (*C*) Alignment of *refZ* region for multiple members of the *Bacillus* genus. (*D*) *RBM*s identified by FIMO (P<1e-10) mapped to chromosomes of other *Bacillus* genus members. Since genome sizes differed, all positions were normalized to a 360° circular chromosome linearized at 180° (x-axis).

Intriguingly, the boundaries of the *oriC*-proximal sites align closely with regions where polar septation occurs over the forespore-destined chromosome (Fig. 2.1A and 2.1D shaded regions) (16, 69). Since *refZ* is conserved in the *Bacillus* genus (Fig. 2.1C) (82), we investigated if the *RBM*s were also conserved by performing a FIMO search (156) of bacterial genomes using the *RBM* consensus (Fig. 2.2). Our analysis showed that the *RBM* consensus was highly conserved throughout the genus of *Bacillus* polar spore formers. Strikingly, the relative locations of the *RBM*s with respect to *oriC* (0°) are also remarkably similar across the genus; most of the species examined (a subset of species are shown in Fig. 2.1D) possessed at least four *RBM*s: two on the left arm of the chromosome (approximately -40° in *B. subtilis*) and two on the right arm (approximately 30° in *B. subtilis*) (Fig. 2.1D) (Fig. 2.2). Our analysis did not reveal any shared genetic contexts, such as being located in or around specific genes or in promoter regions, which might account for the conserved spatial arrangement of the *RBM*s. These results suggest that there is a strong evolutionary pressure to maintain the motifs at specific chromosomal positions, and is consistent with the idea that the location of the *RBM*s is critical for their function.

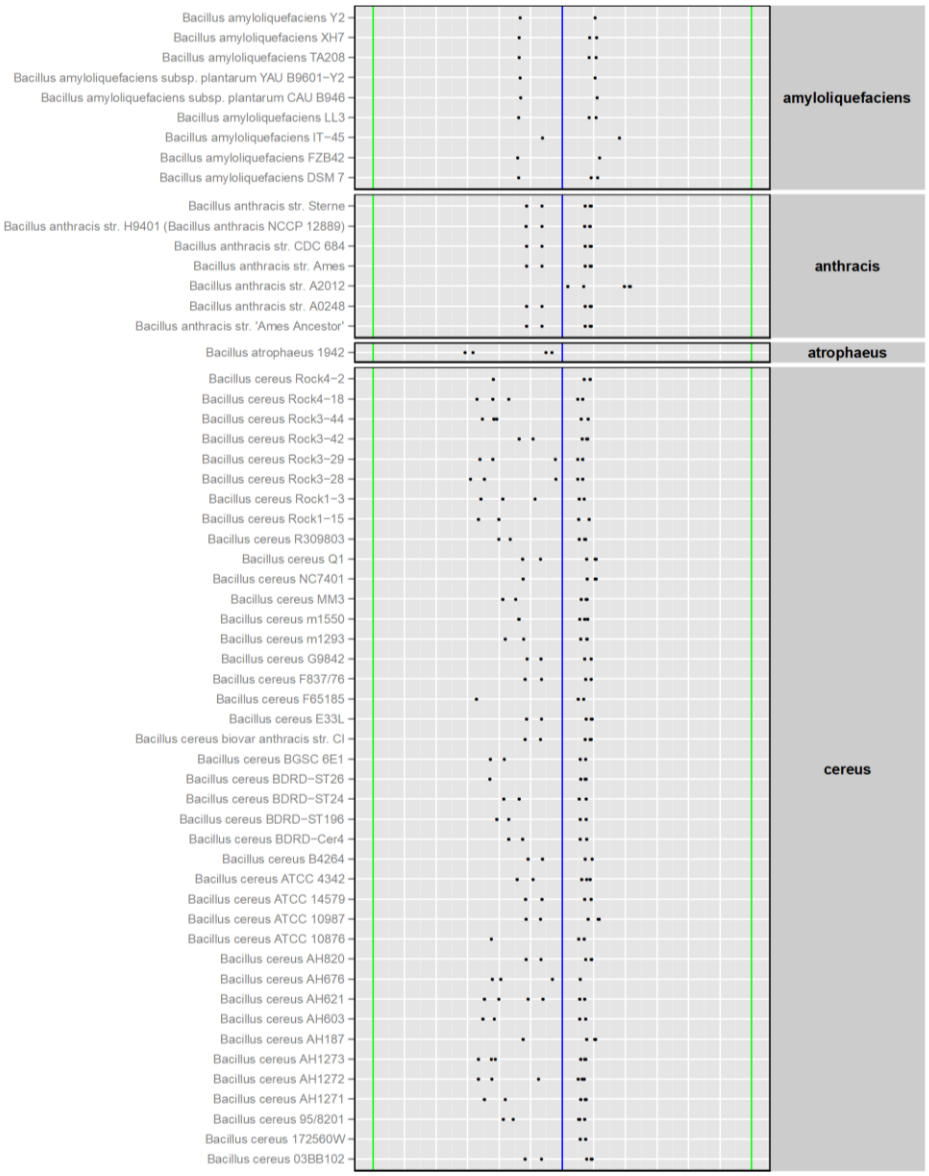

Figure 2.2 *RBM*s identified by FIMO mapped to chromosomes of other members of the *Bacillus* genus. Since genome sizes differed, all positions were normalized to a 360° circular chromosome linearized at 180° (x-axis). Closely spaced *RBM*s are not resolvable.

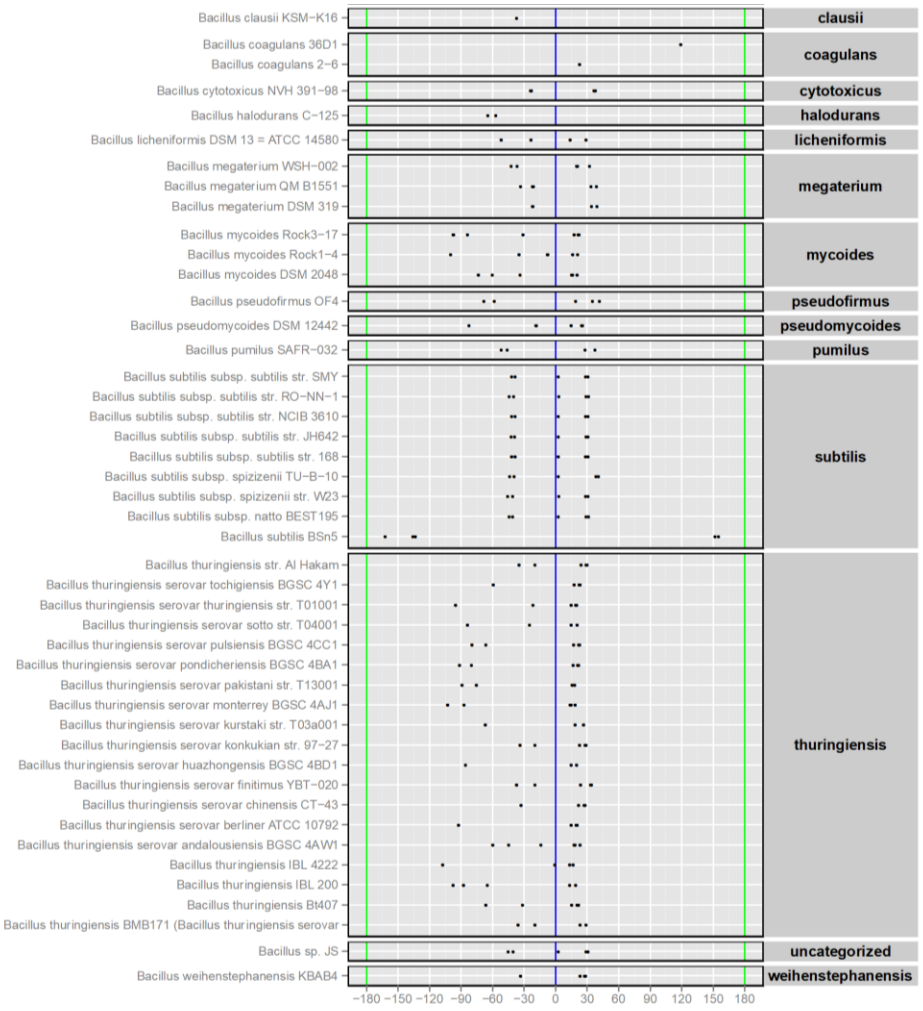

Figure 2.2 Continued.

RefZ-mediated inhibition of cell division is conserved in B. megaterium

RefZ was previously shown to disrupt FtsZ rings when expressed during vegetative growth (82), and our bioinformatic analyses (Fig. 2.1D, Fig. 2.2, and Supplementary text) indicate that RefZ and the *RBM*s are conserved across the *Bacillus* genus. To determine if RefZ's FtsZ inhibitory function (82) is conserved in a distantly related *Bacillus*, we performed a *refZ* swapping experiment between our *B. subtilis* lab strain (*B. subtilis* 168)and *B. megaterium,* another well-characterized and genetically tractable *Bacillus* species (157, 158). We placed *B. megaterium refZ* under the control of an IPTG-inducible promoter (P_{hy}-$refZ_{Bmeg}$) and introduced the construct into the *B. subtilis* chromosome at a non-essential locus. We also performed the reciprocal swap by placing *B. subtilis refZ* under the control of a xylose-inducible promoter (P_{xyl}-$refZ_{Bsub}$) and introducing the construct into *B. megaterium*. Prior to induction, *B. subtilis* harboring P_{hy}-$refZ_{Bmeg}$ possessed an average cell length of 3.4 ± 0.9 μm and divided at regular intervals (Fig. 2.3A). After 60 min of induction, the cells visibly filamented (Fig. 2.3A) and averaged 5.5 ± 2.2 μm in length, ~40% longer on average than the uninduced cells ($P<0.0001$). All cell lengths used to calculate the averages are plotted in Fig. 2.3A. *B. megaterium* harboring P_{xyl}-$refZ_{Bsub}$ possessed an average length of 5.4 ± 2.8 μm before induction. After a 60 min induction, *B. megaterium* cells harboring P_{xyl}-$refZ_{Bsub}$ also filamented (Fig. 2.3B) and exhibited an average cell length of 10.6 ± 6.8 μm, ~2-fold longer ($P<0.0001$) on average than the uninduced control (all data points are plotted in Fig. 2.3B). These results are consistent with the cell filamentation phenotype previously observed following P_{hy}-$refZ_{Bsub}$ expression in *B. subtilis* (82) and suggest that the characterized functions of RefZ are likely to be conserved in other *Bacillus* species.

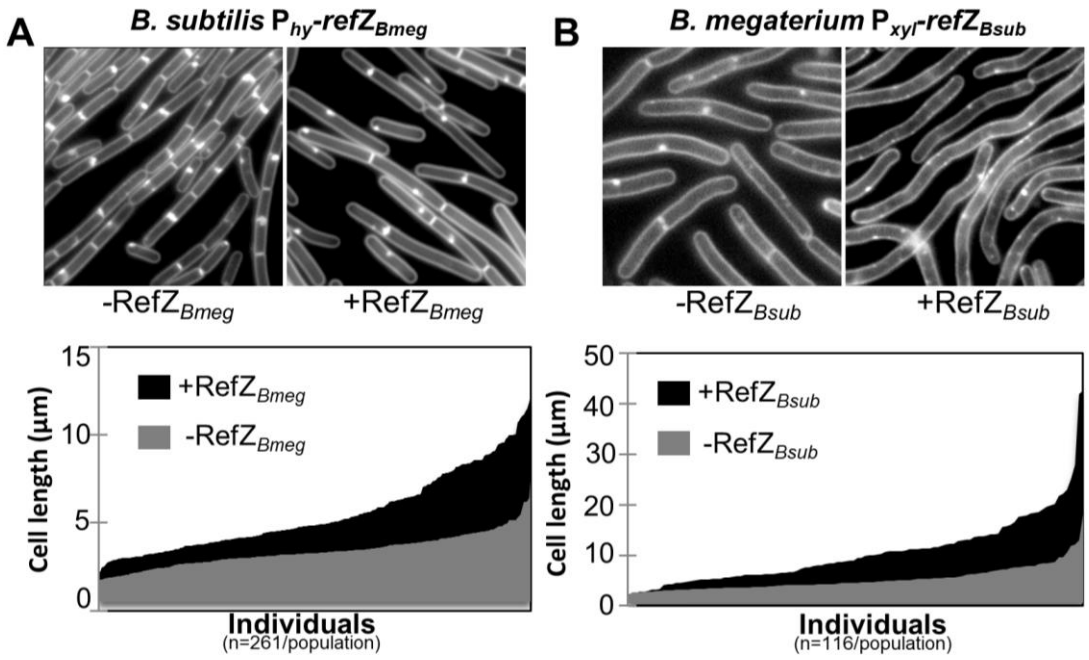

Figure 2.3 Induced expression of RefZ homologs results in cell filamentation across *Bacillus* species. (*A*) Expression of *B. megaterium* RefZ (RefZ$_{Bmeg}$) in *B. subtilis* before and after 60 min induction with 1.0 mM IPTG (top). Quantitation of cell lengths before and after 60 min of RefZ$_{Bmeg}$ induction with 1.0 mM IPTG (bottom). Cell lengths were rank ordered and plotted without spaces along the x-axis to allow for visualization of the entire population. (*B*) Expression of *B. subtilis* RefZ (RefZ$_{Bsub}$) in *B. megaterium* before and after 60 min induction (top). Quantitation of cell lengths before and after RefZ$_{Bmeg}$ expression (bottom). Cell membranes were stained with TMA.

RefZ binds the five oriC-proximal RBMs with similar affinity

RefZ, like the *E. coli* nucleoid occlusion and FtsZ inhibitor, SlmA, is a member of the TetR-family of DNA-binding proteins (138). During sporulation, RefZ is enriched at several sites around the chromosome harboring the consensus *RBM* (82). Integration of an *RBM* at an ectopic site was sufficient to promote enrichment of RefZ at this non-native site, while a mutated *RBM* is not (82). To characterize the binding of RefZ to each of the *oriC*-proximal *RBM*s, we PCR amplified DNA fragments from the chromosome centered on each *RBM* and performed electrophoretic mobility shift assays with RefZ-6His. Each of the *oriC*-proximal *RBM*s exhibited two DNA mobility shifts following incubation with increasing concentrations of RefZ (Fig. 2.4) and displayed similar apparent affinities for RefZ. FEME analysis identified three possible degenerate motifs in the *ter* region (Fig. 2.5). Only one of these motifs, designated as RBM_T (Fig. 2.1B), showed a visible upshift (Fig. 2.4 and Fig. 2.5). The mobility shift pattern differed from the *oriC*-proximal *RBM*s in that the second, higher molecular weight mobility shift was not detectable (Fig. 2.4). The RBM_T site also required a higher concentration of RefZ to induce a mobility shift, suggesting that RefZ likely has a lower apparent affinity for the RBM_T site.

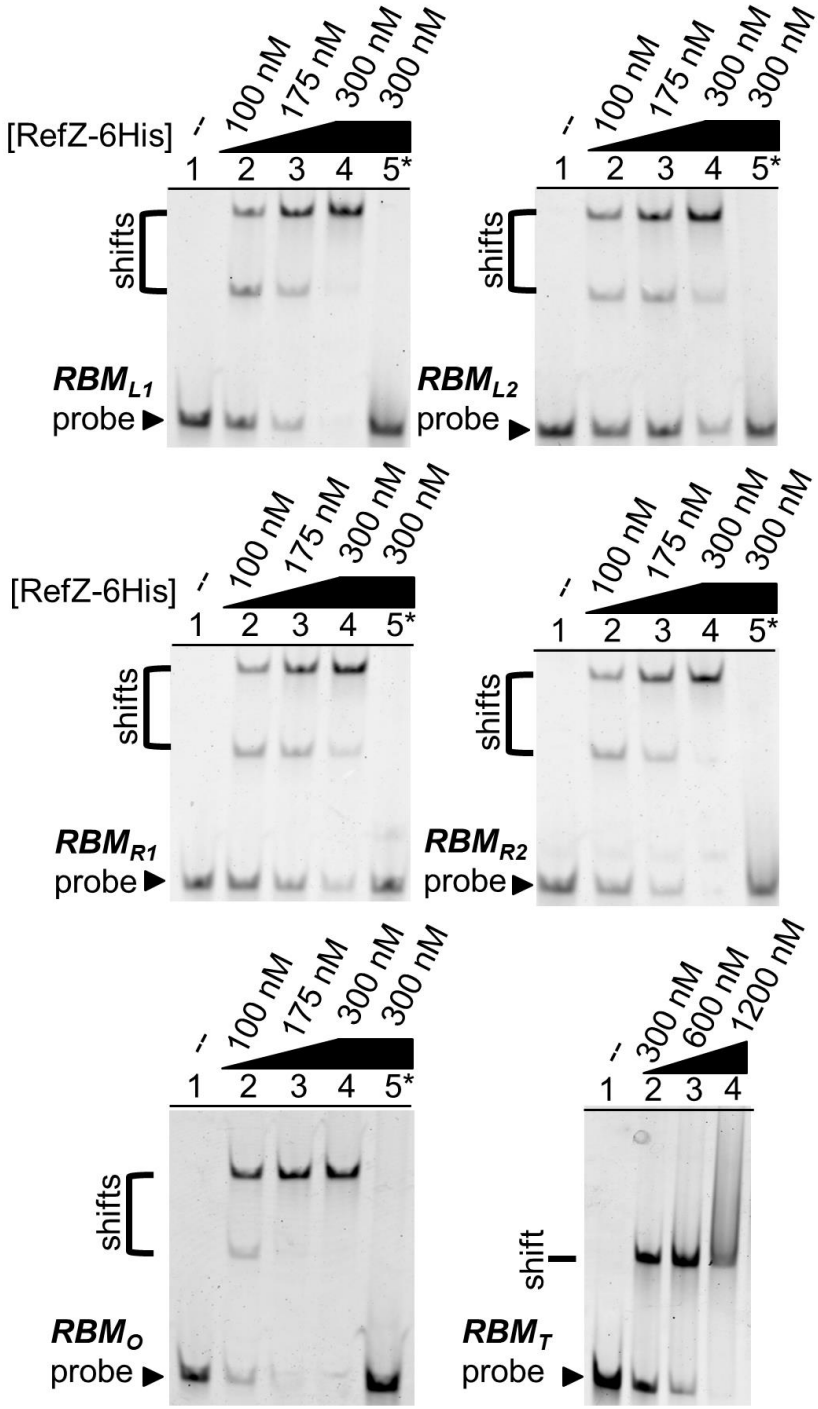

Figure 2.4 Characterization of RefZ-*RBM* interactions. (*A*) Gel shift analysis of DNA fragments (7 nM) centered on the *RBM* indicated incubated with various concentrations of RefZ-6His. Lane 5 (asterisk) of each gel shows the gel shift results for the mutant version of each *RBM* (see Fig. 2.1B) incubated with 300 nM RefZ-6His.

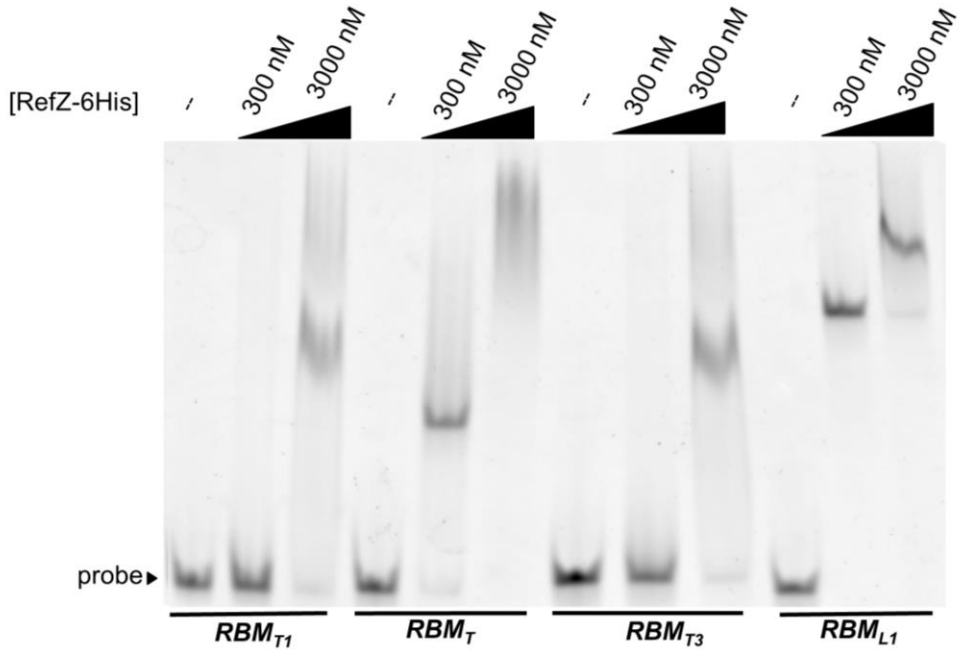

RBM_{T1} 2,629,601ATAATCAACGATTTTATTAA2,629,582
RBM_{T} 2,629,078CCGCTTAAACGGTCGTTCAG2,629,097
RBM_{T3} 2,628,828TTGAACCAGCTTTAAAACAT2,628,847
RBM_{L1} 3,731,586TTAAACAAACGTTTAATCAA3,731,567

Figure 2.5 Characterization of RefZ interaction with degenerate *RBM*s in the terminus region. (*A*) Gel shift analysis of DNA fragments (7 nM) centered on the *RBM* indicated and incubated with various concentrations of RefZ-6His. The *RBM* sequences present in the amplified DNA probes are shown at the bottom for reference. The bases that are invariant in the five *oriC*-proximal *RBM*s are underlined on the RBM_{L1} sequence.

To determine if the DNA flanking each *RBM*, rather than the motif itself, was sufficient for the mobility shift, we amplified the same *RBM* regions from an *RBM* mutant strain (RBM_{5mu}), which harbors seven point mutations in the central palindrome of each of the five *oriC*-proximal *RBM*s (Fig. 2.1B). None of the DNA fragments harboring the mutant *RBM*s were visibly shifted in the presence of the highest RefZ concentration tested (Fig. 2.4, lane 5 for all), corroborating the prior conclusions that the *RBM*s represent RefZ's cognate binding sites (82). Importantly, these data also demonstrate that the *RBM* mutations we introduced on the *B. subtilis* chromosome are loss-of-function with respect to their ability to be specifically recognized by RefZ.

RefZ binds to the oriC-proximal RBM*s *in units of two and four

The presence of multiple mobility shifts suggests that RefZ is capable of binding to the DNA in several states, each of which may have different functional properties. To determine the number of units of RefZ associated with each mobility shift, we performed a mobility shift assay utilizing RefZ fused to epitope tags of different molecular weights, as shown in Fig. 2.6A. When the RefZ-6His and SUMO-RefZ were mixed, a mobility pattern indicative of mixed multimers was formed (Fig. 2.6A and 4B), suggesting that RefZ binds the *RBM*s in units of two and four. The TetR family members SlmA (an inhibitor of FtsZ) and the multidrug export regulator QacR, have been shown through crystallography studies to bind to their cognate binding motifs as a pair of dimers (133, 159). Based on these data, and our observation that RefZ binds to the DNA in units of two and four, we propose that RefZ most likely binds as a dimer to RBM_T and as both a dimer and pair of dimers to the five *oriC*-proximal *RBM*s. We did not observe additional,

higher molecular weight mobility shifts that might be indicative of RefZ further polymerizing along DNA, but we do not exclude this possibility. We also do not exclude the possibility that RefZ is capable of forming a tetramer when associated with DNA, as such a configuration could also be consistent with the mobility pattern observed.

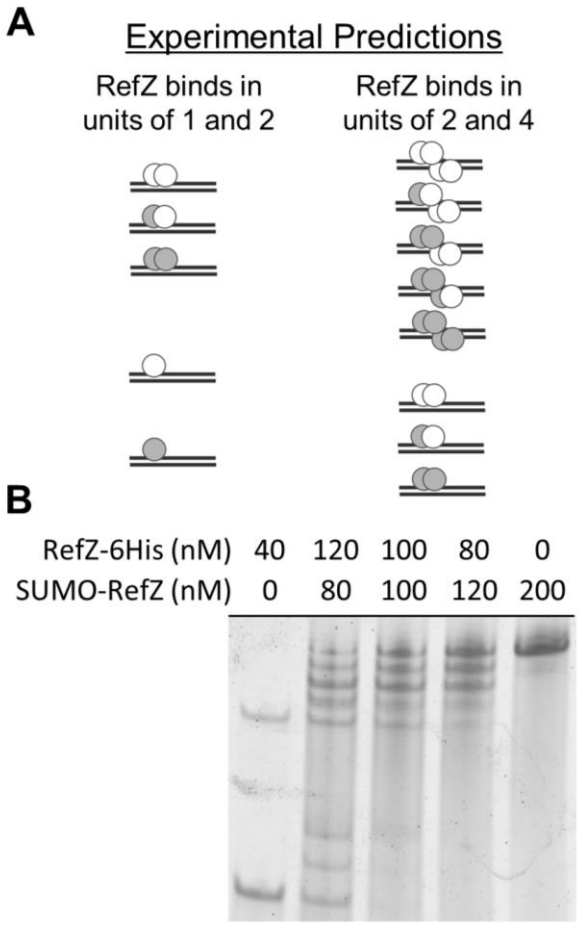

Figure 2.6 RefZ binds to *RBM*s in units of two and four. (*A*) Cartoon showing possible experimental outcomes for RefZ binding to *RBM*-containing DNA (*B*) Gel shift analysis of DNA fragments (10 nM) centered on RBM_O incubated with the indicated concentrations of RefZ-6His and SUMO-RefZ. Unshifted RBM_O probe was run out of the bottom of the gel. The filled arrowheads indicate the position of RefZ-6His mobility shifts. The unfilled arrowheads indicate the position of SUMO-RefZ mobility shifts. The remaining bands correspond to mixed species.

RefZ coordinates one piece of DNA not two

At the time of axial filament formation, the right and left arms of the chromosome are parallel to each other and the long axis of the cell. This may juxtapose *RBMs* on opposing chromosomal arms. If RefZ forms a tetramer when associated with the *RBM* then association to a nearby *RBM* could bridge opposite chromosomal arms to one another allowing RefZ-*RBM* interactions to bridge the arms together in order to organize this chromosomal region in preparation for pumping into the forespore.

If a RefZ tetramer can bridge opposite chromosomal arms, then a RefZ tetrameric complex should be able to coordinate more than one piece of DNA. To test this hypothesis in the mobility shift assay a series of PCR products (100 bp, 150 bp, 200 bp) centered on RefZ's L2 binding motif were designed. PCR products were cleaned and quantified by picogreen. The electrophoretic mobility shift assay was performed as previously described. If RefZ could coordinate two pieces of DNA, seven bands total should appear and three bands for the tetrameric complex: (Band 1, 100 bp and 100 bp; Band 2, 100 bp and 150 bp; Band 3, 150 bp and 150 bp). When 100 bp and 150 bp of DNA were mixed, 6 different bands were observed (Fig. 2.7) and only two bands for the tetrameric complex. This favors the model of of a pair of RefZ dimers bound (a pair of dimers bound to 100 bp and a pair of dimers bound to 150 bp). The absence of a third band for the RefZ dimer of dimers means that there is only one DNA in this complex (Fig. 2.7).

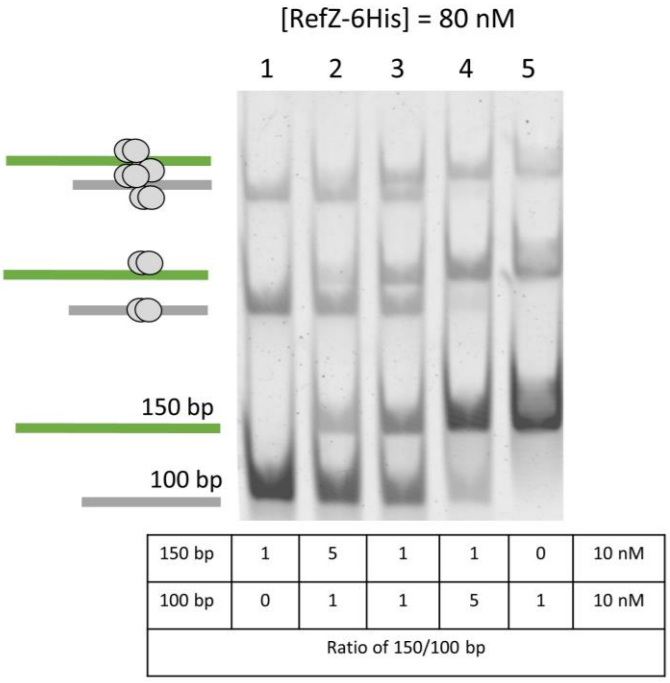

150 bp	1	5	1	1	0	10 nM
100 bp	0	1	1	5	1	10 nM
Ratio of 150/100 bp						

Figure 2.7. RefZ coordinates one piece of DNA not two. 150 bp and 100 bp of *RBM*$_{L2}$ DNA were used in electrophoretic mobility shift assays to determine if RefZ could coordinate more than one piece of DNA. When the ratio of 150 bp to 100 bp was 1:1 (lane 3) six bands are observed. Two of the bands correspond to unbound probe (see schematic on right). The next two complexes represent a dimer of RefZ (dimer bound to 100 bp & dimer bound to 150 bp). Finally the last two complexes correspond to a dimer of dimers (4 units bound to 100 bp and 4 units bound to 150 bp). The absence of a third band for either upshift suggests that only one piece of DNA is coordinated in the complex.

No evidence for RefZ looping DNA

In some of our early RefZ purifications, RefZ was present at molecular weights consistent with tetramers and RefZ forms a visible reversible precipitate (data not shown), hinting that RefZ may have a propensity to multimerize beyond dimers. Since the terminus-organizing protein MatP and Spo0J were shown to form tetramers that create DNA loops by bridging its binding sites (45, 70), we hypothesized that RefZ may act similarly, bridging *RBM*s on opposing chromosomal arms. To test if RefZ could promote DNA looping in vitro, a 591 bp piece of DNA harboring two *RBM*s was constructed (Fig. 2.8A). The 591 bp piece was a stitched amplification from RBM_{L1} and RBM_{R1}.

RefZ-6His was incubated with a piece of DNA harboring two *RBM*s and the DNA visualized using negative staining and electron microscopy (Fig. 2.8B). Lollipop structures were observed in both control and experimental micrographs (Fig. 2.8B). To determine if the loops observed in the samples were of the predicted size, we first quantitated the length distribution of the *RBM*-containing DNA without protein, which peaked between 150 and 190 nm (Fig. 2.8C). We then quantitated the loop sizes in samples with and without RefZ-6His, with the expectation that loops of the predicted size would range from 115 to 146 nm (77% of the total experimentally determined length). Only 15% of loops from DNA only samples fell within the predicted range (Fig. 2.8D). In contrast, 32% of the looped DNA in samples containing RefZ-6His fell within the predicted range, with a notable peak at 130 nm (Fig. 2.8D). When the experiment was repeated the number of predicted size loops became even more similar between control

and experimental samples. From these results we did not feel comfortable concluding that RefZ promotes loop formation, therefore an alternative method was undertaken.

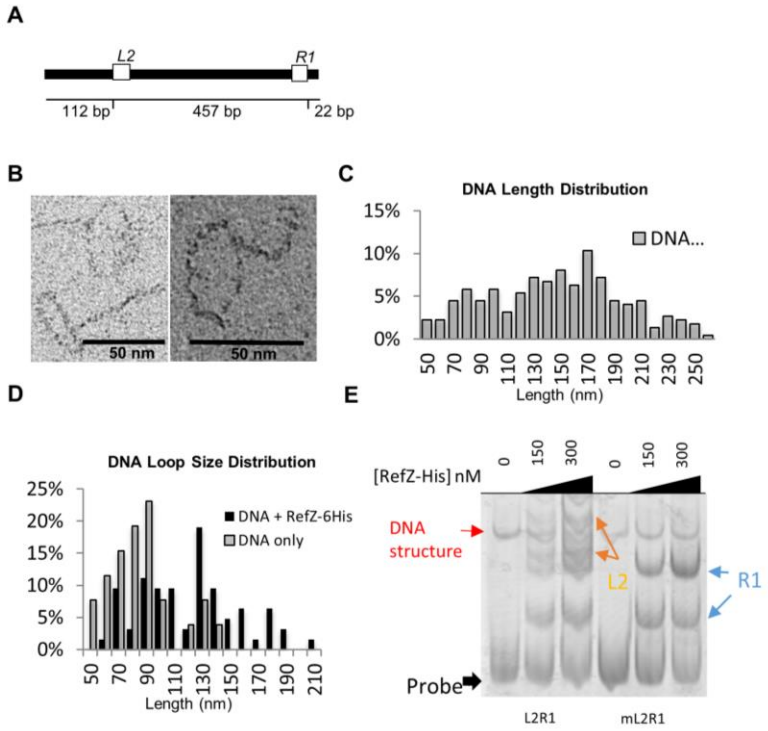

Figure 2.8. DNA looping experiments produce inconclusive results. (A) Schematic of 591 bp DNA harboring two *RBM*s generated by stitching RBM_{L2} to RBM_{R1}. (B) Electron micrographs of observed DNA loops formed in the presence of RefZ-6His, which correspond to correct size. (C) Quantitation of DNA lengths from $RBM_{L2\text{-}R1}$ DNA-only micrographs. (D) Quantitation of DNA loop sizes observed by electron microscopy. (E) EMSA with RefZ-6His and 591 bp stitched fragment of $RBM_{L2\text{-}R1}$ DNA and 591 bp stitched fragment of $RBM_{mL2\text{-}R1}$ DNA. Two upshifts can be observed for RBM_{L2} and RBM_{R1} but not RBM_{L2}.

If RefZ is able to loop the intervening sequence bounded by two *RBM*s, a large upshift corresponding to the loop should be observed in the EMSA assay in addition to the bands of the tetrameric complex. When the 591 bp piece containing two *RBM*s was used in an EMSA, one contaminating band (significantly larger than the probe) appeared prior to addition of any protein (Fig. 2.8E). Addition of protein resulted in four additional upshifts the expectation if the protein bound as a dimer of dimers to both sites. However, no additional band corresponding to a larger looped sequence appeared. This is consistent with RefZ not imposing DNA loops. A control piece of DNA (591 bp) was a stitched amplification of $mRBM_{L1}$ and RBM_{R1} and showed only two upshifts.

RBM DNA localizes in the vicinity of the polar septum

The *RBM*s flank the region of the chromosome captured by polar division (Fig. 2.1A and 2.1D, shaded regions), so we hypothesized that the *RBM*s located on the left and right chromosomal arms would localize in the vicinity of the incipient division plane during sporulation. To examine where the *RBM* DNA localizes during sporulation, we inserted a *tet* operator array immediately adjacent to RBM_{L2} in cells expressing TetR-CFP (Fig. 2.9). The reporter was generally localized in the cell quarter regions (near both poles) 60 to 75 min into sporulation, when most cells begin exhibiting the membrane invaginations characteristic of polar division. The array near RBM_{L2} was localized in the division plane in 91% (n=112) of septating cells (Fig. 2.9A). Operator arrays inserted on the chromosome near RBM_{R1} and RBM_{R2} exhibited similar localization patterns to the array near RBM_{L2} (Fig. 2.10). The localization of the RBM_{L2} array appeared similar in a Δ*refZ* mutant and in an *RBM* mutant harboring loss-of-function mutations in all five

oriC-proximal *RBM*s (*RBM*$_{5mu}$), suggesting that RefZ and the *RBM*s cannot be the sole effectors of organization and/or orientation of this region of the chromosome (Fig. 2.9). Given the limited resolution provided by the operator arrays, we do not rule out the possibility that RefZ and/or the *RBM*s mediate smaller, local changes in the positioning of specific regions of chromosome. The localization of the *RBM*s is consistent with a role in organizing the chromosome and/or regulating FtsZ dynamics at the pole (where polar cell division takes place). However, we do not exclude the possibility that the in vivo localization of the *RBM*s near the incipient septum is coincidental.

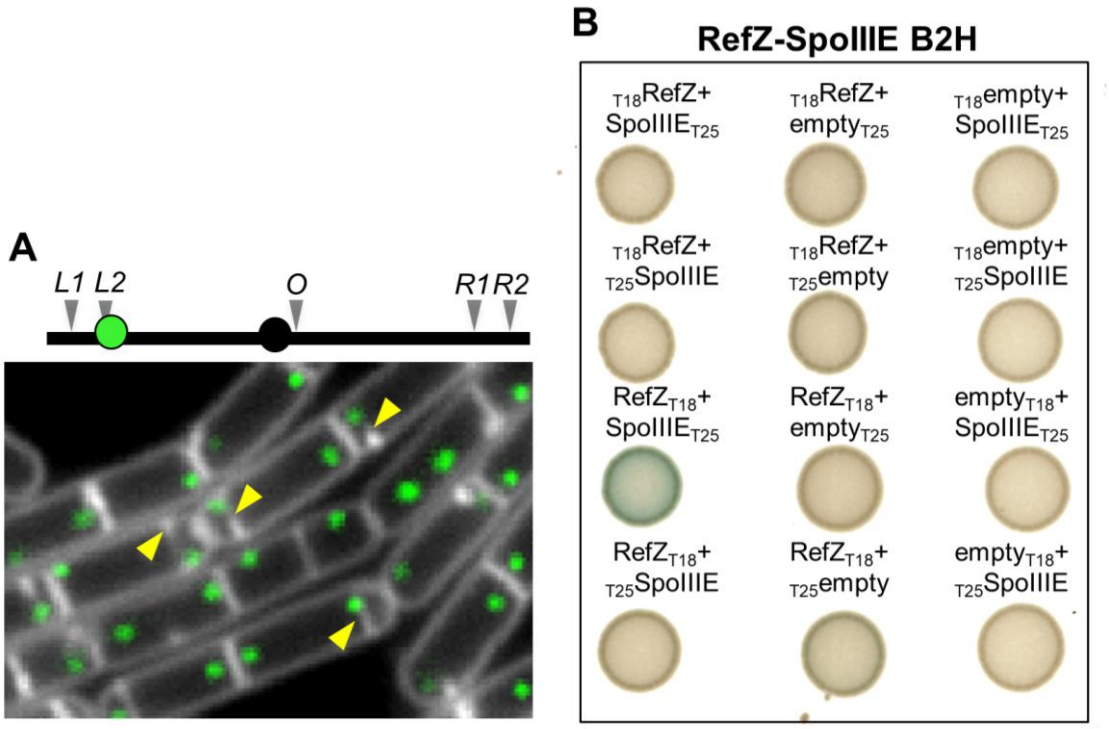

Figure 2.9. *RBM* DNA localizes near the site of polar division. (*A*) Images of sporulating cells (75 min after resuspension) harboring TetR-CFP and a *tetO48* array integrated ~1100 bp from *RBM*$_{L2}$ (the location of array is denoted by green circle in the cartoon). Membranes were stained with TMA (white) and TetR-CFP foci are pseudocolored green. Yellow arrowheads indicate incipient septa. (*B*) Bacterial two-hybrid analysis showing the pairwise interaction between RefZ and SpoIIIE.

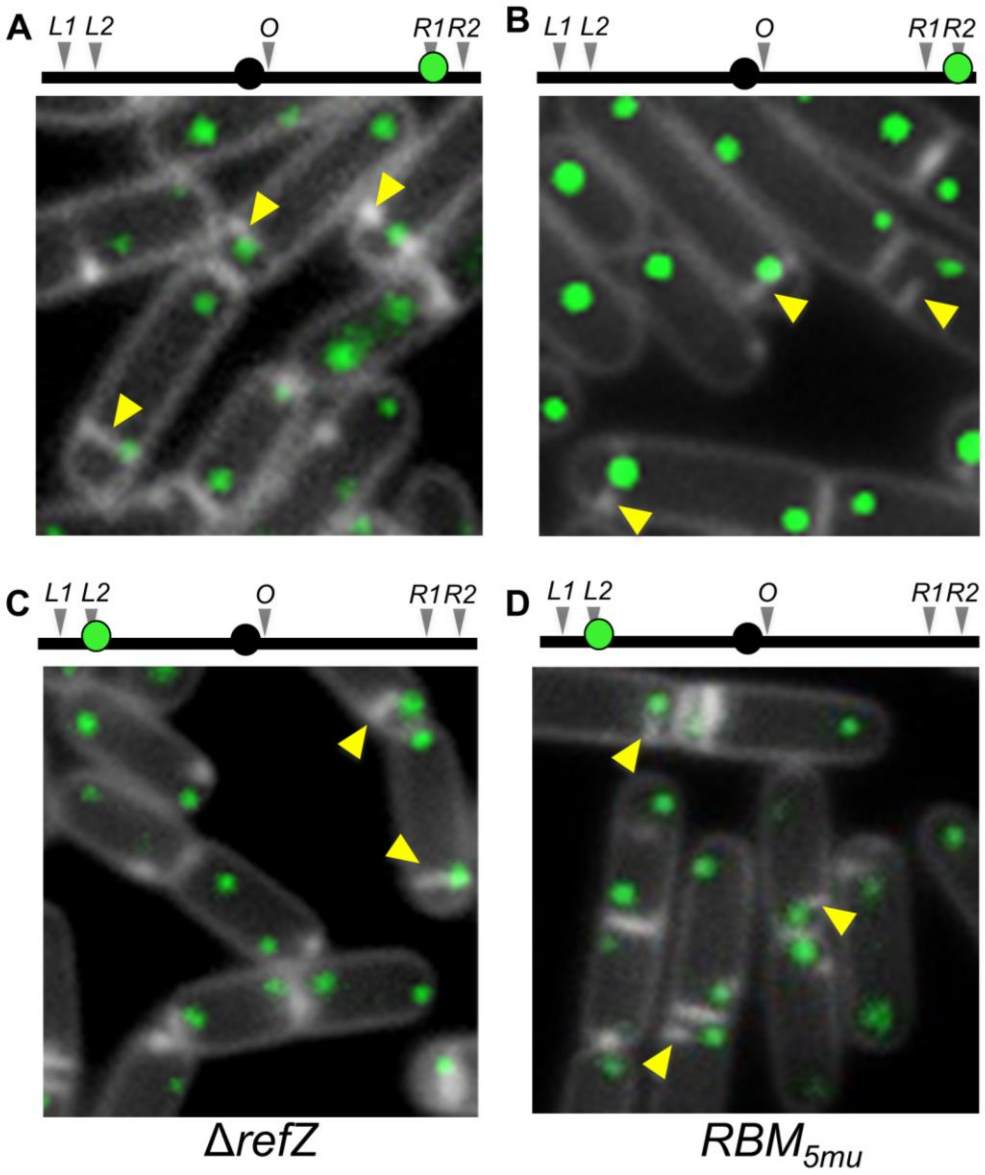

Figure 2.10. Supplementary RBM DNA localizes near the site of polar division. Images of sporulating cells (75 min) harboring LacI-YFP and a $(lacO)_{48}$ array integrated near RBM_{R1} (A) or near RBM_{R2} (B). Membranes were stained with TMA (white) and *LacI*-YFP foci are pseudocolored green. Yellow arrowheads indicate incipient septa. (C) Images of sporulating cells (75 min) harboring TetR-CFP and a $(tetO)_{48}$ array integrated near RBM_{L2} in a Δ*refZ* mutant. (D) Images of sporulating cells (75 min) harboring TetR-CFP and a $(tetO)_{48}$ array integrated near RBM L2 in RBM 5mu. Membranes were stained with TMA (white) and TetR-CFP foci are pseudocolored green. Yellow arrowheads indicate incipient septa.

The DNA pump SpoIIIE was recently shown to localize at the leading edge of the sporulation septum (160). Current data favor a model in which SpoIIIE assembles at least two pumps (one for each chromosomal arm) (24, 160, 161) and the observation of a single focus of SpoIIIE in vivo suggests that these pumps are in close proximity to each other (69, 160-162). The juxtaposition of the *RBM*s to the site of polar division (Fig. 2.1A, 1D) and the fact that SpoIIIE localizes to the leading edge of the septum (160) where it must also assemble on DNA in the division plane, prompted us to investigate the possibility that RefZ might interact with SpoIIIE or another divisome component directly. Such a mechanism could be an efficient way to promote pump assembly at precise locations along the chromosome without requiring that SpoIIIE assemble on DNA at specific sequences. It could also ensure that RefZ is precisely positioned in the cell to affect a role in FtsZ activity at the pole (see discussion). To test these ideas, we performed bacterial two-hybrid analysis with RefZ and several putative interaction partners. We did not detect an interaction between RefZ and the cell division proteins EzrA (conserved by synteny near *refZ*) or FtsZ in the bacterial two-hybrid analysis. In contrast, we detected a positive interaction between full-length RefZ and full-length SpoIIIE (Fig. 2.9B), but not a full-length version of the vegetative DNA pump SftA (Fig. 2.11), suggesting that the observed interaction between RefZ and SpoIIIE is specific.

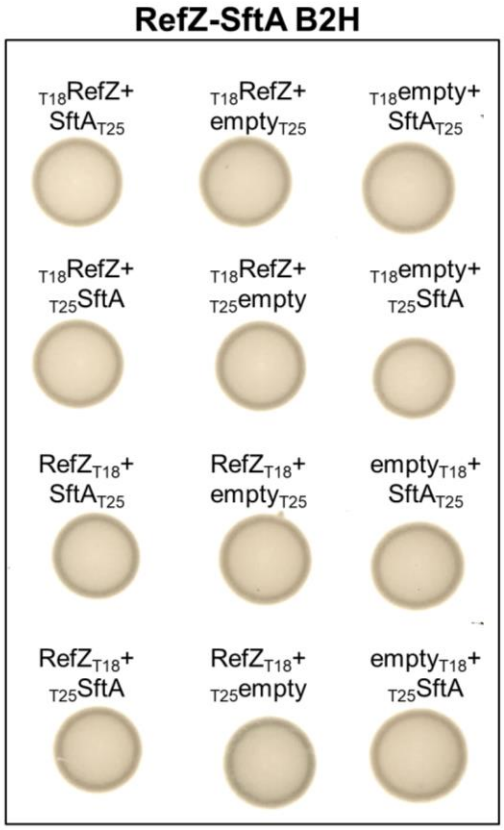

Figure 2.11. Bacterial two-hybrid analysis of interaction between RefZ and SftA.

RefZ promotes precise positioning of the chromosome arms during sporulation

Based on the proximity of the outermost *RBM*s to the region of the chromosome initially captured in the forespore, and RefZ's previously characterized role as a regulator of FtsZ, we hypothesized that by binding to the *RBM*s, RefZ might contribute to defining the region over which cell division takes place on the chromosome. Regions of chromosome initially captured in the forespore can be monitored using a highly sensitive, single-cell assay (69). The assay works by fusing a forespore-specific promoter to a fluorescent reporter and inserting the fusion into the chromosome at the DNA location of interest. The assay is performed in a SpoIIIE mutant that cannot pump the remainder of the chromosome into the forespore, thus ensuring that only reporters captured or "trapped" on the forespore side of the septum will produce fluorescence (69). Using the trapping assay, we found that the Δ*refZ* mutant captures a marker located at -61° (Fig. 2.1A) (approximately 230 kb counter-clockwise from $RBM_{L1)}$, approximately two times more often than wildtype (22% in Δ*refZ* compared to 10% in wildtype) (Fig. 2.12). Introducing a copy of P_{refZ}-*refZ* at the *amyE* locus (28°**)** fully complemented the left-arm trapping defect (Fig. 2.12).

To determine if right arm of the chromosome was also affected in the Δ*refZ* mutant, we repeated the assay with a +51° reporter. This location was selected because it is located approximately 230 kb clockwise from RBM_{R2}, the outermost *RBM* on the right arm (Fig. 2.1B). Similar to the left arm, +51° was trapped in 11% of wildtype and 21% of Δ*refZ* cells. The +51° trapping defect was largely, but not fully complemented by *amyE*::P_{refZ}-*refZ* (Fig. 2.12). It is not clear why right arm complementation differed from left, however, we speculate that the right arm is more sensitive to perturbations from

wildtype (see discussion), including those that might result from shifting P_{refZ}-*refZ* from its native locus (-100°) to *amyE* (28°). Reporters integrated close to RBM_{L1} and RBM_{R2} (-40° and +30°) were also captured approximately two times more often in the forespore in a Δ*refZ* mutant compared to wildtype, suggesting that shift we observe in chromosome capture is not restricted to the -60° and +51° regions (data not shown). We conclude that RefZ contributes to the proper capture of regions located on both the left and right arms of the chromosome during sporulation.

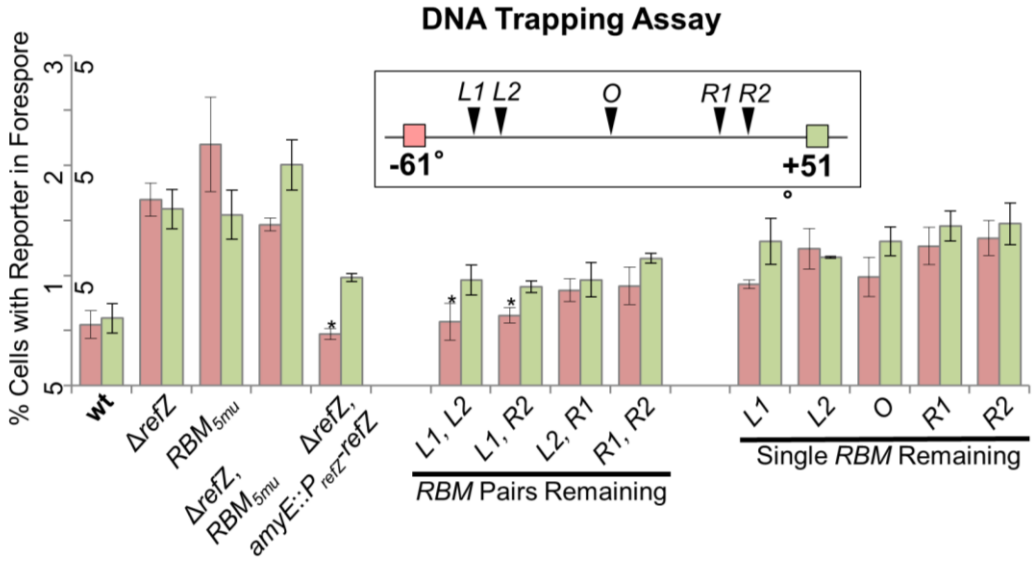

Figure 2.12. RefZ and the *oriC*-proximal RBMs promote the precise positioning of the left and right chromosome arms during sporulation. Single cell analysis indicating the average percentage of cells that captured either the left arm (−61°) or right arm (+51°) reporter in the forespore at the time of polar division. Asterisks indicate samples that did not differ significantly from the wild-type controls. All other samples differed significantly from the wild-type controls ($P < 0.01$). A minimum of 1,500 cells from three biological replicates were counted for each strain.

RBMs are required for wild-type chromosome capture during sporulation

Since RefZ binds to the *RBM*s during sporulation (82), we hypothesized that RefZ would also require one or more of the *RBM*s for wild-type trapping of the chromosome arms. We further hypothesized that a mutant harboring point mutations in all five *oriC*-proximal *RBM*s (*RBM*$_{5mu}$), would phenocopy the Δ*refZ* strain. To test these ideas, we performed the chromosome trapping assay on the *RBM*$_{5mu}$ strain, which harbors point mutations (Fig. 2.1B) in the five *oriC*-proximal *RBM*s. On average, 27% of *RBM*$_{5mu}$ cells trapped the -61° reporter, while 20% of cells trapped the +51° reporter, similar to the Δ*refZ* strain (Fig. 2.12). The *RBM*$_{5mu}$ strain exhibited a wide standard deviation for left arm trapping (trapping ranged from 20% to 34% in 18 independent experiments) that was not observed in the *RBM*$_{5mu}$ Δ*refZ* strain (see below), suggesting the emergence of a RefZ-dependent enhancement of variation in chromosome capture in the absence of its cognate *RBM*s. To test if RefZ and the *RBM*s act in the same genetic pathway to affect chromosome capture, we asked if a double mutant (*RBM*$_{5mu}$ Δ*refZ*) produced a similar trapping defect when compared to the single mutants. We found that 20% of the *RBM*$_{5mu}$ Δ*refZ* population trapped the -61° reporter, while 25% trapped the +51° reporter (Fig. 2.12), consistent with the *RBM*s and RefZ each requiring the other for wild-type function. These results are most consistent with a model in which RefZ binds to one or more of the *RBM*s to achieve its function in chromosome capture.

At least two RBMs are required for a wild-type arrangement of the chromosome

When the five *oriC*-proximal *RBM*s are mutated, septation occurs over a different portion of the forespore-destined chromosome, similar to a Δ*refZ strain.* To determine if

all five *RBM*s are required to support a wild-type arrangement of the chromosome, we performed the trapping assay on nine additional *RBM* mutant combinations (Fig. 2.12). The symmetric distribution of the *RBM*s around *oriC* across the *Bacillus* genus (Fig. 2.1D) supports the idea that *RBM*s positioned on both chromosomal arms are important for RefZ-*RBM* function; however, to test the simplest case in which a single *RBM* is sufficient to maintain wild-type trapping, we first performed the assay on five mutants, each harboring only one remaining functional *RBM*. As shown in Fig. 2.12, no single *RBM* was sufficient to ensure wild-type trapping of either the left (-61°) or right (+51°) arm reporters. However, the single *RBM* remaining mutants trapped the left arm reporter significantly ($P<0.01$) less often than RBM_{5mu}. These results suggest that a single *RBM* on either arm can contribute to left arm trapping. In contrast, right arm was capture was statistically indistinguishable between each of the single *RBM* remaining mutants ($P<0.01$) and RBM_{5mu}.

We next examined trapping in strains harboring various combinations of two intact *RBM*s. Left arm trapping was statistically indistinguishable from wild-type as long as RBM_{L1} and at least one other *RBM* was intact (Fig. 2.12). In contrast, right arm trapping was not restored to wild-type levels ($P<0.01$) for any of the combinations examined, with the RBM_{L1} and RBM_{R2} combination being the combination most similar to wildtype. These results suggest that while the left and right arms both depend on RefZ and the *RBM*s to precisely capture the chromosome, the arms also have different requirements for accomplishing this function. More specifically, the left arm requires RBM_{L1} and at least one other *RBM*, while the right arm appears to require *RBM*s on both the left and right arms.

Discussion

One of the earliest morphological manifestations of *Bacillus* sporulation is the formation of the axial filament, an elongated, *oriC-ter-ter-oriC* conformation of the cell's two chromosomes (1, 149). RacA, Spo0J, and SMC contribute to axial filament formation by condensing the *oriC* region, creating a centromere-like element favorable for chromosome segregation (69, 70, 76, 77, 163). This element is tethered to the cell pole through interactions between RacA (bound to DNA at *ram* sites) and a membrane protein, DivIVA (76, 150). Another protein, Soj, also contributes to *oriC* capture by permitting segregation of approximately 15-20% of origins that otherwise fail to be captured in the forespore (69).

Although much is understood about factors that promote *oriC* segregation during sporulation, very little is known about how the cell manages to reproducibly divide over a precise portion of the forespore-destined chromosome. Wu and Errington observed that two regions located approximately 400 kb to the left and right of *oriC* (encompassing the left and right arm *RBM*s) are still captured in the forespore, even in genetic backgrounds where the remainder of the chromosome (including *oriC*) is generally captured in the mother cell compartment (17). This residual capture requires Spo0J, which led them to hypothesize that Spo0J creates an orientation of the chromosome that positions regions +/-400 kb from *oriC* in the vicinity of the division plane (17). Our data indicate that RefZ and the *RBM*s also contribute to determining the relative positioning of the chromosome arms with respect to the division plane. More specifically, we find that both

a Δ*refZ* mutant and an *RBM* mutant (RBM_{5mu}) show an increased propensity to capture regions of the chromosome that are normally excluded from the forespore.

RefZ and RBMs on both chromosomal arms help define the boundary of chromosome capture

We found that both RefZ, and *RBM*s located on each chromosomal arm are required to support a wild-type chromosome capture, but each arm responds somewhat differently to *RBM* perturbations. In general, for the reporters we tested, the right arm is more sensitive than the left arm to *RBM* mutations, and no combination of left and right *RBM*s tested was sufficient to support wild-type capture of the right arm (Fig. 2.12). In contrast, RBM_{L1} in combination with either RBM_{L2} or RBM_{R2} was sufficient to capture the left arm reporter at wild-type levels. The left arm also harbors the majority of the RacA and Spo0J binding sites (Fig. 2.1A). Therefore, we speculate that the phenotypic consequence of losing *RBM*-dependent organization might be partially dampened on the left arm by RacA-dependent tethering at the cell pole and/or Spo0J-dependent condensation of chromosomal DNA proximal to *oriC*. We found no evidence that deletion of *refZ* in Δ*racA* Δ*soj* or Δ*racA* Δ*soj* Δ*spo0J* mutant backgrounds lead to enhanced capture of reporters on the left and right arms (Miller and Herman unpublished). Thus, while RefZ is important for defining the region of chromosome captured at the time of cell division, this role appears to require that the systems that condense, organize, and segregate the DNA proximal to *oriC* are functioning.

RefZ and RBMs across Bacillus

The chromosomal position of predicted *RBM*s across the *Bacillus* genus reveals several patterns in *RBM* distribution (Fig. 2.1D and Fig. 2.2). In general, there are multiple *RBM*s on each arm that align fairly closely (especially on the right arm) with the region trapped during polar division in *B. subtilis*. In addition, many of the species, including *B. subtilis*, have one or more additional *RBM*s closer to *oriC* (*RBM*$_O$, in *B. subtilis*). The trapping assay data indicates that *RBM*$_O$ contributes to the overall arrangement of the chromosome during sporulation, although we did not pursue its specific role further. It is also important to note that the stringent criteria of our bioinformatics analysis likely underrepresent the number of motifs, which might include *RBM*s closer to *oriC* in other species (Fig 2.2).

We also observe that, compared to the *B. subtilis RBM*s (which were experimentally identified using ChIP-seq), the pathogenic *Bacillus* species (*B. anthracis*, *B. cereus*, and *B. thuringenesis*) have more *RBM*s, some with reduced spacing between them (not resolvable in Fig. 2.1D and 2.2). For example, we identified seven putative *RBM*s in *B. anthracis Ames*, two sets with less than 100 bp between them (83). The same pathogenic strains also encode a slightly different gene organization in the *refZ* region (Fig. 2.1C), the implication of which is not yet clear. Curiously, *B. anthracis Ames* RefZ appears to be generated as two distinct polypeptides, the first of which encodes the DNA-binding domain of the protein. The start and stop codons overlap by 1 nucleotide, consistent with the idea that the polypeptides may be translationally-coupled. The separation of RefZ domains was also found in the other *B. anthracis* strains we examined,

including *B. anthracis Sterne*, indicating that the genetic arrangement of the domains is unlikely to be a sequencing error.

Models for RefZ's role in chromosome organization and cell division regulation

The conservation of *RBM* chromosomal locations across the *Bacillus* genus argues that their role is position-dependent and critical for fitness in the environment, and we propose several models for how RefZ-*RBM* complexes might function in vivo. RefZ could bind to the *RBM*s and, possibly through interactions with SpoIIIE or another component of the cell division apparatus, fine-tune the positioning of the *RBM* DNA with respect to the division plane. One prediction of this model is that the placement of *RBM*s at ectopic sites should lead to a corresponding shift in the portion of DNA that is captured in the trapping assay. When we introduced RBM_{L1} and RBM_{R2} into the RBM_{5mu} strain at ectopic sites positioned 10° counterclockwise from their original positions, the resultant strain trapped the left and right arm reporters like the RBM_{5mu} parent. These data suggest that the region at which RefZ affects chromosome capture (presumably at the native *RBM* sites) may be secondary to other cellular restrictions. For example, the *B. subtilis RBM*s fall within a region that is noticeably devoid of Noc binding sites, possibly representing a "window" of chromosome that is favorable for FtsZ assembly. Introducing *RBM*s outside of this window could negate their contribution to overall organization because FtsZ assembly is already inhibited in those regions. Moreover, the *RBM*s may be present in specific configurations within the 3D landscape of the axial filament (promoted by proteins like RacA and Spo0J) that act upstream of a RefZ's position-sensitive function.

Multiple lines of evidence (82), including those in this study, suggest that RefZ acts as a negative regulator of cell division. If RefZ is a negative regulator of FtsZ activity during sporulation, then how might it function at the pole, where the FtsZ-ring assembles to promote division? We can envision several possibilities that are consistent with the known data. First, early in sporulation (before polar division occurs) RefZ could function as an inhibitor of FtsZ-ring assembly at the cell poles. Then, at the time when FtsZ redistributes from midcell toward the pole, its activity could be localized to another cellular location. Consistent with this model, RefZ-GFP localizes at the poles early in sporulation (60 min) and at midcell around the time of septation (75 min)(82). A non-exclusive model is that RefZ-mediated inhibition of FtsZ is spatially restricted to the immediate vicinity of the *RBM*s. In such a scenario, RefZ might influence the absolute positioning of the FtsZ-ring with respect to specific regions of the chromosome, but not necessarily inhibit polar cell division itself. Similarly, RefZ could function to inhibit additional FtsZ-rings from forming at the same pole of cells that fail to capture *oriC* after the first polar division. Lastly, it is possible that in its native context, RefZ may act as a positive regulator of polar cell division although data to support this interesting possibility are currently lacking.

The remarkable evolutionary conservation of RefZ and the *RBM*s across the genus argues that the system is critical for fitness in the environment. Excluding the sequences that control DNA replication initiation and termination, a relatively small number of well-characterized, non-coding and non-regulatory DNA motifs are conserved in chromosomal position either across multiple genera or among a given genus. The best characterized of these motifs are involved in regulating chromosome segregation and

condensation (164) and *ter* resolution following DNA replication (45). Other motifs are position-dependent even if their sequence degeneracy precludes identification in other species bioinformatically (76, 132, 135, 136). Excitingly, a growing body of evidence suggests that proteins that bind position-dependent motifs are often multifunctional, regulating cellular functions that are also position-dependent such as FtsZ polymerization (131, 135) and DNA translocase activity (165). It is attractive to speculate that many undiscovered chromosomal placeholders exist, possibly regulating processes like cell elongation and chromosome segregation. We anticipate that bioinformatic approaches will be central to navigating this largely unexplored area of prokaryotic biology.

Materials and Methods

General methods

All *B. subtilis* strains were derived from *B. subtilis 168*. *E. coli* and *Bacillus* strains utilized in this study are listed in Table 2.1. Plasmids are listed in Table 2.2. Oligonucleotide primers are listed in Table 2.3. Sporulation was induced by resuspension at 37°C according to the Sterlini-Mandelstam method (166). For microscopy experiments, all samples were grown in volumes of 25 ml in 250 ml baffled flasks in a shaking waterbath set at 280 rpm. For transformation and selection of *B. subtilis*, antibiotics were included at the following concentrations: 100 μg ml^{-1} spectinomycin, 7.5 μg ml^{-1} chloramphenicol, 10 μg ml^{-1} tetracycline, and 1 μg ml^{-1} erythromycin (erm) plus 25 μg ml^{-1} lincomycin (MLS).

Table 2.1 Strain table chapter II

Strain	Description	Reference/Figure
Parental		
B. subtilis PY79	*Bacillus subtilis* laboratory strain	(167)
B. subtilis 168	*Bacillus subtilis* laboratory strain 168 *trpC2*	Bacillus Genetic Stock Center (1A866)
WH320	Chemically mutagenized version of sequenced strain *B. megaterium DSM319*	MoBiTek
DH5α	*F^- endA1 glnV44 thi-1 recA1 relA1 gyrA96 deoR nupG Φ80dlacZΔM15 Δ(lacZYA-argF)U169, hsdR17(r_K^- m_K^+), λ–*	
DHP1	*F-, cya-99, araD139, galE15, galK16, rpsL1 (Strr), hsdR2, mcrA1,mcrB1;*	Obtained from Thomas Bernhardt
AH109	*MATa, trp1-901, leu2-3, 112, ura3-52, his3-200, gal4D, gal80D, LYS2::GAL1UAS-GAL1TATA-HIS3, GAL2UAS-GAL2TATA-ADE2, URA3::MEL1UAS-MEL1TATA-lacZ, MEL1*	Clontech
WH320		
BAM073	*P_{xylA}-$refZ_{Bsub}$ (amp) (tet)*	Fig. 2A
B. subtilis 168		
BAM071	*amyE::P_{hy}-$refZ_{Bmeg}$ (spec)*	Fig. 2B
BJH205	*RBM_{5mu}*	This work
BJH241	*lacA::P_{spoIIQ}-cfp (erm)*	This work
BJW556	*ycgO::P_{ftsW}-tetR-cfp (spec), $(tetO)_{48}$ΩRBM_{L2} region (cat)*	Fig. 2.9
BJH245	*lacA(-61°)::P_{spoIIQ}-cfp (erm), yycR(-7°)::P_{spoIIQ}-yfp (phleo), spoIIIE36-tet*	Fig. 2.12
BJH246	*RBM_{5mu}, lacA(-61°)::P_{spoIIQ}-cfp (erm), yycR(-7°)::P_{spoIIQ}-yfp (phleo), spoIIIE36-tet*	Fig. 2.12
BJH251	*refZ::cat, lacA(-61°)::P_{spoIIQ}-cfp (erm), yycR(-7°)::P_{spoIIQ}-yfp (phleo), spoIIIE36-tet*	Fig. 2.12
BJH253	*refZ::cat, amyE::P_{refZ}-refZ (spec), lacA(-61°)::P_{spoIIQ}-cfp (erm), yycR(-7°)::P_{spoIIQ}-yfp (phleo), spoIIIE36-tet*	Fig. 2.12
BJH292	*RBM_{5mu}, refZ::cat, lacA(-61°)::P_{spoIIQ}-cfp (erm), yycR(-7°)::P_{spoIIQ}-yfp (phleo), spoIIIE36-tet*	Fig. 2.12
BAM076	*+51°::P_{spoIIQ}-cfp (erm)*	This work/Fig. 2.9
BAM077	*RBM_{5mu}, +51°::P_{spoIIQ}-cfp (erm), yycR(-7°)::P_{spoIIQ}-yfp (phleo), spoIIIE36-tet*	Fig. 2.12
BAM078	*+51°::P_{spoIIQ}-cfp (erm), yycR(-7°)::P_{spoIIQ}-yfp (phleo), spoIIIE36-tet*	Fig. 2.12
BAM079	*refZ::cat, +51°::P_{spoIIQ}-cfp (erm), yycR(-7°)::P_{spoIIQ}-yfp (phleo), spoIIIE36-tet*	Fig. 2.12
BAM080	*RBM_{5mu}, refZ::cat, +51°::P_{spoIIQ}-cfp (erm), yycR(-7°)::P_{spoIIQ}-yfp (phleo), spoIIIE36-tet*	Fig. 2.12
BAM081	*refZ::cat, amyE::P_{refZ}-refZ (spec), +51°::P_{spoIIQ}-cfp (erm), yycR(-7°)::P_{spoIIQ}-yfp (phleo), spoIIIE36-tet*	Fig. 2.12
BAM175	*+RBM_{L1} (wt), lacA(-61°)::P_{spoIIQ}-cfp (erm), yycR(-7°)::P_{spoIIQ}-yfp (phleo), spoIIIE36-tet*	Fig. 2.12

Table 2.1 Continued.

Strain	Description	Reference/Figure
Parental		
BAM176	*+RBM_{L1} (wt), +51°::P_{spoIIQ}-cfp (erm), yycR(-7°)::P_{spoIIQ}-yfp (phleo), spoIIIE36-tet*	Fig. 2.12
BAM185	*+RBM_{L2} (wt), lacA(-61°)::P_{spoIIQ}-cfp (erm), yycR(-7°)::P_{spoIIQ}-yfp (phleo), spoIIIE36-tet*	Fig. 2.12
BAM186	*+RBM_{L2} (wt), +51°::P_{spoIIQ}-cfp (erm), yycR(-7°)::P_{spoIIQ}-yfp (phleo), spoIIIE36-tet*	Fig. 2.12
BAM193	*+RBM_{O} (wt), lacA(-61°)::P_{spoIIQ}-cfp (erm), yycR(-7°)::P_{spoIIQ}-yfp (phleo), spoIIIE36-tet*	Fig. 2.12
BAM194	*+RBM_{O} (wt), +51°::P_{spoIIQ}-cfp (erm), yycR(-7°)::P_{spoIIQ}-yfp (phleo), spoIIIE36-tet*	Fig. 2.12
BAM183	*+RBM_{R1} (wt), lacA(-61°)::P_{spoIIQ}-cfp (erm), yycR(-7°)::P_{spoIIQ}-yfp (phleo), spoIIIE36-tet*	Fig. 2.12
BAM184	*+RBM_{R1} (wt), +51°::P_{spoIIQ}-cfp (erm), yycR(-7°)::P_{spoIIQ}-yfp (phleo), spoIIIE36-tet*	Fig. 2.12
BAM357	*+RBM_{R2} (wt) lacA(-61°)::P_{spoIIQ}-cfp (erm), yycR(-7°)::P_{spoIIQ}-yfp (phleo), spoIIIE36-tet*	Fig. 2.12
BAM358	*+RBM_{R2} (wt), +51°::P_{spoIIQ}-cfp (erm), yycR(-7°)::P_{spoIIQ}-yfp (phleo), spoIIIE36-tet*	Fig. 2.12
BAM108	*+RBM_{L1} (wt), +RBM_{R2} (wt), lacA(-61°)::P_{spoIIQ}-cfp (erm), yycR(-7°)::P_{spoIIQ}-yfp (phleo), spoIIIE36-tet*	Fig. 2.12
BAM109	*+RBM_{L1} (wt), +RBM_{R2} (wt), +51°::P_{spoIIQ}-cfp (erm), yycR(-7°)::P_{spoIIQ}-yfp (phleo), spoIIIE36-tet*	Fig. 2.12
BAM117	*+RBM_{L2} (wt), +RBM_{R1} (wt), lacA(-61°)::P_{spoIIQ}-cfp (erm), yycR(-7°)::P_{spoIIQ}-yfp (phleo), spoIIIE36-tet*	Fig. 2.12
BAM116	*+RBM_{L2} (wt), +RBM_{R1} (wt), +51°::P_{spoIIQ}-cfp (erm), yycR(-7°)::P_{spoIIQ}-yfp (phleo), spoIIIE36-tet*	Fig. 2.12
BAM133	*+RBM_{L1} (wt), +RBM_{L2} (wt), lacA(-61°)::P_{spoIIQ}-cfp (erm), yycR(-7°)::P_{spoIIQ}-yfp (phleo), spoIIIE36-tet*	Fig. 2.12
BAM134	*+RBM_{L1} (wt), +RBM_{L2} (wt), +51°::P_{spoIIQ}-cfp (erm), yycR(-7°)::P_{spoIIQ}-yfp (phleo), spoIIIE36-tet*	Fig. 2.12
BAM140	*+RBM_{R1} (wt), +RBM_{R2} (wt), lacA(-61°)::P_{spoIIQ}-cfp (erm), yycR(-7°)::P_{spoIIQ}-yfp (phleo), spoIIIE36-tet*	Fig. 2.12
BAM141	*+RBM_{R1} (wt), +RBM_{R2} (wt), +51°::P_{spoIIQ}-cfp (erm), yycR(-7°)::P_{spoIIQ}-yfp (phleo), spoIIIE36-tet*	Fig. 2.12
BAM151	*+RBM_{L1} (wt), +RBM_{R1} (wt), +RBM_{R2} (wt), lacA(-61°)::P_{spoIIQ}-cfp (erm), yycR(-7°)::P_{spoIIQ}-yfp (phleo), spoIIIE36-tet*	Fig. 2.12
BAM152	*+RBM_{L1} (wt), +RBM_{R1} (wt), +RBM_{R2} (wt), +51°::P_{spoIIQ}-cfp (erm), yycR(-7°)::P_{spoIIQ}-yfp (phleo), spoIIIE36-tet*	Fig. 2.12
BAM156	*+RBM_{L2} (wt), +RBM_{R1} (wt), +RBM_{R2} (wt), lacA(-61°)::P_{spoIIQ}-cfp (erm), yycR(-7°)::P_{spoIIQ}-yfp (phleo), spoIIIE36-tet*	Fig. 2.12
BAM157	*+RBM_{L2} (wt), +RBM_{R1} (wt), +RBM_{R2} (wt), +51°::P_{spoIIQ}-cfp (erm), yycR(-7°)::P_{spoIIQ}-yfp (phleo), spoIIIE36-tet*	Fig. 2.12
DHP1		
CAM247	*spoIIIE-T25 (kan), refZ-T18 (amp)*	Fig. 2.9
CAM243	*spoIIIE-T25 (kan), empty-T18 (amp)*	Fig. 2.9

Table 2.2. Plasmid table chapter II

Plasmid	**Description**	**Reference/Figure/Use**
pDR111	*$P_{hyperspank}$-empty (amp) (spec)*	David Z. Rudner
pJH048	*amyE::$P_{hyperspank}$-$refZ_{B.meg}$ (amp) (spec)*	Fig. 2A
pHIS1522	*P_{xylA}-empty (amp) (tet)*	MoBiTek
pYD029	*P_{xylA}-$refZ_{B.sub}$ (tet)*	Fig. 2B
pJH026	*pminiMAD – RBM_{Omu} (amp) (erm)*	Creating RBM_O point mutants
pJH027	*pminiMAD – RBM_{L2mu} (amp) (erm)*	Creating RBM_{L2} point mutants
pJH028	*pminiMAD – RBM_{L1mu} (amp) (erm)*	Creating RBM_{L1} point mutants
pJH029	*pminiMAD – RBM_{R2mu} (amp) (erm)*	Creating RBM_{R2} point mutants
pJH030	*pminiMAD – RBM_{R1mu} (amp) (erm)*	Creating RBM_{R1} point mutants
pJW119	*$(tetO)_{48}$ΩRBM$_{L2}$ region (amp) (cat) (Cambell vector)*	Fig. 2.9
pAM030	*SUMO-RefZ (amp)*	Fig. 4
pAM125	*spoIIIE-T25 (kan)*	Fig. 2.9/B2H
pJW097	*T18-refZ (amp)*	Fig. 2.9 and Fig. 2.11/B2H
pJW101	*refZ-T18 (amp)*	Fig. 2.9 and Fig. 2.11/B2H
pAM132	*T18-sftA (amp)*	Fig. 2.11/B2H
pAM131	*T25-sftA (kan)*	Fig. 2.11/B2H
pAM130	*sftA-T18 (amp)*	Fig. 2.11/B2H
pAM129	*sftA-T25 (kan)*	Fig. 2.11/B2H
pCH363	*empty-T18 (amp)*	Tom Bernhardt/B2H vector
pCH364	*T18-empty (amp)*	Tom Bernhardt/B2H vector
pKNT25	*empty-T25 (kan)*	Tom Bernhardt/B2H vector
pKT25	*T25-empty (kan)*	Tom Bernhardt/B2H vector
pER19	*Cambell vector*	(168)
pminiMAD	*ori^{BsTs} (amp) (erm)*	{Kearns, 2005 #71}

Table 2.3. Oligonucelotide table chapter II

Oligo	Sequence 5' to 3'
OAM094	AAAAAGCTCTTCCGGTATGAAAGTAAGCACCAAAGACA
OAM095	TTTTTCTCGAGCTAGTTGGTGAGCGCCA
OAM098	CGATGGGAATTCATCATATTACAG
OAM099	TTAACGGGAGGAAATAATTCTATGAGTCGCTCATAGATGACATATAACGATCTGC
OAM100	TAATAAAACAGCGGAAGTCAGCATATACATTAATTTTTACGCTAAAAGCTTGG
OAM101	ATTCGAAAGTGGCTTGAGATTAC
OEB001	TCGACAATTAAAATCTGAATTCCTTC
OEB002	TATGGCTCGTCTTAAAGGCAGTTCTCGGTATCGTGGAGGTC
OEB003	GACCTCCACGATACCGAGAACTGCCTTTAAGACGAGCCATA
OEB004	CATCTTTGTTTCCCAGACAGC
OEB009	ATCAGCGCTCTGGTGATTG
OEB010	TTTTGCACAGCCTTAGCTTC
OEB012	GCGACACCTCATCATAACAA
OEB013	TTCCACCTCGCCGTAGATTC
OEB014	CCGCGCTTATGTACAGCATA
OEB015	AGCTTTAGCGGATCCGTGAT
OEB016	TTAAAGAACCGCTATGTCAG
OEB017	TGTATTCCTATACTACCACG
OEB018	TGGGCCATCTGCTCCATT
OEB019	GAGGACCCGTTTAAATGGAAGC
OEB020	GAAAACGAGAAATTTTCACACTC
OEB021	TTTTCTTCTTTTGACCGGCT
OEB027	ATTGAGAGTGCTAACAGAGGTGATG
OEB028	GTTGCAGAGCTAAATGTGATTTCATC
OEB029	GAAAACAAAACGATTAACTTTCCG
OEB030	GTGCTGTCTTAGGTACATGACAAC
OEB031	GCCTGAGTTCCATGATATCAC
OEB032	CTGCAATTTTCCATCTCTTCATA
OJH063	GGGAAATGTACAATGAAAGTAAGCACCAAAGACAAAATT
OJH064	GCCGGCATGCGGGTTGGTGAGCGCCACGTCTC
OJH112	CCATGGTACCGAAGCTGATTTGGTCAAGGTA
OJH113	GAGCTCGAGTGATTAAAACAAATAGCCCCC
OJH115	ACCGTAACAAGCTTTACACCA
OJH116	CCATGTCGACCAGGGAAAAAAAGTGCTCCTG
OJH117	CTCGAGCTCTTAACTGATCTGCTGCTT
OJH119	CCGAGCCGAATTCTTTCTCTA
OJH120	GGATCGGCCGGCTGGATTCAA
OJH121	GAGCTCGAGTCATTAAAAAAAGCCGTTCCC
OJH123	AATGGAATTCGCCATGATCAATAGCATTCA
OJH124	CATTCGGCCGCATCGGGATTCCTGCTGTAAC
OJH125	CTCGAGCTCTTAAGACTTTCCCGGCTT
OJH127	TCAAGAATTCCTTTCGTCATC
OJH128	CATTCGGCCGCTGGCAGGACTGGATGATCTC
OJH129	CTCGAGCTCTTAAGTGTTTCTATCCGC
OJH147	AATGGAATTCCGGCTGAGCTTTTGCACA
OJH152	TATTTGTTTTAATCACTCGAGCTCTCAAAACGAAAAGGCGGTCAA
OJH153	CAGATCAGTTAAGAGCTCGAGTAATCAAAGAAGACATTCCTTTAC
OJH154	TTTTTTTAATGACTCGAGCTCTTAAACATAATGAGCGTATTTTT
OJH155	GGAAAGTCTTAAGAGCTCGAGTGATGAAGGCTGTCTGGG
OJH156	AGAAACACTTAAGAGCTCGAGTGATTCACTTACAAATGCAGA

Table 2.3. Continued.

Oligo	Sequence 5' to 3'
OJH201	GCGACTCATAGAATTATTTCCTCC
OJH202	ATGTATATGCTGACTTCCGCTGT
OJW167	GCATGCATGCGTAACACACAGGAAACAGCTATGAAAGTAAGCACCAAAGACAA AATTA
OJW168	GCATGGATCCGAACCGCTACCGTTGGTGAGCGCCACGTCTCCT
OJW197	CGCGAATTCGCTGCTTAAAATTGGACCCATACG
OJW198	GCCGCTAGCTGCATGTCCGTTCTGTCAGCC
OKK034	CGCAAGCTTACATAAGGAGGAACTACTATGGCTGTACAGTCAAAAACG
OKK035	TTTGCTAGCCGGTGTTAGGATAATTGAACGCG
OKK060	GCATTCTAGAGTAACACACAGGAAACAGCTATGAGTGTGGCAAAGAAAAAA
OKK061	GCATGAATTCGAACCGCTACCGTTAGAAGAGAGCTCATCATATT
OKK064	GCATTCTAGAGTAACACACAGGAAACAGCTATGAGTTGGCTTCATAAATTT
OKK065	GCATGAATTCGAACCGCTACCGTTTTCGTTTATTAAATCACT
OKK066	GCATGGATCCGGGCAGCGGTATGAGTTGGCTTCATAAATTTTT
OKK067	GCATGAATTCTTATTCGTTTATTAAATCACTTGC

Microscopy

Fluorescence microscopy was performed with a Nikon Ti-E microscope equipped with a CFI Plan Apo lambda DM 100X objective, and Prior Scientific Lumen 200 Illumination system, C-FL UV-2E/C DAPI, C-FL GFP HC HISN Zero Shift, C-FL YFP HC HISN Zero Shift, and C-FL Cyan GFP, filter cubes, and a CoolSNAP HQ2 monochrome camera. Membranes were stained with either TMA-DPH (0.02 mM) or FM4-64 (3 µg ml^{-1}) (Life Technologies) and imaged with exposure times of 200-1000 msec. All images were captured with NIS Elements Advanced Research (version 4.10), and processed with Adobe Photoshop (version 12.0) and ImageJ64 (169). Cells were mounted on glass slides with polylysine-treated coverslips prior to imaging.

RefZ swapping

For the *refZ* swapping experiment, cultures were grown in LB liquid media to midlog, back-diluted to an OD_{600} of ~0.05 and induced with 0.5% (w/v) xylose (BAM073) or 1.0 mM isopropyl-beta-D-thiogalactopyranoside (BAM071). At 60 min post-induction, samples were collected, stained with TMA imaged as described in microscopy.

RefZ-6His protein purification

To obtain RefZ-6His, BL21(λDE3)pLysS cells were freshly transformed with pLM025. To obtain SUMO-RefZ, BL21(λDE3)pLysS was freshly transformed with pAM030. All protein overexpression cultures were grown in Cinnabar high-yield protein expression media (Teknova) supplemented with 25 μg/ml kanamycin, 25 μg/ml chloramphenicol, and 0.1% (w/v) glucose. Overnight starter cultures were avoided. A 25 ml culture in a 250 ml baffled flask was grown in a shaking waterbath at 300 rpm, 37°C to an OD_{600} of approximately 5 and expression was induced by the addition of 1 mM final IPTG. Cultures were grown to an OD_{600} of 10 to 15 and cells were harvested by centrifugation. Pellets were stored at -80°C prior to processing. To lyse cells, pellets were resuspended in 25 ml of lysis buffer (50 mM Tris-HCl [pH 9.0], 300 mM KCl, 25 μl of 1 mg/ml DNaseI, and 50 μl of Protease Inhibitor Cocktail (Sigma). The sample was passaged through a French press cell three times at 10,000 PSI and then spun at 24,000 x g for 30 min to pellet cell debris. The supernatant was applied to a 0.5 ml bed volume of pre-equilibrated Ni-NTA (Qiagen) and washed with 5 ml wash buffer (50 mM Tris-HCl [pH 9.0], 300 mM KCl, 20 mM imidazole, and 10% glycerol). The protein was eluted

with 2 ml elution buffer (50 mM Tris-HCl [pH 9.0], 300 mM KCl, 250 mM imidazole, and 10% glycerol) and collected in eight 250 µl fractions. Peak fractions were pooled (typically ~2 ml total) and the imidazole was removed by buffer exchange using a 10,000 kDa molecular weight cutoff spin filter and 50 mM Tris-HCl [pH 9], 300 mM KCl, 10% glycerol. The purified protein was then stored at -80^{o}C in aliquots until use. Each 25 ml culture typically yielded ~1 mg of protein.

Analysis of RefZ-RBM interaction using electrophoretic gel mobility shift assays

DNA fragments (~150 bp/each) were generated for the gel-shifts by PCR amplification of DNA centered on the native *RBM*s (using *B. subtilis* 168 as template) or mutant *RBM*s (using RBM_{5mu} as template). Fragments were generated using the following primer pairs: RBM_{L1}, oEB012 and oEB013; RBM_{L2}, oEB009 and oEB010; RBM_{O}, oEB014 and oEB015; RBM_{R1}, oEB016 and oEB017; RBM_{R2}, oEB018 and oEB019; RBM_{T1}, oEB027 and oEB028; RBM_{T}, oEB029 and oEB030; RBM_{T3}, oEB031 and oEB032; DNA binding reactions were prepared according to directions of the SYBR Green EMSA Nucleic Acid Gel Stain kit (Life Technologies) except that instead of binding buffer, the samples were prepared in ddH20 [pH 6.7]. Incubation of the samples in KCl or NaCl-based DNA-binding buffers significantly reduced the affinity of RefZ for the *RBM*-containing DNA. After 30 min incubation, 10X DNA loading buffer (45% glycerol, 50 mM EDTA [pH 8], and 1 mM Tris-HCl [pH 8]) was added to a final concentration of 1X and samples were resolved on a 5% Mini-PROTEAN TBE polyacrylamide gel (Biorad). After electrophoresis, the gel was stained with SYBR Green EMSA gel stain (Life Technologies) for 20 min. The gel was then washed and

DNA was visualized with a Typhoon Trio fluorescence imager (GE Healthcare) at an excitation wavelength of 488 nm.

Quantitative forespore chromosome trapping assay

Assays were carried out as previously described (69). An *oriC*-proximal reporter (-7° P_{spoIIQ}-*YFP)* was trapped in the forespores in greater than 99.5% for both wildtype and all of the mutants examined, and thus served as a baseline for σ^F activity. The chromosomal arms harbored either the left (-61° P_{spoIIQ}-*CFP*) or the right (+51° P_{spoIIQ}-*CFP*) reporters. Cell membranes were stained with TMA as described in microscopy. YFP, CFP, and TMA (C-FL UV-2E/C DAPI filter) images were captured 2.5 hrs after cells were resuspended in sporulation media (166). Images for eighteen biological replicates were captured for wild-type and RBM_{5mu}. Images for at least three biological replicates were captured for all other strains. To quantitate the number of cells with the experimental reporters trapped in the forespore, the CFP images were overlaid with the control YFP channel and TMA (membrane stain). Forespores containing YFP, CFP, or both from three independent fields (n>500 cells per trial) were counted manually for each biological replicate. Forespores trapping the -61° or +51° reporters, but not the -7° reporter were also counted, and generally represented less than 0.5% of cells counted. Forespores devoid of any fluorescent signal were rarely observed and were not counted. The percentage of forespores with CFP signal (indicating trapping of the left or right arm reporter) was plotted using Microsoft Excel. The averages and standard deviations are shown in Fig. 2.12. Statistical significance (P-values) was determined using a student's t-test.

Two-hybrid analysis

Bacterial two hybrids were performed as described (170) with the following modifications: cloning was carried out in the presence of 0.2% glucose. Cells harboring the relevant pairwise interactions were grown to early exponential phase in LB with 0.2% glucose, ampicillin (50 μg/ml), and kanamycin (25 μg/ml). Five μl of equivalent OD_{600} cultures were spotted on M9-glucose minimal media plates containing 40 μg/ml X-Gal, 250 μM isopropyl-β-D-thiogalactopyranoside, ampicillin (50 μg/ml), and and kanamycin (25 μg/ml). Plates were incubated at room temperature in the dark for 50 to 70 hrs for color development prior to image capture. We found that spotting liquid cultures on M9-glucose produced clearer, more reproducible differences in color development that were not detectable on LB media or with 37°C incubation.

Strain and plasmid construction

Right Arm (+51°) Reporter Construction

The *+51°::P_{spoIIQ}-cfp (erm)* reporter for the right arm trapping experiments (BAM076) was created by Gibson Assembly (171). Briefly, dsDNA in the *+51°* region were amplified from *Bs168* genomic DNA using primers sets OAM098/OAM099 ("UP") and OAM100/OAM101 ("DOWN"). The reporter portion was generated by PCR amplification of genomic DNA from BJH241, a strain harboring *lacA::PspoIIQ-cfp* (erm)(69), using primer set OJH201/OJH202. The three products were combined in a one-step enzymatic assembly reaction and transformed directly into *B. subtilis 168* selecting for MLS resistance. The final strain was confirmed by PCR.

Plasmid Construction

pAM030 was generated by cloning PCR product from OAM094 and OAM095 amplification of *Bs168* genomic into pTB146 (SapI-XhoI).

pAM125 was generated by cloning PCR product from OKK060 and OKK061 amplification of *Bs168* genomic into pKNT25 (XbaI-EcoRI).

pAM129 was generated by cloning PCR product from OKK064 and OKK065 amplification of *Bs168* genomic into pKNT25 (XbaI-EcoRI).

pAM130 was generated by cloning PCR product from OKK064 and OKK065 amplification of *Bs168* genomic into pCH363 (XbaI-EcoRI).

pAM131 was generated by cloning PCR product from OKK066 and OKK067 amplification of *Bs168* genomic into pKT25 (BamHI-EcoRI).

pAM132 was generated by cloning PCR product from OKK066 and OKK067 amplification of *Bs168* genomic into pCH364 (BamHI-EcoRI).

pJH026 was generated with overlap extension PCR. The "UP" product was amplified from *Bs168* genomic with primer pair OJH128/OJH129. The "DOWN" product was amplified from *Bs168* genomic with primer pair OJH156/ OJH147. The two PCR products were used as template for overlap extension PCR with primer pair OJH128/147. The amplified fragment was cut with EcoRI and KpnI and cloned into pminiMAD cut with the same enzymes.

pJH027 was generated with overlap extension PCR. The "UP" product was amplified from *Bs168* genomic with primer pair OJH112/OJH113. The "DOWN" product was amplified from *Bs168* genomic with primer pair OJH152/ OJH115. The two PCR products were used as template for overlap extension PCR with primer pair OJH112/115. The amplified fragment was cut with EcoRI and KpnI and cloned into pminiMAD cut with the same enzymes.

pJH028 was generated with overlap extension PCR. The "UP" product was amplified from *Bs168* genomic with primer pair OJH116/OJH117. The "DOWN" product was amplified from *Bs168* genomic with primer pair OJH153/ OJH119. The two PCR products were used as template for overlap extension PCR with primer pair OJH116/119. The amplified fragment was cut with SalI and EcoRI and cloned into pminiMAD cut with the same enzymes.

pJH029 was generated with overlap extension PCR. The "UP" product was amplified from *Bs168* genomic with primer pair OJH120/OJH121. The "DOWN" product was amplified from *Bs168* genomic with primer pair OJH154/ OJH123. The two PCR products were used as template for overlap extension PCR with primer pair OJH120/123. The amplified fragment was cut with EagI and EcoRI and cloned into pminiMAD cut with the same enzymes.

pJH030 was generated with overlap extension PCR. The "UP" product was amplified from *Bs168* genomic with primer pair OJH124/OJH125. The "DOWN" product was amplified from *Bs168* genomic with primer pair OJH155/ OJH127. The two PCR products were used as template for overlap extension PCR with primer pair OJH124/127. The amplified fragment was cut with EagI and EcoRI and cloned into pminiMAD cut with the same enzymes.

pJH047 was generated by was generated by cloning PCR product from OKK034 and OKK035 amplification of *Bacillus megaterium* WH320 genomic into pDR111 (HindIII-EcoRI).

pJW087 was generated by was generated by cloning PCR product from OJW152 and OJW153 amplification of PY79 genomic into pGADT7 (EcoRI-BamHI).

pJW089 AD was generated by was generated by cloning PCR product from OJW152 and OJW153 amplification of PY79 genomic into pGBKT7 (EcoRI-BamHI).

pJW096 was generated by cloning PCR product from OJW167 and OJW168 amplification of PY79 genomic into pKNT25 (SphI-BamHI).

pJW097 was generated by cloning PCR product from OJW167 and OJW168 amplification of PY79 genomic into pCH363 (SphI-BamHI).

pJW101 was generated by cloning PCR product from OJW171 and OJW172 amplification of PY79 genomic into pCH363 (EcoRI-BamHI).

pJW119 was generated by cloning PCR product from OJW197 and OJW198 amplification of PY79 genomic into (EcoRI-NheI) into pER19 harboring a $(tetO)_{48}$ fragment at NheI-HindIII site.

pYD029 was generated by cloning PCR product from OJH063 and OJH064 amplification of *Bs168* genomic into pHIS1522 (BsrGI-SphI).

CHAPTER III: REFZ DEFINES THE PRECISE REGION OF CHROMOSOME CAPTURE THROUGH FtsZ DURING *Bacillus* SPORULATION

Introduction

To regulate processes spatially, the distribution of at least some macromolecules within a cell must, by definition, be non-uniform. One way that cells generate subcellular organization to localize cellular activities is to utilize proteins that can partition to and sometimes create membrane curvature (172, 173); these proteins, can then act as platforms to recruit additional factors. Localization can also be controlled by harnessing intrinsic properties of molecules, such as diffusion rates, oligomerization potential, and affinity for other molecules. For example, the ParABS system of *Caulobacter crescentus* generates a nucleoid-dependent protein gradient to segregate chromosomes (63). In this system, The ATPase ParA dimerizes and binds the nucleoid non-specifically in the presence of ATP. DNA-binding restricts ParA mobility establishing a gradient of ParA biased towards the new cell pole. ParB binds to *parS* sites located near the origin of replication (*oriC*), but also interacts with ParA, stimulating ATP hydrolysis and release of ParA from the nucleoid. ParB's affinity for ParA drives the net movement of ParB-*parS* complexes (and *oriC*) toward the pole, thus facilitating chromosome segregation (62, 63).

Another way that cells create subcellular organization is to associate proteins in large, multiprotein complexes to localize, coordinate, and regulate their activities. For example, cell division is accomplished by the coordinated synthesis and turnover of all layers of the cell envelope by the divisome, a multisubunit complex comprised of over 30

proteins (174). Numerous studies indicate that the bacterial envelope is highly organized and possesses topological features utilized by the cell to spatially regulate physiological processes.

In recent years the nucleoid has also emerged as an important cellular landmark utilized by proteins to spatially regulate processes. The activity of a DNA-binding protein is restricted to a specific subcellular location by its affinity for specific DNA motifs. The best characterized examples of this class of proteins are transcription factors, which only affect transcription at promoters they associate with. However, there are also examples of DNA-binding proteins that bind to specific DNA motifs to regulate the initiation of DNA replication (SpoOJ/Soj) (175), mediate DNA repair and recombination (MutL, XerCD) (176, 177), and segregate chromosomes (ParAB, Spo0J/SMC) (62, 63, 68, 69).

Additionally, some DNA-binding proteins simultaneously interact with the nucleoid and the components of the cell envelope to control DNA replication (DnaA, SeqA) (178, 179), organize (RacA, SMC) (34, 74, 76) and segregate (FtsK/SpoIIIE) (162, 180) the chromosome, and regulate cell division (Noc, SlmA) (132, 136). One of the best studied examples of this type of regulation is illustrated by the *Escherichia coli* nucleoid occlusion (NO) factor SlmA. SlmA is a TetR family protein that binds to at least 24 motifs (SBSs) distributed throughout the chromosome except proximal to the terminus (*ter*) region (135). SlmA-SBS complexes are capable of directly inhibiting oligomerization of the cell division protein FtsZ (104, 132, 135). By restricting its activity to sites of SBS enrichment, SlmA can effectively inhibit the formation of FtsZ rings (Z-rings) over the bulk nucleoid without affecting the assembly of Z-rings at midcell (where the *ter* region is

localized at the time of cell division) (104, 132, 135). In this case, SlmA appears to utilize the chromosome as a landmark to localize its FtsZ-inhibitory function.

In addition to nucleoid occlusion, at least two additional systems act to ensure FtsZ rings only assemble at midcell between chromosomes. The Min system utilizes both cell geometry and protein-protein interactions to inhibit FtsZ polymerization in the nucleoid-free regions of the cell. Nucleoid-free regions are present not only near the cell poles, but also at future cell poles on either side of newly initiated midcell division sites (68). More recently, ZapA, ZapB, and the DNA-binding protein MatP, were shown act in the *ter* region to promote midcell FtsZ ring positioning in *E. coli* (118, 119). Thus it appears that cells have evolved multiple, sometimes redundant strategies to ensure daughter cells each inherit intact copies of the genome, thereby safeguarding reproductive success.

Like *E. coli*, *B. subtilis* possesses both a Min system (181) and an NO system (136) that act concertedly to inhibit non-medial Z-ring formation. The NO system of *Bacillus* is also comprised of a DNA-binding protein (Noc) and its cognate binding sites (NBSs) that are distributed throughout the chromosome except near the *ter* region. Noc associates with the cell envelope and NBSs simultaneously, possibly forming a complex that occludes or disrupts the association and nucleation of FtsZ filaments at/along the membrane (130). Noc is a homolog of ParB, a protein involved in regulating replication (175) and segregation of DNA (28, 69, 182).

During *B. subtilis* sporulation, a number of morphological changes occur to facilitate spore formation, including a dramatic adjustment in the location of cell division site. The cell's two chromosomes are stretched from pole to pole in an elongated *oriC-ter-ter-oriC* configuration called the axial filament (15, 16) and FtsZ coalesces at a cell

quarter position and septation occurs over the bulk nucleoid. This new arrangement requires that both Min inhibition of polar cell division and NO inhibition of septation over the nucleoid be relieved (or overcome), indicating additional mechanisms to regulate FtsZ dynamics during sporulation are required. The redistribution of the FtsZ inhibitory protein MinD from a cell quarter position region to the distal pole may contribute to the alleviation of Min inhibition at the cell quarter (183). Regarding NO, Wu et al. have proposed that the axial filament may be arranged such that relatively few Noc binding sites are positioned at the site of incipient septation (130).

The shift of FtsZ from midcell toward the pole is promoted, at least in part, by increasing expression of *ftsZ* and by expression of a membrane-associated sporulation protein, SpoIIE (74). Following septation, the larger mother cell possesses an entire chromosome, whereas the forespore initially captures only one-quarter to one-third of the second chromosome; the remainder of the captured chromosome is threaded through the septum to the mother cell via a DNA pump (SpoIIIE) that assembles around the chromosomal arms at the time of division (16, 162). This unusual arrangement necessitates that SpoIIIE directionally pump the remainder of the second chromosome into the forespore before spore development proceeds. To avoid chromosome breakage, capture a reproducible complement of DNA in the forespore, and pump the forespore-destined chromosome in the correct direction (an event which requires successful capture of *oriC* on the forespore side of the septum), there must be coordination between cell division proteins, SpoIIIE, and the forespore-destined chromosome. How this orchestration occurs at the molecular level remains a mystery.

It is known that precise division over the forespore-destined chromosome requires RefZ, a TetR family protein that is maximally upregulated during early sporulation, first via σ_H, the stationary phase sigma factor (184), and then by Spo0A~P, the activated form of the master response regulator of sporulation (185, 186). RefZ binds to five specific DNA motifs (*RBMs*) located on both chromosomal arms at positions that are conserved across the *Bacillus* genus (82, 83). The *RBMs,* which are positioned along the axial filament at/near the incipient site of polar cell division, are also required for precise chromosome capture (82, 83). The Δ*refZ* mutant has a propensity to overcapture regions of the chromosome adjacent to the *RBMs* in the forespore. Aside from this, there are two other phenotypes associated with perturbation of RefZ activity: first, a Δ*refZ* mutant is modestly delayed in assembly of polar FtsZ rings during sporulation (82). Second, misexpression of RefZ during vegetative growth disrupts Z-rings and inhibits cell division. RefZ's FtsZ-inhibitory activity is lost in variants that do not bind DNA (82). By analogy to the TetR family protein SlmA, these data led us to hypothesize that RefZ-*RBM* complexes might fine-tune FtsZ dynamics/positioning near the site of polar division.

To test this model, we isolated and characterized 10 RefZ loss-of-function (rLOF) variants, each capable of binding *RBMs*, but unable to inhibit cell division under misexpression conditions. When introduced at the wildtype (WT) *refZ* locus, each of the rLOF variants largely phenocopied a Δ*refZ* mutant in that they overcaptured regions on each chromosomal arm in the forespore. These results are consistent with a model in which RefZ plays a role in precise chromosome capture through regulation of FtsZ. To better understand the molecular basis of RefZ's activity, WT RefZ and the rLOFs were overexpressed and purified, and structural and biochemical characterization was carried

out. Collectively, our data suggest RefZ can exist as a monomer or dimer in solution, and moreover, RefZ's dimerization state both on and off DNA, likely controls its capacity to influence FtsZ dynamics in vivo.

Results

Identification of RefZ residues required for regulation of cell division

When RefZ is misexpressed during vegetative growth, it disrupts FtsZ ring formation and inhibits cell division (Fig. 3.1C, WT +IPTG). Cell division can be restored by mutations in *ftsZ* or by doubling the copy number of the *ftsAZ* operon (82). Division is also restored in cells expressing rLOF variants with substitutions (Y43A and Y44A) in the DNA-recognition helix of RefZ's helix-turn-helix (HTH) domain (82), suggesting that the DNA-binding activity of RefZ is required for inhibition of cell division (82). A strain harboring point mutations in the five *oriC*-proximal RefZ binding sites (RBM_{5mu}) phenocopies the trapping defect of the Δ*refZ* mutant, suggesting that RefZ-*RBM* association likely mediates RefZ's role in chromosome capture (83). We hypothesized that RefZ associates with the *RBMs* to modulate FtsZ dynamics in the vicinity of the septum, and that this modulation is responsible for ensuring proper chromosome capture. Furthermore, we predicted that additional regions of RefZ (outside the DNA-binding domain) would be important for RefZ-dependent regulation of FtsZ.

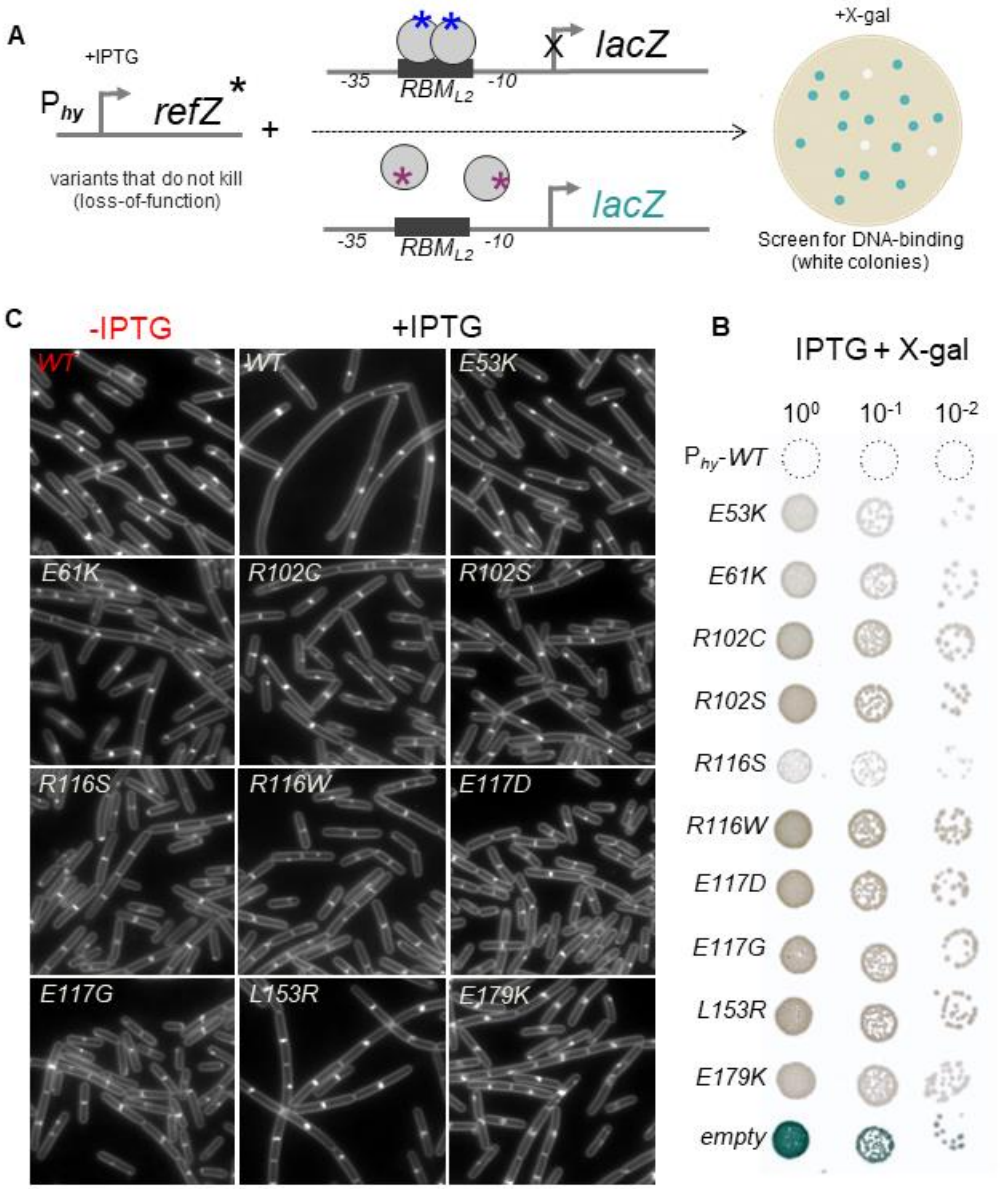

Figure 3.1. Identification and characterization of rLOF variants. **(A)** Schematic of genetic selection and blue/white screening of rLOF *RBM* interactions. *refZ* was mutagenized by PCR, placed under an IPTG promoter, and introduced into the *amyE* locus of the *B. subtilis* chromosome by double crossover recombination (left). In the Δ*minD* Δ*refZ* genetic background, rLOF variants that do not inhibit cell division will survive. An *RBM* was placed between the -35 and -10 of a constitutive promoter upstream of *lacZ*. In the presence of X-gal, expression of rLOFs that cannot bind the *RBM* (due to truncation, misfolding, or specific changes that decrease RefZ's affinity for the *RBM*) results in *lacZ* expression and blue colonies, whereas rLOFs that bind the *RBM* appear white. **(B)** Ten unique rLOF variants were isolated that bind the *RBM* but do not inhibit cell division. rLOF variants in a clean parental selection-screen background were grown in LB to midlog. Cultures were normalized to OD, serially diluted in fresh LB, and spotted on LB plates supplemented with spectinomycin, 1mM IPTG, and X-gal. **(C)** The extent of division inhibition resulting from expression of each rLOF was monitored by fluorescence microscopy 90 min after addition of inducer (1.0 mM IPTG). Misexpression of WT RefZ causes cell filamentation compared to the uninduced control (red). Membranes are stained with TMA.

To test these hypotheses, we designed a powerful, two-step genetic selection and screen to isolate rLOF variants capable of binding to the *RBMs,* but no longer able to inhibit FtsZ (Fig. 3.1A). First, we took advantage of the fact that artificially inducing *refZ* (misexpression) in a background devoid of a functional Min system kills cells on solid medium (82); thus, this background allowed us to select for mutations that restored growth. We therefore used a recipient strain for the selection in which *minD* was deleted (to create a sensitized background) and *refZ* was deleted (to ensure no native RefZ would be expressed). Next, *refZ* was mutagenized by error-prone PCR and assembled into an IPTG-inducible misexpression construct using enzymatic assembly (171). This misexpression construct was marked with a spectinomycin resistance cassette, and flanked by regions of homology to *amyE,* a non-essential locus in the *B. subtilis* chromosome. *B. subtilis* transformation conditions were optimized so the linear assembled DNA products could be introduced directly into cells, allowing simultaneous selection for double crossover integration of the misexpression cassette and RefZ resistance. In this genetic background, expression of WT RefZ from an IPTG-inducible promoter kills cells, whereas expression of rLOFs variants unable to inhibit cell division results in colony formation. Before introducing the mutant library, we also integrated a *lacZ* transcriptional reporter fusion with an *RBM* sequence between the -35/-10 regions of a σ^A-dependent promoter at a second ectopic locus (*sacA*). This reporter allowed as to monitor the ability of the rLOFs to bind DNA. In the presence of inducer and the β-galacosidase substrate X-gal, expression of rLOFs that cannot bind the *RBM* (due to truncation, misfolding, or decreased affinity for the *RBM*) results in blue colonies, whereas expression of rLOFs capable of binding the *RBM* produce white colonies (Fig. 3.1B).

Using this two-step selection/screen we obtained ~1,300 survivors, 37 of which were either white or pale blue when patched onto X-gal and IPTG-containing media, indicating these mutants were capable of repressing *lacZ* expression from the *RBM*-containing promoter. Since resistance to RefZ can also be conferred by suppressor mutations in *ftsZ* (82), the 37 misexpression constructs were transformed into a clean screening background, and resistance and *RBM*-binding were reassessed. Four candidates failed to survive on IPTG plates, indicating the possible presence of suppressor mutations in the primary isolate strain, while an additional four turned blue on X-gal indicator medium. The *refZ* locus was sequenced for the remaining 29 rLOF candidates that maintained LacZ repression.

Ten unique single-point mutations corresponding to the 10 RefZ variants shown in Fig. 3.1B were identified (those with more than one mutation were not characterized further). In a WT background, none of the rLOFs inhibited cell division following misexpression (Fig. 3.1C) (82, 83). Since the variants were capable of binding *RBMs* in vivo, we considered it unlikely that the proteins were misfolded or unstable. Consistent with this conclusion, Western blot analysis of the misexpressed variants showed that each produced full-length protein and was present at levels comparable to WT (Fig. 3.2).

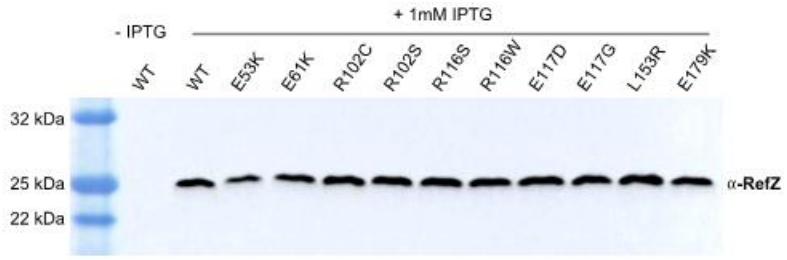

Figure 3.2. rLOFs are present at levels indistinguishable from WT. Western blot analysis demonstrating stable levels of the rLOFs variants following induction. Strains were induced during exponential growth with 1.0 mM IPTG and collected after 45 minutes of growth. Lysate loads were normalized by OD_{600} values and run on a 4-20% Tris-Glycine gel (Lonza) before transfer to nitrocellulose. Polyclonal α-RefZ antibody was used to probe for RefZ. RefZ is absent in the -IPTG lane demonstrating that expression is dependent on the presence of inducer. The native copy of *refZ* (under control of its native promoter) is not expressed during exponential growth. The experiment was repeated with three biological and experimental replicates with equivalent results.

RefZ variants unable to inhibit cell division (rLOFs) overcapture regions of the forespore chromosome

To determine if RefZ-mediated chromosome capture was correlated with the ability to inhibit cell division, we introduced each of the rLOF mutant genes into the native *refZ* locus. The recipient strains harbored either left (–61°) or right (+51°) arm fluorescent reporters fused to a forespore-specific promoter to report on capture of these chromosomal regions in the forespore (83). The resultant strains were induced to sporulate and capture of the reporters in the forespore was assessed using fluorescence microscopy coupled to single cell quantitation (83). We hypothesized that if RefZ acts through FtsZ to mediate precise chromosome capture, then the rLOF variants would phenocopy the Δ*refZ* mutant with regard to chromosome capture. As observed previously (83), a Δ*refZ* mutant and a strain possessing mutant *RBMs* (*RBM_{5mu}*) both exhibited a ~2-fold increase in the frequency of capture for both the left and right arm reporters (Fig. 3.3). Moreover, all but one of the $RefZ^{LOF}$ variants displayed left and right arm overcapture

defects indistinguishable from the Δ*refZ* mutant. The R116S variant phenocopied the Δ*refZ* mutant in left arm capture, but displayed an intermediate defect in right arm capture (Fig. 3.3). These results strongly suggest that the same residues required for RefZ's division inhibition activity are also required for precise chromosome capture. These data are consistent with a model in which RefZ-*RBM* complexes modulate FtsZ activity to influence the location of cell division relative to the chromosome.

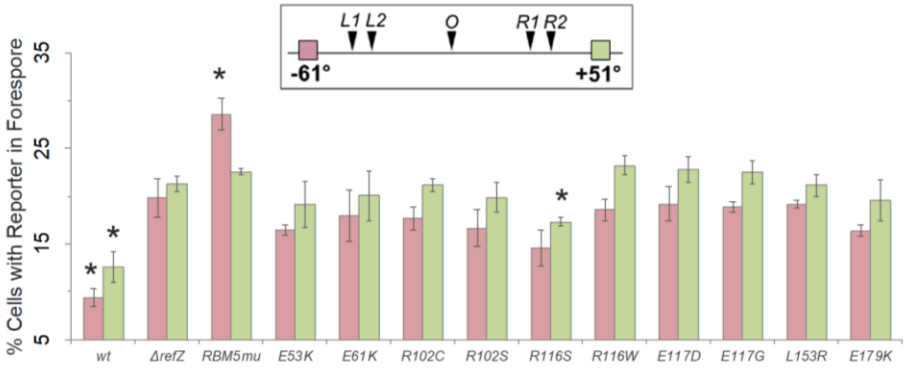

Figure 3.3. Chromsome capture for the rLOF variants. Single cell analysis indicating the average percentage of cells that captured either the left arm (–61°) or right arm (+51°) reporter in the forespore at the time of polar division. Bars represent standard deviations. The rLOF variants, with the exception of R116S (+51°), phenocopy the Δ*refZ* mutant with regard to chromosome capture ($P<0.05$). +51° capture in the R116S variant (*) did not phenocopy the Δ*refZ* mutant ($P = 0.04$), but was distinct from wt ($P<0.05$). A minimum of 1,500 cells from three biological replicates were counted for each strain.

Structural characterization of RefZ

We reasoned that structural characterization of RefZ and mapping of the rLOF variants could provide mechanistic insight for how RefZ targets FtsZ. In order to screen for RefZ crystals, it was necessary to optimize a protocol to overexpress and purify milligrams of soluble protein. RefZ was not soluble when expressed with a GST or N or C-terminal 6XHis tag in LB Lennox broth. However, overexpression of RefZ-6His in Cinnabar Expression Medium (Teknova) produced soluble RefZ. Cinnabar is a high yield, buffered medium with a proprietary composition of vitamins, minerals, and cofactors that allow *E. coli* to achieve OD_{600} values up to 65 units. Although the reasons for increased RefZ solubility in this medium were not determined, similar results were achieved in ProGro (Expression Technologies, Inc.), another commercially available high cell density medium.

Text ref.	Protein:	dsDNA:	(D:P)	[Protein]	Dialysis bx:	Screening/Cond:	Hits:
A	WT RefZ-His	RBM L2 24 bp	1 to 4	8.5 mg/ml	50 mM TrisHCl pH 8.5 , 300 mM KCl	Index, Wizard, Natrix, Peglon, Adventure Hike	10% (v/v) ethanol, Hepes pH 7.5 and 0.2 M MgCl2 (P 41 21 2) 15% (v/v) ethanol, 0.1 M imidazole pH 8.0, and 0.2 M MgCl2 (P 41 21 2)
B	WT RefZ-His (S-met)	RBM L2 24 bp	1 to 4	~5 mg/ml	50 mM TrisHCl pH 8.5 , 300 mM KCl	10% EtOH, Imid pH 8, .2 M MgCl2	no xytls
C	WT RefZ-His	RBM L2 12 bp	1 to 4	~5 mg/ml	50 mM TrisHCl pH 8.5 , 300 mM KCl	Natrix, Peg Ion, Adventure Hike, Crystal screen, Wizard	P 41 21 2
D	WT RefZ-His	RBM L2/L1 41 bp	1 to 4	~4.2 mg/ml	50 mM TrisHCl pH 9 + 300 mM KCl	Natrix, Wizard, Index, Peglon	P 41 21 2
E	WT RefZ-His w/wo AMPPNP	RBM L2 21 bp	2 to 1	~7mg/ml	A (50 mM TrisHCl pH 9 + 300 mM KCl) B(50 mM TrisHCl pH 9)	A (MSG1, Adventure Hike, Natrix, Wizard) B (PEG-ION, Crystal Screen, MSG2, MSG3)	salt xytls and same morphology P 41 21 2
F	E53K-His, R102S-His, R116S-His, E117D-His, E179K-His	RBM L2 41 bp	1 to 1	2.5 ; 2.0 ; 2.0 ; 2.5 ; 2.5 mg/ml	50 mM TrisHCl pH 9 + 300 mM KCl	Wizard, Index, Peg-Ion, Crystal Screen, Natrix, Adventure Hike and Dive	100 mM Hepes pH 8.0, 1.0 M Sodium Acetate, 400 mM Guanidine HCl (R116S) hexagonal plates
F.1	R116S-His	RBM L2 41 bp	1 to 1	~2 mg/ml	50 mM TrisHCl pH 9 + 300 mM KCl	optimized around (100 mM Hepes pH 8.0 1 M Sodium Acetate 400 mM Guanidine HCl)	no single best condition identified xytls appear after 3 months
G	WT RefZ-His	RBM L2 (12 and 21 bp)	varied	~7 mg/ml	50 mM TrisHCl pH 9	detergent screen, additive screen, silver bullet screen (Base conditions taken from screening G: 0.2 M Magnesium Chloride ; 0.1 M Sodium Cacodylate pH 6.5 50% v/v PEG 200)	

Table 3.1 Crystallography screening conditions.

RefZ was purified using nickel chromatography in the following conditions: 50.0 mM Tris-HCl [pH 9.0], 300 mM KCl, and 10% (v/v) glycerol. Under this condition, RefZ still had a tendency to precipitate at the higher concentrations needed for subsequent structural and biochemical analyses. In order to improve solubility, RefZ was combined with a 24 bp fragment of DNA centered on RBM_{L2} at a 4:1 (RefZ:*RBM*) molar ratio prior to dialysis into 50 mM Tris-HCl [pH 8.5] and 300 mM KCl (Table 3.1A). After dialysis RefZ was concentrated using a spin filter with 10,000 MWCO. Under this condition, it was possible to obtain soluble RefZ at concentrations up to ~10.0 mg/ml. Initially 480 different conditions from both commercially available and lab designed crystallization kits were screened using a RefZ concentration of ~8.5 mg/mL (Table 3.1A). The initial screen with the RefZ-*RBM* mixture produced crystals in two conditions: 1) 10% (v/v) ethanol, Hepes [pH 7.5] and 0.2 M $MgCl_2$ and 2) 15% (v/v) ethanol, 0.1 M imidazole [pH 8.0], and 0.2 M $MgCl_2$. Both conditions contained small crystals (less than 100 microns), which diffracted to ~ 4 Å at home radiation source, and were indexed to the P 41 21 2 space group. To obtain larger crystals more suitable for mounting and data collection, optimization around the initial hit condition was carried out by varying pH, salt, protein concentration and RefZ:*RBM* ratio. Ultimately, the largest crystals were obtained with 5.0 mg/ml RefZ, a 4:1 molar ratio of RefZ:*RBM*, 10% ethanol (v/v), 0.1 M imidazole [pH 8.0], and 0.2 M $MgCl_2$. RefZ crystals were cryoprotected by brief soaking in mother liquor containing 20% (v/v) glycerol, and flash frozen in liquid nitrogen before the data collection. These crystals diffracted to 2.8-3.0 Å resolution at an APS synchrotron radiation source, beamline 23ID.

Despite the availability of multiple TetR family protein structures, attempts to solve the phase by molecular replacement failed. To address the phase problem, RefZ expression and solubility were optimized in minimal media for purification of Se-Met RefZ. Soluble protein yields were low and purified Se-Met RefZ did not form crystals under the previously identified conditions (Table 3.1B). In parallel, Pb acetate was successfully soaked into the RefZ crystal, providing an anomalous signal which permitted the phase to be solved by single anomalous dispersion method (SAD). The lead site was at the dimer interface of RefZ, bound to the Y-carboxyl of Glu110. The asymmetric unit contained a single molecule of RefZ with a dimer consistent with the structures of other TetR family proteins generated by crystallographic symmetry. Surprisingly, the unit cell contained no electron density for DNA.

Although the path of the main chain was mostly resolved in the early, experimentally-phased map, building the final model and docking it to the amino acid sequence proved difficult due to the relatively poor resolution and ambiguous electron density; the model building was particularly challenging at the junction between regulatory and DNA-binding domains as well as at the dimer interface. Since the majority of the rLOFs substitutions appeared to map to these regions, more extensive screening was carried out in an attempt to obtain a DNA-containing crystal and/or a different crystal form that might improve the resolution.

RefZ binds in units of two and four to segments of DNA centered on each of the *RBMs* in electrophoretic gel mobility shift assays (83). This observation is consistent with the X-ray crystal structures of other DNA-bound TetR family members (QacR 1JT0 and SlmA 4GCL), which show the proteins binding to DNA as a dimer of dimers, with each

dimer contacting successive major grooves (Chapter I/Fig. 1.12). The SlmA-SBS structure was solved with a 12 bp SlmA binding motif, so screening for RefZ crystals was repeated with a 12 bp DNA fragment $RBM_{L2\text{-}12bp}$ (Table 3.1C). Although $RBM_{L2\text{-}12bp}$ maintained RefZ's solubility at high concentrations, it did not support upshifts by EMSA (data not shown). Moreover, screening with $RBM_{L2\text{-}12bp}$ resulted in crystals of the same morphology and quality (Table 3.1C). To test for crystals with a longer piece of DNA, a new 41 bp probe, $RBM_{L2\text{-}41bp}$ was designed. $RBM_{L2\text{-}41bp}$ supported binding of up to four units of RefZ (Fig. 3.4). Mixing RefZ-6XHis with HSUMO-RefZ and $RBM_{L2\text{-}41bp}$ produced a clear banding pattern and resolution of five distinct protein:DNA upshifts (Fig. 3.4). This is consistent with published results demonstrating that RefZ binds to *RBM*-containing DNA in units of two and four (83) . The splitting of the lower band is not observed in this experiment due to a high total concentration of protein. However, screening with a 41 bp fragment centered on RBM_{L2} as well as one from RBM_{L1} did not produce a different crystal morphology (Table 3.1D).

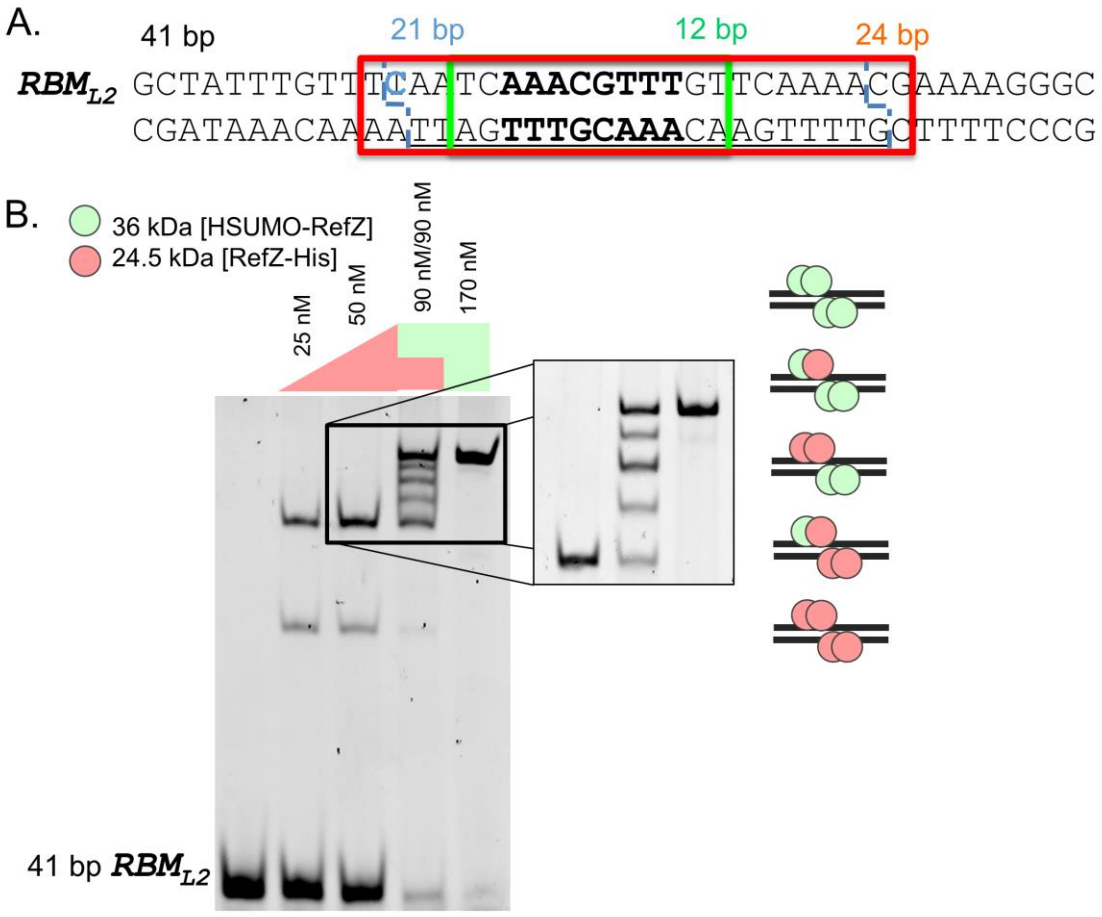

Figure 3.4. RefZ binds *RBM* L2-41bp in units of two and four (A) *RBM* L2 containing dsDNA used for crystal screening. Red, green, and blue boxed areas show the different lengths and respective sequences used for crystal screening. **(B)** RefZ-His and HSUMO-RefZ were co-incubated with 50 nM *RBM* L2-41bp for 10 min and run on a 7.5% TBE gel at 200V for 60 min (gel was pre-run at 120V for 60 min). The inset gel was run for 75 min to achieve separation of the complexes. Gels were stained with SYBR Green prior to imaging.

The crystal packing for some protein-DNA complexes requires end-to-end alignment of DNA molecules and that the length be such that the proteins would be positioned on the same DNA face in the crystal lattice (187). Therefore, the *RBM*-containing fragment was redesigned with compatible one base pair overhangs at the 5' and 3' ends to encourage end-to-end base pairing. A length of 21 bp was used to attempt to place the protein on the same DNA face for DNA packing. The new DNA fragment

RBM$_{L2\text{-}21bp}$, supported RefZ binding in units of two and four by EMSA (data not shown), but further crystal screening did not produce novel morphologies for WT RefZ (Table 3.1E).

The crystal form of WT RefZ had a solvent fraction of 75%, suggesting the crystals were loosely packed (usually, crystals of a protein this size have closer to ~50% solvent fraction), possibly accounting for the relatively poor diffraction quality. To determine if any of the rLOF variants would pack more tightly and/or produce distinct crystals, additional screening was carried out. E53K, R102S, R116S, E117D, and E179K were overexpressed, purified, and and used to screen for crystals under various conditions (Table 3.1F). E53K exhibited stronger affinity for DNA by EMSA, which we hypothesized might increase the chance of obtaining a RefZ-*RBM* complex crystal. All of the rLOF variants crystallized in at least one condition. However, with the exception of R116S, all produced the same, limited resolution crystal form. R116S formed a different crystal in 100 mM HEPES [pH 8.0], 1.0 M sodium acetate, and 400 mM Guanidine-HCl (Table 3.1F.1). However, the crystals took several months to grow and also diffracted poorly.

Finally, the previously identified conditions were screened with additives in an attempt improve the quality of the crystals (Table 3.1G); however, this approach failed. Since attempts to optimize the crystal quality were unsuccessful, more extensive efforts were made to improve the electron density maps with the existing data and to build a model. Iterative building and phasing were employed on the data re-processed in the lower symmetry group (to have a dimer in the asymmetric unit). Eventually a model comprising

a continuous chain of residues 2-200 (out of 207) was successfully built and refined at 2.9 A resolution to r_work = 0.2200 r_free = 0.2466.

The structure of RefZ was compared with other TetR family proteins deposited in the PDB. The top 10 structural similarity hits for RefZ (residues 2-200) from VAST are listed in Table 3.2 by their descending VAST structure-similarity scores, P-value, r.m.s.d, % structural similarity, and alignment length (188). PfmR (3VPR) had the highest structural similarity score. PfmR is a transcriptional repressor from *Thermus thermophilus* HB8 that regulates an operon of eight genes predicted to be involved in fatty acid metabolism (189). RefZ's functional homolog SlmA is the 10th structural similarity match see Table 3.2.

Name	PDB	Score	P-value	RMSD	% ID	Organism
PfmR	3VPR	15.4	10e-14.4	2.2	15.9	*Thermus thermophilus Hb8*
Kstr2	4W97	15.2	10e-14.1	2.5	13.1	*Mycobacterium tuberculosis*
PTR*	3F1B	14.3	10e-12.4	3.1	15.8	*Rhodococcus sp. Rha1*
Aq_1058	2EH3	14.3	10e-12.3	2.8	16.5	*Aquifex aeolicus vf5*
Sco4008	2D6Y	14.1	10e-11.0	2.7	19.8	*Streptomyces CoelicolorA3(2)*
Ycdcy	3LOC	14.1	10e-10.9	3.0	16.8	*E. Coli*
EthR	4M3F	14.0	10e-10.8	3.0	15.6	*Mycobacterium tuberculosis*
PTR*	4NEL	13.9	10e-11.5	3.3	16.5	*Saccharomonospora Viridis*
Rha1	2NP5	13.7	10e-11.1	3.1	14.5	*Rhodococcus sp. Rha1*
SlmA	4GCT	13.6	10e-10.9	2.8	14.0	*E. coli*

Table 3.2 Top 10 structural similarity hits to RefZ by VAST.

The RefZ structure reveals a homodimer with a HTH DNA-binding motif (Fig. 3.5A). Each monomer is composed of ten α-helices connected by loops and turns. The HTH domain is comprised of α1, α2, and α3 (Fig. 3.5B). α3 is the DNA recognition helix that sits in the major groove (141). For all TetR family members, the HTH is structurally similar (141). Figure 3.5B shows a superimposition of RefZ's N-terminal domain (residues 5-49, cyan) to the most structurally similar HTH domain of TetR family (residues 1-47) (QacR: 1JT6 Tan). A pairwise comparison of the corresponding Cα atoms gave an rmsd of 0.7. In the QacR-*IR1* complex (1JT0) QacR binds as a pair of dimers and makes seven contacts to the phosphate backbone of DNA with residues T25, S34, S35, Y40, Y41, H42, K46 (159). Y41 and K46 are conserved in RefZ (Y43 and K48, respectively). K48 is the most conserved residue across the TetR HTH domain (141). Figure 3.5B shows K48 forming hydrogen bonding contacts to the carbonyl oxygen of the peptide backbone for Thr25 and Phe22, stabilizing the HTH (141). To compare RefZ's N-terminal domain to its functional homolog SlmA, we performed the same pair-wise comparison (residues 11–56) (SlmA: 3NXC) to RefZ's N-terminal domain (residues 5-49) resulting in an r.m.s.d of 1.48 (190). SlmA makes 5 contacts to the phosphate backbone (T34, R31, Y49, K55), K55 being equivalent to K48 in RefZ.

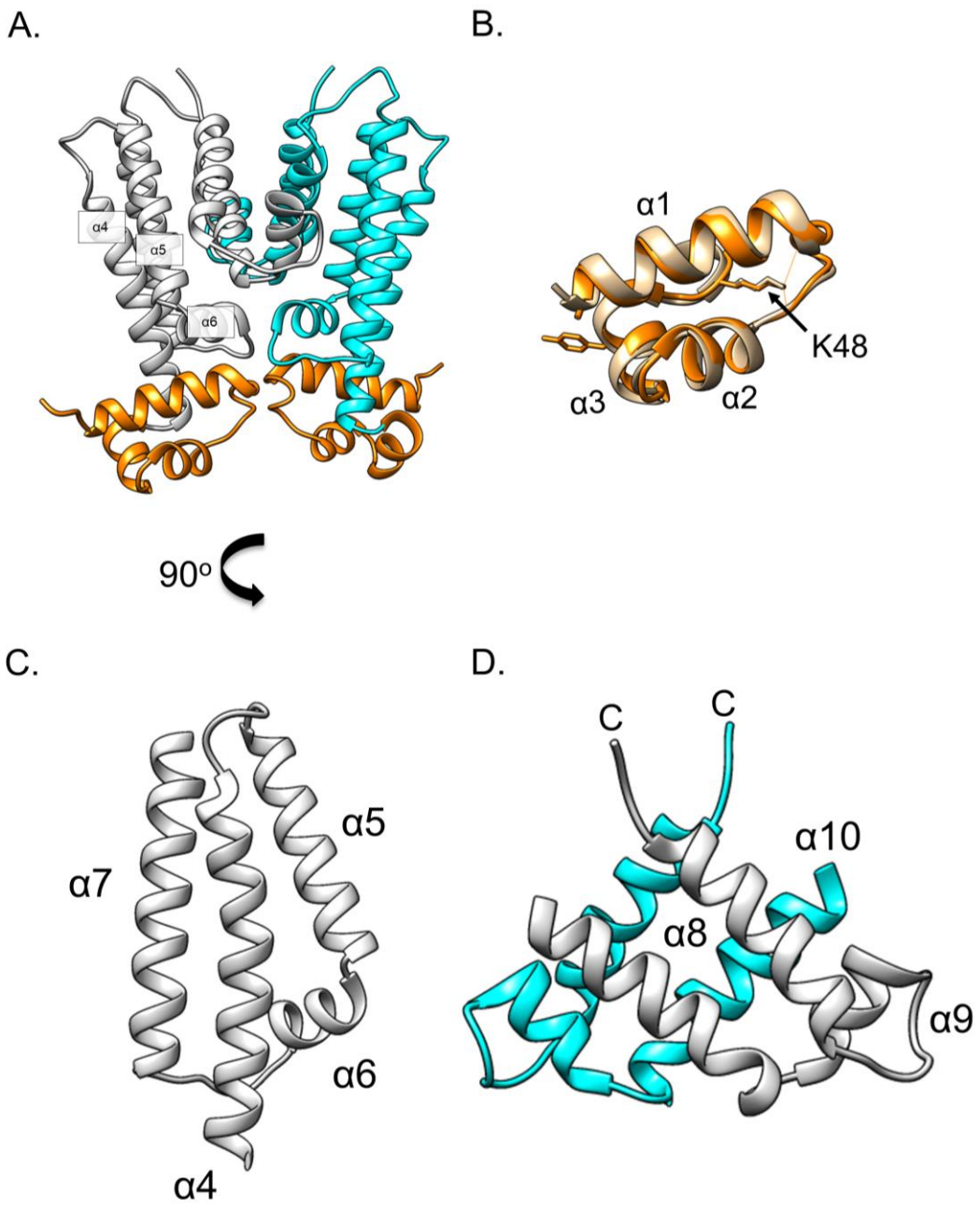

Figure 3.5. 2.9 Å crystal structure of RefZ. (A) RefZ is a homodimer. One monomer is shown in light gray and the other monomer is shown in cyan. **(B)** Superimposition of the HTH domains of RefZ (cyan), SlmA (salmon), and QacR (tan). **(C)** Helices α5, α6, and α7 of RefZ form the characteristic triangular pocket utilized by most TetR family members for ligand binding, while α4 acts like a lid for this pocket. In this conformation of RefZ the pocket is small and not accessible. **(D)** RefZ α8, α10 and α8', α10' form a four helix bundle, typical of the TetR family dimerization interface.

The C-terminal regulatory domain of RefZ (α5-α10) is connected to the HTH domain by α4 (Fig. 3.5A) and contains the dimerization interface. Fig. 3.5C shows RefZ's α4, α5, α6, and α7 helices. For the TetR protein family, DNA binding can be allosterically regulated by ligand binding in the C-terminal regulatory domain (141). Ligands bind in the triangular pocket formed by α5, α6, and α7. For TetR and QacR this causes a conformational change resulting in a pendulum motion from α4 which makes distance between α3 and α3' incompatible with DNA binding (141). Alternatively, ligand binding may rigidify the protein, preventing flexibility required for accessing the DNA-binding conformation (141).

Interestingly, the structures of the TetR family exhibit extensive variability for the distance between α3 and α3' (33.3 to 63.4 Å) in apo (DNA free) conformations. The distance between α3 and α3' must fall within a narrow range to straddle the minor groove and place each HTH in successive major grooves. Consistent with this the crystal structures of most apo forms of the TetR family appear incompatible with DNA binding (141) . This is likely a crystallization artifact manifested because of the flexibility for α3 and α3' prior to motif recognition (141). To assess if the distance between RefZ's α3 and α3' was compatible with straddling the minor groove based on the crystal structure, RefZ was superimposed with the QacR-*IR1* complex (1JT0). As shown in Fig. 3.6A and B, RefZ is improperly placed in the Z plane relative to QacR resulting in a conformation that does not allow a3' to sit deeply in the major groove. The distance between equivalent positions of α3 and α3' for RefZ was 40.4 Å (A39 and A39') compared to 44.8 Å for

QacR (N38 and N38'). In Fig. 3.6C, it becomes apparent that a conformational change is required in order to properly place RefZ' relative to QacR'.

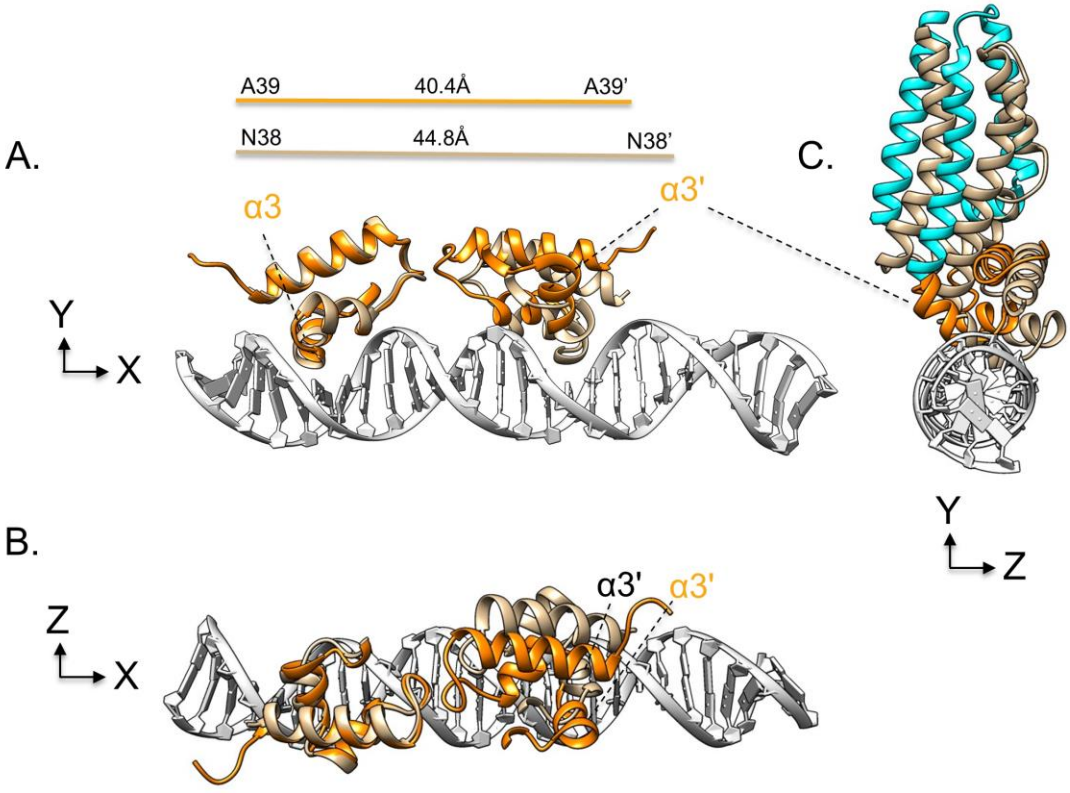

Figure 3.6 RefZ apo structure is incompatible with straddling the minor groove. (A) Front view of superimposition of RefZ's HTH (orange) with the QacR-IR1 complex. In order to properly straddle the minor groove and sit deeper in the major groove RefZ needs to be shifted such that α3' is in the same position as α3' for QacR **(B)** Top view of the HTH. RefZ's α3' is not aligned to QacR's α3' in the Z-plane. **(C)** Side view of RefZ' (cyan and orange HTH) overlaid with QacR (tan). A conformational change needs to take place before α3' can properly sit in the major groove.

RefZ's dimerization interface

Using PISA (Protein interfaces, surfaces and assemblies service) the amt of solvent accessible surface area excluded by dimerization for RefZ was calculated to be 1099.3 $Å^2$ (ΔG = -11.2 kcal/mol) (191). In comparison SlmA (5HBU), EthR and TetR bury 1755.4

$Å^2$ (ΔG = -7.4 kcal/mol), 1479.4 $Å^2$ (ΔG = -19.9 kcal/mol), and 2349.8 $Å^2$ (ΔG = -36.6 kcal/mol) respectively (191). In order to overcome the loss of rotational and translational degrees of freedom dimerization must have a ΔG < 15-20 kcal/mol (146). The solvent accessible surface area must also be > 856 $Å^2$ to favor dimerization (192). This may suggest that RefZ has a weaker propensity to dimerize compared to SlmA and TetR.

Important dimerization contacts for the TetR family usually include the four helix bundle composed of α8, α10, α8' and α10' (141). The four helix bundle of RefZ is shown in Fig. 3.5D. The primary contacts at RefZ's dimerization surface were identified with DimPlot (Fig. 3.7) (193, 194). In the RefZ structure α6, α7, and α9 also participate in dimerization by forming hydrogen bonding contacts. Residues R102 and R106 on RefZ's α6 make contact to the other monomer of RefZ (Fig. 3.7B): R102 donates a hydrogen bond from NH2 to the peptide backbone carbonyl of V108'; R106 forms two hydrogen bonds: $R106_{NH2}$ to $E107_{O}$' and $R106_{NE}$ to $R106_{O}$'. The contacts between α7, α8, α9 and α10 are highlighted in Fig. 3.7B. On α8, $S157_{OH}$ bonds with $S157_{OH}$'. α9 makes two contacts to α7'. $Y168_{OH}$ can donate a hydrogen bond to the side chain carbonyl of E126. The lone pair on $Y168_{OH}$ can be an acceptor of a hydrogen bond from $Y122_{OH}$; and E171 is a hydrogen bond acceptor from K127'. On α10, E189 hydrogen bonds to H150'. Hydrophobic interactions are also important for the dimer interface. Importantly, the L153R substitution was identified as an rLOF variant, and L153' participates in hydrophobic interactions with M160, M161, Y168, and I169 (Fig. 3.8A). The presence of a positively charged side chain in the hydrophobic neighborhood of M160, M161, I169 and Y168 would result in repulsive interactions (Fig. 3.8B) and would be predicted to destabilize the dimer.

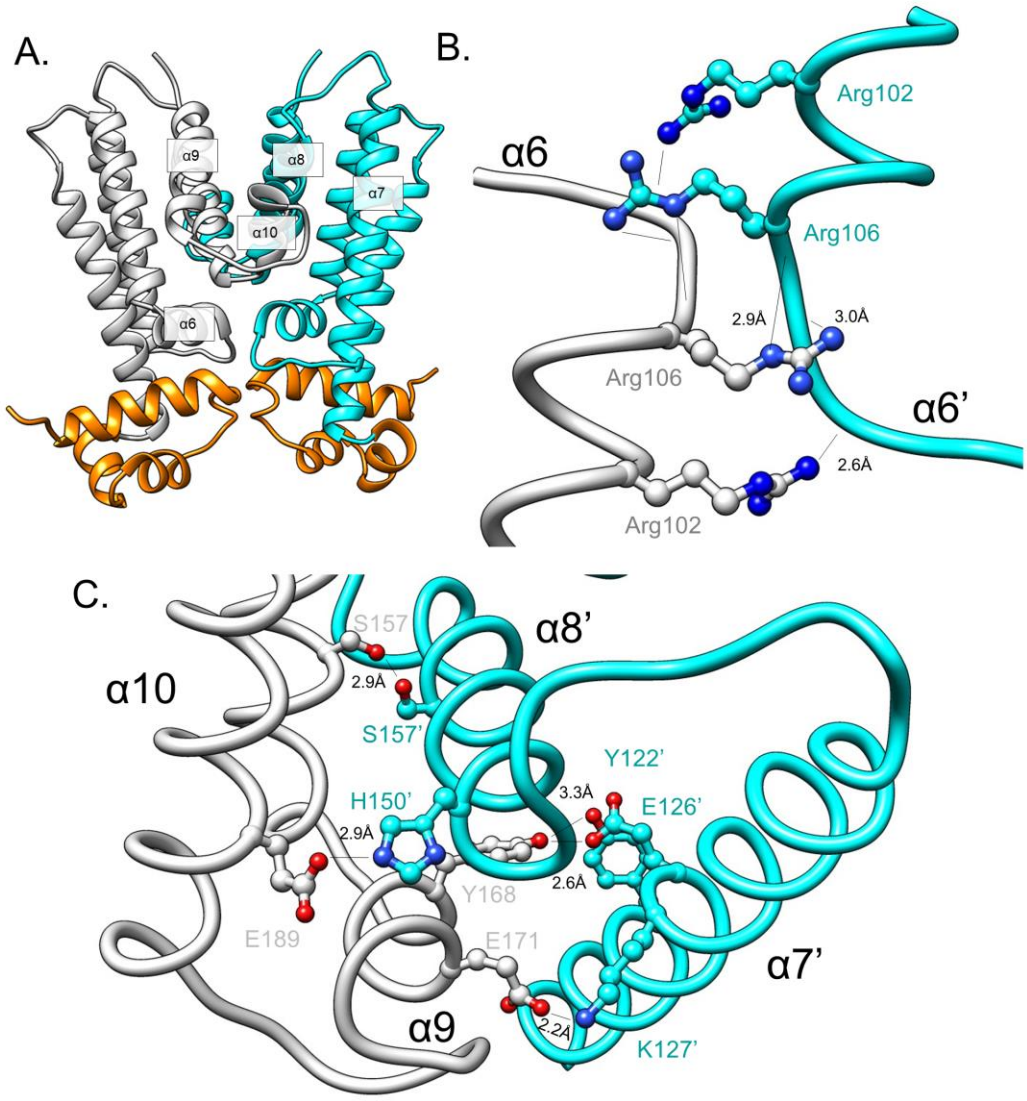

Figure 3.7. Hydrogen bonds formed at the dimerization interface of RefZ. RefZ monomers are shown in light gray and cyan. **(A)** The helices important for H-bonding are labeled. **(B)** R102 hydrogen bonds to the peptide backbone carbonyl of V108'. R106 forms two hydrogen bonds; $R106_{NH2}$ to $E107_{O}$' and $R106_{NE}$ to $R106_{O}$'. **(C)** On α8 $S157_{OH}$ bonds with $S157_{OH}$'. α9 makes three contacts to α7'. $Y168_{OH}$ can donate a hydrogen bond to the side chain carbonyl of E126. The lone pair on $Y168_{OH}$ can be an acceptor of a hydrogen bond from $Y122_{OH}$. E171 is a hydrogen bond acceptor from K127'. Finally on α10 E189 hydrogen bonds to H150'.

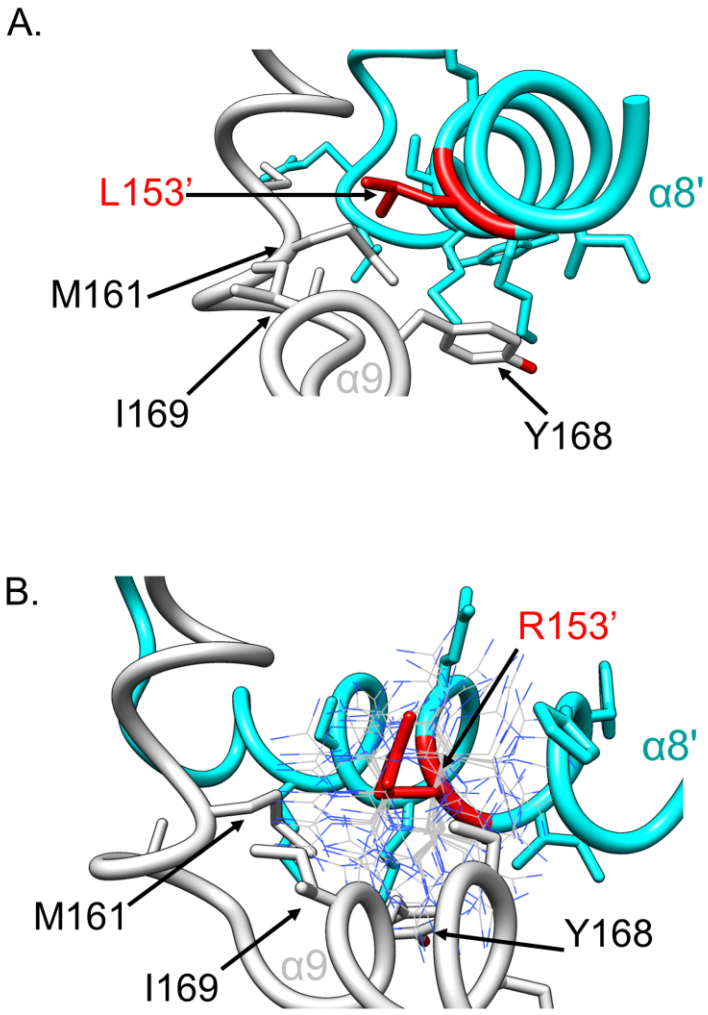

Figure 3.8. Hydrophobic dimerization contact L153. RefZ monomers are shown in light gray and cyan. **(A)** L153 (red) and neighboring residues within 5 Å are shown as sticks. The neighborhood environment of L153 is hydrophobic, consisting of M161, I169 and Y168 **(B)** Replacement of L153 with Arg. R153 could adopt many side chain conformations shown as thin blue and grey sticks. The presence of a positively charged side chain in the hydrophobic neighborhood of M161, I169 and Y168 would result in repulsive interactions and a potential steric clash.

Bacterial two-hybrid analysis of RefZ self-interaction

Three of the rLOF variants (R102C, R102S, and L153R) map on the RefZ dimer interface, potentially implicating RefZ dimerization in regulation of FtsZ. To investigate self-interaction of WT RefZ and the rLOF variants, bacterial two-hybrid (B2H) analysis was conducted. In the B2H, WT RefZ shows a pairwise interaction with itself that is not

observed for the negative controls (Fig. 3.9). RefZ's positive B2H self interaction is likely reporting on RefZ dimerization since all characterized TetR family proteins form dimers, and RefZ is also a dimer in the crystal structure. The B2H is performed in *E. coli*, which lacks *RBM* motifs, indicating that the positive interaction is not mediated through *RBM* binding. Consistent with this hypothesis, a DNA-binding deficient variant, Y43A (82), also displays self-interaction similar to WT (Fig. 3.9B).

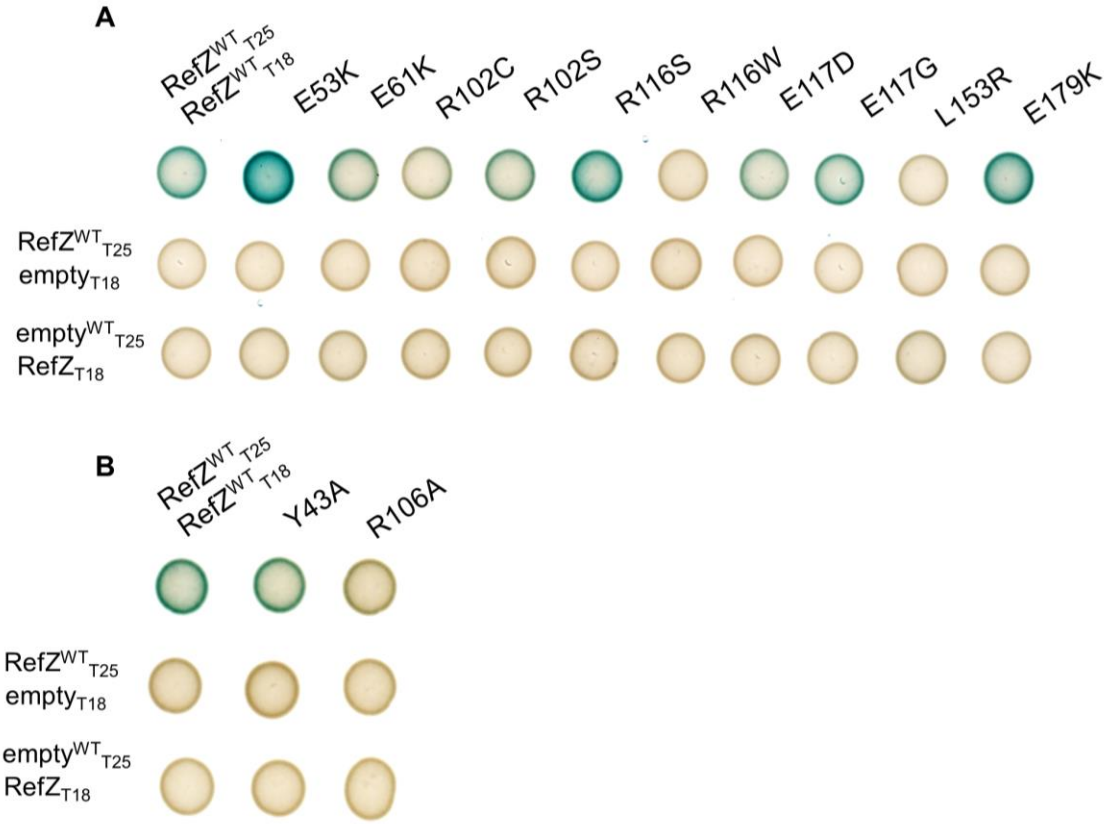

Figure 3.9. rLOF variants exhibit varying degress of self-interaction by B2H. (A) Self-interaction of RefZ compared to rLOF variants in a bacterial 2-hybrid assay (B2H). Pairwise interaction of WT or rLOF T25 and T18 tagged proteins was assayed for by monitoring production of blue LacZ cleavage product following 41 hr of growth (room temperature) on selective M9 minimal plates supplemented with 250 µM IPTG and 40 µg/ml X-gal. One of three biological replicates is shown. **(B)** Self-interaction of RefZ compared to the point mutant Y43A and R106A.

The rLOF variants were classified as loss-of-interaction, gain-of-interaction, or similar to WT based off their B2H results (Fig. 3.9). No detectable self-interaction was observed for the R116W and L153R mutants, and the signal for R102C was greatly reduced. The L153R substitution likely creates a steric clash and introduces a repulsive positive charge at the dimer interface prohibiting dimer formation (Fig. 3.8B). R116 is probably important for the positioning of α6 which is critical for dimerization, therefore a bulky tryptophan residue sidechain may incorrectly position α6 resulting in a loss of self-interaction. R102 makes two hydrogen bonds to α1 of the helix-turn-helix. $R102_{NH}$ is a hydrogen bond donor with the side chain carbonyl of N18. The peptide bond nitrogen of Q19 donates a second hydrogen bond to the lone pair of electrons on $R102_{NH}$ (Fig. 3.10A). Replacement of R102 with cysteine or serine would prevent the hydrogen bonding contact across the dimer interface to the backbone carbonyl of V108' (Fig. 3.7B) and the hydrogen bond contact to the peptide backbone nitrogen of Q19. It is likely that R102S could still hydrogen bond to N18 (Fig. 3.10C). Interestingly R102S had a self-interaction similar to WT RefZ while R102C's self-interaction was harder to detect (Fig. 3.9C). This is possibly due to serine's OH group more readily donating a hydrogen bond than cysteine, although in this structural conformation both are unable to form a hydrogen bond across the interface due to distance restraints. Notably, the R102S substitution is loss-of-function even though it supports dimer formation. R102 is invariant across the *Bacillus* genus and may have a function independent of supporting dimerization. R106 is also invariant in *Bacillus refZ* homologs and makes two hydrogen bonding contacts across the dimer interface (Fig. 3.7B). To test if R106 was important for dimerization, an R106A variant

was generated by site-directed mutagenesis and assessed for self-interaction. Consistent with the structural prediction, R106A showed no self-interaction (Fig. 3.9B).

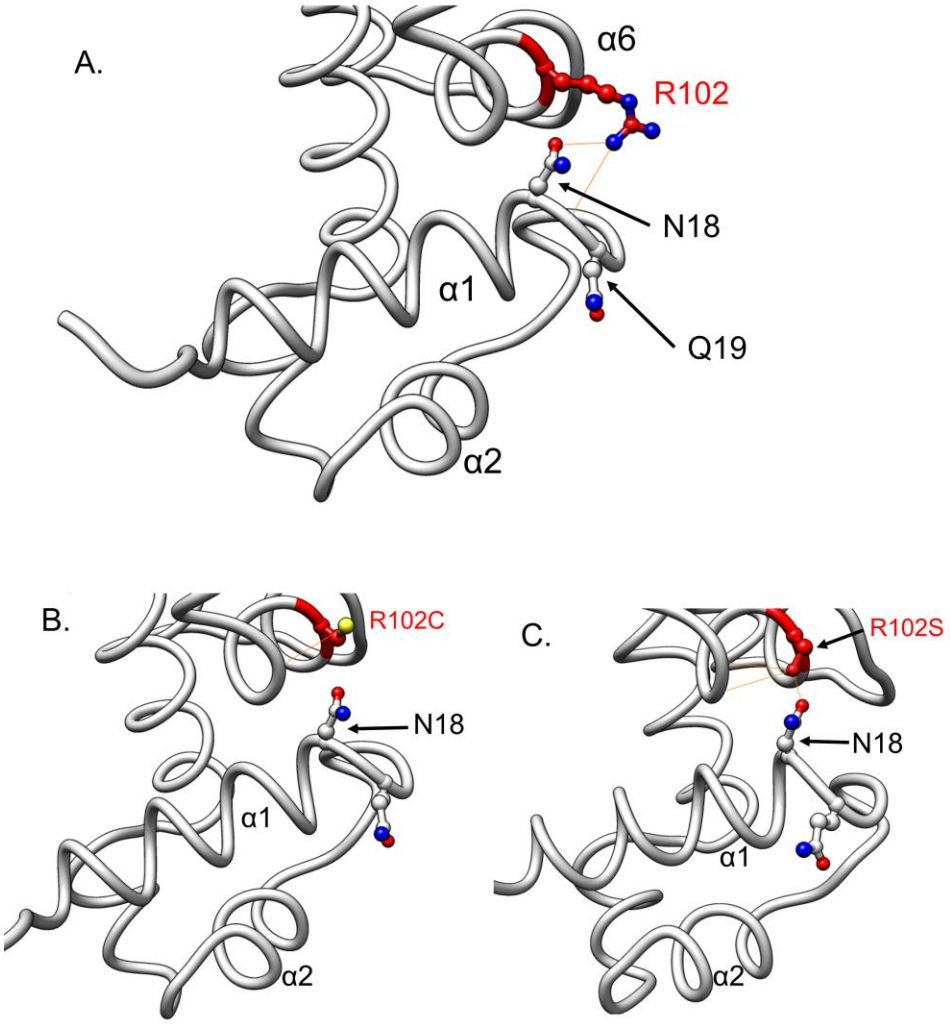

Figure 3.10 Hydrogen bonding of R102. (A) R102 can form two hydrogen bonds with the HTH and one hydrogen bond across the dimer interface. One hydrogen from $R102_{NH2}$ bonds with the oxygen of N18. The other $R102_{NH2}$ bonds with the Q19 peptide bond. **(B)** The rotameric positions are shown for replacement of Arginine with cysteine. Importantly an R102C variant lacks the ability to hydrogen bond with the HTH. **(C)** The R102S variant can only create a hydrogen bond with N18, and this bond is much shorter in R102S than R102.

The E53K, R116S, and E179K mutants show enhanced self-interaction compared to WT (Fig. 3.9A). E53K is positioned on α4, which for TetR and QacR, transmits the conformation change from the regulatory domain to the DNA-binding domain, making the spacing between two HTH domains incompatible with the width of the major groove (Fig. 3X) (138). The E53K substitution may stabilize a conformation of RefZ which more readily binds DNA. Unlike the R116W substitution, the R116S variant has the capacity to hydrogen bond and serine is not a bulky amino acid. This substitution may favor the correct positioning of α6 for dimerization. The variant E179K (positive to negative) has a stronger self-interaction compared with WT, but the structure doesn't offer any clues as to why this would be.

The remaining rLOF variants, R102S, E61K, E117D, and E117G show similar self-interaction to WT (Fig. 3.9). Since six out of ten rLOF variants display either reduced or increased self-interaction, these data suggest that both monomer and dimer forms of RefZ are important for the mechanism of inhibiting FtsZ.

Mapping the RefZ rLOF residues onto the RefZ structure and comparison to SlmA

In the SlmA-DNA-FtsZ CTD crystal structure, SlmA has a narrow hydrophobic groove between α4 and α5 that is bound by an extended conformation of the FtsZ CTD (Fig. 3.11A) (104, 195). Several previously identified SlmA loss-of-function substitutions (104, 195) occur in residues that map to either side of the hydrophobic groove in α4 and α5 in the SlmA-DNA-FtsZ CTD crystal structure (F65, R73, L94, G97, R101, N102) (Fig. 3.11A, green).

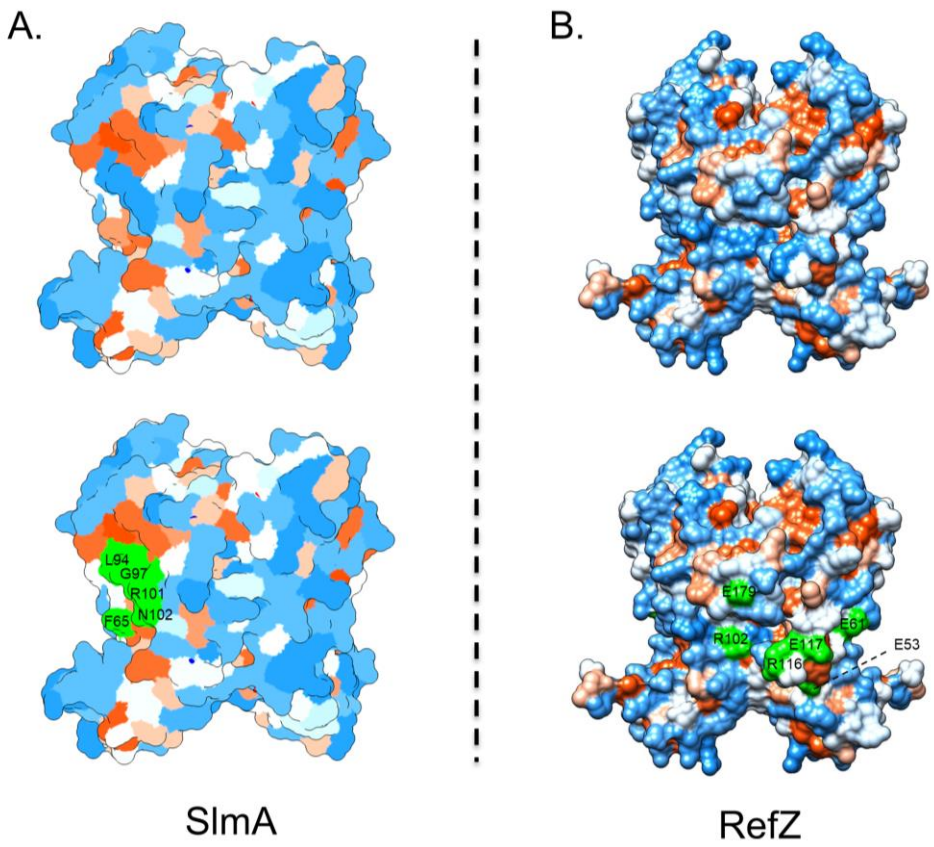

Figure 3.11. RefZ and SlmA do not share the same FtsZ interaction surface. (A) Hydrophobicity of SlmA (5HBU) surface shown without the FtsZ CTD or DNA. Amino acids have been assigned attributes according to the Kyte and Doolittle hydrophobicity scale with Chimera. Residues are color-coded as follows: hydrophobic (red), neutral (white) and hydrophilic (blue). Notably, SlmA has a hydrophobic patch where the CTD binds. SlmA sLOF residues are shown in green. **(B)** Hydrophobicity of RefZ surface. Notably, RefZ has a hydrophobic groove running down the left side of α7. Note the rLOF residues are in a different place than those found for SlmA.

To compare the SlmA-FtsZ interaction interface with the location of the rLOF substitutions we identified in the rLOF screen, RefZ residues not implicated in dimerization (E53, E61, R116, E117, and E179) were mapped to a surface hydrophobicity representation of the RefZ structure (Fig. 3.11B). Surprisingly, relative to the SlmA-FtsZ binding surface, E53, E61, R116, E117, and E179 are positioned on the opposite face of the monomer and closer to the dimerization interface (Fig. 3.11B). Intriguingly, RefZ

does not have a hydrophobic groove in the same position as SlmA, though there are hydrophobic patches near E117 and E61 (Fig. 3.11B). These data suggest that if RefZ regulates FtsZ through interaction with the CTD, then those contacts are likely in a different position from those of SlmA. A different interaction position may be necessitated by the fact that although the CTT (CHAPTER I/Fig. 1.6C) peptide utilized in the SlmA structure is relatively conserved (DIPAFLR in *E. coli* vs. DIPTFLR in *B. subtilis*), the remaining residues of the C-termini are distinct (KQAD in *E. coli* vs. NRNKRG in *B. subtilis*) and the positive charge of the *B. subtilis'* CTD has been shown to be important for FtsZ regulation.

Characterization of rLOF variant DNA-binding using EMSA

Electrophoretic mobility shift analysis of the variants revealed two unique patterns of behavior with respect to specificity and affinity when compared to WT. Three variants (E53K, E61K, and E117G) had higher apparent affinity for non-specific DNA and exhibited a laddering behavior for $RBM_{L2\text{-}150bp}$ and a mutant ($mRBM_{L2\text{-}150bp}$) harboring seven point mutations in the central palindrome of each of the five *oriC*-proximal RBMs (Fig. 3.12). The E53K variant had the most nonspecific behavior, with at least five upshifts observed with the $mRBM_{L2\text{-}150bp}$ (Fig. 3.12). The E61K and E117G variants also exhibited additional upshifts for $RBM_{L2\text{-}150bp}$ and $mRBM_{L2\text{-}150bp}$, though more laddering was observed with E53K and E61K (Fig. 3.12).

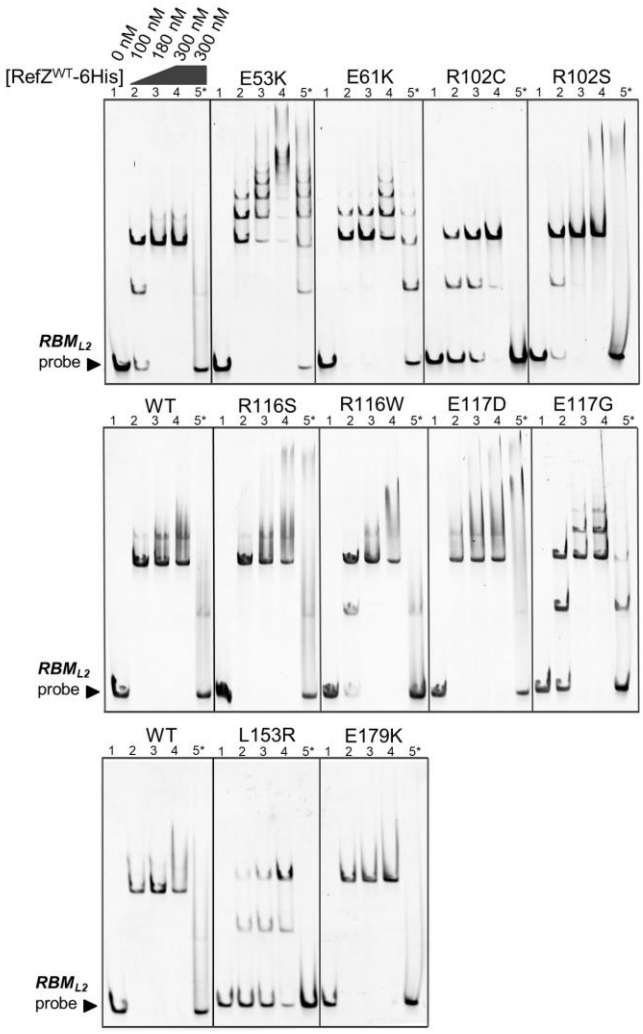

Figure 3.12. Electrophoretic Mobility Shift Assay for rLOF variants. Increasing concentrations of RefZ and rLOFs were incubated with 150 bp RBM_{L2} wt or mutant DNA for 30 min prior to running on a 5% TBE gel for 45 min at 150V. Three replicates of WT are shown so that experimental variability of upshifting can be appreciated. The ability of WT and rLOFs to bind the mutant RBM_{L2mu} DNA is tested in lane 5.

Interestingly, two variants with decreased self-interaction (R102C and L153R) (Fig. 3.9) displayed no upshifts beyond those corresponding to two and four units of RefZ for $RBM_{L2\text{-}150bp}$ and $mRBM_{L2\text{-}150bp}$ (Fig. 3.12). The R102C and L153R variants, which possess substitutions in residues that make contacts at the RefZ dimer interface (Fig. 3.7 and 3.8), also displayed reduced apparent affinity for $RBM_{L2\text{-}150bp}$ compared to WT (Fig.

3.12). TetR family proteins form dimers on DNA, and a RefZ dimer (with two HTH domains) would be expected to have tighter affinity for the *RBM* than a monomer. Therefore, we hypothesize that the R102C and L153R variants have lower apparent affinity for the *RBM* because they possess substitutions on the dimerization interface. Notably, the R116W variant, which also shows reduced self-interaction in the B2H (Fig. 3.9), displays EMSA behavior equivalent to WT. This may suggest that the R116W variant is only effected in self-interaction in solution. Consistent with this hypothesis, R116W is located at on α5, distal to the dimerization interface (Fig. 3.11). These results suggest that the R116W substitution is LOF for a reason independent of reduced capacity to self-interact or bind DNA. One possibility is that R116W causes a distortion that affects the positioning of E117, another residue important for FtsZ inhibition. The remaining variants (R116S, E117D, E117G, and E179K) also exhibited WT behavior in EMSAs, suggesting that the LOF phenotype is not attributable to their capacity to bind *RBM*s.

Thermostability of RefZ and the rLOF variants

To examine the effect of each of the rLOFs on RefZ's thermostability, we employed differential scanning fluorimetry (thermal shift assays). This assay requires higher concentrations of protein than needed for the EMSA. While we previously identified several conditions to keep RefZ and the rLOFs soluble at higher concentrations for crystallization (purification in ddH_2O and presence of *RBM*-containing DNA fragments), these conditions were not compatible with the thermal shift assay, as reactions must be buffered and DNA-binding precludes assessment of thermostability for apo RefZ. Imidazole also has a solubilizing effect on RefZ; however, the presence of imidazole can

destabilize proteins in thermal shift assays. As a compromise, we optimized the imidazole to be at the minimum concentration required to keep RefZ and the rLOF variants in solution for the assay. Under these conditions, WT RefZ displayed a single transition melting curve with a melting temperature (T_m) of 39^{o}C (Fig. 3.13). Variants E61K, E117D, E117G, E179K possessed a similar T_m to WT and also displayed single transition melting curves though, for unknown reasons, the signal for the E117G was considerably reduced (Fig. 3.13). Notably, the most stabilized variant, E53K (+4^{o}C) (Fig. 3.13) displayed the strongest self-interaction by B2H (Fig. 3.9) while the two most destabilized variants, L153R and R102C (-5^{o}C and -4^{o}C) showed complete and considerable loss of interaction in the B2H, respectively (Fig. 3.9), and make contacts on the RefZ dimer interface. These results suggest that the oligomerization state of RefZ may affect its thermostability. Interestingly, R116W displayed two melting transitions, although the significance of this observation is currently unclear (the lower T_m is reported in the inset table in Fig. 3.13). R116S and R102S have a slight decrease in T_m compared to WT -2^{o}C and -3^{o}C, likely reflecting a loss of a few contacts in the protein.

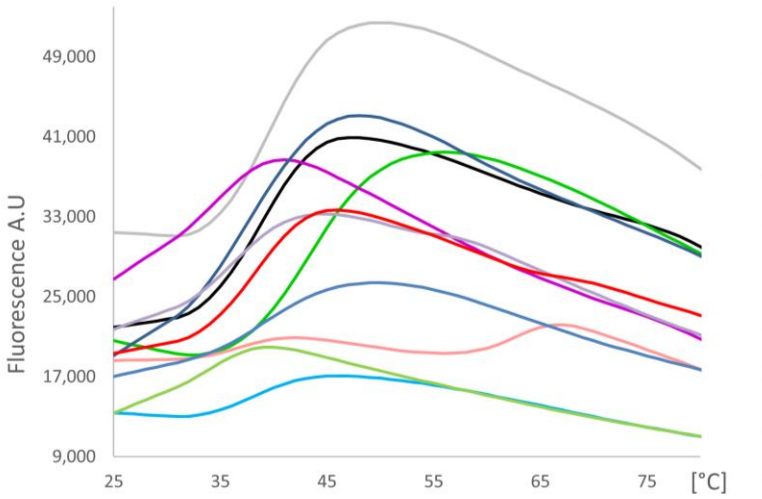

	T_m [C°]	ΔT_m [C°]
WT	39	
E53K	43	+4
E61K	40	+1
R102C	35	-4
R102S	37	-2
R116S	36	-3
R116W	37	-2
E117D	38	-1
E117G	38	-1
L153R	34	-5
E179K	39	0

Figure 3.13. DSF estimates of WT RefZ and rLOF variant stability. Representative sigmoidal melting curves (left). T_m values were calculated by taking the first derivative d(RFU)/dT. ΔT_m is the melting difference between WT and the variants.

RefZ rLOF variants have differences in ATPase activity compared to WT

Purified RefZ possesses a low-level ATPase activity that is stimulated ~10 fold by the presence of Mg^{2+} (Fig. 3.14). This activity was previously discounted as a contaminant, as RefZ lacks obvious motifs associated with canonical ATPases (data not shown). WT RefZ stimulates the hydrolysis of 0.37 ATP/min, and this activity was slightly enhanced by the addition of *RBM*-containing DNA (P=0.03) (Fig. 3.14), suggesting that the source of ATP turnover could be attributed to RefZ. To determine if the ATPase activity could be correlated with function, we determined the rate of ATP hydrolysis for each of the rLOF variants (Fig. 3.14). Surprisingly, R102C and L153R, the variants with substitutions on the dimer interface that also displayed reduced self-interaction by B2H assay, possessed significantly higher activity (~1.5 fold) compared to

WT. In contrast, the E53K variant (strongest self-interaction by B2H) showed a three fold reduction in activity. While the differences in activity observed in some of the variants is suggestive of RefZ possessing an intrinsic ATPase activity, more experiments are needed to rigorously test this hypothesis. At present, the possibility that RefZ co-purifies with an *E. coli* protein possessing ATPase activity cannot be excluded. No TetR family member has yet been reported to possess ATPase activity. However, EthR and DarR, TetR family proteins from *Mycobacterium tuberculosis* and *M. smegmatis*, respectively, have been recently reported to bind nucleotides, specifically c-di-GMP and ci-di-AMP (196, 197). This group also proposed, based on docking analysis, that additional TetR family proteins may bind c-di-GMP at the dimer interface (196).

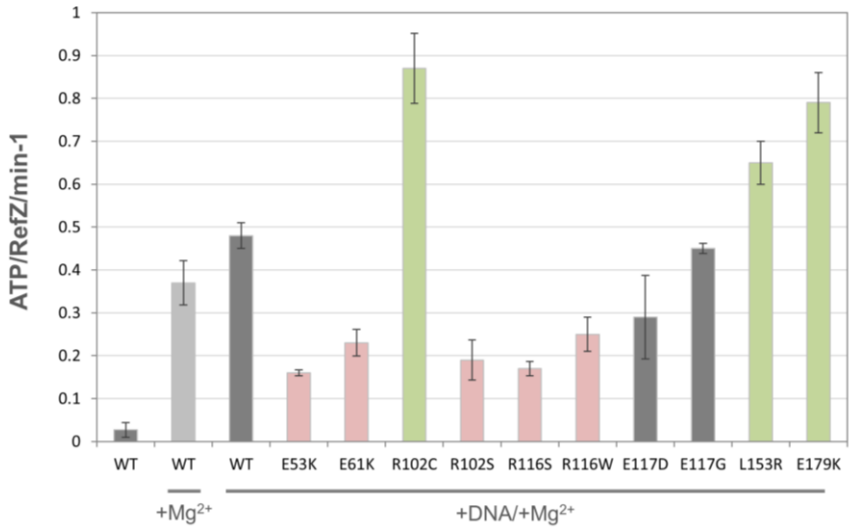

Figure 3.14. Malachite green phosphate assay reveals differences in ATP/RefZ/min^{-1} between WT RefZ and rLOF preps following a 20 min incubation with 1.0 mM ATP. Mg^{2+} was required for this activity and -Mg^{2+} is shown only for WT (far left). WT is shown in the presence and absence of the *RBM$_{L2\text{-}25bp}$*. Pink indicate less activity than WT (P<0.01). The green indicate more activity than WT (P<0.01).

RefZ is thermally destabilized by adenosine triphosphate

Preliminary data suggest RefZ may be able to hydrolyze ATP (Fig. 3.14). To assess if RefZ's thermostability was affected by the presence of ATP, thermal shift analysis was carried out. Ligand binding to the native state usually increases the thermal stability of a protein. However, a protein's thermal stability can also decrease in the presence of a ligand that promotes a less stable protein conformation (198).

Initial experiments using the conditions shown in Fig. 3.13 showed no difference in RefZ thermostability in the presence of ATP. We hypothesized that the imidazole used to solubilize the RefZ might interfere with ATP binding. To test this, the concentration of imidazole was reduced compared to that of the prior experiment. This was possible for WT RefZ because it had higher solubility than some of the rLOF variants. In the lower final concentration of imidazole, RefZ's T_m increased to 49^{o}C (Fig. 3.15), 10^{o}C higher than observed previously (Fig. 3.14). Under these conditions, addition of ATP reduced the T_m by 8^{o}C, highly suggestive of an interaction between RefZ and the nucleotide. If ATP binds RefZ, then this result suggests that imidazole either interferes with ATP binding and/or promotes a conformation of RefZ (at high protein concentrations) that is unable to bind the nucleotide. Moreover, these data suggest that an ATP-bound form of RefZ is less thermally stable in solution. Since the variants predicted to be more monomeric (R102C and L153R) are also less thermostable, it is tempting to speculate that, at least in the absence of DNA, the RefZ monomer is the predominant ATP-bound form. More experiments are needed to explore these different possibilities, including alternative methods for determining if RefZ can bind ATP directly.

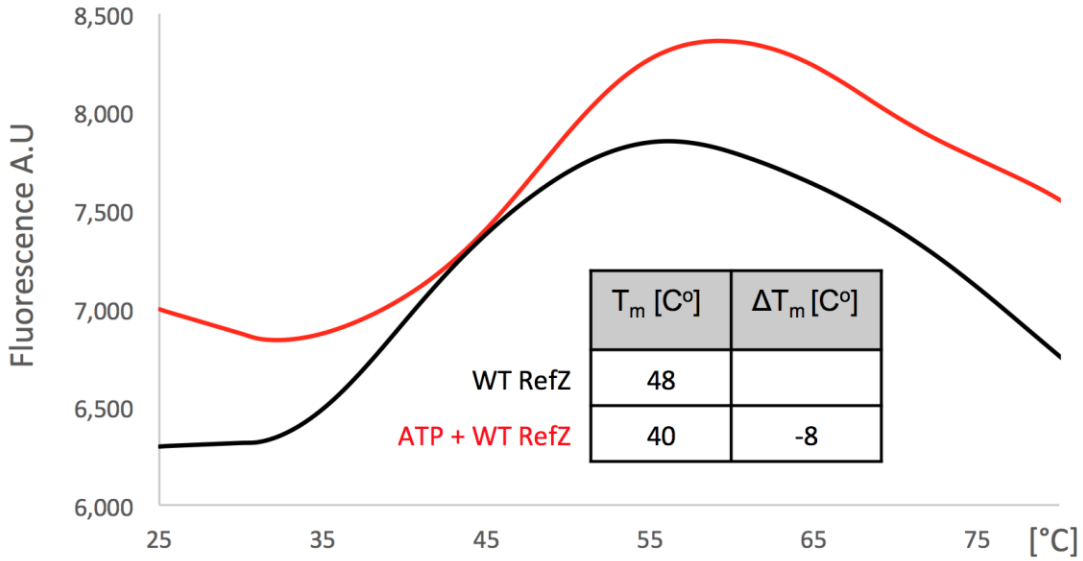

Figure 3.15. DSF sigmodial melting curve of WT RefZ in the presence and absence of ATP. Representative sigmoidal melting curves from three independent runs are shown. T_m values were calculated by taking the first derivative d(RFU)/dT. ΔT_m was calculated as the difference between -/+ATP.

RefZ migrates as an apparent monomer by gel filtration chromatography

Gel filtration chromatography or size exclusion chromatography (SEC) is a separation technique for macromolecules in solution as a function of their shape and size (199, 200). We reasoned that SEC could allow us to distinguish the state of RefZ and the rLOF variants in solution as well as determine the effects of ATP on RefZ's oligomerization state. Using a mobile phase of 50 mM Tris-HCl [pH 9.0], 300 mM KCl, and 10% (v/v) glycerol, WT RefZ eluted from a Supradex 200 column as a single peak corresponding to an apparent molecular weight of a RefZ monomer (Fig. 3.16). Gel filtration can only provide an apparent molecular weight since retention time in the column is directly related to the Stokes radius of the molecule, not to the actual molecular weight (Senisterra and Finerty, 2009; La Verde et al., 2017). SEC of an elongated protein with a larger hydrodynamic radius than a globular protein of equivalent mass will result in an overestimation of true molecular weight (199, 200).

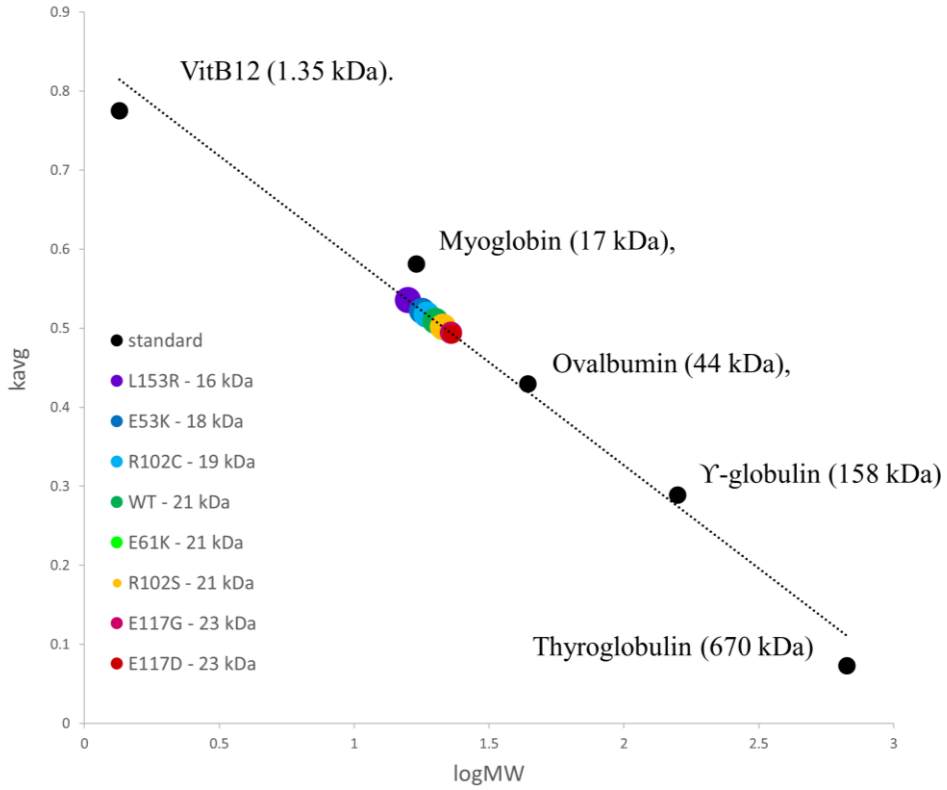

Figure 3.16. Gel filtration chromatography of WT and a subset of rLOF variants on a Supradex 200 column (1.0 mg/ml). Molecular mass estimated using the calculated K_{avg} for standards Thyroglobulin (670 kDa), Y-globulin (158 kDa), Ovalbumin (44 kDa), Myoglobin (17 kDa), and VitB12 (1.35 kDa). The E61K and R102C variants plot to the same position on the standard curve so only R102C is visible.

Several TetR proteins with nearly identical Stokes radii to RefZ elute on SEC columns at the predicted dimeric molecular weight, and some of these were found to be dimers by analytical ultracentrifugation (201). SlmA also elutes as a single peak around 48 kDa, suggestive of a dimeric complex (132). Taken together these results suggest that gel filtration can accurately distinguish monomer from dimer for the TetR family. Based on the B2H data (Fig. 3.9), we think RefZ can exist as a monomer/dimer equilibrium in solution. However, as the dimerization contact for RefZ is not strong, we hypothesize that the dimers are dissociated by passage through gel filtration column.

Several of the rLOF variants, and E53K in particular, showed increased self-interaction in the B2H analysis (Fig. 3.9). To see if E53K or other rLOF variants would have elution profiles distinct from WT, we repeated gel filtration (Fig. 3.16). Under the conditions tested, WT RefZ and each of the variants tested (E61K, R102C, R102S, E117G, E117D, and L153R) all eluted as monomers (Fig. 3.16). We also repeated in the presence of a mobile phase containing 1 mM ATP, and observed a nearly identical elution profile (data not shown). These data indicate that under the conditions tested, RefZ exists as a monomer.

Discussion

Nucleoid occlusion at the pole "tunes" the forespore DNA capture

RefZ is required for the timely redistribution of FtsZ from midcell to the pole (82), and RefZ-*RBM* complexes mediate precise capture of the chromosome by the polar sporulation septum (83). When artificially induced during vegetative growth, RefZ inhibits formation of Z-rings. The observation that Z-ring disruption during vegetative growth also required DNA-binding led us to hypothesize that RefZ might act through a NO mechanism to tune Z-ring positioning for precise chromosome capture. This hypothesis was further bolstered by the fact that RefZ and SlmA (the NO protein of *E. coli*) both belong to the TetR family of DNA-binding proteins. Moreover, the conservation of the *RBM*s and their relative position on the chromosome across the *Bacillus* genus, and the localization of RefZ and the *RBM*s near the site of polar septation (83) argues that RefZ's FtsZ inhibitory activity is spatially constrained by its interactions with the nucleoid.

To determine if RefZ's FtsZ-inhibitory activity was important for chromosome capture, we took advantage of RefZ's misexpression phenotype to isolate 10 rLOF variants capable of binding DNA, but unable to inhibit FtsZ. All 10 of the rLOF variants were unable to support chromosome capture, providing evidence that *B. subtilis* utilizes a NO mechanism to facilitate the positioning of the sporulation septum.

Variant	FtsZ inhibition	Chromosome Capture	Self-Interaction	ΔT_m (°C)	EMSA apparent Kd	EMSA laddering	Specificity for *RBM*	ATPase activity
WT	+	+	++	-	++	++	+++	++
E53K	-	-	++++	+4	++	++++	+	+
E61K	-	-	++	-	++	++++	+	+
R102C	-	-	+	-4	+	-	+++	++++
R102S	-	-	++	-2	++	++	+++	+
R116S	-	-	+++	-3	++	++	+++	+
R116W	-	-	-	-2	++	++	+++	+
E117D	-	-	++	-	++	+	+++	++
E117G	-	-	++	-	++	+++	++	++
L153R	-	-	-	-5	+	-	+++	+++
E179K	-	-	+++	-	++	++	+++	+++
Y43A	-	ND	++	ND	ND	ND	ND	ND
Y44A	-	ND	+	ND	ND	ND	ND	ND
R106A	-	ND	+	ND	ND	ND	ND	ND
E107A	-	ND	++	ND	ND	ND	ND	ND

Table 3.3. Qualitative summary of RefZ and rLOF variant characterization. Activity in the corresponding assays is indicated by (-) for non-functional, and (+) for varying degrees of functionality. Pink indicates a reduction relative to WT. Green indicates an increase relative to WT. Dashed lines in the ΔT_m column signify a difference of less than 1.5°C. ND = not determined.

Role of RefZ oligomerization and RBM-binding in the regulation of FtsZ

To better understand RefZ's mechanism of action at the molecular level, WT RefZ and the rLOFs variants were overexpressed, purified, and analyzed utilizing structural and biochemical approaches (summary of biochemical characterization Table 3.3). The RefZ crystal structure revealed that, like other solved TetR proteins, including SlmA, RefZ is

capable of forming a homodimer. Moreover, mapping of the residues implicated in FtsZ regulation revealed RefZ and SlmA do not share the same interaction interface. Instead, two of the rLOF variants (R102C and L153R) (Fig. 3.17) possessed substitutions in residues predicted to effect dimerization, a result corroborated by B2H analysis (Fig. 3.9). Two other rLOF variants (E53K and E61K) are on α4 which in other TetR family proteins has been shown to transmit the structural changes from allosteric effectors to the DNA-binding domain resulting in the distance between a3 and a3' being incompatible with DNA binding. Both E53K and E61K exhibit increased laddering on $RBM_{L2\text{-}150bp}$ suggestive that these variants might be locked in a "favorable for DNA binding" conformation that cannot be switched by an allosteric effector (possibly the CTD of FtsZ). rLOF residues E179 (light gray monomer) R116' (cyan monomer) and E117' (cyan monomer) (Fig. 3.17) map to both sides of the dimer interface implicating that the RefZ-FtsZ interface is created by dimerization.

B2H analysis indicated that the majority (6/10) of rLOF variants exhibited either reduced or enhanced self-interaction (Table 3.3), suggesting that RefZ's ability to switch between a monomer and dimer state is an integral feature of its FtsZ-regulating mechanism. Since RefZ binds to DNA motifs localized in the vicinity of the incipient asymmetric septum (83), and DNA-binding is required for RefZ to affect FtsZ, the simplest model which accommodates the loss of function for variants (R102C and L153R) is that loss of dimerization precludes some degree of DNA binding during artifical missexpression that is required for killing. Alternatively, the ability to form a dimer in solution may be required for disrupting FtsZ.

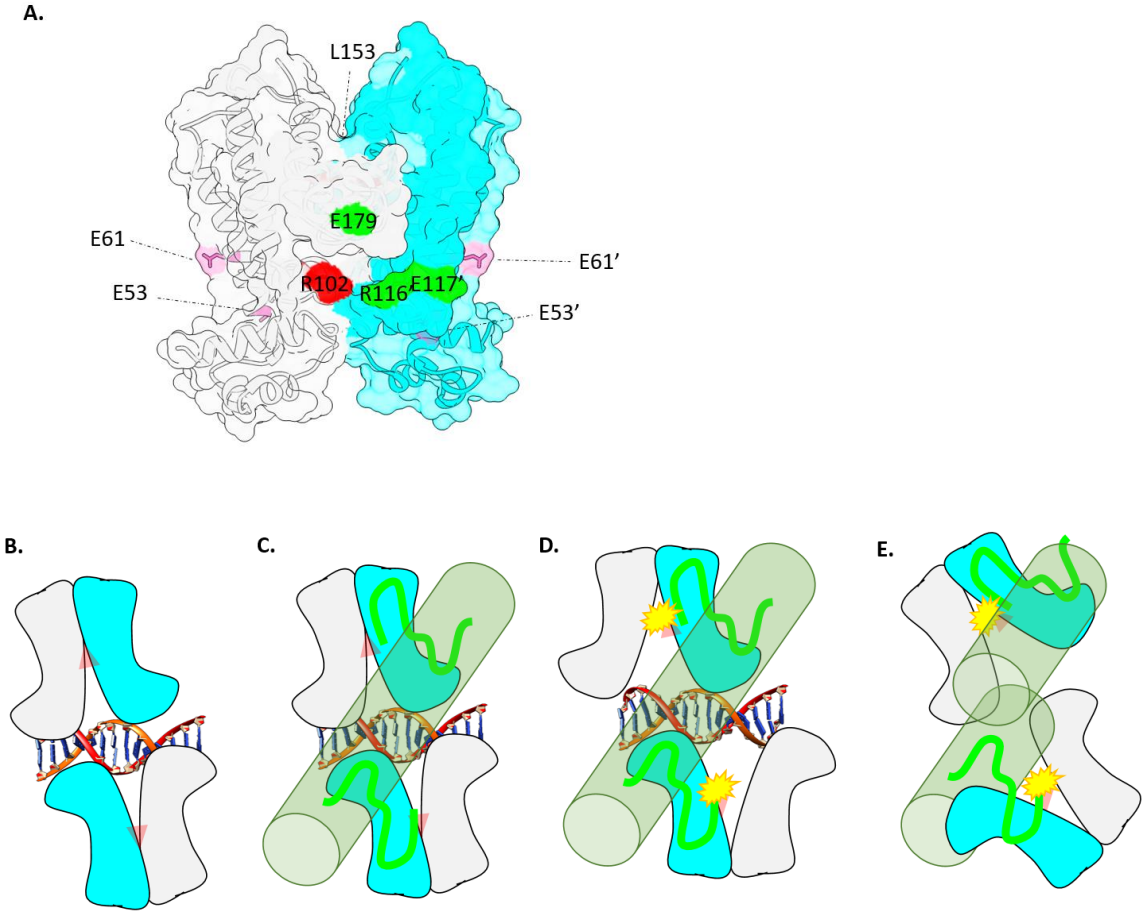

Figure 3.17. Model for RefZ targeting FtsZ (A) Crystal structure of RefZ highlighting the positions of residues implicated in the regulation of cell division. One RefZ monomer is light gray while the other is cyan. (**B)** RefZ (grey) bound to the *RBM* and ATP (red triangle) is activated to interact with the CTD of FtsZ (green cylinder). **(C)** FtsZ CTDs (bright green lines) extend from protofilaments and interact with the *RBM*-bound form of RefZ. **(D)** Interaction between RefZ and the CTD induces ATP hydrolysis, which causes RefZ to change conformation and dissociate from the *RBM*. **(E)** In the process of releasing, RefZ breaks the FtsZ filament, inhibiting filament growth and/or bundling.

We propose that the mechanism for FtsZ antagonism involves detachment of RefZ from the *RBM* (Fig. 3.17) because E53K and E61K both result in increased laddering on $RBM_{L2\text{-}150bp}$ suggesting that they stabilize a conformation of RefZ favorable for DNA binding. The position of these substitutions is on α4 of RefZ which has been shown to transmit the structural changes from allosteric effectors to the DNA-binding domain in other TetR family proteins. One of these mutants, E53K, also exhibited increased self-interaction by B2H, supporting the idea that this variant exists in an increased dimeric state in solution. Consistent with this idea, we observed increased stabilization for E53K in the thermal shift assay (+4^{o}C), while only a minor stabilization (+1^{o}C) was seen for the E61K variant. E53K and E61K may lock RefZ into a conformation which is unable to be allosterically affected by a ligand (presumably the FtsZ CTD).

RefZ is significantly destabilized by ATP in thermal shift assays, consistent with ATP binding. Additional experiments need to be performed to determine if RefZ is a bonafide ATPase, and if so how ATP hydrolysis factors in to RefZ's regulation of FtsZ. However, based on these preliminary data, we propose that, similar to ParA, RefZ utilizes ATP binding and hydrolysis to facilitate cycling between its DNA-bound and DNA-unbound states. Although structurally unrelated to RefZ, ParA also binds to DNA as a dimer, is capable of ATP binding, and dissociates from the DNA when its low-level ATPase activity is stimulated by ParA-ParB interaction (62). Details of our working model are discussed more below and summarized in Fig. 3.19. If ATP hydrolysis occurs upon FtsZ CTD interaction detaching RefZ from the DNA, then it is expected that E53K and E61K would exhibit low ATP hydrolytic activity (Fig. 3.14) since they are unable to be detached by the ligand interaction of the CTD.

The remaining variants (R102S, R116S, R116W, R117D, E117G, and E179K) are loss-of-function for reasons not obviously related to *RBM* binding (Table 3.3). Two variants in this class (R116S and E179K) exhibit enhanced self-interaction in the B2H, the significance of which is currently unclear. One possibility is that they form more stable dimers off of DNA. Conversely, R116W was loss-of-interaction in the B2H, but this variant bound DNA with WT affinity and specificity. This may suggest that the R116W variant is only reduced in its ability to form a dimer in solution, but not on DNA. For the two variants, R102S and E117D, the most obvious distinction is that R102S is on the dimer interface, whereas E117D is on the surface (Fig. 3.17). R102S also showed reduced ATPase activity compared to WT. E117D is the only variant identified in the rLOF screen that phenocopies WT RefZ's functionality in every respect tested except in its ability to inhibit cell division (and by proxy, support chromosome capture) (Table 3.3). The E117D substitution does not affect any of the other activities/properties of RefZ implicated in function (eg. DNA-binding and dimerization). It is striking that E117D displays a complete loss-of-function in the assays for FtsZ inhibition, as the change from a glutamate to an aspartate is conservative. We hypothesize that the shorter sidechain introduced by the aspartate substitution compromises the E117D variants ability to interact with FtsZ's CTD. These findings point toward E117 as a primary candidate for RefZ-FtsZ interaction. Moreover, R102, E117, R116, and E179 are all in close proximity to the dimerization interface and near RefZ's hydrophobic patches (Fig. 3.17 and Fig. 3.11)

Working model for RefZ-mediated NO

Based on available data, we propose a model (Fig 3.18) where RefZ mediates chromosome capture by fine-tuning the position of FtsZ assembly over the forespore-destined chromosome. In our model, RefZ is primed for FtsZ interaction by binding in an ATP-bound form to polarly-localized *RBM* sites. Based on structural studies of other TetR family proteins and the observation that RefZ binds to *RBM*s in units of two and four (83), it most likely does so as a pair of dimers; RefZ may also have the capacity to spread on DNA based on ChIP-seq data (82) and the observation that under some EMSA conditions, RefZ is capable of laddering on DNA (Fig. 3.13). Once bound to DNA, RefZ is poised to interact with CTDs extending from FtsZ protofilaments, likely through contacts (R116, E117, and E179) near the dimerization interface. The RefZ-CTD interaction stimulates RefZ to hydrolyze ATP, leading to a conformational change that simultaneously releases RefZ from the DNA and breaks the FtsZ filament. Given very limited number of *RBMs* present for RefZ binding, and the low levels relative to FtsZ that RefZ achieves upon expression, we think this dynamic system of reloading makes more sense than the a "single bullet" static system where only one bound pair of dimers interacts with FtsZ.

Since our data suggest the activity of RefZ toward FtsZ is inhibitory, this raises the question as to how an inhibitor of FtsZ promotes proper placement of the division apparatus. In our model, RefZ is only a weak inhibitor of FtsZ and its primary function is only to shift the location of Z-ring assembly away from the immediate vicinity of the *RBM*s, rather than to inhibit cell division at the pole. Another paradox raised is why the Δ*refZ* mutant exhibits a delay shifting Z-rings from midcell to the pole during sporulation (82). If RefZ acts as an inhibitor at the pole, then the obvious prediction would be that a

Δ*refZ* mutant would show accelerated Z-ring assembly at the poles. This seeming contradiction can be explained by considering RefZ's localization during sporulation. At early timepoints, just before polar division occurs, RefZ-GFP localizes as foci at the poles. These foci likely represent RefZ-*RBM* complexes, as they are lost in both a DNA-binding mutant (82) an *RBM* mutant (RBM_{mu5}) (Miller, unpublished data). Around the time polar division initiates, the polar RefZ foci disappear from the poles and coalesce near midcell, at or near the membrane (82). The redistribution of RefZ's inhibitory activity to midcell could facilitate disassembly of midcell Z-rings and its dynamic redistribution toward the pole (74).

Materials and Methods

Detailed general material and methods for growth, microscopy, the chromosome trapping assay, and bacterial two-hybrid analysis are described in Chapter II.

Western Blotting

B. subtilis strains were grown in 25 ml CH complete medium in 250 ml baffled flasks in a shaking waterbath at 280 rpm and 37ºC. rLOF expression was induced during early exponential (OD_{600} ~.01) with 1 mM IPTG for 45 min with shaking at 37ºC. 1 ml samples were collected and pellets were resuspended in 25 µl of lysis buffer (20 mM Tris [pH 7.5], 10 mM EDTA, 1.0 mg/ml lysozyme, 10 µg/ml DNase I, 100 µg/ml RNase A, and 1 mM phenylmethylsulfonyl fluoride). Samples were normalized by OD_{600} at the time of harvest in 2X sample buffer (0.25 M Tris [pH 6.8], 4% SDS, 20% glycerol, 10 mM EDTA, 10% (v/v) 2-mercaptoethanol) and run on a 4-20% gradient polyacrylamide gel (Lonza). Protein was transferred to a nitrocellulose membrane (Pall) for 1 hr at 60V, and

blocked in 5% (w/v) nonfat milk in PBS [pH 7.4] containing 0.05% (v/v) Tween-20 for 1 hr at room temperature. Membranes were probed with polyclonal rabbit α-RefZ antibody (1:1,000) at 4ºC overnight, followed by a 1:10,000 dilution of horseradish peroxidase-conjugated goat anti-rabbit immunoglobulin G secondary antibody (Bio-Rad) for 1 hr at room temperature. Washed membranes were incubated with SuperSignal West Femto chemiluminescent substrate (Thermo) according to the manufacturer's instructions prior to detection with an Amersham Imager 600 (GE Healthcare).

Protein overexpression and purification

To overexpress and purify RefZ-His6, pLM025a was transformed into BL21 (DE3) pLysS and plated on LB Lennox solid medium supplemented with kanamycin (25.0 µg/ml), chloramphenicol (25.0 µg/ml) and 0.1% (w/v) glucose. The following day colonies were pooled in ~2 mLs of Cinnabar supplemented with kanamycin (25.0 µg/ml), chloramphenicol (25 µg/ml) and 0.1% w/v glucose. The OD_{600} was measured and used to inoculate 4 x 25 mL of the same medium to an OD_{600} of 0.1. The cultures were grown 6-7 hrs in a shaking waterbath set at 280 rpm and 37ºC until reaching an OD_{600} of ~5. At this point, IPTG was added to a final concentration of 1 mM. The cultures were grown for an additional 3 hrs before harvesting. Cells were harvested by centrifugation for at 9,639 xg for 5 min at 4ºC, supernatant decanted, and pellets stored at -80ºC. Four pellets (~25 mL each) were resuspended in ~40 mL of Lysis buffer (50 mM Tris-HCl [pH 9.0], 300 mM KCl, 10% glycerol, and 10 mM imidazole). 1.0 µl of protease inhibitor (P8465 Sigma-Aldrich) was added per 35 OD units (OD_{600} x Volume Culture). DNase was added to a final concentration of 1 µg/mL of cell lysate. Resuspensions were passed through a

Microfluidizer LM20-30 five times at 10,000 psi. Cell lysate was cleared by spinning at 22,662 x g for 30 minutes at 4°C. A 2 mL column volume of Nickel-NTA agarose beads (Qiagen) was equilibrated with Lysis buffer. Supernatants were passed through the column, after which the resin bed was washed with 10 mL of Wash buffer (50mM Tris-HCl [pH 9.0], 300 mM KCl, 10% glycerol, 20 mM imidazole). 2-4 mL of Elution buffer (50 mM Tris-HCl [pH 9.0], 300 mM KCl, 10% glycerol, 250 mM imidazole) was used to elute RefZ off the column in ~250µl fractions. 2 µl was removed from each fraction for SDS-PAGE analysis, and elutions were immediately stored at -80°C. Elution fractions were thawed and pooled as needed and dialyzed into either Elution buffer (50 mM Tris-HCl [pH 9.0], 300 mM KCl, 10% glycerol, 250 mM imidazole) or ddH_2O using Thermo Scientific Slide-A-Lyzer 7.0 kDa MWCO dialysis cassettes at 4°C with stirring. Buffer was exchanged 3x with 500-1000 mL of either Elution buffer or ddH_2O. Protein concentrations were calculated using Bradford reagent and BSA as standard.

Crystallography screening

Before crystallization RefZ was taken from -80°C, thawed and the concentration determined. dsDNA was added to the given screening ration (Table 3.1) and the protein was dialyzed into the desired screening buffer (Table 3.1). Dialysis was performed 2-3 hrs/buffer change in 500-1000 mL with 3 buffer exchanges. After dialysis the protein was concentrated or directly set in 24 hanging drop vapor diffusion or 96 well sitting drop screening plates. rLOF variants were purified identically and dialyzed and set at concentrations indicated (Table 3.1). Nucleotide was added after dialysis and concentration.

Crystallography

RefZ crystals were grown by hanging drop vapor diffusion using a 4:1 molar ratio of RefZ (5.0 mg/ml RefZ, 50 mM Tris-HCl [pH 8.5], 300 mM KCl) and $RBM_{L2\text{-}24bp}$. The crystallization buffer was 10% ethanol (v/v), 0.1 M imidazole [pH 8.0], and 0.2 M $MgCl_2$. RefZ apo crystals appeared within 24-48 hrs. RefZ crystals were cryoprotected by brief soaking in crystallization buffer containing 20% (v/v) glycerol, and flash frozen in liquid nitrogen before the data collection. The data were collected at APS synchrotron radiation source, beamline 23ID. Pb acetate was successfully soaked into the RefZ crystal, providing an anomalous signal that permitted the phase to be solved by single anomalous dispersion method (SAD). Since crystal quality was poor, iterative building and phasing were employed on the electron density maps and re-processed in the lower symmetry group (to have a dimer in the asymmetric unit). A model comprising a continuous chain of residues 2-200 (out of 207) was successfully built and refined at 2.9 Å resolution to r_work = 0.2329 and r_free = 0.2902.

Annealing of oligos to generate dsDNA for crystallography

Complementary oligonucleotides were resuspended in annealing buffer (10 mM Tris-HCl [pH 7.5], 50 mM NaCl, and 1 mM EDTA) to a concentration of 1 mM according to Sigma's protocol (202). They were annealed in a thermocycler by heating to 95^{o}C for 2 min followed by ramp cooling for 45 min to 25^{o}C. The annealing buffer was removed by dialysis into ddH_2O with a 7.0 kDa MW cutoff dialysis cassette.

Electrophoretic gel mobility shift assays

For Fig. 3.4, 50 nM of OEB091/OEB092 (41 bp) annealed as described above was incubated with RefZ-His and HSUMO-RefZ (concentrations in Fig. 3.4) in 20 mM Tris-HCl [pH 8.5] with *RBM* $_{L2\text{-}41bp}$ for 10 minutes prior to addition of 10X Loading Bx (1 mM Tris-HCl [pH 8.0], 0.5 M EDTA, 50% (v/v) glycerol, 0.04% bromophenol blue). 10µl of the reaction was run at 200V for 60 min on a 7.5% TBE gel pre-run at 120V for 60 min. Inset gel run was run at 200V for 75 min to achieve further separation of the complexes.

For Fig. 3.12, DNA fragments (~150 bp each) were generated for the gel-shifts by PCR amplification of DNA centered on the native *RBM*s (using *B. subtilis* 168 as template) or mutant *RBM*s (using genomic from the RBM_{5mu} harboring strain as template). The fragment from RBM_{L2} was generated using the following primer pairs: oEB009 and oEB010. DNA binding reactions were incubated in 150 mM KCl and 10 mM Tris-HCl [pH 8.0) for 30 minutes. After 30 min incubation, 10X DNA loading buffer (45% glycerol, 50 mM EDTA [pH 8.0], and 1 mM Tris-HCl [pH 8.0]) was added to a final concentration of 1X and samples were resolved at room temperature on a pre-run (100V/60 min) 5% Mini-PROTEAN TBE polyacrylamide gel (Biorad) for 45 min at 150V. After electrophoresis, the gel was incubated with agitation in 1X SYBR™ Green EMSA gel stain (Life Technologies) (diluted from 10,000X stock) in TBE buffer for 5-10 min followed by rinsing in 1X TBE for 5-10 min. DNA was visualized with a Typhoon FLA 9500 using the setting for Fluorescence and LPB (510LP) filter for SYBR™ Green.

Malachite green phosphate release assay for ATPase activity

ATPase reactions were incubated at 25ºC for 20 min. Purified RefZ or rLOF variants were diluted from a storage buffer containing 50 mM Tris-HCl [pH 9.0], 300 mM KCl, 250 mM imidazole, and 10 % (v/v) glycerol to a final concentration of 24 µM in 20 mM HEPES [pH 7.5] and 1 mM $MgCl_2$. The final concentration of imidazole after dilution was nominal, however, due to the effect of imidazole in the thermal shift analysis (see results) a Pearson's Correlation Test was performed to determine if the differences ATPase activity could be attributed to the differences in imidazole concentration; no correlation was detected. Phosphate release was quantified using a malachite green phosphate assay kit (Sigma-Aldrich). Color development was allowed to proceed for 30 min before measuring with the emission wavelength of 620 nm using the Infinite M200 PRO Multimode Microplate Reader (Tecan). All reactions were performed in triplicate using protein stored identically with the same number of freeze thaws. The amount of phosphate released was determined using the average values obtained from three standard curves.

Thermal shift assays

The TSA (Thermal Shift Assay) was performed in a 96 well plate with the CFX96 Touch™ Real-Time PCR Detection System and 5X SYPRO orange. The ramp rate was set to 1ºC/min from 25ºC to 95ºC. To assess rLOF stability compared to WT, variants stored at -80 in 50 mM Tris-HCl [pH 9.0], 300 mM KCl, 250 mM imidazole, and 10% (v/v) glycerol were diluted to 10 µM in 20 mM Tris-HCl [pH 7.5]. To ensure identical reaction conditions, we normalized to the lowest variant concentration, which resulted in a

final storage buffer concentration of 0.16X for WT and rLOF variants. To assess WT RefZ's ability to bind to ATP, purified protein was diluted from a ~10 mg/mL stock stored in 50 mM Tris-HCl [pH 9.0], 300 mM KCl, 250 mM imidazole, and 10% (v/v) glycerol to 10 µM in 20 mM Tris-HCl [pH 7.5] and 1.0 mM $MgCl_2$. The final storage buffer concentration was 0.025X. ATP (0.2 M ATP in 100 mM HEPES [pH 7.5]) was diluted to give a final reaction concentration of 1.0 mM. Identical volumes of ATP storage buffer was added to controls.

Gel filtration chromatography

A Supradex 200 column was equilibrated with 50 mM Tris-HCl [pH 9.0], 300 mM KCl, and 10% (v/v) glycerol. WT RefZ and rLOF stored in ddH_2O were diluted to 1 mg/mL in a volume of 200 µl (50 mM Tris-HCl [pH 9.0], 300 mM KCl, 10% (v/v) glycerol) prior to injection. Samples were prespun at 4^{o}C for 10 min at 21,130 xg in a chilled table top centrifuge. The absorbance at 280 nm was continuously measured and the V_e corresponding to peak maximum was taken from resulting elution profile and used to calculate $K_{av} = (V_e – V_o)/(V_t - V_o)$. V_e= the elution volume (corresponding volume for peak height maximum).V_o = the void volume (7 mL experimentally determined from elution of aggregated complexes for Superdex 200 PC 3.2/30 3.2 × 300 mm). V_t= total volume of the column (24 mL for Superdex 200 PC 3.2/30 3.2 × 300 mm). The apparent molecular mass was estimated using a curve generated from the molecular mass standard (Biorad Gel Filtration Standard cat#151-1901) Thyroglobulin (670 kDa), Y-globulin (158 kDa), ovalbumin (44 kDa), myoglobin (17 kDa), and VitB12 (1.35 kDa).

Table 3.3 Strain table Chapter III

Strain	Description	Reference/Figure
Parental		
B. subtilis 168	*Bacillus subtilis* laboratory strain 168 *trpC2*	Bacillus Genetic Stock Center (1A866)
BL21 (DE3)	*BL21 (DE3) pLysS (cat)*	Expression host
DH5a	*F-, endA1, glnV44, thi-1, recA1, relA1, gyrA96, deoR, nupG, Φ80dlacZΔM15, Δ(lacZYA-argF)U169, hsdR17(r_K^- m_K^+), λ–*	
DHP1	*F-, cya-99, araD139, galE15, galK16, rpsL1 (Strr), hsdR2, mcrA1,mcrB1*	Obtained from Thomas Bernhardt
B. subtilis 168		
BJH188	*Em his nprE18 aprE3 eglS(DELTA)102 bglT/bglS(DELTA)EV lacA::PxylA-comK (ERM)*	Bacillus Genetic Stock Center (1A976)
BJH042	*minD::kan, amyE::*$P_{hyperspank}$*-refZ (WT) (spec)*	Jennifer Herman
BAM043	*minD::kan*	This work
BAM142	*lacA::*P_{xylA}*-comK (erm)*	This work
BAM229	*sacA::*P_{spremo}*-lacZ (cat)*	This work
BAM248	*sacA::*P_{spremo}*-lacZ (cat), refZ::tet*	This work
BAM266	*sacA::*P_{spremo}*-lacZ (cat), refZ ::tet, lacA::*P_{xylA}*-comK (erm)*	This work
BAM168	*sacA::*P_{spremo}*-lacZ (cat), refZ ::tet, lacA::*P_{xylA}*-comK (erm), minD::kan*	This work
BAM1060	*sacA::*P_{spremo}*-lacZ (cat), refZ ::tet, lacA::*P_{xylA}*-comK (erm), minD::kan, amyE::*$P_{hyperspank}$*-refZ (E53K) (spec)*	Original rLOF isolate
BAM1061	*sacA::*P_{spremo}*-lacZ (cat), refZ ::tet, lacA::*P_{xylA}*-comK (erm), minD::kan, amyE::*$P_{hyperspank}$*-refZ (E61K) (spec)*	Original rLOF isolate

Table 3.3 continued.

Strain	Description	Reference/Figure
BAM1062	*sacA::P_{spremo}-lacZ (cat), refZ ::tet, lacA::P_{xylA}-comK (erm), minD::kan, amyE::$P_{hyperspank}$-refZ (R102C) (spec)*	Original rLOF isolate
BAM1063	*sacA::P_{spremo}-lacZ (cat), refZ ::tet, lacA::P_{xylA}-comK (erm), minD::kan, amyE::$P_{hyperspank}$-refZ (R102S) (spec)*	Original rLOF isolate
BAM1064	*sacA::P_{spremo}-lacZ (cat), refZ ::tet, lacA::P_{xylA}-comK (erm), minD::kan, amyE::$P_{hyperspank}$-refZ (R116S) (spec)*	Original rLOF isolate
BAM1065	*sacA::P_{spremo}-lacZ (cat), refZ ::tet, lacA::P_{xylA}-comK (erm), minD::kan, amyE::$P_{hyperspank}$-refZ (R116W) (spec)*	Original rLOF isolate
BAM1066	*sacA::P_{spremo}-lacZ (cat), refZ ::tet, lacA::P_{xylA}-comK (erm), minD::kan, amyE::$P_{hyperspank}$-refZ (E117D) (spec)*	Original rLOF isolate
BAM1067	*sacA::P_{spremo}-lacZ (cat), refZ ::tet, lacA::P_{xylA}-comK (erm), minD::kan, amyE::$P_{hyperspank}$-refZ (E117G) (spec)*	Original rLOF isolate
BAM1068	*sacA::P_{spremo}-lacZ (cat), refZ ::tet, lacA::P_{xylA}-comK (erm), minD::kan, amyE::$P_{hyperspank}$-refZ (L153R) (spec)*	Original rLOF isolate
BAM1069	*sacA::P_{spremo}-lacZ (cat), refZ ::tet, lacA::P_{xylA}-comK (erm), minD::kan, amyE::$P_{hyperspank}$-refZ (E179K) (spec)*	Original rLOF isolate
BAM374	*sacA::P_{spremo}-lacZ (cat), refZ ::tet, lacA::P_{xylA}-comK (erm), minD::kan, amyE::$P_{hyperspank}$-refZ (WT) (spec)*	Figure 3.1B
BAM449	*sacA::P_{spremo}-lacZ (cat), refZ ::tet, lacA::P_{xylA}-comK (erm), minD::kan, amyE::$P_{hyperspank}$-refZ (E53K) (spec)*	Figure 3.1B
BAM462	*sacA::P_{spremo}-lacZ (cat), refZ ::tet, lacA::P_{xylA}-comK (erm), minD::kan, amyE::$P_{hyperspank}$-refZ (E61K) (spec)*	Figure 3.1B
BAM407	*sacA::P_{spremo}-lacZ (cat), refZ ::tet, lacA::P_{xylA}-comK (erm), minD::kan, amyE::$P_{hyperspank}$-refZ (R102C) (spec)*	Figure 3.1B
BAM409	*sacA::P_{spremo}-lacZ (cat), refZ ::tet, lacA::P_{xylA}-comK (erm), minD::kan, amyE::$P_{hyperspank}$-refZ (R102S) (spec)*	Figure 3.1B
BAM443	*sacA::P_{spremo}-lacZ (cat), refZ ::tet, lacA::P_{xylA}-comK (erm), minD::kan, amyE::$P_{hyperspank}$-refZ (R116S) (spec)*	Figure 3.1B
BAM440	*sacA::P_{spremo}-lacZ (cat), refZ ::tet, lacA::P_{xylA}-comK (erm), minD::kan, amyE::$P_{hyperspank}$-refZ (R116W) (spec)*	Figure 3.1B
BAM441	*sacA::P_{spremo}-lacZ (cat), refZ ::tet, lacA::P_{xylA}-comK (erm), minD::kan, amyE::$P_{hyperspank}$-refZ (E117D) (spec)*	Figure 3.1B
BAM403	*sacA::P_{spremo}-lacZ (cat), refZ ::tet, lacA::P_{xylA}-comK (erm), minD::kan, amyE::$P_{hyperspank}$-refZ (E117G) (spec)*	Figure 3.1B

Table 3.3 continued.

Strain	Description	Reference/Figure
BAM411	*sacA::P_{spremo}-lacZ (cat), refZ ::tet, lacA::P_{xylA}-comK (erm), minD::kan, amyE::$P_{hyperspank}$-refZ (L153R) (spec)*	Figure 3.1B
BAM407	*sacA::P_{spremo}-lacZ (cat), refZ ::tet, lacA::P_{xylA}-comK (erm), minD::kan, amyE::$P_{hyperspank}$-refZ (E179K) (spec)*	Figure 3.1B
BJH228	*amyE::$P_{hyperspank}$-refZ (WT) (spec)*	Figure 3.1C & 3.2
BAM457	*amyE::$P_{hyperspank}$-refZ (E53K) (spec)*	Figure 3.1C & 3.2
BAM490	*amyE::$P_{hyperspank}$-refZ (E61K) (spec)*	Figure 3.1C & 3.2
BAM434	*amyE::$P_{hyperspank}$-refZ (R102C) (spec)*	Figure 3.1C & 3.2
BAM436	*amyE::$P_{hyperspank}$-refZ (R102S) (spec)*	Figure 3.1C & 3.2
BAM454	*amyE::$P_{hyperspank}$-refZ (R116S) (spec)*	Figure 3.1C & 3.2
BAM451	*amyE::$P_{hyperspank}$-refZ (R116W) (spec)*	Figure 3.1C & 3.2
BAM455	*amyE::$P_{hyperspank}$-refZ (E117D) (spec)*	Figure 3.1C & 3.2
BAM431	*amyE::$P_{hyperspank}$-refZ (E117G) (spec)*	Figure 3.1C & 3.2
BAM450	*amyE::$P_{hyperspank}$-refZ (L153R) (spec)*	Figure 3.1C & 3.2
BAM428	*amyE::$P_{hyperspank}$-refZ (E179K) (spec)*	Figure 3.1C & 3.2
BJH205	*RBM_{5mu}*	(83)
BJH245	*yycR(-7°)::P_{spoIIQ}-yfp (phleo), lacA(-61°)::P_{spoIIQ}-cfp (erm), spoIIIE36-tet*	(83)/ Figure 3.3
BAM078	*yycR(-7°)::P_{spoIIQ}-yfp (phleo), +51°::P_{spoIIQ}-cfp (erm), spoIIIE36-tet*	(83)/ Figure 3.3
BAM1006	*refZ::refZ (wt) (cat), yycR(-7°)::P_{spoIIQ}-yfp (phleo), lacA(-61°)::P_{spoIIQ}-cfp (erm), spoIIIE36-tet*	Figure 3.3

Table 3.3 continued.

Strain	Description	Reference/Figure
BAM1007	*refZ::refZ (wt) (cat), yycR(-7°)::P_{spoIIQ}-yfp (phleo), +51°::P_{spoIIQ}-cfp (erm), spoIIIE36-tet*	Figure 3.3
BAM1008	*refZ::refZ (E179K) (cat), yycR(-7°)::P_{spoIIQ}-yfp (phleo), lacA(-61°)::P_{spoIIQ}-cfp (erm), spoIIIE36-tet*	Figure 3.3
BAM1009	*refZ::refZ (E179K) (cat), yycR(-7°)::P_{spoIIQ}-yfp (phleo), +51°::P_{spoIIQ}-cfp (erm), spoIIIE36-tet*	Figure 3.3
BAM1010	*refZ::refZ (E117G) (cat), yycR(-7°)::P_{spoIIQ}-yfp (phleo), lacA(-61°)::P_{spoIIQ}-cfp (erm), spoIIIE36-tet*	Figure 3.3
BAM1011	*refZ::refZ (E117G) (cat), yycR(-7°)::P_{spoIIQ}-yfp (phleo), +51°::P_{spoIIQ}-cfp (erm), spoIIIE36-tet*	Figure 3.3
BAM1012	*refZ::refZ (R012C) (cat), yycR(-7°)::P_{spoIIQ}-yfp (phleo), lacA(-61°)::P_{spoIIQ}-cfp (erm), spoIIIE36-tet*	Figure 3.3
BAM1013	*refZ::refZ (R102C) (cat), yycR(-7°)::P_{spoIIQ}-yfp (phleo), +51°::P_{spoIIQ}-cfp (erm), spoIIIE36-tet*	Figure 3.3
BAM1014	*refZ::refZ (R102S) (cat), yycR(-7°)::P_{spoIIQ}-yfp (phleo), lacA(-61°)::P_{spoIIQ}-cfp (erm), spoIIIE36-tet*	Figure 3.3
BAM1015	*refZ::refZ (R102S) (cat), yycR(-7°)::P_{spoIIQ}-yfp (phleo), +51°::P_{spoIIQ}-cfp (erm), spoIIIE36-tet*	Figure 3.3
BAM1016	*refZ::refZ (L153R) (cat), yycR(-7°)::P_{spoIIQ}-yfp (phleo), lacA(-61°)::P_{spoIIQ}-cfp (erm), spoIIIE36-tet*	Figure 3.3
BAM1017	*refZ::refZ (L153R) (cat), yycR(-7°)::P_{spoIIQ}-yfp (phleo), +51°::P_{spoIIQ}-cfp (erm), spoIIIE36-tet*	Figure 3.3
BAM1018	*refZ::refZ (R116W) (cat), yycR(-7°)::P_{spoIIQ}-yfp (phleo), lacA(-61°)::P_{spoIIQ}-cfp (erm), spoIIIE36-tet*	Figure 3.3
BAM1019	*refZ::refZ (R116W) (cat), yycR(-7°)::P_{spoIIQ}-yfp (phleo), +51°::P_{spoIIQ}-cfp (erm), spoIIIE36-tet*	Figure 3.3
BAM1020	*refZ::refZ (R116S) (cat), yycR(-7°)::P_{spoIIQ}-yfp (phleo), lacA(-61°)::P_{spoIIQ}-cfp (erm), spoIIIE36-tet*	Figure 3.3
BAM1021	*refZ::refZ (R116S) (cat), yycR(-7°)::P_{spoIIQ}-yfp (phleo), +51°::P_{spoIIQ}-cfp (erm), spoIIIE36-tet*	Figure 3.3
BAM1022	*refZ::refZ (E117D) (cat), yycR(-7°)::P_{spoIIQ}-yfp (phleo), lacA(-61°)::P_{spoIIQ}-cfp (erm), spoIIIE36-tet*	Figure 3.3
BAM1023	*refZ::refZ (E117D) (cat), yycR(-7°)::P_{spoIIQ}-yfp (phleo), +51°::P_{spoIIQ}-cfp (erm), spoIIIE36-tet*	Figure 3.3

Table 3.3 continued.

Strain	Description	Reference/Figure
BAM1024	*refZ::refZ (E53K) (cat), yycR(-7°)::P_{spoIIQ}-yfp (phleo), lacA(-61°)::P_{spoIIQ}-cfp (erm), spoIIIE36-tet*	Figure 3.3
BAM1025	*refZ::refZ (E53K) (cat), yycR(-7°)::P_{spoIIQ}-yfp (phleo), +51°::P_{spoIIQ}-cfp (erm), spoIIIE36-tet*	Figure 3.3
BAM1026	*refZ::refZ (E61K) (cat), yycR(-7°)::P_{spoIIQ}-yfp (phleo), lacA(-61°)::P_{spoIIQ}-cfp (erm), spoIIIE36-tet*	Figure 3.3
BAM1027	*refZ::refZ (E61K) (cat), yycR(-7°)::P_{spoIIQ}-yfp (phleo), +51°::P_{spoIIQ}-cfp (erm), spoIIIE36-tet*	Figure 3.3

Strain construction

The background used in the rLOF selection-screen (Figure 3.1A, B) was generated by the following transformations in *Bacillus:*

BAM229 was created by transformation of linearized pAM083 (below) into *Bs168* wildtype, selecting for integration of the P_{spremo}-*lacZ* fusion at the *sacA* locus with chloramphenicol (cat5). Genomic DNA from resulting cat^R transformants was prepared and the *sacA* locus screened by PCR with OAM124 and OAM125. The P_{spremo} promoter region (a fusion of the *Phyperspank* promoter to a single RefZ binding motif, RBM_{L2}) was sequenced from the PCR products with OJH133.

BAM248 was created by transformation of BAM229 with genomic DNA isolated from BJH247 (*Bs168 refZ::tet*) selecting for double crossover integration with tetracyclin (tet10) and transformants were confirmed to retain cat^R.

BAM266 was created by transformation of BAM248 with genomic DNA isolated from BJH188 selecting for integration of the P_{xylA}-*comK* fusion at the *lacA* locus with MLS (erm10) and transformants were confirmed to retain cat^R and tet^R.

BAM168 was created by transformation of BAM266 with genomic DNA isolated from BAM043 (*Bs168 minD::kan)* selecting for double crossover integration with kanamycin (kan10) and transformants were confirmed to retain cat^R, tet^R, and erm^R.

Selection for rLOF variants (BAM1060-1069)

The *refZ* open-reading frame was PCR amplified from pJW013 with Phusion polymerase using OAM122 and OAM165 to create the template for mutagenesis. Error-prone PCR using a GeneMorph II Random Mutagenesis Kit was performed according to

the manufacturer's protocol (Agilent Technologies #200550) using OAM122 and OAM166 which introduce 5' sequence homology to $P_{hyperspank}$ and 3' sequence homology to *lacI,* respectively, to create a fragment pool of *refZ* mutants. The mutant pool of *refZ* fragments was combined with the following PCR fragments listed with primer set and template used for PCR (in parentheses):

"***P_{hy}-spec^R-amyE**"* creates homology to the upstream region flanking *amyE* for double crossover and introduces the $P_{hyperspank}$ inducible promoter sequence and a spectinomycin (*spec^R*) cassette for selection
OAM010/OAM013 (genomic DNA isolated from BJH228, *amyE::$P_{hyperspank}$-refZ (spec)*)

"***amyE-lacI***" creates homology to the downstream region flanking *amyE* for double crossover and introduces *lacI* gene for repression of $P_{hyperspank}$ promoter
OAM001/OAM012 (genomic DNA isolated from BJH228, *amyE::$P_{hyperspank}$-refZ (spec)*)

Fragments were combined at equimolar ratios in a one-step enzymatic assembly reaction (Gibson *et al*., 2009) and transformed directly into BAM168 (selection-screen background) selecting for double crossover integration of the $P_{hyperspank}$-*rLOF* mutant library at the *amyE* locus with spectinomycin (spec100) plates supplemented with inducer (1mM IPTG). Surviving transformants were confirmed to also maintain *cat^R*, *tet^R*, *erm^R*,, and *kan^R*. Isolates were then visually screened for LacZ expression on spec100 plates supplemented with IPTG and X-gal. Genomic DNA was isolated and screened by PCR with OJH001 and OJH002 to confirm proper integration and *refZ* genes were sequenced to identify any rLOF mutations.

BAM374 was created by transformation of BAM168 with genomic DNA isolated from BJH228 selecting for integration of the P$_{hyperspank}$-*refZ (WT)* fusion at the *amyE* locus with spectinomycin (spec100) and transformants were confirmed to retain *cat^R*, *tet^R*, *erm^R*,, and *kan^R*.

BAM strains corresponding to Figure 3.1b were created similar to BAM374, except genomic DNA prepared from the original rLOF mutant strains (BAM1060-1069) isolated in the selection-screen were transformed into BAM168 (clean selection-screen background) and integration of each P$_{hyperspank}$-*rLOF* fusion was selected for with spec100. Transformants were also confirmed to retain *cat^R*, *tet^R*, *erm^R*,, and *kan^R*.

BAM strains corresponding to Figure 3.1c and Figure 3.2 were created by transformation of *Bs168* wildtype with genomic DNA prepared from the original rLOF mutant strains isolated in the selection-screen, selecting for integration of each P$_{hyperspank}$-*rLOF* fusion with spec100. Transformants were also confirmed for sensitivity to all other resistances present in the selection-screen background (*catS, tetS, ermS,* and *kanS*).

rLOF Reporter Trapping Strains corresponding to Figure 3.3 (BAM1006-BAM1027) Gibson assembly (171)was performed to produce linear DNA constructs comprised of the following PCR fragments listed with primer set and template used for PCR (in parentheses):

"***UP***" creates region of homology to upstream region flanking *refZ* for double crossover
OAM200/OAM201 (*Bs168 wt*)

"***rLOF****"* amplifies each of the rLOF variants from corresponding misexpression constructs. OAM202/OAM203 (genomic DNA prepared from original rLOF mutant isolates)
OAM202 introduces 27bp to the 5' end of each amplicon with homology to the "*UP*" fragment. OAM203 introduces 24bp to the 3' and of each amplicon with homology to "cat^R" fragment.

"***cat^R***" for selection of transformation with chloramphenicol (cm5)
OJH179/OJH180 (*pKM074*)

"***DOWN***" creates region of homology to downstream region flanking *refZ* for double crossover
OAM204/OAM205 (*Bs168 wt*)

Fragments were combined at equimolar ratios in a one-step enzymatic assembly reaction (171) and transformed directly into both left and right arm reporter trapping backgrounds, BJH245 and BAM078, respectively, selecting for double crossover integration of the rLOF mutants at the native *refZ* locus with chloramphenicol (cat5). Resulting transformants were confirmed to also maintain erm^R, $phleo^R$, tet^R and to exhibit *spo*- phenotypes on DSM plates. Genomic DNA was isolated and screened by PCR with OAM200/205 to confirm proper integration and *refZ* genes were sequenced to confirm the presence of the introduced rLOF mutation with OEB041 and OEB042.

Table 3.4. Plasmid table Chapter III

Plasmid	Description	Reference/Figure/ Use
pJW013	*amyE::$P_{hyperspank}$-refZ (spec) (amp)*	Herman *et al*., 2012
pJW034	*yycR::$P_{hyperspank}$ (cat) (amp)*	Jennifer Herman, unpublished
pJH036	*sacA::$P_{hyperspank}$-lacZ (erm) (amp)*	Ben Mercado
pKM074	*MCS1+2 (cat) (amp)*	Kathleen Marquis
pKM062	*sacA::erm (amp)*	Kathleen Marquis
pAM037	*yycR::P_{spremo} (cat) (amp)*	This work
pAM046	*sacA::cat (amp)*	This work
pAM080	*sacA::P_{spremo} (cat) (amp)*	This work
pAM081	*sacA::$P_{hyperspank}$ (cat) (amp)*	This work
pAM083	*sacA::P_{spremo}-lacZ (cat) (amp)*	This work
pAM084	*sacA::$P_{hyperspank}$-lacZ (cat) (amp)*	This work
pCH363	*empty-T18 (amp)*	Tom Bernhardt/B2H vector
pKNT25	*empty-T25 (kan)*	Tom Bernhardt/B2H vector
pJW097	*refZ(WT)-T18 (amp)*	Miller *et al*., 2016/ Figure 3.9
pJW096	*refZ(WT)-T25 (kan)*	Miller *et al*., 2016/ Figure 3.9
pAM152	*refZ(E53K)-T18 (amp)*	Figure 3.9
pAM162	*refZ(E53K)-T25 (kan)*	Figure 3.9
pAM153	*refZ(E61K)-T18 (amp)*	Figure 3.9
pAM163	*refZ(E61K)-T25 (kan)*	Figure 3.9
pAM154	*refZ(R102C)-T18 (amp)*	Figure 3.9
pAM164	*refZ(R102C)-T25 (kan)*	Figure 3.9
pAM155	*refZ(R102S)-T18 (amp)*	Figure 3.9

Table 3.4. Continued

Plasmid	Description	Reference/Figure/ Use
pAM165	*refZ(R102S)-T25 (kan)*	Figure 3.9
pAM156	*refZ(R116S)-T18 (amp)*	Figure 3.9
pAM166	*refZ(R116S)-T25 (kan)*	Figure 3.9
pAM157	*refZ(R116W)-T18 (amp)*	Figure 3.9
pAM167	*refZ(R116W)-T25 (kan)*	Figure 3.9
pAM158	*refZ(E117D)-T18 (amp)*	Figure 3.9
pAM168	*refZ(E117D)-T25 (kan)*	Figure 3.9
pAM159	*refZ(E117G)-T18 (amp)*	Figure 3.9
pAM169	*refZ(E117G)-T25 (kan)*	Figure 3.9
pAM160	*refZ(L153R)-T18 (amp)*	Figure 3.9
pAM170	*refZ(L153R)-T25 (kan)*	Figure 3.9
pAM161	*refZ(E179K)-T18 (amp)*	Figure 3.9
pAM171	*refZ(E179K)-T25 (kan)*	Figure 3.9
pAM144	*refZ(Y43A)-T18 (amp)*	Figure 3.9
pAM139	*refZ(Y43A)-T25 (kan)*	Figure 3.9
pAM145	*refZ(Y44A)-T18 (amp)*	Figure 3.9
pAM140	*refZ(Y44A)-T25 (kan)*	Figure 3.9
pAM146	*refZ(R106A)-T18 (amp)*	Figure 3.9
pAM141	*refZ(R106A)-T25 (kan)*	Figure 3.9
pAM147	*refZ(E107A)-T18 (amp)*	Figure 3.9
pAM142	*refZ(E107A)-T25 (kan)*	Figure 3.9
pRD001	*amyE::$P_{hyperspank}$-refZ(R106A) (spec) (amp)*	Jennifer Herman
pRD002	*amyE::$P_{hyperspank}$-refZ(E107A) (spec) (amp)*	Herman *et al*., 2012
pRD004	*amyE::$P_{hyperspank}$-refZ(E117A) (spec) (amp)*	Jennifer Herman

Table 3.4. Continued

Plasmid	Description	Reference/Figure/ Use
pRD010	*amyE::$P_{hyperspank}$-refZ(Y43A) (spec) (amp)*	Herman *et al*., 2012
pRD011	*amyE::$P_{hyperspank}$-refZ(Y44A) (spec) (amp)*	Jennifer Herman
pET24b (+)	*C-terminal His-tag*	
pET28a (+)	*N-/C-terminal His-tag*	
pLM025	*refZ(WT)-His6 (kan)*	Larry Mulcahy
pEB002	*refZ(WT) (kan)*	This work
pEB003	*ftsZ (kan)*	This work
pEB004	*refZ(Y43A)-His6 (kan)*	This work
pEB005	*refZ (E117A)-His6 (kan)*	This work
pEB019	*refZ(E53K)-His6 (kan)*	This work
pEB020	*refZ(E61K)-His6 (kan)*	This work
pEB017	*refZ(R102C)-His6 (kan)*	This work
pEB018	*refZ(R102S)-His6 (kan)*	This work
pEB013	*refZ(R116S)-His6 (kan)*	This work
pEB022	*refZ(R116W)-His6 (kan)*	This work
pEB015	*refZ(E117D)-His6 (kan)*	This work
pEB014	*refZ(E117G)-His6 (kan)*	This work
pEB021	*refZ(L153R)-His6 (kan)*	This work
pEB016	*refZ(E179K)-His6 (kan)*	This work
pEB006	pUC19_L2R1	This work
pEB007	pUC19_L2mR1	This work
pEB008	pUC19_mL2mR1	This work

Plasmid construction

pAM037 was generated by cloning the annealed product of oligos OAM139 and OAM140 into pJW034 (XhoI-HindIII)

pAM046 was generated by subcloning the *cat-*^{R} cassette from pKM074 into the backbone of pKM062 (SalI-BamHI)

pAM080 was generated by cloning PCR product of OJH133 and OJH001 from pAM037 into pAM046 (EcoRI-HindIII)

pAM083 was generated by cloning PCR product of OJH185 and OJH186 from pJH036 into pAM080 (HindIII-NheI)

rLOF bacterial 2-hybrid pAM's corresponding to Figure 3.9 were generated by cloning PCR products of OAM148 and OAM149 from genomic DNA prepared from corresponding rLOF Reporter Trapping strains (BAM1006-1026, even numbered strains) or pRD010, pRD011, pRD001, and pRD002 (for Y43A, Y44A, R106A, and E107A, respectively) into both pCH363 (creates *rLOF-T18*; selection with amp100) and pKNT25 (creates *rLOF-T25*; selection with kan25) (SphI-BamHI). Clones confirmed by PCR with OYD070 and OAM149 were sequenced for the presence of the introduced rLOF mutation.

pEB002 (WT RefZ overexpression, untagged) was generated by cloning PCR product from oEB024 and oAM095 amplification of 168 genomic into pET-24b (+) (NdeI and XhoI). The RBS is exactly 10 bp away from the 1st start codon. The native STOP codon was inserted before the C-terminal His tag.

pEB003 (FtsZ overexpression, untagged) was generated by cloning PCR product from oEB022 and oEB023 amplification of 168 genomic into pET-28a (+) (NcoI and EcoRI).

pEB004 (RefZ^{Y43A}-His6) was generated by cloning PCR product from oEB041 and oEB042 amplification of pRD010 into pET-24b (+) (NheI and XhoI).

pEB005 (RefZ^{E117A}-His6) was generated by cloning PCR product from oEB041 and oEB042 amplification of pRD004 into pET-24b (+) (NheI and XhoI).

pEB006 (pUC19_L2R1) generated by cloning overlap extension PCR product from oEB001 and oEB055 amplification (L2 PCR product (oEB001 and oEB002 genomic *Bs168*) & R1 PCR product (oEB003 and oEB055 genomic *Bs168*)) into pUC19 (EcoRI and BamHI)

pEB007 (pUC19_L2mR1) generated by cloning overlap extension PCR product from oEB001 and oEB055 amplification (L2 PCR product (oEB001 and oEB002, genomic *Bs168*) & mR1 PCR product (oEB003 and oEB055, genomic DNA from BJH205)) into pUC19 (EcoRI and BamHI)

pEB008 (pUC19_mL2mR1) generated by cloning overlap extension PCR product from oEB001 and oEB055 amplification (mL2 PCR product (oEB001 and oEB002 genomic DNA from BJH205) & mR1 PCR product (oEB003 and oEB055 genomic DNA from BJH205)) into pUC19 (EcoRI and BamHI)

pEB013 (RefZ^{R116S}-His6) generated by cloning PCR product from oEB041 and oEB042 amplification of genomic DNA from BAM1064 into pET-24b (+) (NheI and XhoI). Confirmed by sequencing.

pEB014 (RefZ^{E117G}-His6) generated by cloning PCR product from oEB041 and oEB042 amplification of genomic DNA from BAM1067 into pET-24b (+) (NheI and XhoI). Confirmed by sequencing.

pEB015 (RefZ^{E117D}-His6) generated by cloning PCR product from oEB041 and oEB042 amplification of genomic DNA from BAM1066 into pET-24b (+) (NheI and XhoI). Confirmed by sequencing.

pEB016 (RefZ^{E179K}-His6) generated by cloning PCR product from oEB041 and oEB042 amplification of genomic DNA from BAM1069 into pET-24b (+) (NheI and XhoI). Confirmed by sequencing.

pEB017 (RefZ^{R102C}-His6) generated by cloning PCR product from oEB041 and oEB042 amplification of genomic DNA from BAM1062 into pET-24b (+) (NheI and XhoI). Confirmed by sequencing.

pEB018 (RefZ^{R102S}-His6) generated by cloning PCR product from oEB041 and oEB042 amplification of genomic DNA from BAM1063 into pET-24b (+) (NheI and XhoI). Confirmed by sequencing.

pEB019 (RefZ^{E53K}-His6) generated by cloning PCR product from oEB041 and oEB042 amplification of genomic DNA from BAM1060 into pET-24b (+) (NheI and XhoI). Confirmed by sequencing.

pEB020 (RefZ^{E61K}-His6) generated by cloning PCR product from oEB041 and oEB042 amplification of genomic DNA from BAM1061 into pET-24b (+) (NheI and XhoI). Confirmed by sequencing.

pEB021 (RefZ^{L153R}-His6) generated by cloning PCR product from oEB041 and oEB042 amplification of genomic DNA from BAM1068 into pET-24b (+) (NheI and XhoI). Confirmed by sequencing.

pEB022 (RefZ^{R116W}-His6) generated by cloning PCR product from oEB041 and oEB042 amplification of genomic DNA from BAM1065 into pET-24b (+) (NheI and XhoI). Confirmed by sequencing.

Table 3.5. Oligonucleotide table Chapter III

Oligo	Sequence 5' to 3'
OEB001	TCGACAATTAAAATCTGAATTCCTTC
OEB002	TATGGCTCGTCTTAAAGGCAGTTCTCGGTATCGTGGAGGTC
OEB003	GACCTCCACGATACCGAGAACTGCCTTTAAGACGAGCCATA
OEB004	CATCTTTGTTTCCCAGACAGC
OEB005	GACTTGCTCCTGCTCAAGCTTTCTCGGTATCGTGGAGGTC
OEB006	GACCTCCACGATACCGAGAAAGCTTGAGCAGGAGCAAGTC
OEB009	ATCAGCGCTCTGGTGATTG
OEB010	TTTTGCACAGCCTTAGCTTC
OEB012	GCGACACCTCATCATAACAA
OEB0013	TTCCACCTCGCCGTAGATTC
OEB014	CCGCGCTTATGTACAGCATA
OEB015	AGCTTTAGCGGATCCGTGAT
OEB016	TTAAAGAACCGCTATGTCAG
OEB017	TGTATTCCTATACTACCACG
OEB018	TGGGCCACTGCTCCATT
OEB019	GAGGACCCTTTAAATGGAAGC
OEB020	GAAAACGAGAAATTTTCACACTC
OEB021	TTTTCTTCTTTTGACCGGCT
OEB022	TATACCATGGCTTTGGAGTTCGAAACAAACATAGAC
OEB023	GCTCGAATTCGGATTAGCCGCGTTTATTACGGT
OEB024	ATACATATGAAAGTAAGCACCAAAGACA
OEB027	ATTGAGAGTGCTAACAGAGGTGATG
OEB028	GTTGCAGAGCTAAATGTGATTTCATC
OEB029	GAAAACAAAACGATTAACTTTCCG
OEB030	GTGCTGTCTTAGGTACATGACAAC
OEB031	GCCTGAGTTCCATGATATCAC
OEB032	CTGCAATTTTCCATCTCTTCATA
OEB033	CAGTTAAACAAACGTTTAATCAA

Table 3.5. Continued

OEB034	TTGATTAAACGTTTGTTTAACTG
OEB035	GTCTTAAACAAACGTTTGATGAA
OEB036	TTCATCAAACGTTTGTTTAAGAC
OEB037	TGTTTAAACAAACGTTTCATTAA
OEB038	TTAATGAAACGTTTGTTTAAACA
OEB039	CACTTAAACAAACGTTTGATTCA
OEB040	TGAATCAAACGTTTGTTTAAGTG
OEB041	TATGGCTAGCATGAAAGTAAGCACCAAAGACA
OEB042	GGTGCTCGAGGTTGGTGAGCGCCACGTCTC
OEB043	TCGTCAGGGAATCCGGA
OEB044	GCAGCTGACGTTTGGCAA
OEB045	TGTATAAAAACGAGCCAGCCG
OEB046	TCCTGTCCCGGAAGCAC
OEB047	TTAATCAAACGTTTGTTCAATTGAACCTGAAAAGGAGAAATT
OEB048	TTGAACAAACGTTTGATTAACAAAATGCAACAAATCAAGTA
OEB049	TTCATCAAACGTTTGTTTAAATTACATAGAAAGACTTTCAA
OEB050	TTAAACAAACGTTTGATGAATTTTTCTTCAAAAAGTTTCAA
OEB051	CTTGATTTGTTGCATTTTGTTAATCAAACGTTTGTTCAATTGAACCTGAAAAGGAGAAAT
OEB052	ATTTCTCCTTTTCAGGTTCAATTGAACAAACGTTTGATTAACAAAATGCAACAAATCAAG
OEB053	TAAGAATTCTTTTTGAGGGTTCTTTTTTTA
OEB054	AATGGATCCTTGAGCAGCGATCATGACCTC
OEB055	AATCGGATCCCATCTTTGTTTCCCAGACAGC
OEB056	AATGGATCCGAAAAGCTTGTTTGATTTGA
OEB057	CTGAACGACCGTTTAAGCGG
OEB058	CCGCTTAAACGGTCGTTCAG
OEB059	GAATAGCGGCGAATCCTG
OEB060	GCCCGAAATTAAAATCCATTC
OEB061	TATGGCTAGCATGAAACAGACGAAACAAAAAGTA
OEB062	GGTGCTCGAGCATATGAACAGCTCTTGGCCA

Table 3.5. Continued

OEB063	GGTGCTCGAGATGTCGTATCAAGCGAAAGCT
OEB064	ATAGGGAACTGACACGTTTTGTTTACCGAGAGCTTTCGCTT
OEB065	AAGCGAAAGCTCTCGGTAAACAAAACGTGTCAGTTCCCTAT
OEB066	GGTGCTCGAGAATTTCCCTGATTAATGTGGAG
OEB067	TTAGTGGTGGTGGTGGTGGTGATGTGGAGTCAATTGTGACTTCC
OEB068	ACATCACCACCACCACCACCACTAATCTGGGAAATTATGTCGACATATC
OEB069	CTCGAGCTAGTTGGTGAGCGCCAC
OEB070	ACGACGGCCAGTGAATTCATGAAAGTAAGCACCAAAGACAA
OEB071	TTGTCTTTGGTGCTTACTTTCATGAATTCACTGGCCGTCGT
OEB072	AGTTGGTCTGGTGTCAAAAATAAATGTCCAGACCTGCAGGC
OEB073	GCCTGCAGGTCTGGACATTTATTTTTGACACCAGACCAACT
OEB074	GGAAGTCACAATTGACTCCACAGTGGAAGTTACTGACGTAAGATTACG
OEB075	CGTAATCTTACGTCAGTAACTTCCACTGTGGAGTCAATTGTGACTTCC
OEB076	GGAAGTCACAATTGACTCCACATGTGGAAGTTACTGACGTAAGATTACG
OEB077	CGTAATCTTACGTCAGTAACTTCCACATGTGGAGTCAATTGTGACTTCC
OEB078	TTTGTCTACCGGGAAGTCACAATGTGGAAGTTACTGACGTAAGATTACG
OEB079	CGTAATCTTACGTCAGTAACTTCCACATTGTGACTTCCCGGTAGACAAA
OEB080	ACAAACGTTTGA
OEB081	TCAAACGTTTGT
OEB083	ACA CTC GAG CTC
OEB084	GAG CTC GAG TGT
OEB085	CGTTTTGAACACTCGAGCTCTTAA
OEB086	TTAAGAGCTCGAGTGTTCAAAACG
OEB087 L1	CAGCAGATCAGTTAAACAAACGTTTAATCAAAGAAGACATT
OEB088 L1	AATGTCTTCTTTGATTAAACGTTTGTTTAACTGATCTGCTG
OEB091 L2	GCCTTTTCGTTTTGAACAAACGTTTGATTAAAACAAATAGC
OEB092 L2	GCTATTTGTTTTAATCAAACGTTTGTTCAAAACGAAAAGGC
OEB093	TGGTAAATATACTGAACGACCGTTTAAGCGGCGTTCCAATG
OEB094	CATTGGAACGCCGCTTAAACGGTCGTTCAGTATATTTACCA

Table 3.5. Continued

OEB095	GTTTTGAACAAACGTTTGATT
OEB096	CAATCAAACGTTTGTTCAAAA
OEB097	ATTGAACAAACGTTTGATTAA
OEB098	TTTAATCAAACGTTTGTTCAA
OEB099	TTTCGTTTTGAACAAACGTTTGATTAAAACG
OEB100	CGTTTTAATCAAACGTTTGTTCAAAACGAAA
OAM122	ATTAAGCTTACATAAGGAGGAACTACTATG
OAM124	GTCGCACTGGCTGTTACTTC
OAM125	CACATGACCAGGAGCTTCGT
OAM139	TCGAGGGTCATTTTGCAAAAGTTGTTGACTTGAACAAACGTTTGATTCATAATGTGTGTA
OAM140	AGCTTACACACATTATGAATCAAACGTTTGTTCAAGTCAACAACTTTTGCAAAATGACCC
OAM148	GCATGCATGCGTAACACACAGGAAACAGCTATGAAAGTAAGCACCAAAGACAAAATTA
OAM149	GCATGGATCCGAACCGCTACCGTTGGTGAGCGCCACGTCT
OAM165	ACCGAATTAGCTTGCATGCGGCTAGCTCTAGTTGGTGAGCGCCAC
OAM166	ACCGAATTAGCTTGCATGCGGCTAGCTCTA
OAM200	CAATGAATGATCTGGCTGTGAG
OAM201	GCTTACTTTCATACGGCTCACTC
OAM202	TAGTATCAAGAGGAAGGAGTGAGCCGTATGAAAGTAAGCACCAAAGACAA
OAM203	TATCTAGAGGGAAACCGTTGTGGTCTAGTTGGTGAGCGCCAC
OAM204	AGGAGGAACTATATCCGGATCTGGACCAACTAGCACCGTTCCAA
OAM205	TTCAAGGCTGTCATAAAGCTC
OJH001	CATATGTAAGATTTAAATGCAACCG
OJH002	CTACAAGGTGTGGCATAATGTGT
OJH133	GCAGGAATTCGACTCTCTAGCTTGAGG
OJH179	CCAGATCCGGATATAGTTCCTCCT
OJH180	ACCACAACGGTTTCCCTCTAGATA
OJH185	CAGGAATTCGACTCTCTAGC
OJH186	CTCAGCTAGCTAACTCACATTAATTGCGTTGC
OYD070	GTGTGGAATTGTGAGCGGATAAC

CHAPTER IV

CONCLUSION

In this dissertation I have provided evidence that a specialized nucleoid occlusion system contributes to the precise positioning of FtsZ during *Bacillus* sporulation. In order to differentiate the spore from the mother cell, 30% of the *Bacillus* chromosome is initially captured in the forespore. This genetic assymmetry results in the initiation of different gene expression programs in the forespore and mother cell. The mechanisms underlying the precise and reproducible capture of the forespore chromosome is not well understood. Here I summarize our findings regarding the TetR family DNA-binding protein RefZ and and what we have learned about the mechanism by which RefZ contributes to precise chromosome capture. Since all life forms must faithfully replicate and segregate their genetic material to daughter cells, understanding how RefZ functions at the molecular level advances our general understanding of the mechanisms utilized in nature to coordinate cell division with chromosome segregation.

The RefZ binding motifs (*RBMs*) are highly conserved across the *Bacillus* genus both in sequence and relative location with respect to *oriC*, in support of the hypothesis that these motifs serve as positional markers along the chromosome for polar septation (83). We showed the *RBM* DNA localizes in the vicinity of the division septa (83). RefZ was named Regulator of FtsZ for its ability to prevent establishment of a midcell FtsZ ring when expressed during vegetative growth and because Z-ring shifting from midcell to the pole is delayed in a Δ*refZ* mutant background (82). Consistent with these phenotypes, suppressors of RefZ-induced cell filamentation and death are isolated in FtsZ (82) (Yi

Duan and Jennifer Herman, unpublished data). Many regulators of FtsZ have been described, but only SlmA has been shown to depend on DNA-binding to regulate FtsZ activity{Cho, 2011, 7kqL}. RefZ's affect on FtsZ is also dependent on DNA-binding, though at present we lack evidence of direct RefZ-FtsZ interaction. Expression of RefZ in *B. megaterium* also produced filamentation suggesting that RefZ's mechanism of action against FtsZ is also conserved across the *Bacillus* genera (83). RefZ binds to the *RBM*s in units of two and four, producing two mobility shifts by EMSA, the same pattern observed for SlmA. Based on structural studies of other TetR family proteins and the observation that RefZ binds to *RBM*s in units of two and four (83), RefZ most likely does so as a pair of dimers; RefZ may also have the capacity to spread on DNA based on ChIP-seq data (82) and the observation that under some EMSA conditions, RefZ is capable of laddering on DNA (Fig. 3.13).

Without RefZ a subpopulation of cells overcaptures regions on the right and left chromosome arms (83). We showed that while no single *RBM* was sufficient to restore wildtype chromosome capture, cells possessing even one *RBM could* support chromosome capture to about 50% of WT, suggesting that even one *RBM* is beneficial (83). Mutating all five of the *oriC*-proximal *RBMs* produced a similar defect in chromosome capture to the *refZ* deletion, suggesting that RefZ and the *RBMs* function in the same pathway and that RefZ mediates proper chromosome capture through interaction with the binding motifs (83). Together this data describes a protein-DNA interaction that utilizes the axial filament arrangement to properly tune the position of the cell division machinery relative to the chromosome.

To investigate if RefZ's FtsZ-inhibitory activity was important for chromosome capture, we took advantage of RefZ's misexpression phenotype to isolate 10 rLOF variants capable of binding DNA, but unable to inhibit FtsZ. All 10 of the rLOF variants were unable to support chromosome capture, providing evidence that *B. subtilis* utilizes a NO mechanism to facilitate the positioning of the sporulation septum. To better understand RefZ's mechanism of action at the molecular level, WT RefZ and the rLOFs variants were overexpressed, purified, and analyzed utilizing structural and biochemical approaches. The RefZ crystal structure revealed that RefZ is similar to the NO protein SlmA and is a homodimer composed of alpha helices α1-α10. However, mapping of the residues implicated in FtsZ regulation revealed the residues implicated in RefZ's inhibitory activity against FtsZ do not occur on the same surfaces as those identified as the SlmA-FtsZ interaction interface. Therefore, RefZ's mechanism of FtsZ regulation is novel and understanding it will illuminate another of nature's solutions for regulating FtsZ

Two rLOF substitutions map to the dimerization interface of RefZ, and B2H analysis shows these substitutions reduce RefZ self-interaction in the absence of the *RBM* (Fig. 3.9). Two other rLOF variants are on α4, which in other TetR family proteins has been shown to transmit structural changes resulting from binding of allosteric effectors (in the C-terminal regulatory domain) to the DNA-binding domain. Allostery for the TetR family usually results in alteration of the distance between α3 and α3' such that it is incompatible with DNA binding in the presence of an effector. Both E53K and E61K exhibit increased laddering on $RBM_{L2\text{-}150bp}$ suggesting that these variants might be locked in a conformation that is more favorable for DNA binding or that is less sensitive to allosteric regulation (possibly induced by RefZ-FtsZ interaction as it is with SlmA-FtsZ

interaction). The remaining rLOF substitutions (shown in Fig. 3.18), E179 (light gray monomer) R116' (cyan monomer) and E117' (cyan monomer), map to the face of RefZ on different monomers. If RefZ and FtsZ do interact directly, then this may suggest that the RefZ-FtsZ interface is created by dimerization.

RefZ is significantly destabilized by ATP binding in thermal shift assays consistent with ATP binding, and the purified protein possesses a low level of ATP hydrolysis activity. In an endpoint assay, several rLOF variants exhibited different levels of ATP hydrolysis, suggesting that the ATPase activity is attributable to RefZ. At the same time, we cannot presently exclude the possibility that the ATP hydrolysis activity we observe is due to a contaminating ATPase in the purified protein. However, based on these preliminary data, I hypothesize a mechanism for RefZ, similar to ParA. ParA binds to DNA nonspecifically in an ATP-dependent manner, and dissociates from the DNA when its low-level ATPase activity is stimulated by ParA-ParB interaction (62). I hypothesize the RefZ-FtsZ interaction stimulates RefZ bound to the *RBM* to hydrolyze ATP, leading to a conformational change that simultaneously releases RefZ from the *RBM* and breaks the FtsZ filament. Recently, ATP was shown to act as a hydrotrope to solubilize proteins at millimolar concentrations (203). Therefore, another possibility to explain RefZ's destabilization in the thermal shift upon ATP addition is that it is due to nucleotide hydrotrope interactions with RefZ.

Sporulation requires a repositioning of FtsZ from the midcell to the cell quarter position. RefZ localizes to the site of polar septation, and exhibits inhibitory activity against FtsZ (82, 83). At a first glance it seems contradictory that an inhibitor would be localized to the polar position at the time FtsZ needs to be respositioned to the pole.

However, in my model, RefZ functions only in the immediate vicinity of the *RBM*'s, which should not prevent FtsZ from assembling at the pole.

A prediction of RefZ being a local inhibitor at the pole would be an accelerated FtsZ assembly at the cell poles in the absence of RefZ. However, the opposite is observed. Without RefZ there is a delay in the shifting of the FtsZ ring to the cell pole (82). This paradox can be explained when RefZ's localization behavior is taken into account. Early in sporulation, before polar division, RefZ-GFP localizes to the cell poles as foci that colocalize with the nucleoid. The polar foci are dependent on DNA binding and are not observed in the RBM_{5mu} mutant (82) (Miller, unpublished data). consistent with the foci representing an *RBM*-bound state (82). Around the time polar division begins, the polar foci are diminished and a brighter focus near midcell, proximal to the membrane is observed (82). We propose that midcell RefZ localization may promote redistribution of FtsZ to the pole by destabilizing FtsZ at midcell. This would result in a delay in FtsZ repositioning in the Δ*refZ* strain. An alternative possibility is that in the absence of RefZ, organization of the chromosome in preparation for assembly of SpoIIIE at/near the incipient division plane is delayed, and this leads to a delay in FtsZ assembly at the pole.

Future directions

Effect of RefZ on FtsZ polymerization in vitro.

Induction of RefZ during vegetative growth (via an inducible promoter) prevents assembly of functional midcell Z-rings, leading to filamentation in a manner reminiscent of induction of other negative regulators of FtsZ such as MinC and MciZ (204, 205). We

purified *B. subtilis* FtsZ and used 90^{o} light scattering to determine the effect of RefZ on FtsZ polymerization. Addition of 2 mM GTP to 5 uM FtsZ caused an increase in light scattering signal from 50 to 400 absorbance units, indicating successful FtsZ polymerization. Addition of RefZ and *RBM*-containing DNA (+/- ATP) did not produce a decrease in the light scattering signal in preliminary experiments. SlmA's FtsZ inhibitory activity is dependent on a high concentration of KCl, which is known to increase the GTP hydrolysis rate and decrease the light scattering signal. MinC's FtsZ inhibitory activity is pH sensitive and can only be observed at pH 7.5. The buffer conditions used to assess SlmA and MinC's activities against *E.coli* FtsZ could not be assessed due to RefZ's poor solubility. In the described buffer conditions, RefZ aggregates, leading to a positive contribution to the light scattering signal even in the absence of FtsZ. We have tested a range of buffering conditions where RefZ appears to remain soluble, but FtsZ is still able to polymerize, but have yet to observe any effect of RefZ-6His on FtsZ polymerization. The lack of inhibitory affects on FtsZ *in vitro* may be due to the fact that the assay could not be performed using equal molar concentrations of RefZ and FtsZ (as was used to observe the inhibitory activity for MinC and SlmA). Thus far, we have not identified a condition that both prevents RefZ from aggregating at the concentrations necessary and is compatible with FtsZ polymerization. It is also possible that RefZ does not interact directly with FtsZ and or depends on other proteins or cofactors not contained in our assays to affect FtsZ dynamics. Alternatively RefZ may affect bundling or an aspect of FtsZ assembly not readily observed using the light scattering assay. Future work can be directed toward investigating this latter possibility using alternative methodologies, such electron microscopy.

RefZ and FtsZ's Interaction

Using a Zetasizer Nano S (Malvern Panalytical), which measures hydrodynamic radius by dynamic light scattering, we detected an increase in the hydrodynamic radius of FtsZ upon addition of 0.1 uM RefZ and 0.1 uM 41 bp RBM_{L2}, suggestive of an interaction between RefZ and the FtsZ filament. Notably, when we tested the effect of three rLOFs on FtsZ particle size, the rLOF variants did not cause the same increase in hydrodynamic radius. E61K showed very little increase in the hydrodynamic radius with increasing concentration. E117G and E53K exhibited a slightly less significant phenotype. To further investigate the possibility that RefZ and FtsZ interact, we will utilize the Pall ForteBio Octet system (Bio-layer interferometry), a more standardized method for detection of protein-protein interactions. Both full length FtsZ and as well as the CTD tail of FtsZ (ADDTLDIPTFLRNRNKRG) will be tested for interaction.

Characterization of RefZ's low-level ATP hydrolysis activity

At present, we cannot rule out that RefZ's low level ATP hydrolysis activity is due to a contaminating ATPase, but based upon the destabilization of RefZ's T_m by ATP, high structural similarity to EthR shown to bind another nucleotid (c-di-GMP), and the fact that several of the rLOFs exhibit reproducible differences in ATP hydrolysis with different protein purifications, we think the activity is likely attributable to RefZ. Important future work should include further purification (eg: nickel affinity chromatography, followed by gel filtration) of RefZ and two rLOF variants (one loss of hydrolysis E53K and one gain

of hydrolysis R102C). To assess RefZ's specific activity and to test if the ATP hydrolysis we observe is enzymatic, the concentration of RefZ will be varied while the ATP concentration is kept high and constant (10 mM). Hydrolysis rates for WT RefZ can be assessed with a NADH-coupled ATPase assay assuming the buffer conditions can be optimized to be compatible with RefZ solubility. Once the rate is determined, the RefZ concentration will be held constant while substrate concentration is increased to obtain a hyperbolic curve from which V_{max} and K_m can be obtained. Subsequent assays would then use substrate concentrations 3 to 4 times the K_m to ensure that rates are only dependent upon enzyme concentration and not substrate. Additionally we will assess if *RBM*-containing DNA stimulates RefZ's activity in a dose dependent manner and then select a biologically relevant concentration of DNA to determine RefZ's V_{max} and K_m in the presence of the *RBM*. Finally we need to repeat this characterization for the variants E53K and R102C so that we can compare these values to those obtained for WT RefZ.

Screening for a RefZ-nucleotide crystal

We screened for crystals +/- dsRBM_{L2} (oEB097 & oEB098) in the presence of ATP, AMP-PNP, ATPγS, and GTP with WT RefZ and the variant R102C, which had the highest ATPase activity in vitro. We obtained one crystal hit in PEG ION F7 (0.1M Succinic Acid; 12% Polyethelyene glycol 3350). Formation of this crystal was dependent on the presence of AMP-PNP. We proceeded with two rounds of optimization of this crystal hit and obtained a data set at 4Å resolution, which was indexed to a unit cell distinct from the apo crystal described in Chapter III and was large enough to contain DNA. Unfortunately the crystals were extremely fragile and couldn't be separated from

one another. Future studies should include performing an additive screen on top of this crystal condition to determine if more separate crystals can be obtained.

RefZ's monomer/dimer state in solution

Dimerization of RefZ may create the FtsZ interaction and contacts (R116, E117, and E179) are anticipated to be important for FtsZ interaction. RefZ may exist only as a dimer when bound to the *RBM* or alternatively as suggested by B2H analysis (which lacked *RBM* DNA), exist as a dimer in solution as well. As an alternative approach to gel filtration (recall we could not observe formation of an obvious dimer under any condition), we performed crosslinking with RefZ. Successful crosslinking depends on the availability of reactive groups at the dimer interface. Unfortunately the RefZ dimer interface is devoid of amide groups, and inconveniently there are a significant number of amides on the surface of RefZ increasing unspecific background crosslinking. RefZ also lacks native cysteines and the carboxyls are not optimally oriented for dimer interface crosslinking either. Consistent with the lack of appropriately positioned and spaced reactive groups, amide cross linking (formaldehyde - 0 Å, DSS - 11.4 Å, and NHS Diazarine LC - 11.4 Å) did not show any significant proportion of dimer for RefZ (data not shown). An alternative interpretation of this data is that the crosslinking was successful and RefZ does not self-associate to any appreciable degree in solution. In the future this limitation could be addressed by designing a functional RefZ molecule with cysteines and amide groups at the dimer interface to facilitate crosslinking.

RefZ has a single tryptophan positioned at the upper dimer interface, Trp_{193}. The local environment of Trp_{193} is fairly hydrophobic and near the C-terminus of the protein.

We hypothesized that the fluorescence of this conveniently located Trp_{193} may quench upon dimerization. This would imply a difference in fluorescence yield for monomers (higher quantum yield) vs. dimers (lower quantum yield) permitting us to distinguish the state of RefZ in solution. In solution, we predict higher protein concentration would favor the dimeric state as long as the protein did not begin to aggregate. We hypothesized that the absorbance (measuring protein concentration at 280 nm) and fluorescence (measuring Tryptophan fluorescence at 330 nm) should decrease at different rates if the protein becomes more monomeric with dilution. We propose to measure the absorbance and fluorescence of WT RefZ and rLOFs over a concentration of 5-20 mM. We predict that variants predicted to be monomeric as judged by B2H should have the same rate of decrease for fluorescence and absorbance when diluted from 5 to 20 mM. Variants that exist as a monomer/dimer equilibrium will become more monomeric with dilution resulting in a slower rate of decrease for fluorescence than that of absorbance. Preliminary data has shown that for WT, the rates of fluorescence and absorption upon dilution of RefZ behave as predicted (absorption decreases at a faster rate than fluorescence). In the future, variants E53K and L153R should be checked to see if they behave as predicted (more dimeric and more monomeric, respectively).

Effect of the FtsZ CTD on binding of RefZ to the RBM

I hypothesize that the CTD of FtsZ will act like an effector of RefZ and cause a conformational change that will release RefZ from DNA by increasing the distance between α3 and α3'. To test this, a peptide corresponding to the FtsZ CTD will be synthesized and used to evalute its effect on RefZ in the EMSA assays. The prediction is

that with increasing concentration, the CTD will result in a decreased apparent affinity of RefZ for *RBM*-containing DNA. This peptide could also be used to examine its effects on RefZ's exchange rate on the *RBM* and rate of ATP hydrolysis.

Obtaining a RefZ-FtsZ co-crystal

By analogy to other characterized negative regulators of FtsZ, I hypothesize that RefZ may bind to FtsZ's CTD and RefZ-mediated disruption of FtsZ polymerization or bundling might be facilitated by a second contact to FtsZ's globular C-terminal domain. There are only a few structures of FtsZ interacting with regulatory proteins (FtsZ:MciZ (204); FtsZ:SulA (206); FtsZ:ZipA(111) FtsZ:SlmA (128) out of the many proteins that regulate FtsZ. Obtaining structural data for RefZ interacting with FtsZ could inform models regarding the mechanism by which RefZ inhibits FtsZ. In preliminary experiments, RefZ and FtsZ were passed over gel filtration to determine if a co-complex would elute. RefZ and FtsZ both eluted at a MW consistent with monomers; no co-complex was formed. Later an analytical SEC column was equilibrated with a buffer compatible with FtsZ polymerization that included ATP and $MgCl_2$. Under this set of conditions FtsZ eluted around the void volume consistent with it being a polymer. Addition of RefZ did not result in a co-complex peak below the void volume. We cannot exclude that RefZ interacts with polymerized FtsZ. However, the peak height of RefZ +/- FtsZ was not considerably reduced, which suggests that under these conditions, RefZ did not associate with FtsZ (data not shown). We have also screened over 500 conditions for RefZ:FtsZ crystals at a 1:1 FtsZ:RefZ ratio in the presence of dsDNA at 5 and 10 mg/ml. A single crystal hit was identified in the conditions where FtsZ is known to crystallize,

and this crystal possessed a similar morphology to an FtsZ-only crystal; therefore this was not pursued. Future studies should include a screen with just the CTD of *B. subtilis* FtsZ (similar to those performed with to obtain a co-crystal of the *E. coli* FtsZ CTD with SlmA) as well as conditions that include the AMP-PNP.

REFERENCES

1. Piggot PJ & Hilbert DW (2004) Sporulation of Bacillus subtilis. *Curr Opin Microbiol* 7(6):579-586.

2. Errington J (2003) Regulation of endospore formation in Bacillus subtilis. *Nat. Rev. Microbiol.* 1(2):117-126.

3. Sonenshein AL, Hoch JA, & Losick R (Bacillus subtilis: From Cells to Genes and from Genes to Cells. *Bacillus subtilis and Its Closest Relatives*), pp 3-5.

4. Nicholson WL (2002) Roles of Bacillus endospores in the environment. *Cell. Mol. Life Sci.* 59(3):410-416.

5. Kelly CP, Pothoulakis C, & LaMont JT (1994) Clostridium difficile colitis. *N. Engl. J. Med.* 330(4):257-262.

6. Shapiro RL, Hatheway C, & Swerdlow DL (1998) Botulism in the United States: a clinical and epidemiologic review. *Ann. Intern. Med.* 129(3):221-228.

7. Tam NKM, *et al.* (2006) The intestinal life cycle of Bacillus subtilis and close relatives. *J. Bacteriol.* 188(7):2692-2700.

8. Ehling-Schulz M, Fricker M, & Scherer S (2004) Bacillus cereus, the causative agent of an emetic type of food-borne illness. *Mol. Nutr. Food Res.* 48(7):479-487.

9. Kotiranta A, Lounatmaa K, & Haapasalo M (2000) Epidemiology and pathogenesis of Bacillus cereus infections. *Microbes Infect.* 2(2):189-198.

10. Xu Zhou K, Li N, Christie G, & Wilson DI (2017) Assessing the Impact of Germination and Sporulation Conditions on the Adhesion of Bacillus Spores to Glass and Stainless Steel by Fluid Dynamic Gauging. *J. Food Sci.* 82(11):2614-2625.

11. Faille C, *et al.* (2010) Morphology and physico-chemical properties of Bacillus spores surrounded or not with an exosporium: consequences on their ability to adhere to stainless steel. *Int. J. Food Microbiol.* 143(3):125-135.

12. Burkholder PR & Giles NH, Jr. (1947) Induced biochemical mutations in Bacillus subtilis. *Am. J. Bot.* 34(6):345-348.

13. Aguilar C, Vlamakis H, Losick R, & Kolter R (2007) Thinking about Bacillus subtilis as a multicellular organism. *Curr. Opin. Microbiol.* 10(6):638-643.

14. Vachon V, Laprade R, & Schwartz J-L (2012) Current models of the mode of action of Bacillus thuringiensis insecticidal crystal proteins: a critical review. *J. Invertebr. Pathol.* 111(1):1-12.

15. Webb CD, *et al.* (1997) Bipolar localization of the replication origin regions of chromosomes in vegetative and sporulating cells of B. subtilis. *Cell* 88(5):667-674.

16. Wu LJ & Errington J (1998) Use of asymmetric cell division and spoIIIE mutants to probe chromosome orientation and organization in Bacillus subtilis. *Mol. Microbiol.* 27(4):777-786.

17. Wu LJaE, J. (2003) RacA and the Soj-Spo0J system combine to effect polar chromosome segregation in sporulating Bacillus subtilis. *Mol Microbiol* 49(6):1463-1475.

18. Król E, de Sousa Borges A, Kopacz M, & Scheffers D-J (2017) Metal-dependent SpoIIE oligomerization stabilizes FtsZ during asymmetric division in Bacillus subtilis. *PLoS One* 12(3):e0174713.

19. Wang ST, *et al.* (2006) The forespore line of gene expression in Bacillus subtilis. *J. Mol. Biol.* 358(1):16-37.

20. Frandsen N, Barak I, Karmazyn-Campelli C, & Stragier P (1999) Transient gene asymmetry during sporulation and establishment of cell specificity in *Bacillus subtilis*. *Genes Dev* 13(4):394-399.

21. Hilbert DW & Piggot PJ (2004) Compartmentalization of gene expression during Bacillus subtilis spore formation. *Microbiol. Mol. Biol. Rev.* 68(2):234-262.

22. Higgins D & Dworkin J (2012) Recent progress in Bacillus subtilis sporulation. *FEMS Microbiol. Rev.* 36(1):131-148.

23. El Najjar N, *et al.* (2018) Study of DNA translocases in Bacillus subtilis by single molecule tracking reveals strikingly different dynamics of SftA, SpoIIIE and FtsA. *Appl. Environ. Microbiol.*:AEM.02610-02617.

24. Burton B & Dubnau D (2010) Membrane-associated DNA transport machines. *Cold Spring Harb. Perspect. Biol.* 2(7):a000406.

25. Marquis KA, *et al.* (2008) SpoIIIE strips proteins off the DNA during chromosome translocation. *Genes Dev.* 22(13):1786-1795.

26. Driks A (1999) Bacillus subtilis spore coat. *Microbiol. Mol. Biol. Rev.* 63(1):1-20.

27. Alberts B, *et al.* (2002) *Chromosomal DNA and Its Packaging in the Chromatin Fiber* (Garland Science).

28. Badrinarayanan A, Le TBK, & Laub MT (2015) Bacterial Chromosome Organization and Segregation. *Annu. Rev. Cell Dev. Biol.* 31(1):171-199.

29. Cutter AR & Hayes JJ (2015) A brief review of nucleosome structure. *FEBS Lett.* 589(20 Pt A):2914-2922.

30. Schmitt AD, Hu M, & Ren B (2016) Genome-wide mapping and analysis of chromosome architecture. *Nat. Rev. Mol. Cell Biol.* 17(12):743-755.

31. Ramani V, Shendure J, & Duan Z (2016) Understanding Spatial Genome Organization: Methods and Insights. *Genomics Proteomics Bioinformatics* 14(1):7-20.

32. Croft JA, *et al.* (1999) Differences in the localization and morphology of chromosomes in the human nucleus. *J. Cell Biol.* 145(6):1119-1131.

33. Naumova N, *et al.* (2013) Organization of the Mitotic Chromosome. *Science* 342(6161):948-953.

34. Wang X, Brandão HB, Le TBK, Laub MT, & Rudner DZ (2017) Bacillus subtilis SMC complexes juxtapose chromosome arms as they travel from origin to terminus. *Science* 355(6324):524-527.

35. Wang X, Llopis PM, & Rudner DZ (2013) Organization and segregation of bacterial chromosomes. *Nat. Rev. Genet.* 14(3):191-203.

36. Chintakayala K, *et al.* (2013) E. coli Fis protein insulates the cbpA gene from uncontrolled transcription. *PLoS Genet.* 9(1):e1003152.

37. Le TBK, Imakaev MV, Mirny LA, & Laub MT (2013) High-Resolution Mapping of the Spatial Organization of a Bacterial Chromosome. *Science* 342(6159):731-734.

38. Claret L & Rouviere-Yaniv J (1997) Variation in HU composition during growth of Escherichia coli: the heterodimer is required for long term survival. *J. Mol. Biol.* 273(1):93-104.

39. Swinger KK (2003) Flexible DNA bending in HU-DNA cocrystal structures. *EMBO J.* 22(14):3749-3760.

40. Huisman O, *et al.* (1989) Multiple defects in Escherichia coli mutants lacking HU protein. *J. Bacteriol.* 171(7):3704-3712.

41. Kar S, Edgar R, & Adhya S (2005) Nucleoid remodeling by an altered HU protein: reorganization of the transcription program. *Proc. Natl. Acad. Sci. U. S. A.* 102(45):16397-16402.

42. Schumacher MA, Lee J, & Zeng W (2016) Molecular insights into DNA binding and anchoring by the Bacillus subtilis sporulation kinetochore-like RacA protein. *Nucleic Acids Res.* 44(11):5438-5449.

43. Hégarat FL, Salti-Montesanto V, Hauck Y, & Hirschbein L (1993) Purification and characterization of the HU-like protein HPB9 from the Bacillus subtilis nucleoid. *Biochimica et Biophysica Acta (BBA) - Gene Structure and Expression* 1172(1-2):101-107.

44. Köhler P & Marahiel MA (1997) Association of the histone-like protein HBsu with the nucleoid of Bacillus subtilis. *J. Bacteriol.* 179(6):2060-2064.

45. Mercier R, *et al.* (2008) The MatP/matS Site-Specific System Organizes the Terminus Region of the E. coli Chromosome into a Macrodomain. *Cell* 135(3):475-485.

46. Dupaigne P, *et al.* (2012) Molecular Basis for a Protein-Mediated DNA-Bridging Mechanism that Functions in Condensation of the E. coli Chromosome. *Mol. Cell* 48(4):560-571.

47. Nolivos S, *et al.* (2016) MatP regulates the coordinated action of topoisomerase IV and MukBEF in chromosome segregation. *Nat. Commun.* 7:10466.

48. Lutkenhaus J (2012) The ParA/MinD family puts things in their place. *Trends Microbiol.* 20(9):411-418.

49. Uhlmann F (2016) SMC complexes: from DNA to chromosomes. *Nat. Rev. Mol. Cell Biol.* 17(7):399-412.

50. Niki H, Jaffe A, Imamura R, Ogura T, & others (1991) The new gene mukB codes for a 177 kd protein with coiled - coil domains involved in chromosome partitioning of E. coli. *EMBO J.*

51. Soppa J, *et al.* (2002) Discovery of two novel families of proteins that are proposed to interact with prokaryotic SMC proteins, and characterization of the Bacillus subtilis family members ScpA and ScpB. *Mol. Microbiol.* 45(1):59-71.

52. Hirano T, Kobayashi R, & Hirano M (1997) Condensins, chromosome condensation protein complexes containing XCAP-C, XCAP-E and a Xenopus homolog of the Drosophila Barren protein. *Cell* 89(4):511-521.

53. Lioy VS, *et al.* (2018) Multiscale Structuring of the E. coli Chromosome by Nucleoid-Associated and Condensin Proteins. *Cell* 172(4):771-783.e718.

54. Nolivos S & Sherratt D (2014) The bacterial chromosome: architecture and action of bacterial SMC and SMC-like complexes. *FEMS Microbiol. Rev.* 38(3):380-392.

55. Kamada K, Miyata M, & Hirano T (2013) Molecular basis of SMC ATPase activation: role of internal structural changes of the regulatory subcomplex ScpAB. *Structure* 21(4):581-594.

56. Wang X, *et al.* (2015) Condensin promotes the juxtaposition of DNA flanking its loading site in Bacillus subtilis. *Genes Dev.* 29(15):1661-1675.

57. Yano K & Niki H (2017) Multiple cis-Acting rDNAs Contribute to Nucleoid Separation and Recruit the Bacterial Condensin Smc-ScpAB. *Cell Rep.* 21(5):1347-1360.

58. Breier AM & Grossman AD (2007) Whole-genome analysis of the chromosome partitioning and sporulation protein Spo0J (ParB) reveals spreading and origin-distal sites on the Bacillus subtilis chromosome. *Mol. Microbiol.* 64(3):703-718.

59. Nasmyth K (2002) Segregating sister genomes: the molecular biology of chromosome separation. *Science* 297(5581):559-565.

60. Austin S & Abeles A (1983) Partition of unit-copy miniplasmids to daughter cells. *J. Mol. Biol.* 169(2):373-387.

61. Ebersbach G, Briegel A, Jensen GJ, & Jacobs-Wagner C (2008) A self-associating protein critical for chromosome attachment, division, and polar organization in caulobacter. *Cell* 134(6):956-968.

62. Lim HC, *et al.* (2014) Evidence for a DNA-relay mechanism in ParABS-mediated chromosome segregation. *Elife* 3:e02758.

63. Surovtsev IV, Lim HC, & Jacobs-Wagner C (2016) The Slow Mobility of the ParA Partitioning Protein Underlies Its Steady-State Patterning in Caulobacter. *Biophys. J.* 110(12):2790-2799.

64. Ptacin JL, *et al.* (2010) A spindle-like apparatus guides bacterial chromosome segregation. *Nat. Cell Biol.* 12(8):791-798.

65. Lasker K, Mann TH, & Shapiro L (2016) An intracellular compass spatially coordinates cell cycle modules in Caulobacter crescentus. *Curr. Opin. Microbiol.* 33:131-139.

66. Danilova O, Reyes-Lamothe R, Pinskaya M, Sherratt D, & Possoz C (2007) MukB colocalizes with the oriC region and is required for organization of the two Escherichia coli chromosome arms into separate cell halves. *Mol. Microbiol.* 65(6):1485-1492.

67. Wang X, Reyes-Lamothe R, & Sherratt DJ (2008) Modulation of Escherichia coli sister chromosome cohesion by topoisomerase IV. *Genes Dev.* 22(17):2426-2433.

68. Wang X, Montero Llopis P, & Rudner DZ (2014) Bacillus subtilis chromosome organization oscillates between two distinct patterns. *Proc. Natl. Acad. Sci. U. S. A.* 111(35):12877-12882.

69. Sullivan NL, Marquis KA, & Rudner DZ (2009) Recruitment of SMC by ParB-parS organizes the origin region and promotes efficient chromosome segregation. *Cell* 137(4):697-707.

70. Graham TGW, *et al.* (2014) ParB spreading requires DNA bridging. *Genes Dev.* 28(11):1228-1238.

71. Lee PS & Grossman AD (2006) The chromosome partitioning proteins Soj (ParA) and Spo0J (ParB) contribute to accurate chromosome partitioning, separation of replicated sister origins, and regulation of replication initiation in Bacillus subtilis. *Mol. Microbiol.* 60(4):853-869.

72. Wagner JK, Marquis KA, & Rudner DZ (2009) SirA enforces diploidy by inhibiting the replication initiator DnaA during spore formation in Bacillus subtilis. *Mol. Microbiol.* 73(5):963-974.

73. Levin P (2009) Faculty of 1000 evaluation for The conserved sporulation protein YneE inhibits DNA replication in Bacillus subtilis. *F1000 - Post-publication peer review of the biomedical literature*.

74. Ben-Yehuda S & Losick R (2002) Asymmetric cell division in B. subtilis involves a spiral-like intermediate of the cytokinetic protein FtsZ. *Cell* 109(2):257-266.

75. Lenarcic R, *et al.* (2009) Localisation of DivIVA by targeting to negatively curved membranes. *EMBO J.* 28(15):2272-2282.

76. Ben-Yehuda S, *et al.* (2005) Defining a centromere-like element in Bacillus subtilis by Identifying the binding sites for the chromosome-anchoring protein RacA. *Mol. Cell* 17(6):773-782.

77. Sharpe ME & Errington J (1996) The Bacillus subtilis soj-spo0J locus is required for a centromere-like function involved in prespore chromosome partitioning. *Mol. Microbiol.* 21(3):501-509.

78. Lee PS, Lin DC-H, Moriya S, & Grossman AD (2003) Effects of the chromosome partitioning protein Spo0J (ParB) on oriC positioning and replication initiation in Bacillus subtilis. *J. Bacteriol.* 185(4):1326-1337.

79. Becker EC & Pogliano K (2007) Cell-specific SpoIIIE assembly and DNA translocation polarity are dictated by chromosome orientation. *Mol. Microbiol.* 66(5):1066-1079.

80. Kloosterman TG, *et al.* (2016) Complex polar machinery required for proper chromosome segregation in vegetative and sporulating cells of Bacillus subtilis. *Mol. Microbiol.* 101(2):333-350.

81. Duan Y, Huey JD, & Herman JK (2016) The DnaA inhibitor SirA acts in the same pathway as Soj (ParA) to facilitate oriC segregation during Bacillus subtilis sporulation. *Mol. Microbiol.* 102(3):530-544.

82. Wagner-Herman JK, *et al.* (2012) RefZ facilitates the switch from medial to polar division during spore formation in Bacillus subtilis. *J. Bacteriol.* 194(17):4608-4618.

83. Miller AK, Brown EE, Mercado BT, & Herman JK (2015) A DNA-binding protein defines the precise region of chromosome capture duringBacillussporulation. *Mol. Microbiol.* 99(1):111-122.

84. Romberg L & Levin PA (2003) Assembly dynamics of the bacterial cell division protein FTSZ: poised at the edge of stability. *Annu. Rev. Microbiol.* 57:125-154.

85. Bi E & Lutkenhaus J (1991) FtsZ ring structure associated with division in Escherichia coli. *Nature* 354(6349):161-164.

86. den Blaauwen T, Hamoen LW, & Levin PA (2017) The divisome at 25: the road ahead. *Curr. Opin. Microbiol.* 36:85-94.

87. de Boer PAJ (2010) Advances in understanding E. coli cell fission. *Curr. Opin. Microbiol.* 13(6):730-737.

88. Erickson HP, Anderson DE, & Osawa M (2010) FtsZ in bacterial cytokinesis: cytoskeleton and force generator all in one. *Microbiol. Mol. Biol. Rev.* 74(4):504-528.

89. Peters PC, Migocki MD, Thoni C, & Harry EJ (2007) A new assembly pathway for the cytokinetic Z ring from a dynamic helical structure in vegetatively growing cells of Bacillus subtilis. *Mol. Microbiol.* 64(2):487-499.

90. Löwe J & Amos LA (1998) Crystal structure of the bacterial cell-division protein FtsZ. *Nature* 391(6663):203-206.

91. Buske PJ & Levin PA (2012) Extreme C terminus of bacterial cytoskeletal protein FtsZ plays fundamental role in assembly independent of modulatory proteins. *J. Biol. Chem.* 287(14):10945-10957.

92. Redick SD, Stricker J, Briscoe G, & Erickson HP (2005) Mutants of FtsZ targeting the protofilament interface: effects on cell division and GTPase activity. *J. Bacteriol.* 187(8):2727-2736.

93. Weart RB & Levin PA (2003) Growth Rate-Dependent Regulation of Medial FtsZ Ring Formation. *J. Bacteriol.* 185(9):2826-2834.

94. Lu C, Stricker J, & Erickson HP (1998) FtsZ from Escherichia coli, Azotobacter vinelandii, and Thermotoga maritima—quantitation, GTP hydrolysis, and assembly. *Cytoskeleton* 40(1):71-86.

95. Li Z, Trimble MJ, Brun YV, & Jensen GJ (2007) The structure of FtsZ filaments in vivo suggests a force - generating role in cell division. *EMBO J.* 26(22):4694-4708.

96. Fu G, *et al.* (2010) In vivo structure of the E. coli FtsZ-ring revealed by photoactivated localization microscopy (PALM). *PLoS One* 5(9):e12682.

97. Yang X, *et al.* (2017) GTPase activity-coupled treadmilling of the bacterial tubulin FtsZ organizes septal cell wall synthesis. *Science* 355(6326):744-747.

98. Bisson-Filho AW, *et al.* (2017) Treadmilling by FtsZ filaments drives peptidoglycan synthesis and bacterial cell division. *Science* 355(6326):739-743.

99. Chen Y & Erickson HP (2009) FtsZ filament dynamics at steady state: subunit exchange with and without nucleotide hydrolysis. *Biochemistry* 48(28):6664-6673.

100. Romberg L, Simon M, & Erickson HP (2001) Polymerization of Ftsz, a bacterial homolog of tubulin. is assembly cooperative? *J. Biol. Chem.* 276(15):11743-11753.

101. Miraldi ER, Thomas PJ, & Romberg L (2008) Allosteric models for cooperative polymerization of linear polymers. *Biophys. J.* 95(5):2470-2486.

102. Chen Y, Bjornson K, Redick SD, & Erickson HP (2005) A rapid fluorescence assay for FtsZ assembly indicates cooperative assembly with a dimer nucleus. *Biophys. J.* 88(1):505-514.

103. Chen Y & Erickson HP (2005) Rapid in vitro assembly dynamics and subunit turnover of FtsZ demonstrated by fluorescence resonance energy transfer. *J. Biol. Chem.* 280(23):22549-22554.

104. Schumacher MA & Zeng W (2016) Structures of the nucleoid occlusion protein SlmA bound to DNA and the C-terminal domain of the cytoskeletal protein FtsZ. *Proc. Natl. Acad. Sci. U. S. A.* 113(18):4988-4993.

105. Oldfield CJ, *et al.* (2008) Flexible nets: disorder and induced fit in the associations of p53 and 14-3-3 with their partners. *BMC Genomics* 9 Suppl 1:S1.

106. Gardner KAJ, Moore DA, & Erickson HP (2013) The C-terminal linker of Escherichia coli FtsZ functions as an intrinsically disordered peptide. *Mol. Microbiol.* 89(2):264-275.

107. Krupka M, *et al.* (2017) Escherichia coli FtsA forms lipid-bound minirings that antagonize lateral interactions between FtsZ protofilaments. *Nat. Commun.* 8:15957.

108. Duman R, *et al.* (2013) Structural and genetic analyses reveal the protein SepF as a new membrane anchor for the Z ring. *Proc. Natl. Acad. Sci. U. S. A.* 110(48):E4601-4610.

109. Haney SA, *et al.* (2001) Genetic analysis of the Escherichia coli FtsZ.ZipA interaction in the yeast two-hybrid system. Characterization of FtsZ residues essential for the interactions with ZipA and with FtsA. *J. Biol. Chem.* 276(15):11980-11987.

110. Szwedziak P, Wang Q, Freund SMV, & Löwe J (2012) FtsA forms actin-like protofilaments. *EMBO J.* 31(10):2249-2260.

111. Mosyak L, *et al.* (2000) The bacterial cell-division protein ZipA and its interaction with an FtsZ fragment revealed by X-ray crystallography. *EMBO J.* 19(13):3179-3191.

112. Loose M & Mitchison TJ (2014) The bacterial cell division proteins FtsA and FtsZ self-organize into dynamic cytoskeletal patterns. *Nat. Cell Biol.* 16(1):38-46.

113. Errington J & Wu LJ (2017) Cell Cycle Machinery in Bacillus subtilis. *Subcell. Biochem.* 84:67-101.

114. Land AD, Luo Q, & Levin PA (2014) Functional domain analysis of the cell division inhibitor EzrA. *PLoS One* 9(7):e102616.

115. Cleverley RM, *et al.* (2014) Structure and function of a spectrin-like regulator of bacterial cytokinesis. *Nat. Commun.* 5:5421.

116. Gündoğdu ME, *et al.* (2011) Large ring polymers align FtsZ polymers for normal septum formation. *EMBO J.* 30(3):617-626.

117. Rodrigues CDA & Harry EJ (2012) The Min system and nucleoid occlusion are not required for identifying the division site in Bacillus subtilis but ensure its efficient utilization. *PLoS Genet.* 8(3):e1002561.

118. Buss JA, Peters NT, Xiao J, & Bernhardt TG (2017) ZapA and ZapB form an FtsZ-independent structure at midcell. *Mol. Microbiol.* 104(4):652-663.

119. Bailey MW, Bisicchia P, Warren BT, Sherratt DJ, & Männik J (2014) Evidence for divisome localization mechanisms independent of the Min system and SlmA in Escherichia coli. *PLoS Genet.* 10(8):e1004504.

120. Lutkenhaus J (2007) Assembly dynamics of the bacterial MinCDE system and spatial regulation of the Z ring. *Annu. Rev. Biochem.* 76:539-562.

121. Eswaramoorthy P, *et al.* (2011) Cellular architecture mediates DivIVA ultrastructure and regulates min activity in Bacillus subtilis. *MBio* 2(6).

122. Bonanno JB, *et al.* (2009) Crystal structure of the septum site-determining protein minC from Salmonella typhimurium.

123. Cordell SC, Anderson RE, & Lowe J (2001) Crystal structure of the bacterial cell-division inhibitor MinC from T. maritima.

124. Castellen P, Sforça ML, Gueiros-Filho FJ, & de Mattos Zeri AC (2015) Backbone and side chain NMR assignments for the N-terminal domain of the cell division regulator MinC from Bacillus subtilis. *Biomol. NMR Assign.* 9(1):1-5.

125. Shen B & Lutkenhaus J (2009) The conserved C-terminal tail of FtsZ is required for the septal localization and division inhibitory activity of MinC(C)/MinD. *Mol. Microbiol.* 72(2):410-424.

126. Shen B & Lutkenhaus J (2010) Examination of the interaction between FtsZ and MinCN in E. coli suggests how MinC disrupts Z rings. *Mol. Microbiol.* 75(5):1285-1298.

127. Hu Z & Lutkenhaus J (2000) Analysis of MinC reveals two independent domains involved in interaction with MinD and FtsZ. *J. Bacteriol.* 182(14):3965-3971.

128. Du S, Park K-T, & Lutkenhaus J (2015) Oligomerization of FtsZ converts the FtsZ tail motif (conserved carboxy-terminal peptide) into a multivalent ligand with high avidity for partners ZipA and SlmA. *Mol. Microbiol.* 95(2):173-188.

129. Blasios V, *et al.* (2013) Genetic and biochemical characterization of the MinC-FtsZ interaction in Bacillus subtilis. *PLoS One* 8(4):e60690.

130. Adams DW, Wu LJ, & Errington J (2015) Nucleoid occlusion protein Noc recruits DNA to the bacterial cell membrane. *EMBO J.* 34(4):491-501.

131. Bernhardt TG & de Boer PA (2005) SlmA, a nucleoid-associated, FtsZ binding protein required for blocking septal ring assembly over chromosomes in *E. coli*. *Mol Cell* 18(5):555-564.

132. Tonthat NK, *et al.* (2011) Molecular mechanism by which the nucleoid occlusion factor, SlmA, keeps cytokinesis in check. *EMBO J.* 30(1):154-164.

133. Tonthat NK, *et al.* (2013) SlmA forms a higher-order structure on DNA that inhibits cytokinetic Z-ring formation over the nucleoid. *Proceedings of the National Academy of Sciences* 110(26):10586-10591.

134. Du S & Lutkenhaus J (2014) SlmA antagonism of FtsZ assembly employs a two-pronged mechanism like MinCD. *PLoS Genet.* 10(7):e1004460.

135. Cho H, McManus HR, Dove SL, & Bernhardt TG (2011) Nucleoid occlusion factor SlmA is a DNA-activated FtsZ polymerization antagonist. *Proc. Natl. Acad. Sci. U. S. A.* 108(9):3773-3778.

136. Wu LJ, *et al.* (2009) Noc protein binds to specific DNA sequences to coordinate cell division with chromosome segregation. *EMBO J.* 28(13):1940-1952.

137. Ramos JL, *et al.* (2005) The TetR Family of Transcriptional Repressors. *Microbiol. Mol. Biol. Rev.* 69(2):326-356.

138. Cuthbertson L & Nodwell JR (2013) The TetR Family of Regulators. *Microbiol. Mol. Biol. Rev.* 77(3):440-475.

139. Hinrichs W, *et al.* (1994) Structure of the Tet repressor-tetracycline complex and regulation of antibiotic resistance. *Science* 264(5157):418-420.

140. Schumacher MA & Zeng W (2016) Structure of the E. coli nucleoid occlusion protein SlmA bound to DNA and the C-terminal tail of the cytoskeletal cell division protein FtsZ.

141. Yu Z, Reichheld SE, Savchenko A, Parkinson J, & Davidson AR (2010) A comprehensive analysis of structural and sequence conservation in the TetR family transcriptional regulators. *J. Mol. Biol.* 400(4):847-864.

142. Grkovic S, Brown MH, Schumacher MA, Brennan RG, & Skurray RA (2001) The staphylococcal QacR multidrug regulator binds a correctly spaced operator as a pair of dimers. *J. Bacteriol.* 183(24):7102-7109.

143. Aravind L, Anantharaman V, Balaji S, Babu MM, & Iyer LM (2005) The many faces of the helix-turn-helix domain: transcription regulation and beyond. *FEMS Microbiol. Rev.* 29(2):231-262.

144. Harteis S & Schneider S (2014) Making the bend: DNA tertiary structure and protein-DNA interactions. *Int. J. Mol. Sci.* 15(7):12335-12363.

145. Mirny L, *et al.* (2009) How a protein searches for its site on DNA: the mechanism of facilitated diffusion. *J. Phys. A: Math. Theor.* 42(43):434013.

146. Harrison SC & Aggarwal AK (1990) DNA recognition by proteins with the helix-turn-helix motif. *Annu. Rev. Biochem.* 59:933-969.

147. Ptacin JL & Shapiro L (2013) Chromosome architecture is a key element of bacterial cellular organization. *Cell Microbiol* 15(1):45-52.

148. Wu LJ & Errington J (2004) Coordination of cell division and chromosome segregation by a nucleoid occlusion protein in Bacillus subtilis. *Cell* 117(7):915-925.

149. Bylund JE, Haines MA, Piggot PJ, & Higgins ML (1993) Axial filament formation in Bacillus subtilis: induction of nucleoids of increasing length after addition of chloramphenicol to exponential-phase cultures approaching stationary phase. *J Bacteriol* 175(7):1886-1890.

150. Ben-Yehuda S, Rudner DZ, & Losick R (2003) RacA, a bacterial protein that anchors chromosomes to the cell poles. *Science* 299(5606):532-536.

151. Gholamhoseinian A, Shen Z, Wu JJ, & Piggot P (1992) Regulation of transcription of the cell division gene ftsA during sporulation of Bacillus subtilis. *J Bacteriol* 174(14):4647-4656.

152. Gonzy-Treboul G, Karmazyn-Campelli C, & Stragier P (1992) Developmental regulation of transcription of the Bacillus subtilis ftsAZ operon. *J Mol Biol* 224(4):967-979.

153. Levin PA, Losick R, Stragier P, & Arigoni F (1997) Localization of the sporulation protein SpoIIE in Bacillus subtilis is dependent upon the cell division protein FtsZ. *Mol Microbiol* 25(5):839-846.

154. Dworkin J & Losick R (2001) Differential gene expression governed by chromosomal spatial asymmetry. *Cell* 107(3):339-346.

155. Wu LJ & Errington J (1994) Bacillus subtilis SpoIIIE protein required for DNA segregation during asymmetric cell division. *Science* 264(5158):572-575.

156. Grant CE, Bailey TL, & Noble WS (2011) FIMO: scanning for occurrences of a given motif. *Bioinformatics* 27(7):1017-1018.

157. Rossler D, *et al.* (1991) Phylogenetic diversity in the genus Bacillus as seen by 16S rRNA sequencing studies. *Syst Appl Microbiol* 14(3):266-269.

158. Eppinger M, *et al.* (2011) Genome sequences of the biotechnologically important Bacillus megaterium strains QM B1551 and DSM319. *J Bacteriol* 193(16):4199-4213.

159. Schumacher MA, *et al.* (2002) Structural basis for cooperative DNA binding by two dimers of the multidrug-binding protein QacR. *EMBO J.* 21(5):1210-1218.

160. Fiche JB, *et al.* (2013) Recruitment, assembly, and molecular architecture of the SpoIIIE DNA pump revealed by superresolution microscopy. *PLoS Biol* 11(5):e1001557.

161. Yen Shin J, *et al.* (2015) Visualization and functional dissection of coaxial paired SpoIIIE channels across the sporulation septum. *Elife* 4:e06474.

162. Burton BM, Marquis KA, Sullivan NL, Rapoport TA, & Rudner DZ (2007) The ATPase SpoIIIE transports DNA across fused septal membranes during sporulation in Bacillus subtilis. *Cell* 131(7):1301-1312.

163. Lin DC & Grossman AD (1998) Identification and characterization of a bacterial chromosome partitioning site. *Cell* 92(5):675-685.

164. Livny J, Yamaichi Y, & Waldor MK (2007) Distribution of centromere-like parS sites in bacteria: insights from comparative genomics. *J Bacteriol* 189(23):8693-8703.

165. Stouf M, Meile JC, & Cornet F (2013) FtsK actively segregates sister chromosomes in Escherichia coli. *Proc Natl Acad Sci U S A* 110(27):11157-11162.

166. Harwood CRaC, S.M. (1990) *Molecular Biological Methods for Bacillus* (Wiley, New York).

167. Youngman PJ, Perkins JB, & Losick R (1983) Genetic transposition and insertional mutagenesis in Bacillus subtilis with Streptococcus faecalis transposon Tn917. *Proc Natl Acad Sci U S A* 80(8):2305-2309.

168. Hanvey JC, *et al.* (1992) Antisense and antigene properties of peptide nucleic acids. *Science* 258(5087):1481-1485.

169. Rasband WS (2014) ImageJ (U.S. National Institutes of Health, Bethesda, Maryland).

170. Karimova G, Pidoux J, Ullmann A, & Ladant D (1998) A bacterial two-hybrid system based on a reconstituted signal transduction pathway. *Proc Natl Acad Sci U S A* 95(10):5752-5756.

171. Gibson DG, *et al.* (2009) Enzymatic assembly of DNA molecules up to several hundred kilobases. *Nat. Methods* 6(5):343-345.

172. Updegrove TB & Ramamurthi KS (2017) Geometric protein localization cues in bacterial cells. *Curr Opin Microbiol* 36:7-13.

173. Antonny B (2011) Mechanisms of membrane curvature sensing. *Annu Rev Biochem* 80:101-123.

174. Du S & Lutkenhaus J (2017) Assembly and activation of the *Escherichia coli* divisome. *Mol Microbiol* 105(2):177-187.

175. Scholefield G, Whiting R, Errington J, & Murray H (2011) Spo0J regulates the oligomeric state of Soj to trigger its switch from an activator to an inhibitor of DNA replication initiation. *Mol Microbiol* 79(4):1089-1100.

176. Grilley M, Welsh KM, Su SS, & Modrich P (1989) Isolation and characterization of the *Escherichia coli mutL* gene product. *J Biol Chem* 264(2):1000-1004.

177. Modrich P (1989) Methyl-directed DNA mismatch correction. *J Biol Chem* 264(12):6597-6600.

178. Hansen FG & Atlung T (2018) The DnaA Tale. *Front Microbiol* 9:319.

179. Leonard AC & Grimwade JE (2015) The orisome: structure and function. *Front Microbiol* 6:545.

180. Aussel L, *et al.* (2002) FtsK Is a DNA motor protein that activates chromosome dimer resolution by switching the catalytic state of the XerC and XerD recombinases. *Cell* 108(2):195-205.

181. Bramkamp M, *et al.* (2008) A novel component of the division-site selection system of *Bacillus subtilis* and a new mode of action for the division inhibitor MinCD. *Mol Microbiol* 70(6):1556-1569.

182. Funnell BE (2016) ParB partition proteins: complex formation and spreading at bacterial and plasmid centromeres. *Front Mol Biosci* 3:44.

183. Marston AL, Thomaides HB, Edwards DH, Sharpe ME, & Errington J (1998) Polar localization of the MinD protein of Bacillus subtilis and its role in selection of the mid-cell division site. *Genes Dev* 12(21):3419-3430.

184. Britton RA, *et al.* (2002) Genome-wide analysis of the stationary-phase sigma factor (sigma-H) regulon of *Bacillus subtilis*. *J Bacteriol* 184(17):4881-4890.

185. Molle V, *et al.* (2003) The Spo0A regulon of Bacillus subtilis. *Mol. Microbiol.* 50(5):1683-1701.

186. Fujita M, González-Pastor JE, & Losick R (2005) High- and low-threshold genes in the Spo0A regulon of Bacillus subtilis. *J. Bacteriol.* 187(4):1357-1368.

187. Chung YS & Guarné A (2012) Iterative optimization of DNA duplexes for crystallization of SeqA-DNA complexes. *J. Vis. Exp.* (69):e4266.

188. Gibrat JF, Madej T, & Bryant SH (1996) Surprising similarities in structure comparison. *Curr Opin Struct Biol* 6(3):377-385.

189. Agari Y, Sakamoto K, Kuramitsu S, & Shinkai A (2012) Transcriptional repression mediated by a TetR family protein, PfmR, from T*hermus thermophilus* HB8. *J Bacteriol* 194(17):4630-4641.

190. Pettersen EF, *et al.* (2004) UCSF Chimera--a visualization system for exploratory research and analysis. *J Comput Chem* 25(13):1605-1612.

191. Krissinel E & Henrick K (2007) Inference of macromolecular assemblies from crystalline state. *J Mol Biol* 372(3):774-797.

192. Ponstingl H, Henrick K, & Thornton JM (2000) Discriminating between homodimeric and monomeric proteins in the crystalline state. *Proteins* 41(1):47-57.

193. Laskowski RA & Swindells MB (2011) LigPlot+: multiple ligand-protein interaction diagrams for drug discovery. *J Chem Inf Model* 51(10):2778-2786.

194. Wallace AC, Laskowski RA, & Thornton JM (1995) LIGPLOT: a program to generate schematic diagrams of protein-ligand interactions. *Protein Eng* 8(2):127-134.

195. Cho H & Bernhardt TG (2013) Identification of the SlmA active site responsible for blocking bacterial cytokinetic ring assembly over the chromosome. *PLoS Genet.* 9(2):e1003304.

196. Zhang H-N, *et al.* (2017) Cyclic di-GMP regulates Mycobacterium tuberculosis resistance to ethionamide. *Sci. Rep.* 7(1):5860.

197. Zhang L, Li W, & He Z-G (2013) DarR, a TetR-like transcriptional factor, is a cyclic di-AMP-responsive repressor in Mycobacterium smegmatis. *J. Biol. Chem.* 288(5):3085-3096.

198. Cimmperman P, *et al.* (2008) A quantitative model of thermal stabilization and destabilization of proteins by ligands. *Biophys. J.* 95(7):3222-3231.

199. Senisterra GA & Finerty PJ, Jr. (2009) High throughput methods of assessing protein stability and aggregation. *Mol Biosyst* 5(3):217-223.

200. La Verde V, Dominici P, & Astegno A (2017) Determination of Hydrodynamic Radius of Proteins by Size Exclusion Chromatography. *Bio-protocol* 7(8).

201. Rodikova EA, *et al.* (2007) Two HlyIIR dimers bind to a long perfect inverted repeat in the operator of the hemolysin II gene from Bacillus cereus. *FEBS Lett.* 581(6):1190-1196.

202. Anonymous (Protocol for Annealing Oligonucleotides.

203. Patel A, *et al.* (2017) ATP as a biological hydrotrope. *Science* 356(6339):753-756.

204. Bisson-Filho AW, *et al.* (2015) FtsZ filament capping by MciZ, a developmental regulator of bacterial division. *Proc. Natl. Acad. Sci. U. S. A.* 112(17):E2130-2138.

205. de Oliveira IF, *et al.* (2010) Characterization of ftsZ mutations that render Bacillus subtilis resistant to MinC. *PLoS One* 5(8):e12048.

206. Cordell SC, Robinson EJH, & Lowe J (2003) Crystal structure of the SOS cell division inhibitor SulA and in complex with FtsZ. *Proc. Natl. Acad. Sci. U. S. A.* 100(13):7889-7894.